

Decoding calcium spiking:

The calcium ion-binding properties of CCaMK

Author: David John Kenneth Swainsbury

A thesis submitted for the degree of Doctor of Philosophy at the University of East Anglia

Work conducted within the Bornemann research group
Department of Biological Chemistry
John Innes Centre
Norwich Research Park
Norwich
NR4 7UH

Date of submission: September 2011

This copy of the thesis has been supplied on condition that anyone who consults it is understood to recognise that its copyright rests with the author and that use of any information derived there from must be in accordance with current UK Copyright Law. In addition, any quotation or extract must include full attribution.

Abstract

Most land plants form symbiotic interactions with arbuscular mycorrhizal fungi. This aids soil penetration and the uptake of key nutrients, particularly phosphorus. Legumes form additional symbioses with rhizobial bacteria, which leads to the formation of root nodules where nitrogen is fixed from the atmosphere. This is of great interest in modern agriculture as legumes do not require nitrogenous fertilisers. These two symbioses share a common signalling pathway that centres on calcium spiking, which is specific to the symbiont. These are thought to be decoded by calcium and calmodulin dependent protein kinase (CCaMK). CCaMK consists of three domains. These are a Ser/Thr kinase domain, an autoinhibitory domain containing a calmodulin binding site and a visinin-like domain containing three active and one inactive calcium ion-binding EF-hands. The presence of a calmodulin binding site and intrinsic EF-hands make CCaMK unique among protein kinases. It was shown that calcium ion-binding induces autophosphorylation leading to an enhancement of CaM binding and that CaM binding leads to substrate phosphorylation. However, the affinity and kinetics of calcium and CaM binding have not been fully characterised. To this end we have undertaken a study of calcium ion-binding to constructs of the CCaMK visinin-like domain and visinin-like domain with autoinhibition. It has been discovered that calcium ions bind to CCaMK EF-hands two and three with an affinity of 200 nM, and the fourth EF-hand with a significantly higher affinity. The binding of calcium ions is diffusion rate limited and induces tertiary structural changes in the protein. These leads to elongation of the visinin-like domain and alterations in its interactions with the autoinhibitory domain. Dissociation of calcium ions is complete within one second. This means that calcium ion-bound CCaMK is unable to persist between spikes, which have an interval of 90 s. The binding of CaM slows the dissociation of calcium ions; however dissociation of CaM and calcium ions is still too rapid to retain activity between spikes. This means that calcium ion-binding to CCaMKs visinin-like domain, or CaM in complex with CCaMK is unable to decode calcium spikes. This means that other processes, such as autophosphorylation, may be the mechanism by which calcium signals are decoded to give rise to specific symbiotic interactions.

Table of contents

Abstract	II
Table of contents	III
List of tables	VII
List of figures	VIII
Acknowledgements	XI
List of abbreviations	XIII
1. Chapter one – Introduction to calcium signalling, plant microbe symbiosis and CCaMK	1
1.1 Calcium signalling	2
1.1.1 <i>Calcium transport and storage</i>	2
1.1.2 <i>Control of calcium signalling</i>	3
1.1.3 <i>Calcium signals and sensors</i>	4
1.1.4 <i>The EF-hand</i>	4
1.2 Plant-microbe symbiosis	7
1.2.1 <i>An introduction to nodulation</i>	7
1.2.2 <i>An introduction to Mycorrhization</i>	8
1.2.3 <i>The common symbiosis pathway</i>	8
1.2.4 <i>Nod-specific Genes</i>	12
1.2.5 <i>Myc-specific genes</i>	13
1.2.6 <i>Calcium spiking</i>	14
1.3 Calcium and calmodulin dependent protein kinase.....	16
1.3.1 <i>Organisation of CCaMK</i>	16
1.3.2 <i>CCaMKs in plants</i>	18
1.3.3 <i>Function of CCaMK</i>	18
1.3.4 <i>Proposed mechanism of CCaMK activation</i>	20
1.4 Introduction to calmodulin.....	23
1.4.1 <i>Functions of calmodulin</i>	25
1.4.2 <i>Calcium ion-binding</i>	25
1.4.3 <i>Target recognition and binding</i>	26

1.4.4	<i>CaM and CMLs in nodulation</i>	28
1.5	calmodulin dependent protein kinase II	28
1.5.1	<i>Structure of CaMKII</i>	30
1.5.2	<i>CaMKII Mechanism</i>	30
1.5.3	<i>Kinetic and affinity studies of CaMKII</i>	31
1.5.4	<i>Modelling CaMKII activation</i>	32
1.5.5	<i>Comparison of CCaMK with CaMKII</i>	37
1.6	Neuronal calcium sensors	37
1.6.1	<i>Structure of the NCS</i>	38
1.6.2	<i>Mechanism of Activation</i>	38
1.7	Aims and objectives of this project	39
2.	Chapter two – Structural aspects of CCaMK and conformational changes upon calcium ion-binding	41
2.1	Results.....	41
2.1.1	<i>Identification of mtCCaMK homologues</i>	41
2.1.2	<i>Identification of the visinin-like domain boundary</i>	44
2.1.3	<i>Prediction of the kinase domain boundary and additional features</i>	44
2.1.4	<i>Cloning, expression and purification of CCaMK and CCaMK constructs</i>	47
2.1.5	<i>Determination of the calcium ion-binding stoichiometry of CCaMK</i>	55
2.1.6	<i>Determination of the CCaMK regulatory domain oligomerisation state</i>	62
2.1.7	<i>Determination of the visinin-like and autoinhibitory domains secondary structure</i> .63	
2.1.8	<i>Evidence of overall conformational changes in CCaMK</i>	66
2.1.9	<i>Monitoring of hydrophobic exposure upon calcium ion-binding</i>	71
2.1.10	<i>Low resolution structures of the CCaMK regulatory domains and calmodulin</i>	72
2.2	Discussion	82
2.3	Materials and Methods.....	86
2.3.1	<i>BLAST analysis</i>	86
2.3.2	<i>Disorder prediction</i>	86
2.3.3	<i>Coiled-coil prediction</i>	86
2.3.4	<i>Experimental determination of the visinin-like domain boundary</i>	86
2.3.5	<i>Threaded model of CCaMK kinase and autoinhibitory domains</i>	87
2.3.6	<i>Cloning of mtCaM1, mtCCaMK and CCaMK-constructs</i>	87
2.3.7	<i>Expression and purification of CaM1, CCaMK and CCaMK constructs</i>	88
2.3.8	<i>Determination of extinction coefficients</i>	91

2.3.9	<i>Screening of buffer conditions for the full length protein</i>	91
2.3.10	<i>Analytical gel filtration of visinin-like domain and visinin-like domain with autoinhibition</i>	91
2.3.11	<i>Electrospray ionisation mass spectrometry</i>	91
2.3.12	<i>Analytical ultracentrifugation</i>	92
2.3.13	<i>Circular dichroism spectroscopy</i>	92
2.3.14	<i>ANS fluorescence spectroscopy</i>	93
2.3.15	<i>Shape determination by small angle X-ray scattering (SAXS)</i>	93
3.	Chapter three – Affinity and thermodynamics of calcium ion-binding to CCaMK EF-hands	95
3.1	Results.....	95
3.1.1	<i>Determination that the CCaMK EF-hands are independent and non-interacting</i>	95
3.1.2	<i>Determination of the calcium ion-affinity of the CCaMK visinin-like domain</i>	99
3.1.3	<i>Effect of EF-hand mutation on the calcium ion-affinity</i>	109
3.2	Discussion	110
3.3	Experimental procedures.....	112
3.3.1	<i>Removal of calcium ions from protein samples</i>	112
3.3.2	<i>Electrospray ionisation mass spectrometry</i>	113
3.3.3	<i>Isothermal titration calorimetry of calcium ion-binding to the CCaMK visinin-like domain</i>	113
3.3.4	<i>Titration of CaCl₂ into the visinin-like domain monitored by tyrosine fluorescence</i>	114
4.	Chapter Four – The kinetics of calcium ion-dissociation from the CCaMK EF-hands	115
4.1	Results.....	115
4.1.1	<i>Calcium ion-dissociation rate constants from the visinin-like domain and visinin-like domain with autoinhibition</i>	115
4.1.2	<i>Dissection of the calcium ion-dissociation from the individual EF-Hands</i>	126
4.1.3	<i>Calculation of the calcium ion-association rate constants</i>	129
4.2	Discussion	129
4.3	Experimental procedures.....	133
4.3.1	<i>Calcium ion-dissociation monitored by Quin-2 fluorescence</i>	133
4.3.2	<i>Calcium ion-dissociation monitored by Quin-2 absorbance</i>	133

4.3.3	<i>UV/Vis spectroscopy of calcium ion-sensitive dyes</i>	134
4.3.4	<i>Simulation of calcium spiking and CCaMK calcium ion-binding in silico</i>	134
5.	Chapter five – Characterisation of CaM binding to the CCaMK visinin-like domain with autoinhibition	135
5.1	Results.....	135
5.1.1	<i>Conformation of complex formation between the CCaMK visinin-like domain with autoinhibition and CaM</i>	135
5.1.2	<i>Determination of the CaM dissociation rate constant from the visinin-like domain with autoinhibition</i>	139
5.1.3	<i>Binding and kinetics of CaM to the CCaMK visinin-like domain with autoinhibition</i>	144
5.2	Discussion	149
5.3	Experimental Procedures	152
5.3.1	<i>Analytical gel filtration of the CCaMK visinin-like domain with autoinhibition, CaM and the visinin-like domain with autoinhibition/CaM complex</i>	152
5.3.2	<i>Analytical ultracentrifugation of the CCaMK visinin-like domain with autoinhibition, CaM and the CCaMK visinin-like domain with autoinhibition/CaM complex</i>	152
5.3.3	<i>Tryptophan fluorescence spectroscopy of the visinin-like domain with autoinhibition to monitor CaM binding</i>	152
5.3.4	<i>Calcium ion-dissociation from the visinin-like domain with autoinhibition/CaM complex monitored by Quin-2 absorbance</i>	152
5.3.5	<i>CaM dissociation from the CCaMK visinin-like domain with autoinhibition monitored by tryptophan fluorescence</i>	152
5.3.6	<i>Surface Plasmon resonance</i>	153
6.	Chapter six - General discussion	154
7.	Chapter seven – Outlook and future work	160
	References	163

List of tables

1. Chapter one – Introduction to calcium signalling, plant microbe symbiosis and CCaMK	1
Table. 1.1. CaM binding affinity and rate constants in the presence of CaM binding proteins...	27
2. Chapter two – Structural aspects of CCaMK and conformational changes upon calcium ion-binding	41
Table. 2.1. Theoretical mass to charge (m/z) ratios for the ESI-MS spectra of CCaMK visinin-like domain.....	58
Table. 2.2. Analytical ultracentrifugation of CCaMK regulatory domain constructs.....	62
Table. 2.3. Secondary structure of CCaMK regulatory domains and EF-hand mutants.....	64
Table. 2.4. Fitted parameters from SAXS data curves.....	77
Table. 2.5. PCR primers for TOPO cloning and Quick-Change mutagenesis.....	87
Table. 2.6. Map of the 96 conditions screened in the thermofluor assay.....	90
3. Chapter three – Affinity and thermodynamics of calcium ion-binding to CCaMK EF-hands.....	95
Table. 3.1. ITC and ICP-OES data for calcium ion-binding to the CCaMK visinin-like domain.....	104
4. Chapter Four – The kinetics of calcium ion-dissociation from the CCaMK EF-hands.....	115
Table. 4.1. Kinetics of calcium ion binding to CCaMK	123
5. Chapter five – Characterisation of CaM binding to the CCaMK visinin-like domain with autoinhibition	135
Table. 5.1. Analytical ultracentrifugation of the CCaMK visinin-like domain with autoinhibition, CaM and the visinin-like domain with autoinhibitor/ CaM complex.	138
Table. 5.2. Measured rate constants for CaM and calcium ion-dissociation from the visinin-like domain with autoinhibition/CaM complex at 15 °C.....	144

List of figures

1. Chapter one – Introduction to calcium signalling, plant microbe symbiosis and CCaMK	1
Figure. 1.1. Structure of EF-hand binding loops.	6
Figure. 1.2. Symbiote entry and the structures of Nod and Myc factors.	10
Figure. 1.3. Overview of the Nod and Myc factor signalling pathways.	14
Figure. 1.4. Nuclear calcium spiking measured in <i>M truncatula</i> root hair cells.....	16
Figure. 1.5. Outline of the features of <i>M. truncatula</i> CCaMK.	17
Figure. 1.6. Scheme of CCaMK activation based upon publications from the Poovaiah group..	23
Figure. 1.7. Crystal structures of CaM and CaM in complex with a target peptide.	24
Figure. 1.8. Structure of CaMKII.	29
Figure. 1.9. Kinetic parameters of CaMKII during calcium spiking.	36
Figure. 1.10. NMR structures of recoverin.	39
2. Chapter two – Structural aspects of CCaMK and conformational changes upon calcium ion-binding.....	41
Figure. 2.1. Alignment of <i>M. truncatula</i> CCaMK against other CCaMKs.....	42
Figure. 2.2. Alignment of CCaMK against entries of CaM kinases in the PDB and members of the NCS protein family.	43
Figure. 2.3. CCaMK structural predictions.....	46
Figure. 2.4. Threaded model of CCaMK kinase-domain with autoinhibition	46
Figure. 2.5. SDS Page gels of protein preparations.	49
Figure. 2.6. Analytical gel filtration of full length CCaMK.	50
Figure. 2.7. UV/Vis spectra between 240 and 340 nm.	54
Figure. 2.8. Analytical gel filtration of CCaMK regulatory domain constructs.	55
Figure. 2.9. Manual alignment of CCaMK EF-hand binding loops.	57
Figure. 2.10. Electrospray ionisation mass spectra of the CCaMK visinin-like domain.	62
Figure. 2.11. Far-UV CD spectra.....	65
Figure. 2.12. Near-UV CD spectra of the CCaMK regulatory domain constructs.	67

Figure. 2.13. Near-UV CD spectra of the CCaMK visinin-like domain and visinin-like domain EF-hand mutants.	69
Figure. 2.14. ANS fluorescence spectra.....	71
Figure. 2.15. SAXS data for calmodulin in the apo and calcium ion-bound forms.....	76
Figure. 2.16. SAXS data for the visinin-like domain in the apo and calcium ion-bound forms..	79
Figure. 2.17. Comparison of SAXS data for the visinin-like domain and visinin-like domain with autoinhibition.	80
Figure. 2.18. Comparison of SAXS P(r) curves for the visinin-like domain EF-hand mutants. .	82
Figure. 2.19. Model of CCaMK regulatory domain rearrangements upon calcium binding.	85
3. Chapter three – Affinity and thermodynamics of calcium ion-binding to CCaMK EF-hands.....	95
Figure. 3.1. Calcium ion titration monitored by ESI-MS.	99
Figure. 3.2. Isothermal titration calorimetry of calcium ion-binding to the CCaMK visinin-like domain.....	103
Figure. 3.3. Titration of CaCl ₂ into the CCaMK visinin-like domain monitored by tyrosine fluorescence.	108
Figure. 3.4. Isothermal titration calorimetry of calcium ion-binding to the CCaMK visinin-like domain mutants.	110
Figure. 3.5. Predicted calcium ion-occupancy of CCaMK over the measured concentration range of a calcium spike.....	111
4. Chapter Four – The kinetics of calcium ion-dissociation from the CCaMK EF-hands.....	115
Figure. 4.1. Calcium ion-binding and dissociation data for Quin-2.....	117
Figure. 4.2. Calcium ion-dissociation from the visinin-like domain construct monitored by Quin-2 fluorescence.	119
Figure. 4.3. UV/Vis spectra of ion-calcium sensitive dyes.....	120
Figure. 4.4. Stopped-flow spectrophotometry time courses of calcium ion-dissociation from the visinin-like domain and visinin-like domain with autoinhibition.	126
Figure. 4.5. Stopped-flow traces of calcium ion-dissociation from the visinin-like domain EF-hand mutants.	128

Figure. 4.6. Simulation of calcium spiking and calcium ion-bound protein oscillations.....	132
5. Chapter five – Characterisation of CaM binding to the CCaMK visinin-like domain with autoinhibition	135
Figure. 5.1. Analytical gel filtration of the CCaMK visinin-like domain with autoinhibition, CaM and the visinin-like domain with autoinhibition/CaM complex.....	136
Figure. 5.2. Fluorescence spectra of CaM binding to the visinin-like domain with autoinhibition.	137
Figure. 5.3. Dissociation kinetics of the CCaMK visinin-like domain with autoinhibition/CaM/calcium ion complex.....	143
Figure. 5.4. CaM binding to the visinin-like domain with autoinhibition monitored by surface plasmon resonance.	148
Figure. 5.5. Proposed mechanism of CaM dissociation from the visinin-like domain with autoinhibition.	151
6. Chapter six - General discussion.....	154
Figure. 6.1. Updated activation scheme for CCaMK with data from this thesis.	156
Figure. 6.2. Effects of CCaMK EF-hand mutation on the efficiency of symbiotic interactions in <i>M. truncatula</i>	158

Acknowledgements

The work presented in this thesis would not have been possible without the help and guidance of my supervisors, colleagues, collaborators, family and friends.

I would like to begin by thanking my supervisor, Dr. Stephen Bornemann. From the point at which I began this project, Dr. Bornemann has offered help, support and guidance whenever required. I have never felt like a question was too stupid (I am sure there were many silly questions!) and he has always been able to find time, even when the diary was full. Dr. Bornemann has always encouraged me to make the most of the opportunities that have been available to me, whether that was to attend a Friday seminar, attend training courses or present my work to an international conference, even though I did not have the confidence to do so. His encouragement, when things were not going well and I felt like progress was nothing but a distant dream, was invaluable in keeping the project on track. This encouragement and guidance has helped me grow both professionally and personally. He has also redefined the word patience on many occasions, and I hope I have not been the cause of too much stress! I could not have asked for a better supervisor, and for all this I am eternally grateful.

I would also like to thank my secondary supervisor, Prof. Giles Oldroyd for his input to the work, and providing an enjoyable collaboration with his research group, from which this project originated. Ben Millar and Dr. Akira Miyahara deserve particular mention. I also thank Prof. Ray Dixon, my advisor, for his input and Dr. David Lawson for help, advice and allowing me to pretend to be a crystallographer. It is a shame that I was unlucky in producing crystals and we did not have the chance to work more closely. Additionally, I thank members of the Bornemann group, Dr. Abdul Rashid, Dr. Karl Syson, Farzana Miah and Dr. Liang Zhou, and former members Dr. Nicola Gilberthorpe and Anne-Claire Marquis for their advice and support.

I would also like to acknowledge members of the department of Biological Chemistry, who have been friendly and always willing to help. This department has made JIC such a wonderful place to work over the course of this project.

There are also some specific acknowledgements for experiments detailed in this thesis. I would like to thank Dr. Fiona Husband and Dr. Phil Johnson at the Institute of Food Research for assistance with the circular dichroism experiments. I thank Dr. Mike Naldrett and Dr. Gerhard Saalbach for collaboration in the electrospray ionisation mass spectrometry experiments, Dr. Tom Clarke at the University of East Anglia for assistance with the analytical ultra centrifugation experiments, and Dr. Dmitri Svergun and Dr. Weifeng Shang for collaboration with the small angle X-ray scattering.

Finally, I would like to thank my friends and family for their support, especially my wife, Sarah Swainsbury. Sarah has always known exactly what to say through the highs and lows of the past

four years and is a top-notch proof-reader to boot! I would not have been able to keep a level-head without her love and support.

This work was funded by the BBSRC Doctoral Training Account awarded to the JIC.

List of abbreviations

- AM – arbuscular mycorrhizal
- ANS – 1-anilinonaphthalene-8-sulfonic Acid
- BLAST – basic local alignment search tool
- CaM – calmodulin (full name calcium modulating protein)
- CaMKII – calmodulin dependent protein kinase II
- CBL – calcineurin B-like protein
- CCaMK – calcium and calmodulin dependent protein kinase
- CIPK – CBL interacting protein kinase
- DLS – dynamic light scattering
- D_{\max} – maximum particle diameter
- EGTA - ethylene glycol tetraacetic acid
- ENOD – early nodulin gene
- EDC – ethyl-3-(3-dimethylaminopropyl) carbodiimide
- ER – endoplasmic reticulum
- HEPES – 4-(2-hydroxyethyl)-1-piperazineethanesulfonic acid
- ICP-OES - inductively coupled plasma optical emission spectrometry
- IDA - iminodiacetic acid
- InsP₃ – inositol-1,4,5-triphosphate
- ITC – isothermal titration calorimetry
- NCS – neuronal calcium sensor protein
- NHS – *N*-hydroxysuccinimide
- NMDA – *N*-methyl-D-aspartate
- NSD – normalised spatial discrepancy
- NSP – nodulation signalling pathway
- NTA – nitrilotriacetic acid
- OD – optical density
- PDB – protein data bank
- P(r) – pair distance distribution
- qPCR – quantitative real time polymerase chain reaction
- IPD3 – interacting protein of DMI3
- rISD – Reflection in source decay
- SPR – surface plasmon resonance
- R_g – radius of gyration
- RIP1 – *Rhizobium* induced peroxidase 1
- SAXS – small angle X-ray scattering

TCEP – tris(2-carboxyethyl)phosphine

T_m – melting temperature

1. Chapter one – Introduction to calcium signalling, plant microbe symbiosis and CCaMK

The legumes are a group of plant species in the family *Leguminosae* which includes *Medicago truncatula*, clover, pea and peanuts. Legume plants are able to form a unique symbiotic relationship with rhizobial bacteria to form a specialised organ, the root nodule, where nitrogen fixation takes place. This form of symbiosis is thought to have evolved 60 million years ago. Additionally, 90% of land plants (including the legumes) are able to form mycorrhizal interactions. In this symbiosis, mycorrhizal fungi extend into the surrounding soil and increase nutrient uptake to the plant, particularly of phosphorous in the form of phosphate. This interaction is much more ancient having evolved approximately 450 million years ago. In return for these services, the plant provides the symbiont with carbon sources to aid its growth (1).

These symbiotic processes are of great importance in terms of environmental and agricultural science. Legumes are able to fix large amounts of nitrogen without the environmental impact of artificial fertilisers, which cause damage to various ecosystems via leeching of nitrates. Furthermore fertilisers contribute to global warming through the release of nitrous oxide into the atmosphere and production of carbon dioxide during their manufacture. Additionally the cost of fertilizer has a major impact on food prices, which are rising at an alarming rate. By understanding symbiosis, it may be better exploited to overcome some of the major problems of modern agriculture.

Chimeric calcium and calmodulin-dependant protein kinase (CCaMK) is involved in nodulation and mycorrhizal factor signalling to initiate the formation of two symbiotic relationships in plants (2). Does not make infection threads 3 (DMI3), identified through mutant screens, is the CCaMK from *M. truncatula* (3). CCaMKs have been demonstrated to show similarity to two animal proteins, calmodulin dependant protein kinase II (CaMKII), which is involved in neuronal calcium signalling and visinin, a neuronal calcium sensor protein (NCS) (4). *M. truncatula* has been selected for the study of these interactions by some researchers due to its small, diploid genome, short life cycle and ease of transformation, which make it an ideal genetic tool to dissect the symbiotic processes (5). Interactions with rhizobia and mycorrhizal fungi share a common signalling pathway in the initial stages of symbiosis, which involves calcium spiking signals and CCaMK as a core component (1). The work undertaken in this thesis aims to understand the links between calcium spiking and CCaMK through a detailed biochemical understanding of calcium ion-binding to CCaMK both directly to its visinin-like domain, and via the calcium relay calmodulin (CaM). The aim of these studies is to understand how CCaMK is able to decode calcium spiking signals, and how it is able to differentiate between specific calcium signals

generated in response to either rhizobia or mycorrhizal fungi to lead to specific processes required for symbiosis.

1.1 CALCIUM SIGNALLING

Calcium ions (Ca^{2+}) are important second messengers in eukaryotic cells and are known to play a role in a vast array of cellular activities. In animals, calcium signals are well documented in the control of many processes such as fertilisation, secretory functions, neural signalling and memory (6). In plants, calcium is known to be an important signalling factor in response to certain stresses and signals, including stomal closing under cold conditions (7) and nodule formation (8).

1.1.1 *Calcium transport and storage*

As calcium ions are such a potent signalling molecule, tight regulation of their cytoplasmic concentration is essential for cell viability. This is achieved through a complex array of calcium stores, pumps and channels, which all work to ensure that calcium concentrations only rise in a controlled manner and only when the correct stimulus is present.

Calcium is highly abundant outside of the cell membrane as well as within certain sub-cellular compartments. These stores include the mitochondrion, golgi and endoplasmic reticulum (ER). Additionally, calcium is stored in plants in vacuoles and in the chloroplast. To allow calcium to enter the cytoplasm from these stores, it must pass through specialised channels, which are often triggered by a specific signalling molecule. In animal cells, examples include inositol-1,4,5-triphosphate (InsP_3) and ryanodine (RYR) receptors in the ER, which are activated by InsP_3 and RYR, respectively. On the plasma membrane *N*-methyl-D-aspartate (NMDA) receptors, activated by NMDA, also allow calcium entry when their respective ligands bind. Additionally, various voltage-gated channels, and calcium-dependent calcium channels have been characterised. Calcium-dependent calcium channels are known to amplify signals by activating additional channels when the calcium concentration reaches a threshold. This facilitates the rapid elevation of calcium commonly observed in calcium signalling (9-10).

In plants, calcium channels have been less well characterised. Plants do not contain InsP_3 receptor channels. Channels identified in plants include several voltage gated channels and slowly activating vacuolar (SV) channels (11). Calcium channels formed by glutamate receptor-like genes are found in pollen tubes and are regulated by pistil D-Serine (12). An SV channel, TPC1 in *Arabidopsis*, has been shown to be regulated by calcium through EF-hand motifs and displays calcium-dependant calcium release allowing it to be regulated by the calcium signal itself (13).

Once calcium has activated its targets, it is important that it is removed from the cytoplasm and returned to basal concentrations rapidly so that undesirable responses are avoided. The removal of calcium is facilitated by calcium pumps, which utilise energy from a proton gradient ($\text{H}^+/\text{Ca}^{2+}$ antiporters) or ATP (calcium ATPases). These pumps act to pump calcium out of the cell as well as to reload calcium stores in preparation for the next calcium signal (14).

The final stage is to reload the calcium stores by transporting calcium from outside of the cell into the depleted sub-cellular compartments. In animal cells this occurs through the production of a complex at the cell surface membrane induced by a drop in calcium ion-concentrations within the ER. This event involves various channels and accessory proteins that bridge the gap between the ER and the outside of the cell followed by calcium diffusion (15).

1.1.2 *Control of calcium signalling*

Calcium signalling is under extensive control that ensures that the signal itself occurs at the right place and time, and that the appropriate receptors are available to interpret it. This is achieved through the localisation in space and temporal control of both calcium ions and the calcium sensors. The description in this section is based upon characterisation of calcium signalling in animal cells. However, the same principles are likely to apply in plants.

Calcium flux will only occur when particular upstream events take place that lead to the activation of the calcium channels and subsequent release of calcium from stores. One of the best examples of this is the intracellular signalling molecule InsP_3 which is produced in response to a vast number of stimuli and activates the InsP_3 receptor calcium channels. When bound, InsP_3 activates the channel allowing calcium to flow down the concentration gradient leading to an increase in the cytoplasmic calcium concentration (16). As well as the timing of calcium flux, its duration and amplitude is also tightly regulated. This is governed by the length of time the calcium channels are active, the delay between calcium ion-concentration increase and the activation of calcium pumps, and the rate at which calcium ions diffuse through the cell (17). Combined, these effects lead to the precise shaping of a calcium spike, and the frequency at which they occur.

Calcium signals are strictly localised within the cell in regions, which can be as small as tens of nanometres across (18). This is achieved through a complex interplay between localised channels, calcium buffers and calcium removal systems. Calcium channels of specific types cluster for signalling so that the release event is confined to the target area (18-19). The degree to which this clustering takes place can have an effect on the calcium signal. Tighter clustering will lead to faster release and a lower dependence on buffers to raise local calcium ion-concentrations (19). Calcium buffers act to allow the cell to resist small fluctuations in the calcium concentration and to control the rate of calcium diffusion (19-20). The cytoplasmic concentration of buffers ranges from 100 to 300 μM in animal cells, the majority of which are stationary and serve to limit the spread of calcium ions by diffusion. Examples of calcium buffers include calbindin 9Dk, calbindin D28K and parvalbumin, which are EF-hand containing proteins. In chromaffin cells (neuroendocrine cells located in the adrenal gland), 25% of the buffers are highly mobile and have a major effect on the rate of calcium ion diffusion by chaperoning calcium ions through the cell, which owing to the high concentrations of protein and stationary calcium buffers, is not an ideal environment for diffusion of free calcium ions (20-21).

The final element of signal localisation is the arrangement of calcium stores and the removal of calcium from the cytoplasm. One of the main organelles to perform this function is the mitochondrion, which has been shown to arrange specifically around areas where calcium is released. This arrangement forms a barrier often referred to as the “mitochondrial firewall” (14, 22). This barrier is highly effective at preventing the further diffusion of calcium due to the mechanism by which mitochondria sequester and release calcium ions. The mitochondrion itself is able to rapidly absorb high levels of free calcium but release it at a much slower rate, which is below the threshold of target activation, thus blocking the diffusion of a signal into other areas of the cytoplasm (14).

1.1.3 *Calcium signals and sensors*

The overall function of calcium signals is to activate downstream targets to bring about specific responses. With the temporal, spatial and amplitude control of calcium, the overall signal is often highly specific to a group of sensors along with their desired output. Calcium signals can occur in spiking regimes controlled by frequency (FM signalling) or amplitude (AM signalling), or as a single calcium flux (6, 23). The response of a protein (calcium sensor) to these signals is determined by its calcium binding properties, which are tuned in terms of calcium ion-binding affinity, association and dissociation rate constants. This means that a signal must be of the correct amplitude, duration and frequency to fully activate its target.

Calcium sensors act to detect calcium signals by binding free calcium and initiating specific responses. This group of proteins can be subdivided into two further groups, which are the calcium relays and calcium responders. Calcium relays, such as CaM or the NCS, have no enzymatic activity. Instead these proteins undergo a conformational change and bind to a range of targets regulating their activity (11, 24). The calcium responders are proteins that have their enzymatic activity directly regulated by calcium via an intrinsic calcium sensing domain. Calcium-dependant protein kinases (CDPKs) are an example, which detect calcium through a binding domain and undergo conformational changes to relieve autoinhibition (11, 25).

1.1.4 *The EF-hand*

Most calcium binding proteins bind calcium through a helix-loop-helix motif named the EF-hand. EF-hands are found in a vast array of the calcium binding proteins. This section is based upon an extensive review by Gifford *et al.* (26). The typical binding sequence is located in a loop between two helices of the EF-hand. This consists of 12 residues providing seven ligands in a pentagonal bipyramid conformation. The side chains of residues 1 (X), 3 (Y) and 5 (Z) provide ligands from their side chains. These are aspartate residues in 100, 76 and 52% of EF-hands, respectively. The next ligand in position 7 (-Y) is provided by a backbone carboxyl, this is a threonine in 23% of cases but this residue has much higher variability owing to the fact that its side chain is not involved in coordination of the calcium ion. Position 9 (-X) provides a ligand via a bound water molecule where shorter side chains, such as that from aspartate (32% of cases), are

found. Alternatively it may provide a direct ligand in cases where a longer side chain, for instance from a glutamate, is present. The final two ligands are provided by a bidentate side chain in position 12 (-Z), which is either glutamate at 92% frequency, or aspartate. Also worthy of note is the position 6 glycine residue, which is present in 96% of cases. This residue facilitates a 90° turn (ϕ = approximately 60°, ψ = approximately 20°). Due to the high torsional strain of this conformation, it is only possible with a glycine residue as the introduction of a side chain would cause it to be sterically unfavourable. The structure and amino acid sequences of the EF-hands are shown in Figure 1.1. The ability of calcium ions to be coordinated by seven ligands allows EF-hand containing proteins to be specifically activated by calcium ions. This is because magnesium ions can only form up-to six coordinate complexes. As the seven coordinate structure is required to induce conformational changes, magnesium ions have little, if any effect on the protein and therefore bind with much lower affinity.

EF-hands occur in pairs, which assists in the folding of their structure and allows for cooperativity in many cases. A hydrophobic core forms through bundling of the helices and a short antiparallel beta sheet forms between the loops (Figure 1.1C). This pairing of hands and the interactions between them also occurs in proteins that bind an odd number of calcium ions. In these cases, the paired inactive hand serves a structural role within the protein.

The affinity of an EF-hand is determined by many factors. One of the main ways in which this is modulated is through the residues chelating the calcium ion. The presence of a glutamate in position 9 is thought to give a higher affinity than those with an aspartate as this removes the need to chelate Ca^{2+} through a water molecule. The removal of a water from the coordination sphere increases solvent entropy thus increasing the free energy of the interaction. In position 12, glutamate also confers a higher affinity than aspartate as the smaller side chain requires a more tightly packed structure in order to achieve correct positioning. Additional to these direct effects, differences in the non-chelating residues both in and surrounding the loop can act to fine-tune the local dielectric constant, which is an important determinant of affinity. Another way in which the affinity is manipulated is through the binding of a target after the calcium induced conformational change. In CaM, the binding of calcium induces conformational changes that lead to the exposure of hydrophobic surfaces. This subsequently leads to CaM binding its target as it is unfavourable to expose hydrophobic surfaces to aqueous solvent. Target binding increases the affinity of CaM for calcium ions, has been shown to be significantly lower without an available CaM binding site (Discussed in section 1.4 “introduction to calmodulin”).

The structural changes generally occur through a closing of the EF-hand around the calcium ion. This causes the helices to exert a physical force on the remainder of the protein causing a change in its conformation. These alterations can be widespread, having an effect throughout the protein as is the case in CaM. However the extent and nature of a conformational change is usually very specific to the protein in which it occurs (26).

A

EF-loop position	1	2	3	4	5	6	7	8	9	10	11	12
coordinating ligand	X _{sc}		Y _{sc}		Z _{sc}		-Y _{bb}		-X _{sc*}			-Z _{sc2}
most common	Asp 100%	Lys 29%	Asp 76%	Gly 56%	Asp 52%	Gly 96%	Thr 23%	Ile 68%	Asp 32%	Phe 23%	Glu 29%	Glu 92%
also frequently observed		Ala Gln Thr Val Ile Ser Glu Arg	Asn	Lys Arg Asn	Ser Asn		Phe Lys Gln Tyr Glu Arg	Val Leu	Ser Thr Glu Asn Gly Gln	Tyr Ala Thr Leu Glu Lys	Asp Lys Ala Pro Asn	Asp

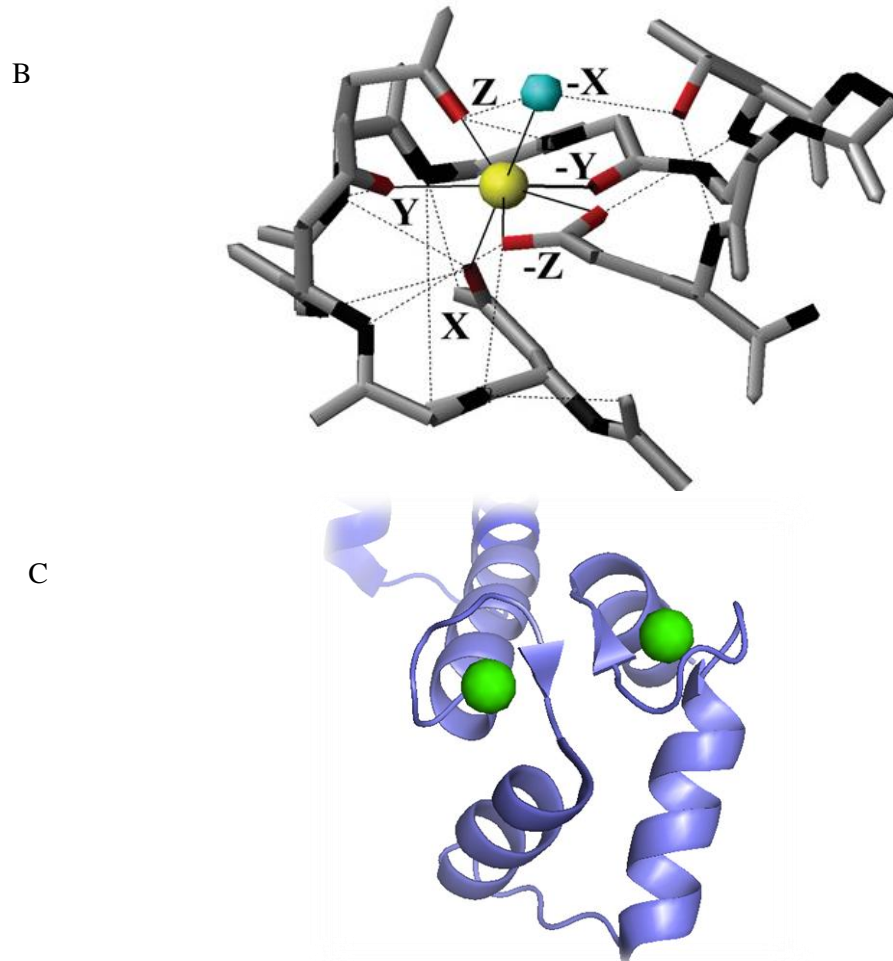


Figure. 1.1. Structure of EF-hand binding loops. A, list of amino acids commonly found in each position of the calcium ion-binding loop of EF- hands. B, the 12 residue binding sequence chelating a single calcium ion (yellow) from a crystal structure of *Paramecium tetraurelia* CaM. Oxygen atoms providing a ligand have been highlighted in red, NH backbone atoms in black and the bridging water molecule in blue. Hydrogen bonds are illustrated with broken lines, and interactions with the calcium ion are shown with solid lines. A and B were taken from a review by Gifford *et al. Biochem J* (2007) 405 p199-211 (26). C, EF-hand pair from the C-terminal lobe of potato CaM with calcium ions (green spheres) bound. This figure was produced from a crystal structure of PCM6 (27).

1.2 PLANT-MICROBE SYMBIOSIS

1.2.1 *An introduction to nodulation*

Nodulation is a process where plants form new organs, root nodules, within which the fixation of atmospheric nitrogen takes place. The root nodule is populated by rhizobial bacteria which have differentiated into bacteroides. The low oxygen environment created within nodules is required by rhizobial nitrogenase enzymes to fix nitrogen. This is combined with nutrient exchange between the two symbionts to allow the production of ammonia, which is assimilated by the plant. This process is restricted in nature to the legume family of plants, and one closely related non-legume *Parasponia* (28). It is also known that the symbiotic pairing between plants and rhizobia is species specific. For instance, *M. truncatula* forms specific symbiosis with *Sinorhizobium meliloti*. This form of symbiosis is thought to have evolved around 60 million years ago (1-2).

The observable stages of nodule formation have been well documented and were reviewed by Oldroyd in 2001 (2) and since updated with new discoveries and further characterisation of signalling, genes and pathways (See references below and within sections 1.2.3 “the common symbiosis pathway”, 1.2.4 “Nod-specific genes” and 1.3 “Calcium and calmodulin dependent protein kinase”) . The initiation of the process involves the release of flavonoids from the plant roots, which are detected by the free-living rhizobia in the soil. This leads to alterations within the bacterium, which includes the release of Nod factors. Nod factors are perceived by the plant at nanomolar concentrations and initiate morphological and genetic alterations within the root of the plant. These Nod factors have been chemically identified as chitin-based molecules consisting of four glucosamine residues modified with an N-acyl group at the non-reducing end. These molecules are also acetylated and an O-sulphate group is located on the reducing end. These modifications differ between the rhizobia that produce them and are thought to confer the specificity between symbionts (2). The structure of Nod factor produced by *S. meliloti* is shown in Figure 1.2 C.

Initially, rhizobia attach to growing root hair cells. Simultaneous perception of Nod factor leads to root hair curling, which eventually envelops the bacteria within an infection pocket where they divide. Dividing bacteria descend through the root hair cell in a specialised membrane-isolated channel called the infection thread, which descends into the root cortex. Here, bacteria are released from the infection threads into membrane bound compartments within dividing cortical cells, termed the nodule primordium, where they eventually differentiate into larger cells called bacteroids and become specialised in nitrogen fixation. This leads to the formation of pink nodules on the plant root (2) (Figure 1.2 A). The processes involved in infection via root hairs will be the focus of the Nod signalling pathway described below.

A second method by which bacteria can invade is via direct entry to the cortex through cracks in the epidermis formed between cells at lateral root bases, which also requires Nod factor. This form of symbiosis is thought to be more common in the semi aquatic legumes such as *Sesbania*, which can switch its infection mode from root hair to crack entry when its roots are submerged (2, 29-30).

It has been observed that artificial Nod factors applied in the absence of rhizobia are capable of initiating many of the signalling processes. Artificial Nod factors have been instrumental to the understanding of Nod signalling (2). Model legumes such *M. truncatula*, *lotus japonicas*, and lily have been used to study this process.

1.2.2 *An introduction to Mycorrhization*

The symbiotic interaction with arbuscular mycorrhizal (AM) fungi is more widespread than nodulation and occurs in most land plants. This process is thought to have evolved around 450 million years ago facilitating plant colonisation of the land. Genes required for symbiosis are well conserved with key signalling components, including CCaMK, being found in mosses and liverworts (31). It is worth noting that mycorrhization does not occur in *Arabidopsis*, as a result rice has been adopted as a model non-legume to study mycorrhization. This symbiosis is essential for efficient uptake of nutrients by plants from the soil, particularly of phosphate and nitrate (1-2).

AM fungi respond to plant strigolactone signals with hyphal morphological changes and excrete Myc factors, which are perceived by the plant to allow the symbiotic interactions to begin. These Myc factors have been shown to have a similar structure to Nod factors. They are also chitin-based molecules of four glucosamine residues, N-acylated at the non reducing end. It has been shown that sulphated and non-sulphated Myc factors are produced and a mixture of these is most effective in the initiation of symbiotic responses from the plant (32). The structure of sulphated Myc factor is shown in Figure 1.2 D.

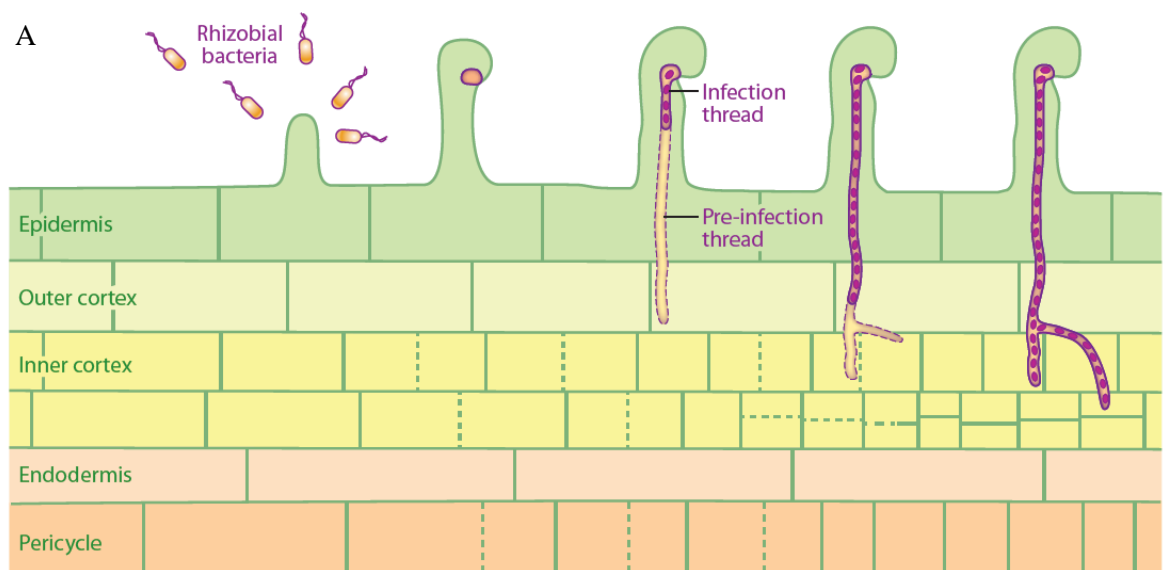
AM fungi contact the root and form appressorium. Growth from these proceeds into root cortex via the pre penetration apparatus, which channels the fungus through epidermal cells. In the cortex, they form highly branched structures in membrane bound pockets within cortical cells called arbuscules, where nutrient exchange takes place (2, 33) (Figure 1.2 B).

1.2.3 *The common symbiosis pathway*

Study of the initial responses to Nod factor has identified a set of genes required for signalling that are required for interaction with rhizobia. It has also been found that several of these genes are required for the interaction with AM fungi. Collating the data shows that the Nod or Myc factors are perceived by specific cell surface receptors and then the two pathways converge on DMI (does not make infection threads) genes and calcium spiking within the nucleus before the pathways split into shared, mycorrhization or nodulation specific responses, shown in Figure 1.3 (1, 34-35). The calcium spiking observed for cells stimulated with AM fungi or Nod factor appears to be different raising the issue of a calcium signal decoder in this system (Figure 1.4). The Initial stages of signalling were reviewed by Oldroyd *et al.* in 2005 (1) and have been significantly updated since

by new research. An overview of the core signalling pathway is shown in Figure 1.3. It is also known that once a root hair cell is initiated in the Myc or Nod process, it cannot be diverted. This is evident from the fact that a cell previously treated with Nod factor cannot begin calcium spiking in response to AM fungi (36). Additionally, signalling is known to occur independently in root hair cells, which do not synchronise calcium spiking when multiple cells are simultaneously treated with Nod factor (8, 37).

The receptors of NOD and Myc factors are receptor-like kinases, which contain LysM domains in the extracellular region. LysM domains are commonly used for the binding of saccharides. These receptors are likely to be formed by heterodimers of two receptor proteins. Mutants of either of the Nod receptors NFP and LYK3 are incapable of all Nod factor responses (38). Recently it has been suggested that the receptor NFP may be shared between the two pathways (32).



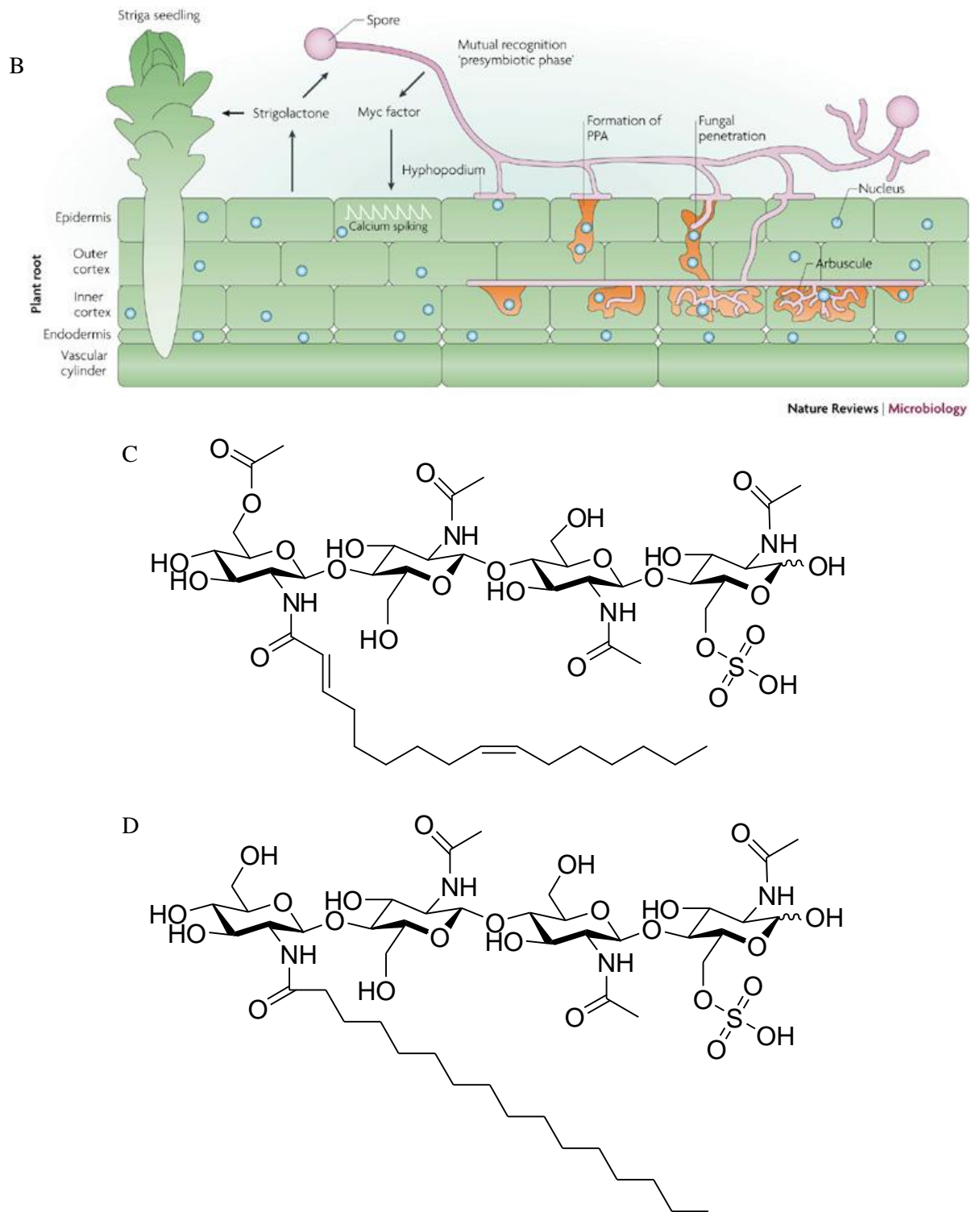


Figure. 1.2. Symbiote entry and the structures of Nod and Myc factors. A, Overview of bacterial entry into cells. Free-living rhizobia release Nod factor and attach to growing root hairs. Root hair curling envelops the bacterium in an infection pocket, and infection threads (preceded by a pre-infection thread) channel the bacteria to the cortex where nodule formation takes place. Figure taken from Oldroyd *et al. Annual reviews Genetics* (2011) 45 with permission of authors (39). B, Overview of AM fungal entry into the root cortex. Strigolactone is released from the plant

and perceived by AM fungal spores. Spores form hyphae and release Myc factor inducing the Sym pathway in the plant. The fungus contacts the plant and forms Hyphopodium (specialised appressorium) and then growth descends into the cortex via pre penetration apparatus (PPA), where arbuscules form. Figure taken from publication by Parniskie, *Nature reviews Microbiology* (2008) 6 p763-775 (33) with permission of publisher. C, Nod factor from *S. meliloti*. (redrawn from review by Oldroyd 2001 (2)) D, Sulphated Myc factor produced by *G. intraradices* redrawn from Maillet *et al.* 2011 (32). Both molecules share a chitin oligosaccharide backbone modified by N-acylation and O-sulphation. The primary differences between these examples are the double bonds in the N-acyl group, which are absent in the sulphated Myc factor, and the additional acetylation of the Nod factor. *G. intraradices* secretes a second major Myc factor lacking the sulphate at the reducing end and with an 18:1 Δ 9Z alkyl chain (not shown) (32).

DMI1 (alternative names Castor and Pollux) is a putative cation channel with plastid localisation and DMI2 (alternative name SymRK) is a receptor-like kinase (1). Mutants in these genes are blocked for both nodulation and mycorrhization (3, 40-41). It has also been observed that mutants in these two genes are blocked for calcium spiking (37) and the expression of nodulation marker genes ENOD11, ENOD40 and RIP1 in response to Nod factor (3, 40). These mutants are also blocked for calcium spiking in response to AM fungi. DMI1 and DMI2 Mutants allow the formation of appressorium on root surface but the fungus cannot penetrate the root (36). Additionally, these mutants are blocked for root hair branching in response to Nod factors (3). Root hair branching has also shown as a response to Myc factor stimulation. However, the effect of DMI1 and 2 mutation on Myc factor induced root hair branching is not currently known (32).

DMI3 is a calcium and calmodulin dependent protein kinase (CCaMK). Like DMI1 and 2, mutants in this protein are unable to form symbioses with AM fungi or rhizobia, or express nodulation marker genes (3, 40). CCaMK is also required for mycorrhizal symbiosis in rice (42). However, unlike DMI1 and 2 mutants, DMI3 mutant cells are not impaired for calcium spiking. This suggests that CCaMK lies downstream of calcium spiking. Additionally the ability of this gene to be regulated by both calcium ions and CaM, as discussed in Section 1.3 “calcium and calmodulin dependent protein kinase”, makes it an ideal candidate for the decoder of calcium signals. Knockdowns of CCaMK by RNAi produced far fewer nodules than wild-type plants. These nodules also took longer to develop and showed reduced nitrogen fixation activity. In addition many nodules were white or mosaic showing that they were either free of bacteria or the bacteria had not distributed correctly. This showed that CCaMK is essential for rhizobial dissemination in the nodule and nodule development (43). It should be noted that the RNAi experiments did not completely block CCaMK expression, which may be why a different phenotype was seen to the CCaMK mutant. Another interesting phenotype of CCaMK mutants in an increased sensitivity to Nod factor with regard to the initiation of calcium spiking suggesting

that CCaMK, or components downstream of CCaMK, may be involved in a negative feedback mechanism (44).

Downstream of CCaMK, interacting protein of DMI3 (IPD3) also named Cyclops, has been identified as a phosphorylation target of CCaMK and is required for both nodulation and mycorrhization (41). Cyclops is discussed in detail in Section 1.3 “calcium/calmodulin dependent kinase”. Finally, the GRAS family transcription factor nodulation signalling pathway 2 (NSP2) has been placed in the common symbiosis pathway after initially being identified as a Nod specific component. This protein is localised to the nucleus and acts downstream of CCaMK (45). Mutants of NSP2 cannot form infection threads or root nodules and show no ENOD11 expression. These mutants are also blocked for cortical cell division in response to nod factor. These genes do display rhizobium induced peroxidase (RIP1, used as a marker gene for nodulation) (46) expression, although much later than wild-type. Root hair deformation and growth is also reduced in response to Nod factor in these mutants (47). It is not yet known whether NSP2 is a target for CCaMK phosphorylation.

It is likely that components of the common symbiosis pathway remain undetected. For instance the second messengers responsible for the triggering of calcium spiking are not known, nor are the proteins responsible for their generation and perception. However, the discovery that n-butanol inhibits calcium spiking in *Sesbania* suggests that phospholipase-D may be involved in spiking because it specifically inhibits this enzyme. The calcium channels and pumps, which will generate the calcium spiking signal itself, are also not known at this time. However likely candidate channels have been identified recently in the Oldroyd group (unpublished data). Other genes have also been identified that are required for the generation of calcium spiking and nodulation in response to Nod factor. These include nuclear pore proteins such as Nup133 (48) NENA and Nup85 (49). However the role of the nuclear pore is yet to be identified in this system. Another gene common to both symbioses, vapyrin is thought to be required for vesicle transport. Restructuring of membrane is known to be required for the formation of infection threads to allow rhizobial entry, and to allow AM fungal entry (50).

As the two pathways share so many components, which are highly conserved between legumes and non-legumes, it is thought that the Nod pathway evolved from the more ancient AM symbiosis (2).

1.2.4 *Nod-specific Genes*

Two receptor genes are required for Nod factor perception, these are named NFR1 and NFR5 in lotus (LYK3 and NFP in *M. truncatula*, respectively). It is proposed that these two proteins form a complex to specifically bind Nod factor and activate downstream responses (38). Cip73 has been identified as a specific gene for nodulation and a substrate for CCaMK and is thought to be involved in nodule organogenesis (51).

NSP1 appears to be a transcription factor specific to nodulation as NSP1 mutants are unaffected in their response to Myc factor (32). Mutants in this protein show reduced RIP1 and ENOD11 expression (40).

Downstream of the Nod factor pathway, many genes are expressed, some of which have been identified. These include the Early nodulins (ENODs) ENOD11, 12, 40 and RIP1, which are expressed within a few hours. ENOD12 and RIP1 are expressed in the epidermis whereas ENOD40 is expressed in the cortex (see review by Oldroyd, 2001) (52). It should be noted that ENOD11 was found to be induced by purified Myc factors suggesting that this gene may actually be shared between the two pathways (32). Another downstream gene, NIN, is required for nodule organogenesis demonstrating a promoting role in this process. NIN also appears to be able to inhibit nodulation and has a role in restricting the number of nodules produced suggesting it has a dual role in regulating nodule formation (53). Many other genes have been noted as being upregulated by Nod factor. These include defence and stress response genes within one hour of infection with rhizobia. This may suggest that the rhizobia are initially seen as a threat before being allowed into the plant root. In addition a Ca²⁺ ATPase is upregulated within one hour of inoculation, which may be important in calcium spiking. Cytoskeletal genes are expressed within 6-24 h and cell proliferation genes within 24-72 h (54). Other genes of note that are upregulated are six nodule-specific CaM like proteins (55), which may have an impact on calcium decoding. It should be noted that it is not known how many of these genes are specific to rhizobial infection.

Also downstream of the Nod signalling pathway, cytokinins have been determined to be instrumental in the infection process by stimulating cortical cell division and nodule organogenesis. Other genes such as LIN, thought to be associated with protein turnover are also known to be associated with cortical cell division (56).

It has been reported that Rhizobia produce succinoglycans as well as Nod factors. Rhizobia lacking the genes to produce these compounds are recognised as threats by the plant leading to the expression of defence genes and thus these bacteria fail to produce root nodules. The mechanism by which this occurs is not understood (57). However this does raise the possibility of parallel pathways alongside Nod factor perception.

Other common signalling molecules can impact on nodulation and appear to be involved in the regulation of this process. Ethylene is known to inhibit nodulation at high concentrations, and can reduce the calcium spiking frequency at low concentrations (30, 52), as can jasmonic acid (30). It is thought that these hormones control the rhizobial entry method in hydroponic roots in *Sesbania* (30).

1.2.5 *Myc-specific genes*

The Myc receptor is likely to be formed by a pair of receptors, as is the case for Nod factor. NFP has been proposed as a shared component. However the remainder of the Myc factor receptor complex is currently unknown.

Genes specific to Myc factor signalling are less well characterised than those for Nod factor. However many Myc specific genes are now being identified. The Myc specific transcription factor RAM1 has been identified as being required for calcium spiking in response to purified Myc factors and may be the mycorrhization equivalent of NSP1 (Oldroyd, unpublished).

Few genes, which are expressed as a result of the Myc pathway, have been identified. One example is a pair of two blue copper proteins. However the exact functions of these genes are currently unknown (58).

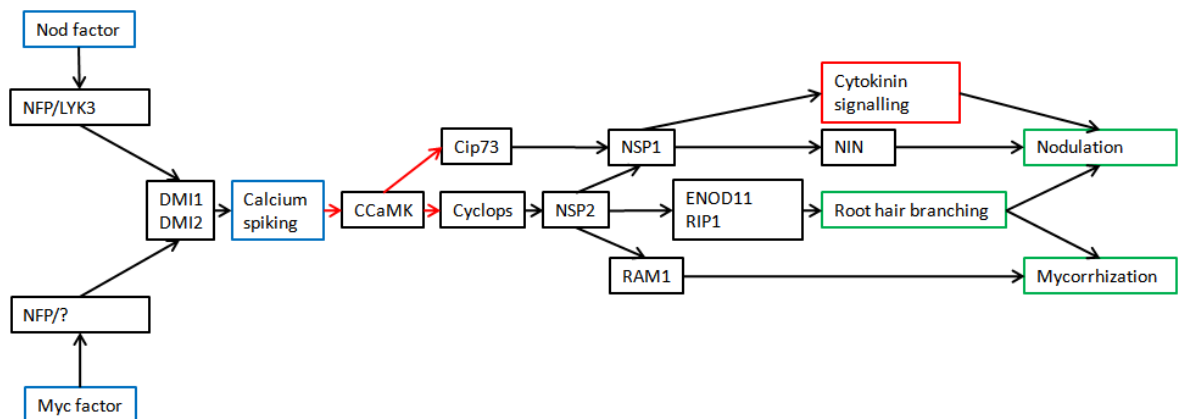


Figure 1.3. Overview of the Nod and Myc factor signalling pathways. Proteins are highlighted in black, Blue highlights denote specific signalling molecules and red highlighting denotes a process, which does not have its components shown. Green highlighting denotes observed physiological changes. Red arrows show direct links between components whereas black arrows show unknown links between components.

1.2.6 Calcium spiking

The possibility of parallel pathways to confer specificity to Nod and Myc factors has not been ruled out. The main arguments to support this hypothesis are the fact that root hair deformation occurs in response to rhizobia without the need for calcium spiking. Also, calcium flux in the root hair tip appears to relate to another set of responses (discussed below) (2, 8, 59). Additionally the ability of non-legume CCaMKs to complement legume CCaMK mutants for nodulation (for instance rice CCaMK can complement lotus) (35) suggests that CCaMK is not a key specificity component because a non-legume CCaMK would have had no evolutionary pressure to be able to induce nodulation. However, the theory that Nod signalling evolved to take advantage of the ancient Myc signalling pathway (2) does not rule out the possibility that modification of CCaMK was not a requirement in Nod signalling evolution.

Despite these caveats, the characteristics of the common symbiosis pathway make the decoding of calcium spiking by CCaMK an attractive hypothesis. After all, CaMKII and CaM have been shown to effectively decode calcium spiking in animals as discussed in Section 1.5 “calmodulin dependent protein kinase II”.

Calcium spiking in response to Nod factor is well characterised. One to three minutes after the application of high concentrations (<10 nM) purified Nod factor, an initial influx of calcium ions is seen in the cytoplasm at the root hair tip, which is required for bacterial infection (Moriere *et al.* unpublished). This does not occur with low concentrations of Nod factor (~1 nM) (2, 8, 59). Then, 3.5-12 minutes after nod factor application, regular calcium oscillations begin in the nucleus, originating from the nuclear periphery (8, 37). These spikes are asymmetrical (8, 35) with 16% of the spike duration in the increasing calcium ion-concentration phase, and 61% of the duration in the decreasing concentration phase. The remainder of the spike period is at basal calcium ion-concentration (30). The spikes occur at an interval of 90 s in *M. truncatula* (30, 36) and the free calcium ion-concentration has been measured at a range of 5 – 800 nM in *Medicago sativa* (8) and is likely to be the same in *M. truncatula* in which the calcium ion-concentration peaks between 443 and 669 nM above baseline during spiking (36). Mathematical analysis of the Nod factor induced calcium spikes shows that the periodicity arises from a chaotic system. This means that there is a deterministic process governing the generation of spikes, which can be predicted if the properties of the calcium pumps and channels are known. However, the system is highly sensitive to perturbation by noise meaning the spike intervals can vary slightly in a manner that is difficult to predict over long time periods (36). Currently the components required to generate the calcium spiking are unknown and require identification and characterisation to understand in detail how the calcium spiking pattern is generated. A typical calcium spiking trace in response to Nod factor is shown in Figure 1.4 A.

In *Sesbania*, nuclear calcium spiking is also observed at lateral root bases in response to Nod factor. These spikes have a shorter period than *M. truncatula* root hair spikes at 55.5 s and a more symmetrical profile of 39% increasing concentration, 61% decreasing. CCaMK is also required for nodule development by crack invasion demonstrating that calcium signalling and decoding is important in nodule formation by both invasion strategies (30).

Nuclear calcium spiking has also been recorded in response to AM fungi. These spikes appear to me more irregular than Nod factor induced spikes with an average interval of around 30 s. However, unlike Nod spikes, there is a high level of variation on the spike interval. Nevertheless this spiking pattern appears to be chaotic rather than random meaning that a specific set of processes govern its generation (36). It should be noted that the measurement of spiking in response to AM fungi is severely limited. Initiating calcium spiking with fungi removes the ability to exert fine temporal control over its initiation. This means that only a segment of the calcium spiking is being measured. This means that it cannot be determined whether the beginning of spiking is being observed, or the end of spiking where the characteristics have been observed to break down (Oldroyd group, personal communication). Recent experiments with purified Myc factors have shown the generation of calcium spiking with a much more regular interval. These spikes are much more similar to Nod factor spiking than those generated with AM fungi (Oldroyd

and Morris, Unpublished). Future characterisation of this spiking pattern will elucidate the differences between them, which in turn will be compiled with our understanding of CCaMK to test the hypothesis that calcium spiking is being decoded to give the specific outputs for nodulation or mycorrhization. A typical calcium spiking trace in response to AM Fungi is shown in Figure 1.4 B.

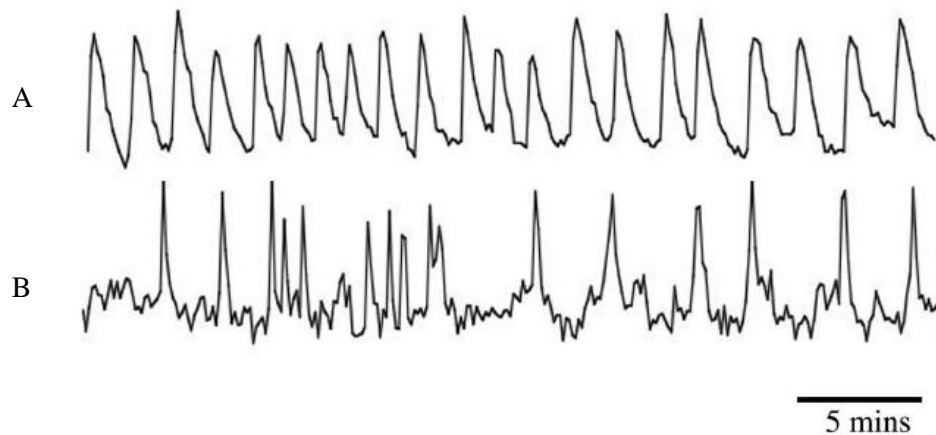


Figure. 1.4. Nuclear calcium spiking measured in *M. truncatula* root hair cells. A, Root hair nuclear calcium spiking trace in response to purified Nod factor. B, calcium spiking in response to AM fungi. Figure has been adapted from Kosuta *et al. PNAS* (2008) 105 p9823-9828 with permission of authors (36).

1.3 CALCIUM AND CALMODULIN DEPENDENT PROTEIN KINASE

1.3.1 Organisation of CCaMK

Chimeric calcium and calmodulin dependent protein kinase (CCaMK) of *M. truncatula* (gene name DMI3) is a 58.6 kDa protein consisting of 523 amino acid residues (4). The protein is arranged into three domains, a serine/threonine kinase domain, an autoinhibitory domain overlapping with a CaM binding domain and a visinin-like calcium ion-binding domain, containing 3 EF-hands as shown in Figure 1.5 (4, 60). The presence of a CaM binding domain and an intrinsic calcium sensing domain allow for dual regulation by calcium ions. This dual regulation is unique among the calcium regulated kinases characterised to date, which are either directly regulated by calcium, or by the calcium relay CaM. (60-61).

It has been revealed that CCaMK has similarity to 2 proteins, which are well characterised in animal systems. The kinase domain including the autoinhibitory region, residues 1-338, shows similarity with animal CaMKII and has been found to contain motifs typical of kinases. The CaM binding site shows especially high identity at 79% identity with mammalian CaMKII and 43 and 50% with yeast and *Aspergillus* CaMKII, respectively. Additionally this region is predicted to form an amphipathic alpha helix, which is typical for CaM binding (60-61). Although the level of similarity is insufficient for complete and detailed homology modelling, there is enough identity to

indicate that the fold is similar and to produce basic threaded models. This similarity allows many predictions to be made regarding the structure and mechanism of the kinase domain by comparison with CaMKII, which will be discussed below.

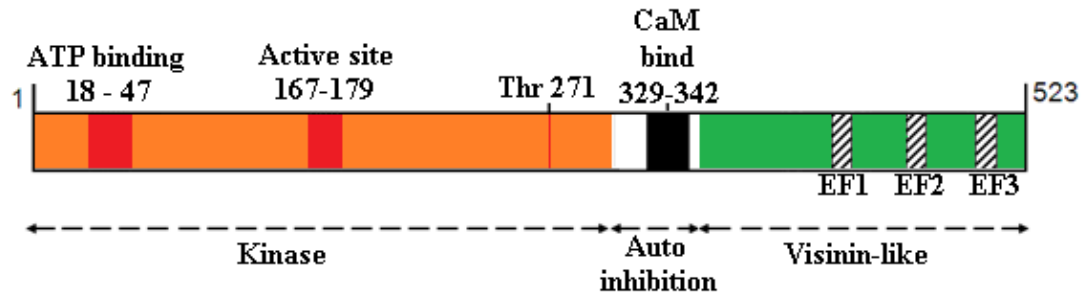


Figure. 1.5. Outline of the features of *M. truncatula* CCaMK. The core serine/threonine kinase domain is shaded orange with important structural elements labelled and shaded red. The autoinhibitory domain has no shading and the CaM binding site in black. The visinin-like domain is shaded in green with EF-hands shaded with diagonal lines. Labels show *M. truncatula* CCaMK residue numbers for the features, which have been identified in CCaMKs of *M. truncatula*, *Lotus* and lily.

The visinin-like domain does not display any homology to the C-terminus of CaMKII. This region of the protein (350-523) displays 32-35% identity with the animal visinin-like proteins (4, 60), which belong to the neuronal calcium sensor (NCS) family. These percentages are also above the required threshold to presume a similar fold thus allowing the NCSs to act as a basis to formulate hypothesis on the nature of CCaMK calcium binding. These proteins typically contain two or three active EF-hands and perform a wide range of functions (62). These proteins will be discussed in greater detail in section 1.6 “neuronal calcium sensors”. Based upon this evidence it is thought that CCaMKs originate from a 2 gene fusion of sequences that were functionally different and from diverse origins (63).

A third family of proteins to which CCaMK is similar is the calcium dependent protein kinases (CDPKs). These proteins contain a kinase domain, an autoinhibitory domain and a C-terminal EF-hand containing calcium ion-binding domain. This domain is more similar to CaM than is the visinin-like domain of CCaMK (4), furthermore these proteins do not appear to bind CaM. Instead they alleviate autoinhibition through an internal mechanism involving modification of the interactions between the calcium-binding and autoinhibitory domains. CDPKs have been reviewed by Harmon *et al.* in 2000 (25). CCaMK on the other hand requires CaM in order to phosphorylate its targets (51, 61, 64-66) (discussed below) and therefore functions by a different mechanism to the CDPKs.

In *Arabidopsis*, which has no CCaMK homologue, the novel protein *Arabidopsis thaliana* calcium/calmodulin-dependant protein-Kinase (AtCK) has been identified. AtCK is similar to

CCaMK in that it has a CaM binding sequence and a domain resembling a visinin-like domain however, the ability to bind calcium has been lost through degeneration of its EF-hands. This protein retains regulation by CaM through a CaM binding site in the autoinhibitory domain. This indicates that AtCK is regulated in a similar fashion to CCaMKs but has different functions *in vivo* (67).

1.3.2 CCaMKs in plants

CCaMKs are widespread throughout the plant kingdom and isoforms have been identified in legumes and non-legumes. These proteins are also unique to plants and have not been identified in any other groups of organisms. Most of the current experiments into CCaMK are conducted using isoforms from *M. Truncatula*, *Lilium longiflorum* (trumpet lily) and *Nicotiana tabacum* (tobacco). CCaMKs have also been identified in pea (gene name Sym9), rice, apple and moss to name but a few. CCaMKs are relatively well conserved, as DMI3 shares 69-91% identity with these examples (4, 42, 63, 68) indicating that the three-dimensional structure and biophysical characteristics are probably highly similar.

Interestingly, tobacco contains two isoforms of CCaMK suggesting that a duplication event has occurred during its evolution. These CCaMKs are both 517 amino acids in length and have diverged by 15 amino acid substitutions, one of the most notable being a serine to alanine substitution in the CaM-binding domain (69).

1.3.3 Function of CCaMK

It is clear that CCaMK plays a pivotal role in the establishment of rhizobial and mycorrhizal symbioses. To date, it remains unclear how CCaMK is able to differentiate between the Nod and Myc factor induced calcium spiking signals. CCaMK is predominantly expressed in roots and nodules and expression is low or undetectable in all other tissues except in anthers. However, no mutant CCaMK phenotypes have been identified in anther development despite upregulation of CCaMK during early stages of this process (31, 42-43, 63-64). CCaMK has been shown to localise to the nucleus (43, 45), where calcium spiking is observed in response to Nod and Myc factors (8).

Through genetic and molecular techniques potential targets of CCaMK have been identified. Histone H3A has been reported as a good target *in vitro* (61). However the biological relevance of this observation is not clear. CCaMK is also reported to phosphorylate the synthetic GS peptide and syntide-2, which were commonly used as artificial substrates for characterisation of protein kinase activity (61, 65). In anthers, a homologue of elongation factor 1 α (EF1 α) has been identified as a target of CCaMK. Once activated, EF1 α has many functions such as regulation of the cytoskeleton through binding to actin and microtubules. CCaMK has been shown to interact with the C-terminus of EF1 α and phosphorylate it at Thr257 (31). To date it has not been shown that EF1 α is involved in the NOD signalling pathway.

Recently a novel protein, Interacting Protein of DMI3 (IPD3, also known as Cyclops) has been shown to associate with CCaMK. IPD3 is a 58 kDa protein and is predicted to have a mostly alpha

helical structure. Database searches reveal that no similar proteins have been characterised to date. Additionally to this it has been shown to be strongly co-expressed in roots and nodules with CCaMK and co-localise to the nucleus. It has been shown that these two proteins interact *in vitro* (66, 70). Additional analysis of the interactions between CCaMK and IPD3 revealed that the interaction is specific to the kinase domain of CCaMK. Moreover the kinase activity is required for infection as mutants of CCaMK which have ATP binding or kinase activity disabled did not interact in a yeast two hybrid screen. The same experiments showed that the interaction with IPD3 is between residues 81-366. This means that a predicted coiled-coil in the first 67 amino acids is not required for the interaction. Residues 81-366 have been shown to be necessary for dimerisation of IPD3, which may play a role in complex formation *in vivo* (66). CCaMK phosphorylation assays have demonstrated that IPD3 is phosphorylated by CCaMK. This activity is dependent on both calcium and calmodulin (66). Two major sites have been identified on IPD3 and there are potentially many other phosphorylation sites on the protein. The main two are Ser50 and 154. Simultaneous mutation of these residues to aspartate to mimic the phosphorylated form was demonstrated to induce spontaneous nodulation. This shows that the phosphorylation of IPD3 by CCaMK is physiologically relevant (M. Parniske, oral presentation, plant calcium signalling conference, Sep 2010, Münster, Germany). IPD3 mutants have been shown to be impaired in both nodulation and mycorrhization. Loss of IPD3 leads to no infection threads forming upon inoculation with rhizobia (66), and an inability to form arbuscules when inoculated with AM fungi (41, 66). When this protein was mutated to prevent expression along with the expression of an autoactive CCaMK spontaneous nodules were able to form (66). Together these data suggest that Cyclops is important for the initial stages of infection, and has a role in nodule organogenesis. However, it is not the only downstream component of CCaMK able to induce nodule organogenesis.

A large-scale analysis of phosphorylated proteins in nodulation identified many proteins (3404 sites in all), and several potential consensus sequences. Of note was phosphorylation of IPD3 at Ser43 or 50 and Ser 155, which is consistent with *in vitro* phosphorylation of IPD3. Nup133 was also identified suggesting that CCaMK may regulate the nuclear pore by phosphorylation (71). It should be considered that it is not known whether identified proteins are CCaMK targets from this analysis but these results may lead to future identification and characterisation of targets for CCaMK.

Another substrate of CCaMK was identified by yeast two hybrid screening of *lotus* proteins using CCaMK as bait. This identified CIP73, a 73 kDa protein of 691 amino acids. This protein contains a Scythe_N ubiquitin like-domain at its N-terminus. The C-terminal region of the protein has no significant identity to characterised proteins. Like IPD3, CIP73 has been shown to express predominantly in roots and co-localise with CCaMK to the nucleus, where the two proteins interact. Additional analysis of the interaction revealed that CIP73 interacts with the kinase domain

of CCaMK and failed to interact with kinase dead mutants, or constructs containing the autoinhibitory domain (including the full length protein) in yeast two hybrid studies. However interaction with the full length protein was demonstrated in pull down assays and *in vivo*. Residues 80-160 of CCaMK were found to be sufficient for interaction. Analysis of CIP73 constructs found that its C-terminal residues (413-691) are required for the interaction with CCaMK and therefore the C-terminus of CIP73 has been termed the CCaMK interacting domain. It was also determined that Cip73 can form homodimers in these studies. Phosphorylation assays revealed that the N-terminal region of CIP73 is phosphorylated by CCaMK in a calcium and CaM dependent manner; however the specific site of phosphorylation has not been identified. The consequences of phosphorylation are also yet to be identified. This protein is known to be required for nodulation as RNAi plants of CIP73 show a phenotype where infection threads fail to reach the cortex indicating a role for CIP73 in nodule organogenesis. Interestingly knockdown of CIP73 had no effect on mychroization indicating that this protein is specific to the nodulation pathway. A role for this protein has been proposed in protein folding and degradation, due to the ubiquitin-like domain and evidence for an interaction with HSP70-interacting protein. This suggests that protein turnover during nodule formation may be indirectly controlled by CCaMK. However further work is required to confirm this hypothesis. Two isoforms of CIP73 have been identified in *M. truncatula* and rice (51).

1.3.4 Proposed mechanism of CCaMK activation

From previous works described in several publications on CCaMK, a basic scheme for activation can be presented. Briefly, calcium ions bind to the three EF-hands of the CCaMK visinin-like domain inducing autophosphorylation. The autophosphorylated CCaMK is enhanced for CaM binding. Finally, the binding of CaM relieves autoinhibition allowing targets to become phosphorylated. This scheme is summarised in Figure 1.6 and current knowledge of each stage of the processes described in detail below.

The first step of CCaMK activation is the binding of calcium to the visinin-like domain, which induces a conformational change leading to autophosphorylation of the kinase domain at Thr271 in mtCCaMK (267 in lily CCaMK) (61, 72-73). The calcium ion-binding to the visinin-like domain has been indicated by mobility shift on an SDS gel when CCaMK is mixed with a calcium solution (61). It should be noted that this shift may be due to charge, conformational changes or both. The K_D for calcium-ions has been predicted to be in the nM range by analogy to other neuronal calcium sensor proteins (72).

The autophosphorylation event induces further conformational changes that increase the affinity for CaM approximately 8-fold from 55.3 nM to 6.5 nM (72-73) and increases the phosphorylation of targets (61). However, the equivalent mutation *in vivo* in *M. truncatula* CCaMK leads to spontaneous nodulation suggesting a loss of negative regulation of CCaMK has occurred, questioning a key feature of this model (64, 74). Autophosphorylation may occur by an

interoligomeric mechanism rather than intraoligomer. This is supported by the observation that autophosphorylation rates increase as the lotus CCaMK concentration was increased (64). This may be explained by a threaded model produced by Sathyanarayanan *et al.* in which the autophosphorylated threonine residue was too far from the active site to be phosphorylated by its own kinase domain (73). However, kinetic data by Sathyanarayanan *et al.* on lily CCaMK (72) was misinterpreted as interoligomer due to a levelling of the autophosphorylation rate at high concentrations of CCaMK. Interoligomer data would be expected to show an exponential increase in the autophosphorylation rate as CCaMK concentrations rise (due to a second order kinetic process) meaning the curve shape observed by Sathyanarayanan *et al.* is incorrect for this interpretation. Unpublished work by A. Miyahara *et al.* in the Oldroyd group suggests that the autophosphorylation mechanism may be intraoligomer in *M. truncatula* CCaMK. The dependence of the rate of autophosphorylation on the CCaMK concentration was observed to be linear rather than exponential (suggesting a first order kinetic process). It should be noted that the oligomerisation state of CCaMK is not currently known. From this it is also clear that the mechanism of autophosphorylation requires further investigation.

Deletion of the visinin-like domain abolishes autophosphorylation showing that calcium ion-binding to CCaMK is absolutely required for this process. Interestingly deletion of the visinin-like domain of CCaMK did not alter the affinity for CaM, and synthetic peptides appear to have a similar CaM affinity suggesting that the CaM binding site itself is unaltered by calcium ion-binding to CCaMK (61, 72). Synthetic peptides containing the autophosphorylation site can also mimic the autophosphorylation dependent increase in CaM affinity (73). However, the EF-hands are required for maximal activity of CCaMK as constructs with all or part of the visinin-like domain deleted show reduced phosphorylation of target peptides in the presence of calcium ions and CaM (61, 75).

The CaM binding site has been experimentally determined to lie between residues 322 and 356 in lily CCaMK (61) (329-342 are the equivalent positions in *M. truncatula* CCaMK). Upon the binding of CaM, autoinhibition is relieved allowing the binding and subsequent phosphorylation of substrates, as indicated by a 20-25 fold increase in kinase activity over the autophosphorylated CCaMK (61). A mechanism is proposed whereby CaM binding removes the autoinhibitory domain from the active site and allows substrates to interact. This is by analogy to CaMKII, which operates by this mechanism as discussed in section 1.5 “calmodulin dependent protein kinase II”. Evidence to support this hypothesis has been collected through experiments where the autoinhibitory domain or the visinin-like and autoinhibitory domains of CCaMK are deleted. These constructs produce an autoactive kinase capable of phosphorylating targets independent of calcium ions and CaM. When expressed in the plant this autoactive kinase induces expression of the nodulation marker gene ENOD11 and spontaneous nodule formation in the absence of rhizobia. This indicates that phosphorylation of targets by CCaMK is required for nodule organogenesis (74). Additional evidence was collected in an experiment where a synthetic peptide of the autoinhibitory domain

was shown to act as a competitive inhibitor of the kinase-only construct of CCaMK. This peptide was shown to compete with substrate binding in a kinase domain only construct but did not affect ATP binding, which is also modulated by the relief of autoinhibition in CaMKII. It is suggested that the lack of a histidine in the CCaMK autoinhibitory domain, which interacts with the ATP binding site in CaMKII may provide an explanation for this (75). CaM has been shown to bind to CCaMK only in the presence of calcium ions (60-61) with K_D of 55 nM (61, 72), which is reduced to 6.5 nM upon autophosphorylation (72). The affinity of CaM for calcium ions has been estimated in the μ M range by analogy to other CaMs (72); however, the affinity for CaM is known to increase in the presence of target peptides (76) (Discussed in section 1.4 “introduction to calmodulin”). The affinity of calcium ions for CaM in the presence of CCaMK is currently not known.

Another intriguing consequence of CaM binding is the inhibition of further autophosphorylation meaning that calcium ion and CaM binding to CCaMK have opposing effects (61) and A. Miyahara *et al.* (unpublished). However it has been observed that this effect does not occur when HIIS and GS peptides are used as substrates (61). Additionally this mechanism was not observed in *zea mays* CCaMK (65). From these studies it is clear that the effect requires further investigation to determine the biological effect of this mechanism.

It has been shown that different CaM isoforms from tobacco had a different effect on tobacco CCaMK. PCM1 was found to be better at inhibiting autophosphorylation than PCM6 and to have a slightly lower IC_{50} (estimated at 400 nM for PCM1 and 200 nM for PCM6). These two CaM isoforms had no differential effects on lily CCaMK (IC_{50} at 400 nM) suggesting that selecting the correct CaM for study may be essential in the understanding of CCaMK (69).

The rates at which targets are phosphorylated have only been assessed qualitatively. It has been shown that HIIS phosphorylation goes to completion after approximately ten minutes (61) and Syntide-2 phosphorylation was complete after four minutes (65). It is clear that these activities are slower than autophosphorylation, which was complete after 1 minute (65) showing that autophosphorylation is going to be the preceding step. For future understanding and modelling of CCaMK activity *in vivo*, the exact rates of autophosphorylation and phosphorylation of biologically relevant targets must be measured.

The final stage CCaMK goes through is phosphorylation-dependent inactivation. This process results in the rapid formation of a sedimentable enzyme formed through self-association. Additionally this process was shown to be pH dependent with pH 6.5, 7.5 and 8.5 leading to 67%, 33% and 84% inactivation after 2 minutes in 200 μ M ATP respectively. It was also observed that an increase in the ATP concentration reduced sedimentation of the enzyme. This process appears to be abolished when ADP-PNP is used as a non-hydrolysable analogue of ATP to prevent autophosphorylation, or when the autophosphorylatable Thr271 is mutated to an alanine. *In vivo* this process may act to regulate the length of time CCaMK is active ensuring that overstimulation does not occur, however this has only been observed to occur in *in vitro* experiments and therefore it is

not known whether this process is biologically relevant (77). Conceivably, protein aggregation within a cell would not be a favourable process meaning that this mechanism is likely to be an artefact of the experimental conditions. It is therefore assumed that, like in CaMKII (78), calcium ion and CaM dissociation along with dephosphorylation by a yet-to-be determined phosphatase return CCaMK to its inactive state.

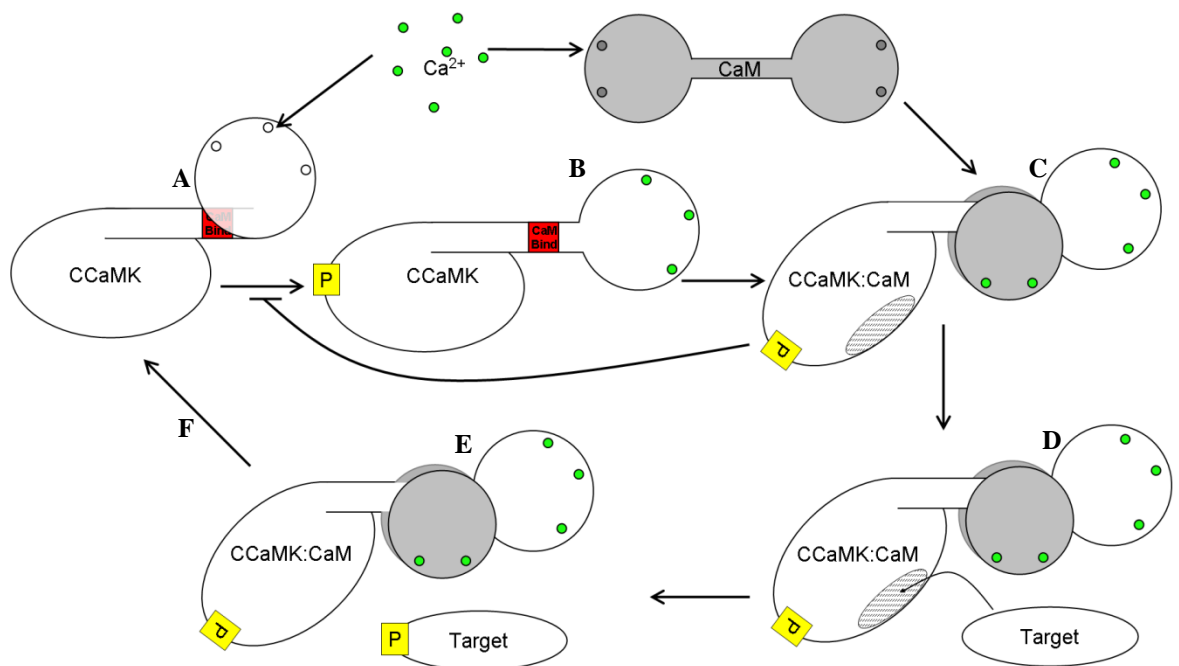


Figure. 1.6. Scheme of CCaMK activation based upon publications from the Poovaiah group. Each protein species has been labelled, CaM is shaded grey and calcium ions are shaded green for clarity. A, calcium ions bind to CCaMK and CaM. B, autophosphorylation of CCaMK occurs enhancing CaM affinity approximately 8-fold from 55.3 nM to 6.5 nM (72). C, CaM binding relieves autoinhibition and kinase activity is increased 20-25-fold (61). Additionally CaM bound CCaMK inhibits further autophosphorylation (61). D, target proteins bind to CCaMK. E, Target proteins are phosphorylated. F, CCaMK is returned to the inactive state by calcium ion-dissociation and dephosphorylation. It should be noted that although included in this diagram, autophosphorylation does not appear to be required for activity and therefore non-phosphorylated CCaMK can also progress through this cycle.

1.4 INTRODUCTION TO CALMODULIN

Calmodulin (CaM) is an abundant protein in eukaryotes and assists in many cellular functions. For instance it is known to be required for regulation of DWARF1 in *Arabidopsis*, which regulates brassinosteroid synthesis and plant growth (79), and CCaMK (discussed in section 1.3 Calcium and calmodulin dependent protein kinase). In animals many proteins have been identified as CaM

regulated including CaMKII (discussed in section 1.5 “calmodulin dependent protein kinase II). As a result, CaM is found in many cell types and CaM interacting proteins are very common in eukaryotic genomes. CaMs are highly conserved proteins with approximately 70% identity between animal and plant isoforms (80). The reason for this is most likely that CaMs are multi-potent and essential in eukaryotes thus rendering most mutations fatal. CaMs also tend to be ubiquitously expressed in plant cells (24).

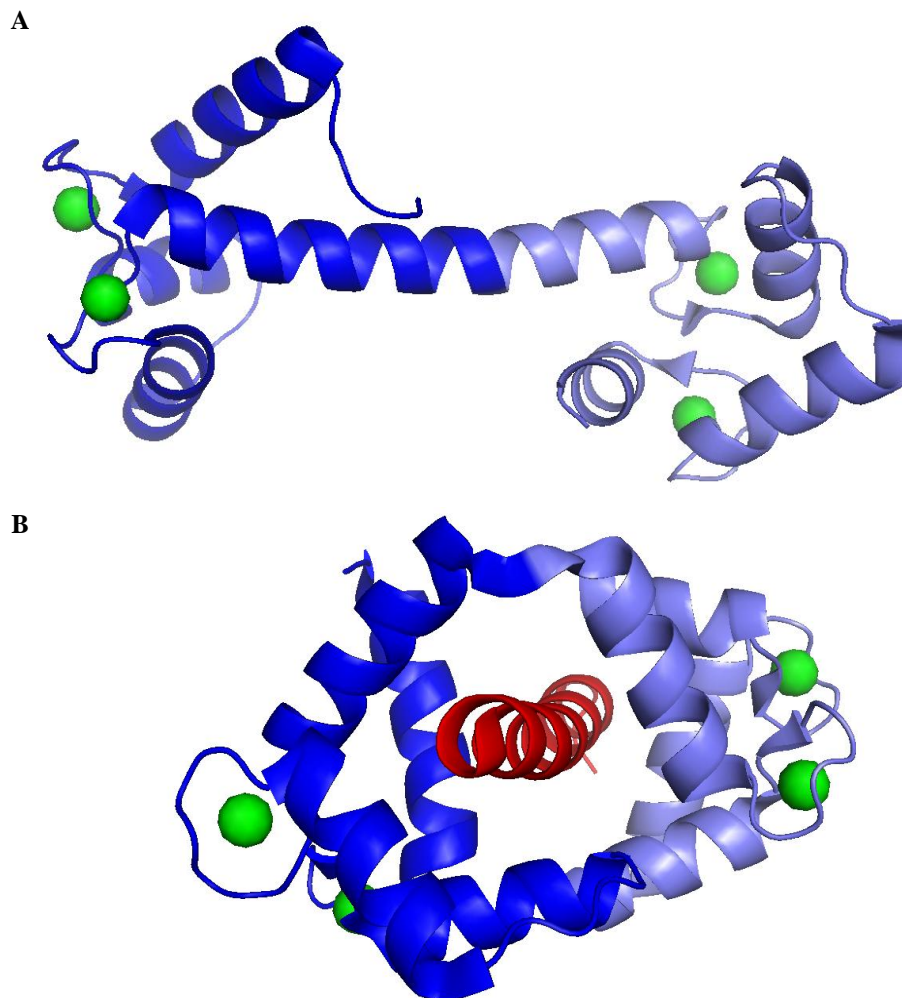


Figure. 1.7. Crystal structures of CaM and CaM in complex with a target peptide. A, potato CaM isoform 6 with calcium ions bound (PDB file 1rfj) (27). B, calcium ion-bound *Drosophila* CaM bound to a synthetic peptide derived from the CaM binding site of Rat CaMKI (PDB file 1MXE) (81). Calcium ions are shown in space fill representation in green. CaM is shown in cartoon representation with the N-terminal lobe in dark blue and the C-terminal lobe in pale blue. The CaMKI peptide is shown in red.

CaMs are typically small, acidic proteins containing four calcium ion-binding EF-hands. Potato CaM isoform 6 was the first plant CaM to have its structure solved. It was found that its structure is very similar to animal CaMs. It is a dumbbell shaped protein consisting of two lobes, termed the N and C-terminal lobes, each containing two EF-hands. The two lobes are linked by a central helix. On each lobe there is a hydrophobic patch, which is the point of interaction with hydrophobic regions of target peptides to form the CaM/target complex (27). Structures of CaM are shown in Figure 1.7. (Discussed briefly in section 1.1.4 “the EF-hand” and expanded upon below).

1.4.1 Functions of calmodulin

The primary function of CaM is to act as a calcium induced regulator of its target proteins. CaM works by a simple mechanism whereby it binds calcium to its four EF-hand motifs; it undergoes a conformational change, which increases its affinity for a target peptide leading to binding. Once bound, CaM modulates the activity of its target.

1.4.2 Calcium ion-binding

The biochemistry of plant CaMs is poorly characterised. However, animal CaMs have been extensively characterised. As the sequence identity is so high between them, the binding characteristics are expected to be very similar. This is supported by evidence that bovine and wheat CaMs have overlapping activation curves giving similar CaM half maximal activation concentrations for 5'-cyclic nucleotide phosphodiesterase (82).

The two calcium ion-binding domains of CaM do not have the same affinity for calcium. This leads to the designation of the N terminal domain the ‘low affinity domain’ and the C-terminal domain the ‘high affinity domain’ (83).

The two lobes of CaM are independent in their calcium ion-binding. Within the lobes, two calcium ions are bound cooperatively (84). Calcium ion-binding to each lobe initiates conformational changes allowing it to bind to its target. In addition, calcium ion-binding melts the central helix of CaM allowing it to wrap around its target and position both lobes in the correct orientation to interact with the target simultaneously as illustrated in Figure 1.7 B (81).

An extensive study on *Drosophila* CaM by Peersen *et al.* characterised calcium ion-binding to CaM in the presence of target peptides (76). In this study it was found that apo CaM had calcium ion-affinities of 2 and 13 μM for the N and C-terminal lobes, respectively. Additionally it was found that the dissociation rate constants for the two domains differ giving rise to biphasic calcium ion-dissociation kinetics. The rate constants were 11.8 s^{-1} and $\geq 850 \text{ s}^{-1}$ at 25 °C for the N and C-terminal lobes, respectively. This broadly agreed with data collected on bovine CaM in a much earlier study in which a slow rate constant of 9.1 s^{-1} at 28 °C was determined. It is worth noting that in bovine CaM the fast rate can be measured by lowering the temperature. At 11 °C rate constants of 293 and 2.1 s^{-1} were determined showing that the affinity and kinetics of calcium ion-binding to each of the two lobes of CaM are accessible experimentally. In addition the rate constants of CaM dissociation from a target peptide cannot be separated from calcium ion-dissociation from the

complex meaning that conformational changes between CaM and calcium ion-dissociation are not rate limiting in these processes (85).

As well as the kinetics and affinity of calcium ion-binding to CaM, the thermodynamics have also been studied. It was determined that the entropy change of binding calcium ions to SynCaM (A synthetic CaM sequence, refer to references within Gilli *et al.* 1998) is positive (44 - 66 J mol⁻¹ K⁻¹ for the four sites). Binding was exothermic for two of the calcium ion-binding sites, and endothermic for the remaining two. This means that the binding of two calcium ions is driven by both entropy and enthalpy whereas the binding of the remaining calcium ions is driven only by entropy. Further analysis on the effect of magnesium on the affinity and thermodynamics of calcium ion-binding revealed that magnesium ions have no effect. This shows that the EF-hands of CaM are specifically tuned to calcium ion-binding (86).

1.4.3 Target recognition and binding

Calmodulin binds to amphiphilic α -helices of variable sequences which share low levels of sequence identity. These helices are 12-30 residues in length and with a net positive charge (reviewed by Du & Poovaiah in 2005) (79). The N-terminus of CaM associates with the C-terminus of the CaM binding site, and the C-terminus of CaM interacts with the N-terminus of the binding site (76). The interaction between the proteins is formed through non-specific van-der-waals forces through the burying of exposed hydrophobic residues. The nature of this interaction goes some way to explaining CaMs multipotency (87).

It is well documented that CaM binding domains have the ability to tune the calcium binding properties of CaM. This occurs through stabilisation of the EF-hands of CaM upon formation of a complex raising the overall affinity calcium ions when a target is present by driving the equilibrium further towards the calcium ion-bound form. The higher affinities are accompanied by a reduction in the dissociation rate constant of calcium ions. This rate constant reduction can be up to 350 fold in the presence of a target compared with CaM alone. This suggests that off rate constant has a large influence on the affinity of CaM for calcium ions. The degree of affinity enhancement ranges greatly from as low as 13 fold to 220 fold in experiments with synthetic peptides. This means that the affinity for calcium ions is increased from the μ M range in the apo form to the nM range, which is physiologically relevant for calcium spiking in plants responding to Nod factor as discussed in Section 1.2 “plant microbe symbiosis”. Although impressive, the maximal enhancement may be artificial due to the use of synthetic sequences. An enhancement of 220 fold would most likely lead to activated CaM at resting calcium ion-concentrations *in vivo*. This leads to the conclusion that the data presented from fragment analysis may not resemble the actual enhancements of the full length target protein. Nevertheless this mechanism of affinity enhancement is important for the tuning of CaM and target protein properties to the specific calcium signals *in vivo*. Selected data from Peersen *et al.* are shown in Table 1.1 (76).

Peptide	Ca ²⁺ affinity enhancement ^a	K_D c-term	K_D n-term	k_d c-term	k_d n-term
		μM		s^{-1}	
None	1x	2.0 ± 0.1	13.0 ± 0.6	11.8 ± 0.10	≥850 ± 70
PhK5	12x	0.24 ± 0.08	0.9 ± 0.2	0.90 ± 0.01	13.2 ± 0.20
CaATPase	62x	0.09 ± 0.01	0.2 ± 0.1	0.69 ± 0.03	12.1 ± 0.05
smMLCK	44x	0.10 ± 0.06	0.2 ± 0.1	0.70 ± 0.02	12.5 ± 0.60
skMLCK	220x	0.02 ± 0.01	0.08 ± 0.06	0.36 ± 0.01	6.40 ± 0.60
MKII	240x	0.03 ± 0.01	0.04 ± 0.01	0.49 ± 0.03	6.00 ± 0.40

Table. 1.1. CaM binding affinity and rate constants in the presence of CaM binding proteins

Table showing values for tuning of calcium ion-binding properties of CaM taken from Peersen *et al. Protein Science* (1997) 6 p794-807 with permission from publisher (76). None denotes CaM in the absence of binding peptide. All other rows show data for CaM in the presence of peptides derived from the following proteins: phosphorylase kinase (PhK5), calcium ATPase plasma membrane calcium ion pump (CaATPase), smooth and skeletal myosin light chain kinases (smMLCK and skMLCK) and CaM kinase IIa (MKII)

^aAffinity enhancement calculated as the ratio of ($[Ca]_{1/2} CaM/[Ca]_{1/2} CaM$ -Peptide)

The identities of the high and low affinity lobes of CaM are retained when a binding peptide is present. However the two domains are independently manipulated. In the CaM binding peptide from *CaM kinase IIa (MKII)*, the N-terminal lobe affinity is increased 325-fold whereas this is just 67-fold in the C-terminal lobe. This imbalance of enhancement is common with the N-terminal affinity enhancement usually 3-5 times stronger than that of the C-terminal domain (76).

Due to the multipotency of CaM, it is likely that the specificity of target activation is likely to be a result of signal and protein localisation within cells, and timing of protein expression. CaMs have been shown to localise, upon the binding of calcium, where a localised target may be interacted with. This appears to be the case in plants (see reviewed by Yang & Poovaiah and McCormack *et al.* (24, 80). The tuning of CaMs properties to its target has also been proposed as a mechanism by which specific complexes can be formed in different calcium signals which has been modelled for the differential activation of CaMKII and protein phosphatase 2B by Stefan *et al.* (88).

There have been three different CaM activation mechanisms identified. The first is active site remodelling, whereby a conformational change in the active site of the protein leads to its activation. This has been shown to occur in anthrax adenyl cyclase. Secondly, CaM-induced dimerisation can occur, as in the calcium ion-induced potassium channels. The final mechanism is the displacement of autoinhibitory domains such as in CaMKII (discussed in section 1.5.2

“CaMKII mechanism”) and CCaMK (Discussed in section 1.3 “calcium and calmodulin dependent protein kinase”). CaM binds to the autoinhibitory/CaM binding domain and displaces it, allowing full access to the active site yielding a fully activated kinase (80, 89-91). The regulation mechanism of CaMKII will be discussed in Section 1.5 “calmodulin dependent protein kinase II”.

1.4.4 *CaM and CMLs in nodulation*

Associated with the formation of the nodule, multiple CaM and CMLs have been identified. A typical calmodulin, CaM1 has been found to be expressed throughout nodule development in *M. Truncatula* (92) and 2 CMLs have also been identified to be expressed at the correct time and location for NOD signalling (54).

These CMLs and CaM require further characterisation to determine whether they are involved in the activation of CCaMK. It is also evident that the specific properties of CaM interaction with CCaMK must be understood in order to understand its role in CCaMK activation fully.

1.5 CALMODULIN DEPENDENT PROTEIN KINASE II

Calmodulin dependent protein kinase II (CaMKII) is a highly conserved CaM dependent kinase involved in many neuronal processes in animals in response to calcium signals. CaMKII has been shown to play a major role in learning and memory (89-90, 93).

Neuronal cells undergo high frequency calcium spiking upon stimulation. These spikes are short in duration (on the ms time scale) with intervals on the second to millisecond timescale and raise the cytoplasmic calcium ion-concentration from approximately 100 nM to the μ M range. Calcium release in neurons is mostly under the regulation of *N*-methyl-D-aspartate (NMDA) and voltage-dependent calcium channels (9-10, 94).

CaMKII monomers dimerise through the formation of a coiled-coil interaction between their autoinhibitory helices (91, 93). These dimers, through interaction of the association domains at the core, form a large dodecameric complex with various ratios of the four subunits. These consist of two rings containing six subunits, each stacking to form a complex with $6 \times 2 \times 2$ fold symmetry shown in Figure 1.8 (89-91, 93, 95-97).

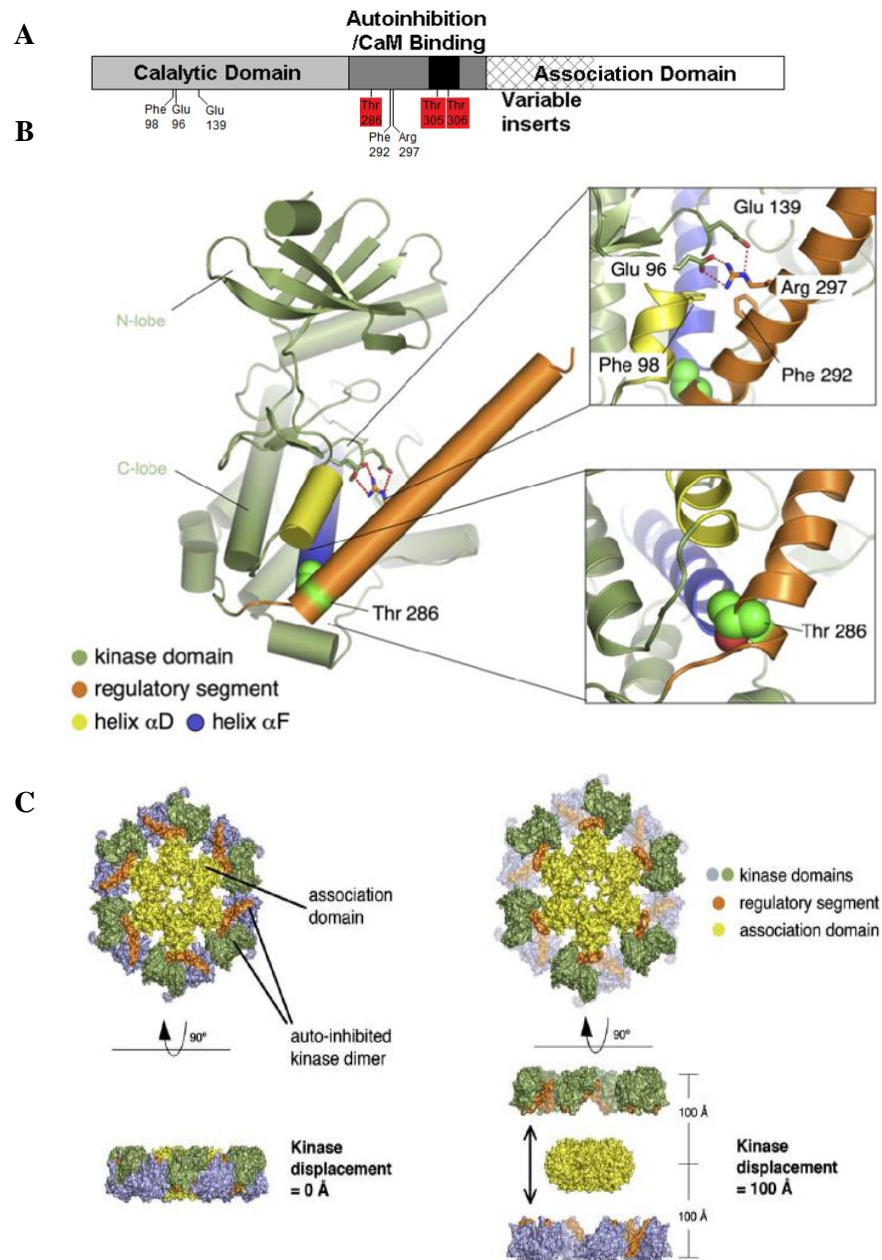


Figure. 1.8. Structure of CaMKII. A, linear representation of the CaMKII sequence. This is a generalised structure for all isoforms with key regulatory residues labelled. Residues highlighted in red are autophosphorylation sites, and those not highlighted are involved in interactions between the kinase and autoinhibitory domains. B, 3D structure of CaMKII kinase (green) and regulatory (orange) domains. Expanded views show the autophosphorylated threonine residue (lower) and contacts between the autoregulatory domain and active site (upper). Residues Phe292 and Arg297 from the autoinhibitory domain, form contacts with Phe98, Glu96 and Glu139 in the kinase domain to stabilise the autoinhibited conformation in the absence of CaM or Thr286 phosphorylation. C, model based on crystallographic data and small angle x-ray scattering. This model shows two potential conformations whereby the kinase domains are displaced by 100 Å from the core as a result of conformational changes induced by CaM binding. Images B and C Reprinted from Cell

123, by Rosenberg et al. Structure of the Autoinhibited Kinase Domain of CaMKII and SAXS Analysis of the Holoenzyme. p849-860. © 2005, with permission from Elsevier (91).

1.5.1 *Structure of CaMKII*

CaMKII exists in four splice variants (α , β , γ , δ). The most common are the 50 kDa α , and 60 kDa β forms. All isoforms contain three domains, a serine/threonine kinase domain, an autoregulatory domain containing a CaM binding site and an association domain. Within the kinase and autoinhibition domains, there are three phosphorylation sites, which are important for activity. These are Thr287 at the base of the regulatory domain, and Thr305 and Thr306 in the CaM binding site (89-91, 95-96, 98-100). The main source of variation between the four variants is the inclusion of variable inserts within the association domain, which plays a major role in the formation of the multimeric complex (89-90, 95). The monomer structure of CaMKII is summarised in Figure 1.8 A and B. Structural studies of CaMKII have revealed that the autoinhibitory domain is mostly α -helical and covers the active site of the enzyme. This acts as a pseudo-substrate occupying the protein binding pocket and blocking both substrate and ATP binding (89-91). Upon the binding of CaM the autoinhibitory domain is removed from the active site and the ATP binding site is altered allowing substrate binding and phosphorylation.

1.5.2 *CaMKII Mechanism*

The activation of CaMKII involves a two-step process that yields an autophosphorylated enzyme with CaM independent activity.

Firstly, CaM binds to the CaM-binding site and displaces the autoinhibitory helix. This breaks the interactions with the active site allowing ATP and substrate to bind. CaM binding also exposes the autophosphorylation site. The mechanism of the initial autophosphorylation has been shown to be an intra-holoenzyme process as the rate at which it occurs is concentration independent. The use of x-ray crystallographic data and small angle x-ray scattering has allowed the mechanism of autophosphorylation to be understood at the molecular level. In this model CaM binds to the autoinhibitory segment and releases the kinase domain causing it to be displaced from the core of the complex. When the same process occurs in an adjacent kinase, the two catalytic domains come into close proximity and a trans-autophosphorylation can occur. This requirement for CaM binding to adjacent kinases within a complex gives rise to cooperativity enhancing the calcium decoding sensitivity of the system (89-91). In this mechanism CaM binding alone governs the rate at which autonomous kinase is produced. Therefore to understand this process in the context of a calcium spiking signal, the biophysics of CaM binding must be fully characterised. Autophosphorylation enables CaM-independent kinase activity by reducing the inhibitory potency of the autoinhibitory domain approximately 10-fold leaving the enzyme with approximately 70% activity when CaM dissociates. The location of Thr286 is at the base of the autoinhibitory domain, where phosphorylation can disrupt the interaction between domains, as shown in Figure 1.8 B.

Furthermore the affinity for CaM increases by three orders of magnitude leading to the retention of CaM at the end of a calcium spike. This may aid rapid phosphorylation of remaining subunits under some conditions to accelerate the formation of autophosphorylated kinases with maximal activity. The increase in the affinity of CaM is achieved through a large reduction in the k_d , possibly due to the exposure of additional CaM binding residues in the autoinhibitory helix. This process is referred to as ‘CaM trapping’ (89-91, 100-101). Once autophosphorylated, CaM dissociation does not render the complex inactive. Instead, on subunits where CaM dissociates, a rapid secondary autophosphorylation of the CaM binding domain at residues Thr305 and Thr306 occurs, which prevents the rebinding of CaM (‘CaM capping’). The most probable function of this is to remove CaMKII capable of CaM binding from the pool of CaM binding proteins to reduce competition (89-90). It should be noted that with high frequency signals CaM capping is not predicted to occur. This is because retention of CaM between spikes prevents exposure of Thr305 and Thr306 (78).

Calcium spiking is decoded by accumulating CaM bound CaMKII. When the spiking frequency is rapid CaM does not have time to fully dissociate before the next spike meaning additional CaM bound CCaMK is accumulated during the next spike. High frequency spiking (e.g. 4 Hz) leads to high levels CaM bound CCaMK whereas low frequency (0.5 Hz) spiking leads to low levels. The level of CaM bound CaMKII relates directly to the amount of autophosphorylated autonomous CaMKII produced, which means that spiking is decoded into the proportion of CaMKII that is activated. As dephosphorylation is slow, active CaMKII can be retained after calcium spiking has ended. Dephosphorylation of CaMKII requires phosphatases as CaMKII has no intrinsic phosphatase activity. CaM dissociation and dephosphorylation are required to return CaMKII to its inactive state. This simple model was reviewed by Hudmon and Schulman in 2002 (89-90).

1.5.3 *Kinetic and affinity studies of CaMKII*

CaMKII has been shown to reach different levels of autonomy based on the frequency at which calcium signals occur over a given time. It has been also been shown that different isoforms respond differently to a calcium spiking frequency. This means that CaMKII complexes may be tuned to detect a particular type of signal through the mixture of isoforms present in a particular complex (89-90, 93, 102-103). Additionally to this, sub-cellular localisation is thought to play a major role in the phosphorylation of CaMKII targets. CaMKII has been shown to specifically localise to particular areas of cells depending on the function it is to perform (89-90, 104). It has also been demonstrated that particular proteins associate with the CaMKII complex to facilitate this process (89-90). Recent advances in the understanding of CaMKII have come from complex computational models. It is known that each stage of the activation and deactivation process is important for determining the amount of active CaMKII over a given calcium spiking program. Precise measurement of these rate constants, binding constants and protein concentrations within

cells has allowed for detailed models, which demonstrate the ability of CaMKII to decode calcium spiking *in vivo*.

CaM association to CaMKII in the presence of calcium is diffusion rate limited (measured rate constant of $1.5 \times 10^8 \text{ M}^{-1} \text{ s}^{-1}$). This means that in the context of calcium spiking signal CaM binding is almost instantaneous with the beginning of the calcium spike. The amount of CaM/CaMKII complex produced is dictated by affinities for CaM and calcium ions, and the concentrations of each component. The dissociation rate of CaM from CaMKII is reasonably fast, 2.2 s^{-1} was measured by Meyer *et al.* When CaMKII is autophosphorylated at Thr286 this rate is significantly reduced to $<0.001 \text{ s}^{-1}$. These rate constants correspond to CaM affinities of 14.5 and $<0.02 \text{ nM}$ for the non-phosphorylated and phosphorylated CaMKII, respectively. This means that the system can be adapted to retain CaM bound CaMKII between spikes by trapping CaM in the autophosphorylated form (100).

As discussed in section 1.4 “introduction to calmodulin”, the N and C-lobes of CaM have different affinity and kinetics for their target. This is also the case with CaMKII. In a study by Jama *et al.* the effect of mutation of individual EF-hands of CaM and the effect on CaM binding, and CaMKII auto and target phosphorylation were characterised. They found that calcium ions dissociated from CaM bound to a CaMKII peptide at a rate of 0.3 s^{-1} for the C-lobe. The N-lobe calcium ion-dissociation was too fast to be measured.

In the presence of wild-type CaM, autophosphorylation was biphasic with rate constants of 5 s^{-1} and 0.006 s^{-1} of similar amplitude. Mutation of either lobe reduced the amplitude of the fast phase, and slowed the slow phase significantly showing that binding of both lobes is required for autophosphorylation at the maximal rate (105).

1.5.4 Modelling CaMKII activation

To dephosphorylate CaMKII, phosphatases are required. It was reported in an experiment by De Koninck and Schulman (described below) that CaMKII has no significant intrinsic phosphatase activity. This means that once phosphorylated in the absence of phosphatase, CaMKII remains autonomous and accumulates with each spike until maximum activation is reached. Under this regime the spike frequency and duration only influence the rate of accumulation rather than a pseudo steady-state of active CaMKII.

De Koninck and Schulman demonstrated that CaMKII autophosphorylation is dependent on calcium spike frequency *in vitro* by exposing CaMKII immobilised in PVC tubing to pulses of calcium ions in the presence of ATP and CaM. This was achieved by pulsing solutions of CaCl_2 or EGTA with an exchange time of 20 ms thus producing square waves of calcium. They found that half maximal activity was achieved at 80 nM CaM for αCaMKII , approximately three times more than for βCaMKII under steady-state conditions. It was found that at a frequency of 1 Hz, 200 ms pulses of CaCl_2 αCaMKII gave little autonomy, 2.5 Hz gave approximately 30% autonomy and 4 Hz yielded $>60\%$ autonomy after 6 s exposure to calcium ions. This shows that the effect of

frequency is significant on the autophosphorylation of CaMKII. It was proposed that higher frequencies do not leave enough time for complete CaM dissociation therefore making it easier to bind CaM to adjacent CaMKII monomers to allow autophosphorylation to occur. In the same work it was discovered that spike length also influenced autonomy demonstrating that the exact timings of the calcium spiking are important for CaMKII activity. Data from this work is shown in Figure 1.9 A. (102).

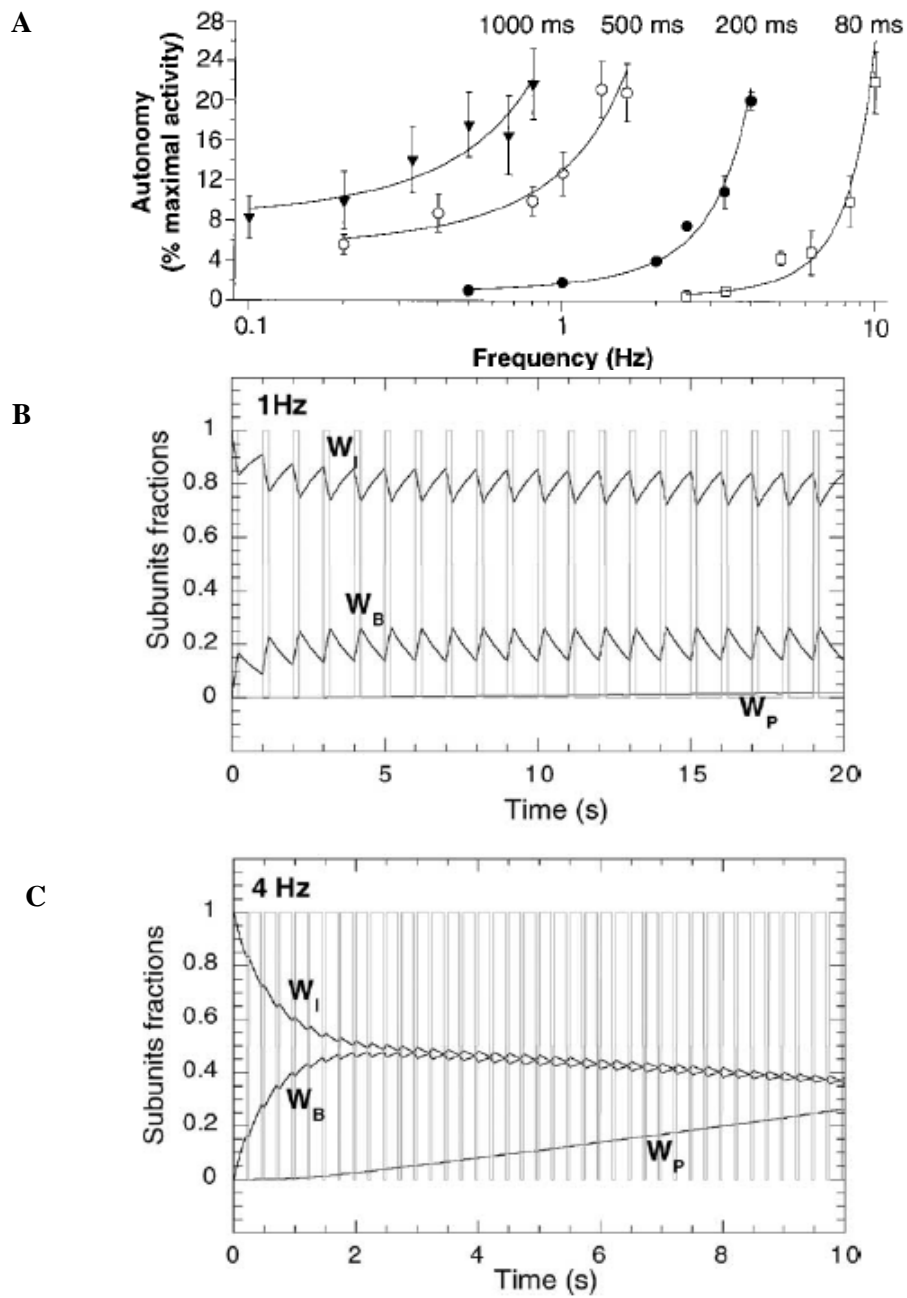
A model produced by Dupont *et al.* used biophysical parameters of CaM binding and autophosphorylation. In this model the steps of CaM binding, autophosphorylation and dissociation from both the phosphorylated and non-phosphorylated kinase were considered. All steps except autophosphorylation were considered to be reversible. The requirement for neighbouring subunits to be CaM bound for autophosphorylation was also considered and CaM capping was ignored. This model produced data that agreed well with the observed autophosphorylation by De Koninck & Schulman. Additionally, they found that CaM trapping had little effect on the output of the model suggesting that CaM binding and dissociation from the non-phosphorylated CaMKII was the biggest determiner of autonomy. Modelling of CaM kinetics showed that at 1 Hz almost all of the CaM dissociated between spikes leading to low levels of autonomy. At 4 Hz significant amounts of CaM remained bound allowing greater accumulation of autonomous CaMKII. Outputs from the Dupont *et al.* simulation is shown in Figure 1.9 B and C (106).

A recent model by Pepke *et al.* was much more complex and accounted for rate constants and affinities corresponding to CaM in partially loaded states. Like the model discussed above, autophosphorylation was assumed to be irreversible. In this model the concentration of CaMKII was 80 μM , CaM was 20-40 μM . Calcium spikes were simulated to mimic neuronal calcium spikes at low (1-5 μM), medium (5-50 μM) and high (50-250 μM) maximal calcium ion concentrations, which mimics calcium transients in different regions of the cell. (See references within (107)). Because of the high protein concentrations involved, the concentrations of calcium ions are limiting. This means that the calcium ion-saturated form of CaM does not dominate during a calcium spike. It was predicted that a burst of formation of CaM with one calcium ion bound to the N-lobe occurred, which then dissociates. Then accumulation of CaM with one calcium ion bound to the slower association, but higher affinity C-lobe occurs. In the presence of CaMKII the profiles of calcium ion-binding change such that CaM with two ions bound to the C-terminus dominates. This is owing to affinity enhancement of CaM for calcium ions when bound to CaMKII. As autophosphorylated CaMKII can enhance the affinity of CaM for calcium ions further, CaM in this complex can also accumulate the calcium ion-saturated form of CaM. In frequency based simulations it was found that the CaM with two calcium ions bound dissociated between spikes at low frequency (0.5 Hz). At high frequency this species is retained. When the next spike occurs these proteins can be converted to the saturated form driving maximal autophosphorylation activity. This model therefore suggested that the part loaded forms of CaM are significant in the

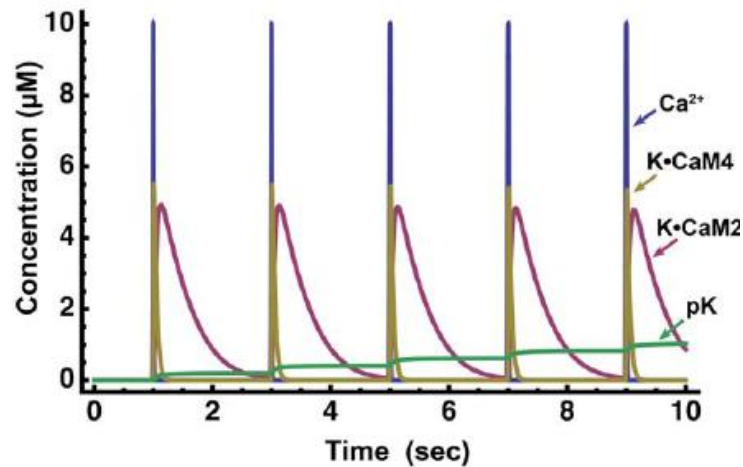
interpretation of calcium spiking. When accounting for the autophosphorylation of part saturated kinase, it was found that autophosphorylation was reduced significantly over models where only saturated CaM can bind and allow autophosphorylation. That is because the blocking of CaM binding by part loaded forms artificially enhances the preference of the system to saturate CaM. This is because the affinity enhancement of the individual lobes of CaM for calcium ions is ignored and several possible species, which will compete for calcium ions are not modelled. It is therefore important to consider rate constants and affinities for all calcium ion-loaded forms of CaM when modelling. An output from this model is shown in Figure 1.9 D and E (107).

When phosphatase is added into mathematical modes of CaMKII, the effect of frequency on rate of activation, and maximal activity levels becomes much more significant. This is because the rate of dephosphorylation is balanced against the rate of autophosphorylation allowing a pseudo-steady-state to be reached. Therefore phosphatase is proposed to be a major factor *in vivo*. (78).

Together the modelling of CaMKII highlights the importance of accurate measurement of all biophysical parameters of CaMKII activation.



D



E

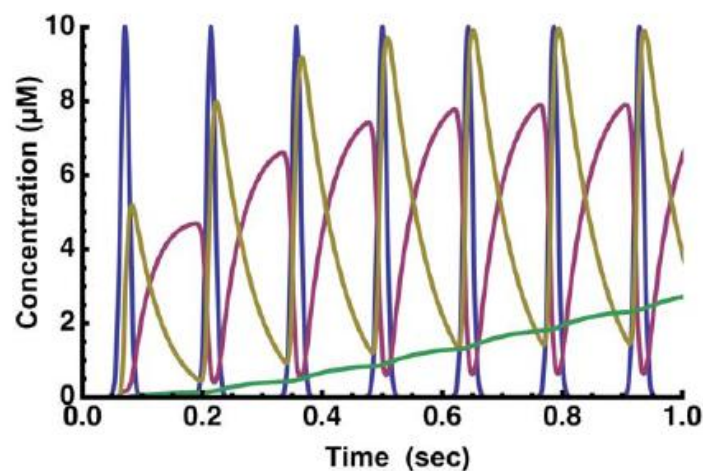


Figure. 1.9. Kinetic parameters of CaMKII during calcium spiking. A, percent autonomy of CaMKII as a function of frequency by *in vitro* analysis. Each curve represents a different pulse duration, as illustrated. Figure taken from De Kroninck and Schulman (1998) *Science* 279 p227-230 (102). Reprinted with permission from AAAS. B and C, modelled concentrations of inactive (W_I), CaM bound (W_B) and autophosphorylated CaMKII (W_P) during calcium spikes at 1 and 4 Hz, respectively, using a simple model. Figure reprinted from *Cell* vol 34 Dupont *et al.* Sensitivity of CaM kinase II to the frequency of Ca^{2+} oscillations: a simple model p485-497 © 2003 with permission from Elsevier (106). C and D, simulated concentrations of calcium ions, CCaMK with calcium ion-saturated CaM bound, CaM with the C-lobe saturated with calcium ions and autophosphorylated CaMKII at 0.5 and 7 Hz, respectively, using a dynamic model. Ca^{2+} shows the concentration of calcium ions, K·CaM4 is calcium ion-saturated CaM bound to CCaMK, K·CaM2 is CaM with calcium ions bound to the C-terminal lobe bound to CCaMK and pK is the autophosphorylated CaMKII. Figure taken from Pepke *et al.* *PLoS Computational biology* (2010) 6 e1000675 (107).

1.5.5 Comparison of CCaMK with CaMKII

Although CCaMK and CaMKII are likely to share significant structural similarity and autoinhibition is likely to operate through a similar mechanism (4), it is clear that there are several key differences between these enzymes.

CCaMK lacks the association domain of CaMKII, which is located at the C-terminus and drives formation of the dodecameric complex (89-90). This means that CCaMK is unlikely to form large complexes through this mechanism. If CCaMK is found to self-associate then it must occur through a different mechanism to CaMKII.

The presence of a calcium ion-binding visinin-like domain at the C-terminus of CCaMK demonstrates that overall regulation of this enzyme will differ. This is because this domain is not found in any other known CaM dependent kinases. Biochemical characterisation of CCaMK to date has revealed several other important differences to CaMKII. Firstly, the primary autophosphorylation site of CCaMK is within the kinase domain rather than the end of the autoinhibitory domain, which suggests that autophosphorylation regulates the CCaMK through a different mechanism. It is also known that the CaM trapping effect of autophosphorylation is much weaker in CCaMK than it is in CaMKII as CaM affinity is only enhanced eight-fold, rather than approximately 1000-fold. Additionally, autophosphorylation of CCaMK does not require CaM binding, whereas this is essential for the autophosphorylation of CaMKII. By contrast, CaM binding has been shown to inhibit autophosphorylation in CCaMK (72). It is also important to note that autonomous activity after autophosphorylation has not been reported in CCaMK. These comparisons reveal that substitution of the C-terminal association domain of CaMKII with a calcium ion-binding visinin-like domain in CCaMK, combined with the different mechanism of autophosphorylation, leads to a very different overall activation mechanism. This will require extensive characterisation to understand how CCaMK is able to decode the calcium spiking signals observed in root hair nuclei.

1.6 NEURONAL CALCIUM SENSORS

The neuronal calcium sensor (NCS) family of proteins are characterised by small calcium binding proteins typically 190-200 amino acids in length. This growing family contains many sub-families of proteins including recoverin, visinin, hippocalcin, neurocalcin and calcineurin-B (62, 108-109). Like CaM, NCSs act as calcium relays and can modulate the function of many target proteins (87, 108-109). These proteins are found mostly in the brain of vertebrates. The NCS proteins are involved in a wide range of functions. Visinin is expressed specifically in retinal cone cells implying an important role in sight (110). A visinin-like protein has been shown to bind double stranded RNA in the central nervous system (111), and another visinin-like protein modulates agonist sensitivity of an acetylcholine receptor (112). Calcineurin-B is a neuronal modulator of the serine/threonine phosphatase calcineurin-A (113).

In plants the calcineurin B-like proteins (CBLs) have been discovered. CBLs have been demonstrated to regulate a set of protein kinases named the CBL interacting protein kinases (CIPKs) (87, 114-115). Analysis of the *Arabidopsis* and rice genomes revealed that these plants have 10 CBLs and 30 and 25 CIPKs, respectively (87, 114-115). It is known that some CBLs are capable of regulating multiple CIPKs. CBLs and CIPKs are also known to be expressed developmentally and in response to various stresses. Subcellular localisation is also thought to play a major role in the CIPK/CBL networks. CBL4 (originally names SOS3) is known to interact with CIPK24 and regulates salt homeostasis in response to salt stress (87, 114-115). The CBLs respond to cytosolic elevations in calcium that do not oscillate (116).

1.6.1 Structure of the NCS

As a family, the NCS share a number of common structural features and vary in their levels of sequence identity, which can be as low as 20% (87). The NMR structures of apo and calcium ion-bound recoverin are shown in Figure 1.10. These proteins contain two pairs of EF-hands separated by a short connecting loop. Additionally they contain short helices at the N and C termini (108-109, 117-118). Further to this, many members of both the NCS and CBLs are covalently modified by addition of a myristoyl group to the N-terminus, which gives these proteins the ability undergo calcium-dependent association with membranes (87, 108-109, 114, 117). The NCSs bind calcium ions over the low μM to nM range (62, 113).

The number of active EF-hands in these proteins varies. Calcineurin B has all four EF-hands active (113). In the NCSs EF-hand 1 is always inactivated by a Cys-Pro pair in EF-hand one. EF-hand 4 is inactive in some cases, including in recoverin, which contains a Lys-Glu salt bridge. (108-109, 117). In the plant CBLs EF-hand one is inactivated by the loss of one or more oxygen-containing side chains. Additionally one or two additional EF-hands may be inactivated in CBLs (117).

1.6.2 Mechanism of Activation

Upon the binding of calcium the protein undergoes a conformational change, which allows their association to a membrane through exposure of the myristoyl group. This activation mechanism is often referred to as the calcium-myristoyl switch (87, 108-109, 112, 117-118). In recoverin, the activation mechanism has been well defined by comparison of the apo and calcium-ion bound NMR structures (Figure 1.10). In the apo form, the myristoyl group is buried within a hydrophobic pocket where it is unable to access the membrane. When calcium binds, a 45° rotation of the N-terminal lobe relative to the C-terminal lobe occurs with a conserved glycine residue (Gly96) within the inter-lobe region, acting as a hinge. Rotation of the backbone also occurs at Gly42, located in the degenerate EF-hand one binding loop, changing the inter-helical angle of EF-hand one. Together these conformational changes lead to the undocking and “swing out” of the myristoyl group from a hydrophobic pocket allowing localisation to the membrane and the interaction with target proteins (117).

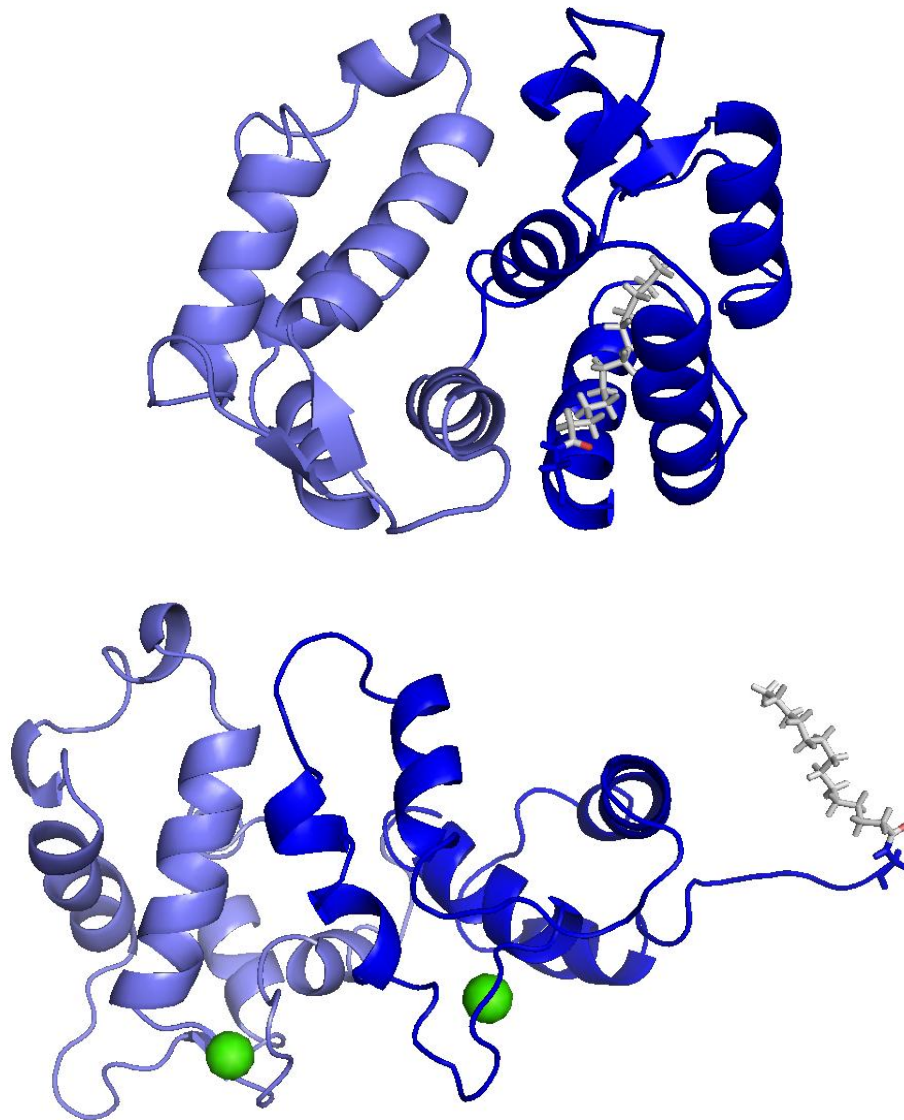


Figure. 1.10. NMR structures of recoverin. A, apo recoverin showing the myristoyl group buried within a hydrophobic pocket and B, calcium ion bound recoverin with the myristoyl group exposed to the solvent. NMR structures were determined by Ames *et al.* (117). The protein is shown in ribbon representation with the N-terminal glycine in stick representation to show the covalent link to the myristoyl group, also shown in stick representation. The N-terminal lobe is shaded dark blue and the C-terminal lobe is shaded in light blue. Calcium ions are shown in green in sphere representation.

1.7 AIMS AND OBJECTIVES OF THIS PROJECT

Although the published work described in section 1.3 “calcium and calmodulin dependent protein kinase” provides some understanding of the mechanism by which CCaMK is activated, the

rate constants of calcium ion and CaM-binding, which are expected to be critical by comparison to CaMKII, are not known. The molecular mechanisms by which calcium ion-binding affects the autoinhibitory domain allowing subsequent autophosphorylation are also unknown.

This raises additional questions with regards to the regulation of CCaMK. Firstly, how is the visinin-like domain affected by calcium ion-binding. To answer this question many experiments were undertaken to understand the consequences of calcium ion-binding to the visinin-like domain at the structural level, which are described in chapter two.

Although important to the understanding of CCaMK, the structural aspects of the visinin-like domain alone cannot allow an understanding of how calcium ion-binding is interpreted by CCaMK. To understand this, two further questions must be answered. Firstly, what is the affinity of the visinin-like domain for calcium ions and is it relevant to the biological range of 5-800 nM measured by Ehrhardt *et al.* (8). This question will be addressed in chapter three. The second question is what is the dissociation rate of calcium ions from the visinin-like domain and is it slow enough to allow persistence between spikes. This will be addressed in chapter four.

As CaM binding is also critical for kinase activation, an additional set of questions to be addressed relate to CaM binding. These are what is the affinity of CaM for CCaMK, what is the dissociation rate of CaM from CCaMK, and are CaM binding and kinetics similar for CCaMK and CaMKII. It is also important to know whether the rate constants of CaM dissociation are slow enough to allow for persistence of active CCaMK between calcium spikes.

By answering these questions it will be possible to update the activation scheme in Figure 1.6 and assign rate constants and affinities to these processes. This will move us a step closer to being able to predict how CCaMK responds to calcium spiking signals *in vivo*.

2. Chapter two – Structural aspects of CCaMK and conformational changes upon calcium ion-binding

To date the structure of CCaMK has been poorly characterised. Understanding the structure of CCaMK will allow for a better understanding of the mechanism of its activation, which will in turn influence computational modelling of calcium signal decoding.

Here bioinformatics have been used to make structural predictions of the properties of CCaMK. Additionally a divide and conquer approach has been used to understand the structural properties of the CCaMK visinin-like and autoinhibitory domains experimentally. It has been discovered that calcium ion-binding induces tertiary level structural changes in CCaMK, which may alter the interaction between the visinin-like and autoinhibitory domains and lead to an increase in the exposure of hydrophobic residues in a manner comparable to the animal NCS family of proteins and CaM.

2.1 RESULTS

2.1.1 Identification of mtCCaMK homologues

Despite the known homology of mtCCaMK to CaMKII, visinin (60), and the CDPKs (4) it was necessary to repeat this analysis to ensure that it is up-to-date. Previously, mtCCaMK had been reported to share 73.5% identity with lily CCaMK, as well as similar percent identity with rice and tobacco (4). Additional homologues of mtCCaMK were identified by searching against the non-redundant protein sequences database using the National Center for Biotechnology Information (NCBI) Basic Local Alignment Search Tool (BLAST). This analysis showed that mtCCaMK shares 99% identity with alfalfa (*M. sativa*) CCaMK, differing by a single amino acid change at residue 278. This analysis also revealed that mtCCaMK also shares 86-94% identity with legume CCaMKs such as pea (*Pisum sativum*) at 90% identity and *Lotus japonicus* at 86% identity. mtCCaMK shares 69-84% identity with non-legume CCaMKs from higher plants, examples of which include Easter lily (*Lilium longiflorum*), rice (*Oryza sativa*), and maize (*Zea mays*) CCaMKs with 73%, 61% and 69% identity, respectively. mtCCaMK is more distantly related to moss CCaMKs, which were revealed to share 52-65% identity. This includes juniper haircap moss (*Polytrichum juniperinum*) CCaMK, which shares 54% identity. Most of the variation appears within the kinase domain between residues 30 and 90 as shown in Figure 2.1. This region encompasses the second half of the ATP binding site. All other sites appear to be well conserved.

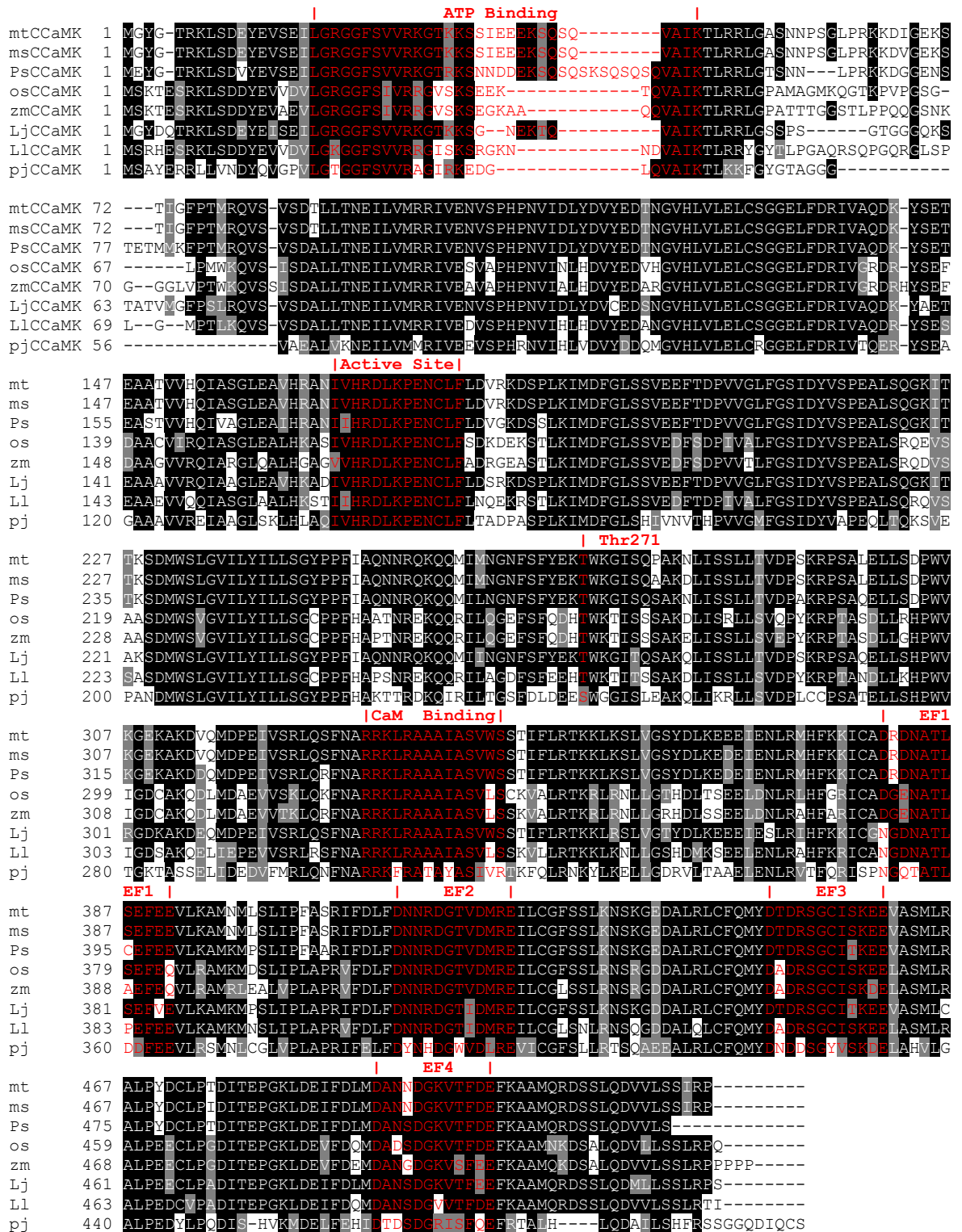


Figure. 2.1. Alignment of *M. truncatula* CCaMK against other CCaMKs. mtCCaMK was aligned against CCaMKs from *M. sativa* (msCCaMK), *Pisum sativum* (psCCaMK), *Oryza sativa* (osCCaMK), *Zea mays* (zmCCaMK), *Lotus japonicus* (LjCCaMK), *Lilium longiflorum* (LlCCaMK) and *Polytrichum juniperinum* (pjCCaMK). Alignment is annotated with predicted features according to the mtCCaMK sequence, which have been highlighted in red.

As the CaM kinases are well characterised at the structural level, CCaMK was searched against the PDB to find suitable proteins for comparison in order to make structure based predictions. In agreement with previous data reported by Patil *et al.* (60), CCaMK was found to share homology with animal CaMKII, with 35% identity to bovine CaMKII in the PDB (PDB code 2BDW). Homology was also found to the visinin-like proteins with 33% identity to *Xenopus* visinin-like protein 1.

Further inspection of the BLAST output revealed that CCaMK has homology to a wide range of protein kinases. A BLAST search against the PDB showed that Human CaMKI D shares 35% identity and human CaMK4 shares 38% identity with the CCaMK kinase and autoinhibitory domains. Taken together, all hits indicate that the CCaMK kinase and autoinhibitory domains share 31 - 40% identity with the CaM kinase protein family.

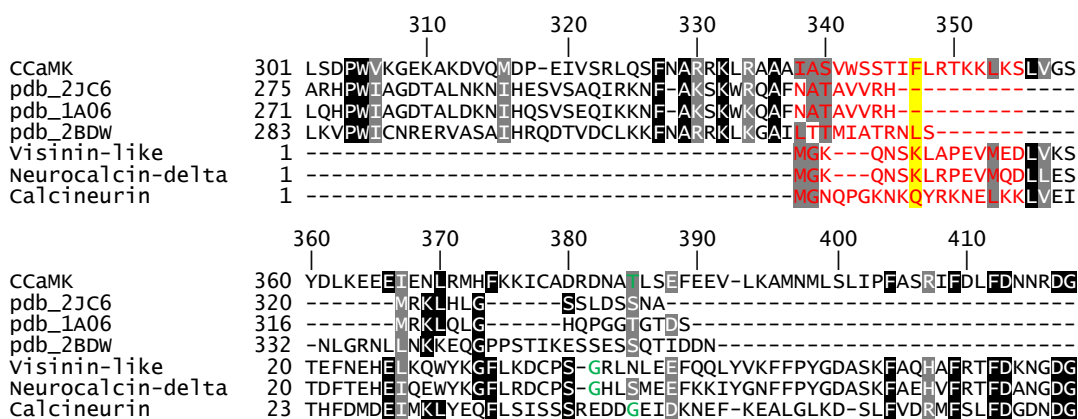


Figure. 2.2. Alignment of CCaMK against entries of CaM kinases in the PDB and members of the NCS protein family. CCaMK was aligned against human calmodulin-dependent protein kinase 1 D (PDB 2JC6), Rat calmodulin-dependent protein kinase 1 (PDB 1A06), *C. elegans* kinase domain of calcium/calmodulin activated kinase II (PDB 2BDW), rat visinin-like protein 1, bovine neurocalcin-delta and *N. fowleri* calcineurin B. The displayed region of the alignment corresponds to the end of alignments with the CaM kinases and the beginning of alignments with the NCS proteins. Numbering on the top row has been added according to mtCCaMK residue numbers. The predicted region of the domain boundary is highlighted in red, and the residue selected for the visinin-like domain construct, Phe346 (to add a small linker after residue 350 before the His-tag) is also highlighted in yellow. Residues highlighted in green are the conserved glycine residues in EF-hand one of the NCS, and the equivalent residue (substituted to Thr in position 385) in CCaMK. Note that the alignment of the CCaMK EF-hand one to the NCS EF-hand one is poor due to the low sequence identity in this region. This is due to the evolutionary divergence of the first EF-hand of CCaMK and the NCS.

To assess the homology of the visinin-like domain in isolation, the C-terminal domain of CCaMK was searched against the non-redundant sequences database. A BLAST of CCaMK

residues 330-523 revealed that CCaMK shares 30-38% identity with the NCS protein family. Examples include 38% identity with *Puccinia graminis* (stem rust) neuronal-calcium sensor 1 and 32% identity to bovine neurocalcin-delta. In addition to the animal proteins, homology was also found to CBLs in plants (reviewed by S. Luan) (87) such as *Arabidopsis* CBL4 (alternative name SOS3) (115), which has 32% identity to the CCaMK visinin-like domain.

The BLAST search against the PDB also revealed that CCaMK has 29-43% identity to the solved structures of the CDPKs (data not shown). These proteins are homologous to the entire CCaMK sequence; however, they lack the CaM binding site found in CCaMK and CaMKII (See review by A. Harmon) (25). However, as these proteins do not rely on CaM binding they are not suitable as analogies to the activation mechanism of CCaMK.

2.1.2 Identification of the visinin-like domain boundary

Multiple alignments were combined to locate the domain boundary between the autoinhibitory and visinin-like domains. This analysis showed that the boundary lies between residues 338-355 where alignments to CaM kinases end, and alignments to NCS proteins begin as shown in Figure 2.2 To predict the regions of CCaMK likely to be unfolded and help inform decisions on constructs and domain boundaries, the FoldIndex server (119) was used, as shown in Figure 2.3 C. A drop in confidence in the fold prediction by FoldIndex (Figure 2.3 C) also supports this prediction. Taken together these data show that residue 350 is likely to represent the domain boundary as this is where alignments to solved CaMK structures end. Additionally the level of sequence identity before this to the NCS is poor. The drop in confidence in the FoldIndex prediction at residue 350 supports that the domain boundary may be at this position. However, as the alignments to CaMKs and the NCS overlap this is an ambiguous boundary and therefore could not be determined precisely.

2.1.3 Prediction of the kinase domain boundary and additional features

FoldIndex predicted that a large area of the CCaMK N-terminus would not be folded, including the ATP binding site. Additionally, a stretch of the C-terminus including EF-hand four was predicted to be unfolded. As these areas were large and encompass key regions of the protein, they were not useful in the determination of domain boundaries. Other regions of disorder were predicted within the protein sequence. Most noteworthy was residues 266-277, which surround the autophosphorylatable Thr271 residue that is thought to be essential for protein function. This suggests the possibility of a flexible loop in this region.

As CaMKII uses coiled-coils to form dimers locally within CaMKII dodecomers (91), coiled-coils could be important in the function of CCaMK. To identify potential coiled-coils the Coils server (120) was used as shown in Figure 2.3 D. This analysis predicted a potential coiled-coil between residues 350 and 383 at the beginning of the visinin-like domain and within the non-functional EF-hand one. Coils also gave an indication that a coiled-coil may be present within the ATP binding site with lower confidence. These coiled-coils may be of significance for protein-

protein interactions and will be discussed further with relation to experimental data later in this chapter.

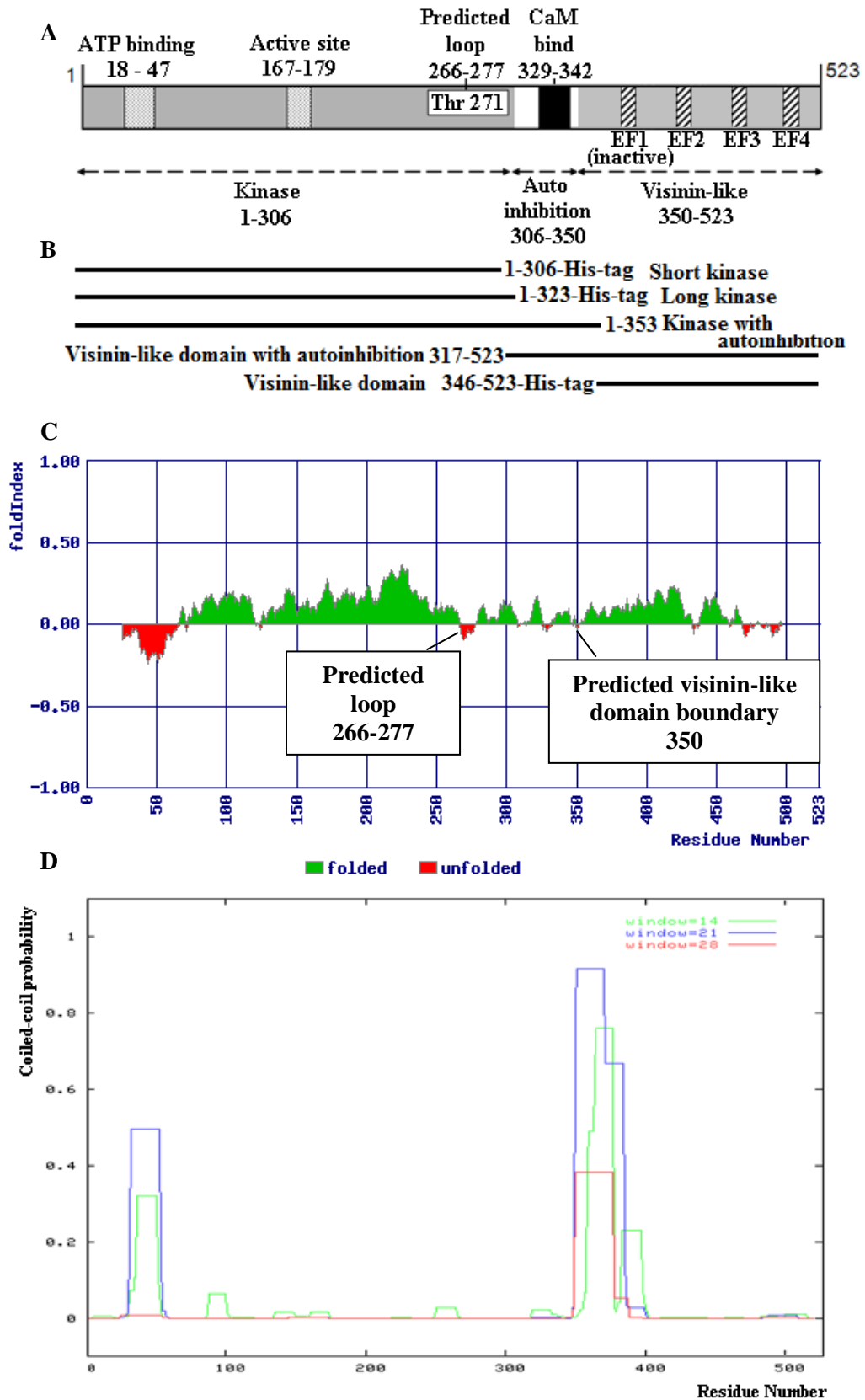


Figure. 2.3. CCaMK structural predictions. A, illustration of CCaMK annotated with important sites and predicted domain boundaries. B, map of CCaMK constructs, which have been cloned into pET101. Labels show construct names, amino acid ranges and added $6 \times$ His-tags. His-tags were not added to constructs containing the CaM binding site. C, FoldIndex (119) output for the full CCaMK sequence. Positive values, highlighted in green, show residues predicted to be folded, and negative values, highlighted in red, show residues predicted to be unfolded. D, Coils (120) output for the full CCaMK sequence. Higher values indicate higher probability of a region forming a coiled-coil.

In order to visualise predicted structural features of CCaMK and assist in the prediction of domain boundaries between the kinase and autoinhibitory domains, a threaded model was produced based upon CaMKII, which is shown in Figure 2.4. From this model it can be predicted that the Thr271 lies adjacent to the autoinhibitory domain, which may be significant for its function.

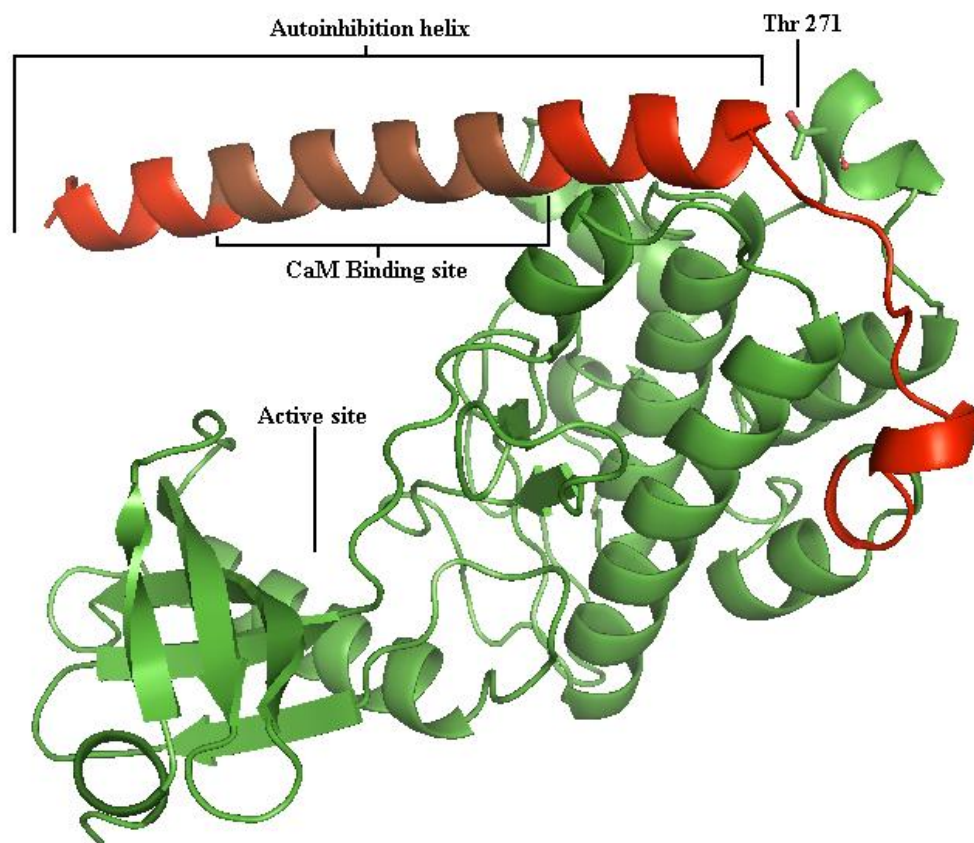


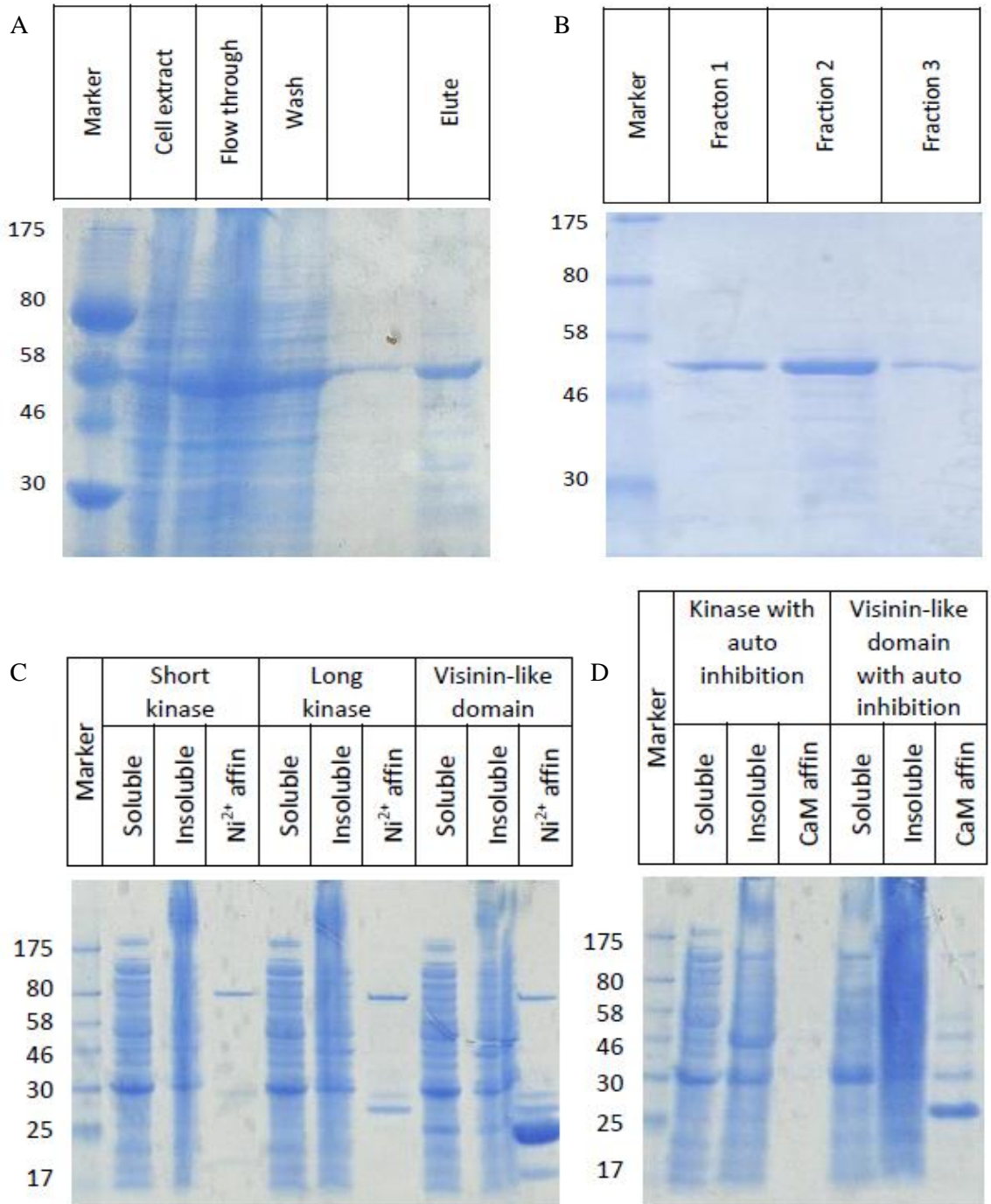
Figure. 2.4. Threaded model of CCaMK kinase-domain with autoinhibition. This model was produced using Swiss PDB Viewer with bovine CaMKII (PDB file 2bdw) as a template (91). The kinase domain is shown in green, the autoinhibitory domain is shown in red with the CaM binding site in brown. The autophosphorylation site Thr271 is shown in stick representation, and is predicted to reside on a short helical section within a loop adjacent to the autoinhibitory domain.

By comparing the threaded model to previous publications on CaMKII regarding the kinase/autoinhibition domain boundary, predictions could be made as to where this lies on CCaMK. A limited proteolysis experiment with chymotrypsin on rat CaMKII by Yamagata *et al.* showed that an active kinase-only fragment could be produced by cutting at residue Ile271 (121), which is located at the end of the loop connecting the autoinhibitory helix to the kinase domain. Aligning this on the threaded model revealed that residue 306 is the equivalent position in CCaMK. A crystallographic study of CaMKII reported interactions between the first few residues of the autoinhibitory helix and the core of the kinase domain (91). This may suggest that the loop connecting the autoinhibitory helix to the kinase domain is required for correct folding and that the true boundary may be closer to the beginning of the autoinhibitory helix. To account for this possibility in CCaMK another potential domain boundary was identified at residue 323, which is close to the beginning of the autoinhibitory helix in the threaded model.

2.1.4 Cloning, expression and purification of CCaMK and CCaMK constructs

The full length CCaMK was found to express best in LB medium at 18 °c. At 37 °c the protein was found to express in the insoluble fraction. As CCaMK contains a CaM binding site, it was enriched using CaM affinity resin (GE Healthcare). This resin contains Bovine CaM immobilised on sepharose beads. This allowed CCaMK to be bound in the presence of CaCl₂ and eluted when EDTA was added. This method was based upon work by Takezawa *et al.* (61) and yielded approximately 3 mg of CCaMK with good purity as shown in Figure 2.5 A.

After purification, CCaMK appeared to be highly unstable. The majority of the protein would elute in the void volume of the Superdex 10/30 GL S200 gel filtration column, as shown in Figure 2.6 in the blue chromatogram. Nevertheless CCaMK was highly enriched after gel filtration as shown in Figure 2.5 B. It was also observed that the protein had a solubility limit of approximately 0.6 mg ml⁻¹ and would precipitate after a few days storage. Additionally, reliable DLS data could not be collected (data not shown).



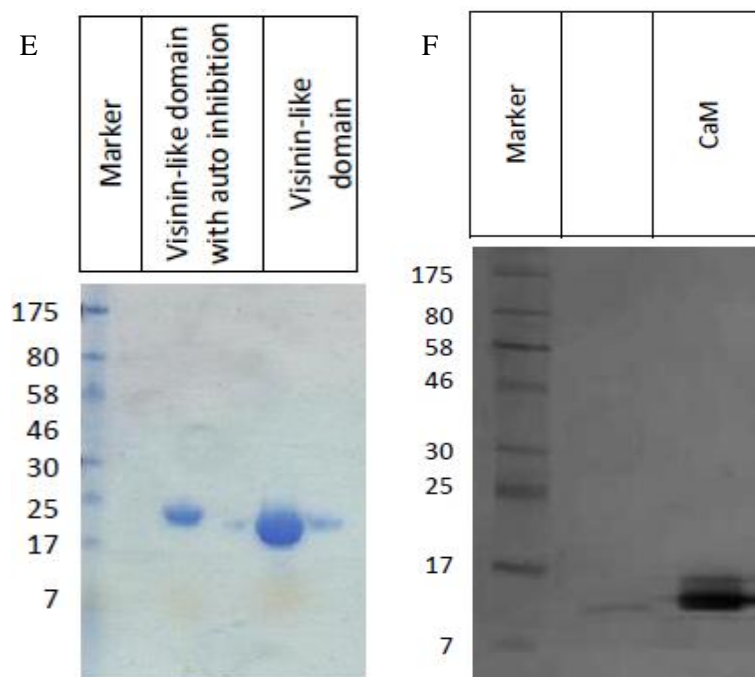


Figure. 2.5. SDS Page gels of protein preparations. A, Whole cell extracts of CCaMK expressed in BL21 (DE3) PlysS cells, the flow through and proteins removed by washing the CaM Sepharose 4B resin (GE Healthcare) and the product eluted with the addition of 2 mM EDTA are also shown. B, SDS PAGE gel of CCaMK after gel filtration on a Superdex 200 13/30 GL gel filtration column (GE healthcare). The elution volume was approximately 8.3 ml. (shown in Figure 2.6). C SDS page gels of His-tagged constructs or D, constructs containing the CaM binding site expressed in BL21 (DE3) PlysS cells. Soluble and insoluble fractions are shown along with eluted products from nickel affinity column or CaM sepharose column. Bands at approximately 80, 30 and 17 kDa are contaminants. E, SDS page of CCaMK visinin-like domain and visinin-like domain with autoinhibition nickel affinity products after gel filtration on a Superdex 200 13/30 GL gel filtration column (GE healthcare). Elution volumes were approximately 16 ml for both constructs (Figure 2.8). F, CaM1 after preparation on a phenyl Sepherose column and gel filtration on a superdex 75 16/60 gel filtration column (GE healthcare) (Image F provided by L. Zhou (unpublished)).

To improve the stability of full length CCaMK a range of conditions were screened using the thermal-shift (thermfluor) assay (122) (data not shown). This method utilises a fluorescent dye, Sypro Orange, which increases fluorescence upon binding to hydrophobic regions of proteins. As Sypro Orange has similar excitation and emission wavelengths to a common qPCR dye, SYBR green, melting curves can be monitored using a qPCR thermocycler. This was achieved for CCaMK in 96 well qPCR plates over a temperature range of 20-95 °c. When the protein unfolds, the binding of Sypro Orange increases, which leads to an increase in fluorescence signal. These data provide melting curves and allow melting temperatures to be determined. As melting

temperature is related to stability, more favourable buffer conditions lead to an increase in the melting temperature of the protein. This analysis showed that the pH 7.5 tris buffer containing 100 mM NaCl gave a melting temperature (T_m) of 37 °c. Changing this to pH 8 EPPS or pH 8.5 tris raised the T_m to 40 and 40.5 °c respectively. As differences of 1 °c are considered to be significant, these improved conditions were deemed to be the same. In the additive screen, water was used as a reference, which had a T_m of 36 °c. Enhancements were seen with the addition of 2 mM AMP-PNP (38 °c) and glycerol (36.5, 37 and 37.5 °c for 1, 5 and 10% v/v, respectively).

Further conditions were screened using a filter based assay in which the full length CCaMK was incubated with buffer containing either 0.15 M ammonium sulphate, 0.4M RbCl, 1% w/v glycine, 40% glycerol, 0.1% triton-X 100 or 5 mM DTT. Samples were then passed through 100 000 molecular weight cut-off filters and the flow through was analysed on SDS gels to determine relative amounts of non aggregated protein qualitatively (data not shown). Hits were then followed up using analytical gel filtration.

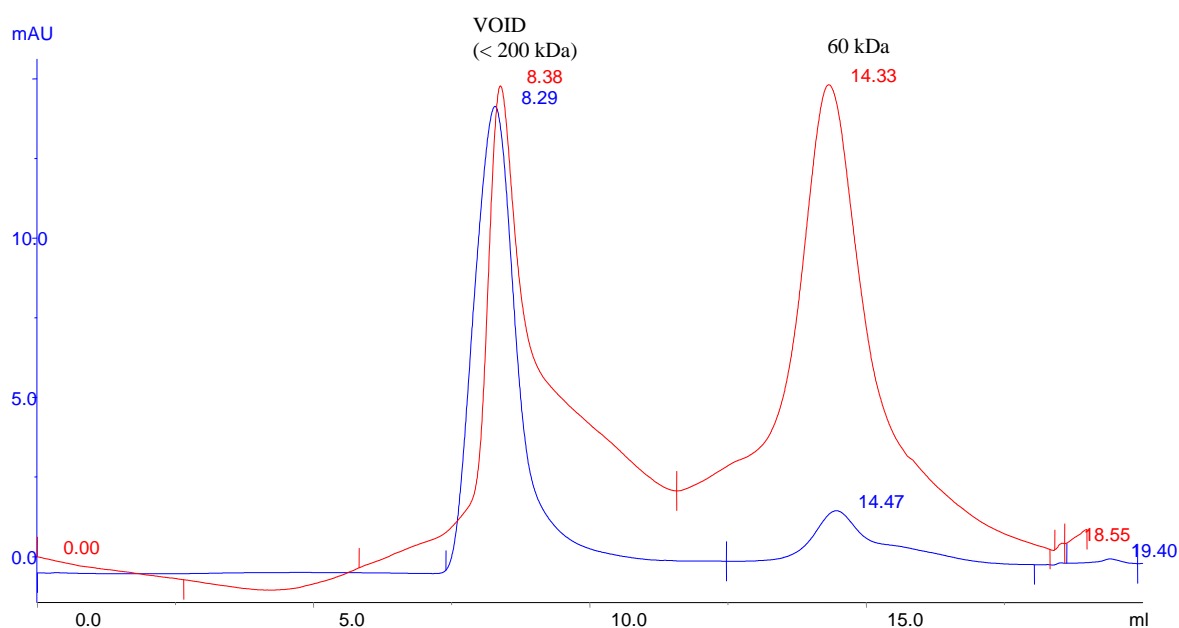


Figure. 2.6. Analytical gel filtration of full length CCaMK. The chromatograms show gel filtration profiles of CCaMK. 50 mM Tris-HCl pH 7.5 containing, 1 M NaCl and 2 mM EDTA (blue). 50 mM HEPES pH 8.0 containing 10 mM MgCl₂, 2 mM EDTA, 1 mM DTT, 0.5 mM ADP and 10 % glycerol (red). Labels show the elution volume and the estimated molecular weight for each peak. Chromatograms have been normalised to the same maximum absorbance level. Gel filtration was performed on an ÄKTA HPLC using a Superdex 10/300 GL S200 analytical gel filtration column and data were processed using the Unicorn software package (GE Healthcare). The expected monomer size of CCaMK is 58 kDa.

In summary, these analyses revealed that stability was enhanced in pH 8 HEPES with the addition of MgCl₂, ADP, glycerol and DTT. In addition it was determined that NaCl reduced stability. A gel filtration profile in the preferred buffer can be seen in Figure 2.6 in the red chromatogram. This suggested that approximately 50% of the protein existed in its monomeric form, whereas the ratio was in the favour of the aggregate form in pH 7.5 Tris-HCl containing 1 M NaCl and 2 mM EDTA. Despite this, significant quantities of the full length CCaMK were in the aggregated form. This meant that although stability was enhanced, the full length CCaMK was still unsuitable for biophysical characterisation.

To produce proteins suitable for biophysical characterisation, constructs of CCaMK were produced. It was hoped that these constructs would allow for the production of pure and stable proteins in high quantities that were suitable for the studies undertaken. These constructs would allow for the study of CCaMK in a divide and conquer approach to characterise CCaMK. The constructs cloned are summarised in Figure 2.3 B.

To experimentally determine the domain boundary between the autoinhibitory and visinin-like domains the visinin-like domain with autoinhibition was subjected to limited proteolysis with trypsin. In the presence of excess CaCl₂, a stable fragment was identified by SDS PAGE and sequenced by reflection in-source decay (rISD) sequencing (data not shown). This analysis revealed that there is an accessible trypsin site at S39 (residue 355 in full length sequence). Additionally a stability test to identify spontaneous breakdown products of this construct yielded a product of the same mass (approximately 19.2 kDa by MALDI-MS). Together these data suggest that the domain boundary is in the region of residue 355 further supporting the bioinformatics prediction. No peptides were removed from the C-terminus of the protein suggesting that this region is folded and stable. When proteolysis was performed in excess EDTA multiple fragments were produced meaning that the sample could not be analysed by mass spectrometry. The same limited proteolysis experiment failed to yield any fragments when performed on the full-length CCaMK (data not shown). This may be due to aggregation preventing access to the trypsin sites by burying them within the aggregate particle. Alternatively the addition of the kinase domain may sterically block the site at residue 355 in the full length protein. Based upon these data, and the bioinformatic predictions in section 2.1.2 “Identification of the visinin-like domain boundary”, it was decided that 350 is a logical choice for the visinin-like domain boundary. For the cloning of some constructs it was decided that additional amino acids were required to act as a linker to improve exposure of the His-tag and reduce interference with the function of the protein. This means that the visinin-like domain construct began at residue 346, and the kinase domain with autoinhibition ended at 353. Additional amino acids were also used as a linker for the visinin-like domain with autoinhibition. Therefore this construct began at residue 317 instead of 323 (the second kinase domain boundary determined in section 2.1.3 “prediction of the kinase domain boundary and additional features”).

For the cloning of kinase domain-only constructs addition of linking regions before the His-tag was not performed. This is because of interactions in this region relate to autoinhibition of the kinases in CaMKII (91), which could be altered by the additional sequence giving some autoinhibition when it was not desired. Therefore it was decided that these should end at residues 306 and 323, which were the boundaries identified in section 2.1.3 “prediction of the kinase domain boundary and additional features”.

Constructs of CCaMK were cloned into pET101 successfully as confirmed by sequencing (data not shown). Of the five constructs produced, only the two lacking the kinase domain were successfully expressed and purified.

The short and long kinase constructs (1-306 and 1-323 respectively) did not show any expression in cell extracts by SDS PAGE, nor could any target protein be isolated by small-scale histidine affinity chromatography (Figure 2.5 C). Similarly, the kinase with autoinhibition (1-353) showed no detectable expression in lysates and CaM affinity chromatography failed to yield any protein (Figure 2.5 D). Expression was attempted in LB, with a IPTG concentrations of either 0.5 or 1 mM, and autoinduction media. Additionally growth at 18 °C and 37 °C in *E. coli* BL21*(DE3), BL21 (DE3) pLysS and BL21 (DE3) pLysE were tested.

The visinin-like domain and visinin-like domain with autoinhibition both expressed well in auto induction media, and could be purified with yields of approximately 3-4 mg l⁻¹ and 1 mg l⁻¹ of culture, respectively. The visinin-like domain with autoinhibition was purified by CaM affinity as described for the full length CCaMK. The visinin-like domain construct was purified using the poly histidine-tag at the N-terminus. It was found that optimal binding occurred in the presence of 10 mM imadazole, and that 500 mM imadazole was sufficient for complete elution from the column. Both constructs were further purified by gel filtration to yield products where the target protein was the only visible band on an SDS gel as shown in Figure 2.5 C, D and E.

Mutants of the Visinin-like domain with inactive EF-hands were produced by mutating the first aspartic acid in the EF-hand binding loop (sequences shown in Figure 2.9) to alanine. The choice of mutation was based upon publication by Putkey *et al.*, which was successful in disabling the EF-hands of Troponin C (123) and Peterson *et al.*, which was successful in disabling EF-hands of CaM (124). Mutants in EF-hands two, four and two-four double mutants were produced in a similar yield to wild-type. Mutation in EF-hand three and the two-three double mutation lead to a reduced yield of approximately 33% that of wild-type. The three-four double mutant showed no evidence of expression and could not be purified. These mutations were confirmed to inactivate the target site by mass spectrometry, which is described below in section 2.1.5 “determination of the calcium ion-binding stoichiometry of CCaMK”.

Analytical gel filtration demonstrated that both the visinin-like domain and visinin-like domain with autoinhibition were monodisperse in both their calcium and magnesium ion-bound, and apo forms as shown in Figure 2.8. However, as the elution volumes corresponded to molecular weights

of approximately 30-40 kDa, which is between the expected sizes for monomer or dimer, accurate molecular masses of each species could not be determined. Additionally peak shifts observed for the visinin-like domain and visinin-like domain with autoinhibition in excess EDTA, CaCl₂ or MgCl₂ cannot be taken as significant (Figure 2.8 A and B) as shifts of similar magnitude were observed in the soybean trypsin inhibitor control samples, which is not known to bind metal ions (Figure 2.8 C).

CaM was prepared by hydrophobic exchange with phenyl sepharose. This method utilised the exposure of hydrophobic residue upon calcium ion binding. When calcium ions were bound, CaM bound to the Phenyl Sepharose resin. It could then be eluted by adding EDTA, which causes conformational changes leading to the burial of hydrophobic residues. This method for CaM purification was previously described by Fromm & Chua (141). CaM was then purified further by gel filtration as shown in Figure 2.5 F.

UV/Vis spectra of each protein construct were collected (shown in Figure 2.7). The molar extinction coefficient at 280 nm was estimated for the visinin-like domain with autoinhibition using the ExPASy ProtParam server to be 9970 M⁻¹ cm⁻¹. Extinction coefficients for the visinin-like domain construct and CaM were determined by measuring absorbance at 280 nm and calculating the values using exact concentrations as determined by amino acid analysis. Extinction coefficients at 280 nm were calculated to be 4745 and 2545 M⁻¹ cm⁻¹ for the visinin-like domain construct and CaM respectively. This represents a 5% and 41% error in the predicted values of 4470 M⁻¹ cm⁻¹ and 1490 M⁻¹ cm⁻¹ for the visinin-like domain and CaM, respectively. Experimental determination of the extinction coefficients was necessary as both the visinin-like domain and CaM lack tryptophan residues and predicted extinction coefficients based upon the absorbance of tyrosine and phenylalanine alone can be unreliable.

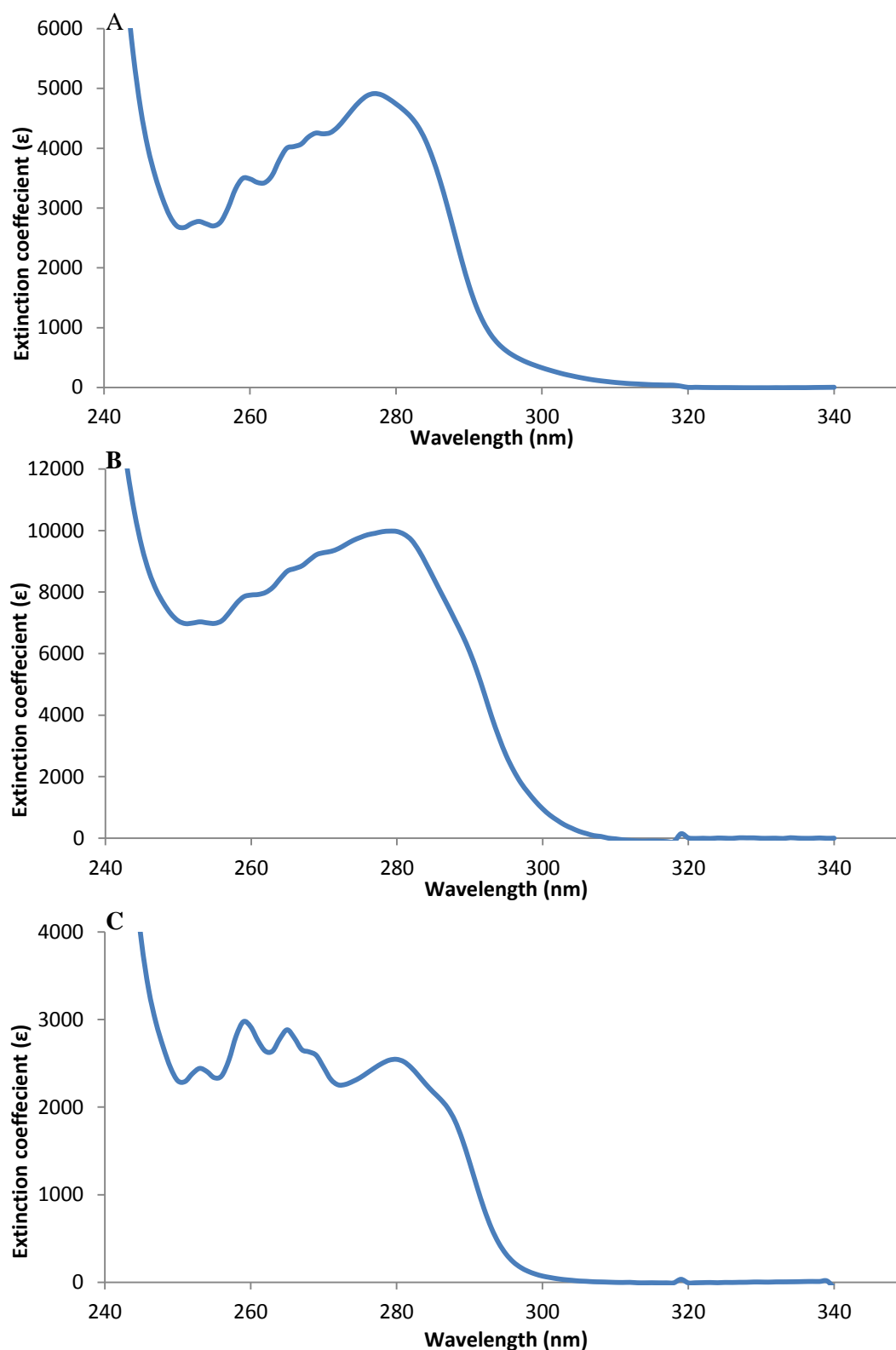


Figure. 2.7. UV/Vis spectra between 240 and 340 nm. Spectra of A, visinin-like domain B, visinin-like domain with autoinhibition and C, CaM1. Spectra are plotted as a function of the molar extinction coefficient. Spectra have been corrected for scatter by aggregate particles by subtracting a straight line throughout with the slope observed between 320 and 340 nm. The spike in the spectra at 319 nm is due to the change from the visible to the UV lamp.

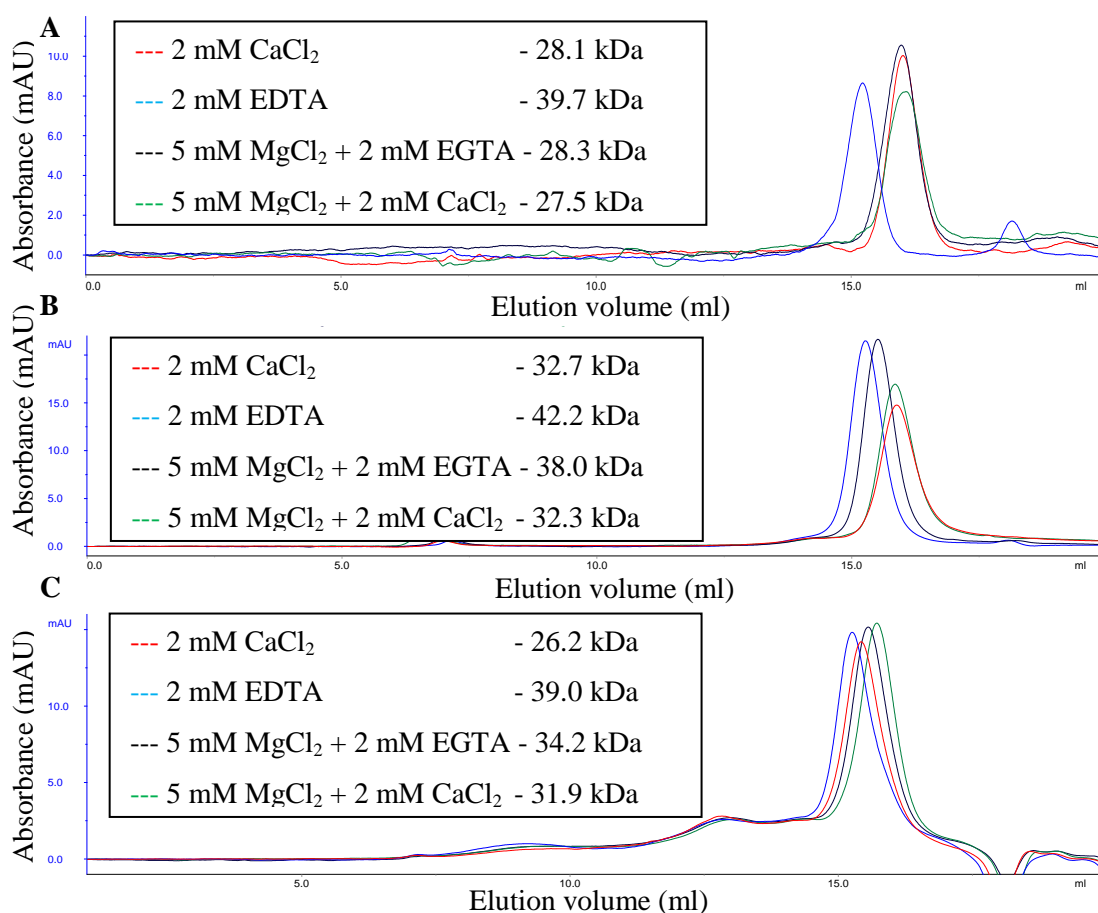


Figure 2.8. Analytical gel filtration of CCaMK regulatory domain constructs. Gel filtration chromatograms of A, visinin-like domain (expected mass 21.1 kDa). B, visinin-like domain with autoinhibition (23.5 kDa) and C, soybean trypsin inhibitor control (20.1 kDa). Gel filtration was performed in buffers containing either 2 mM CaCl₂ (red chromatograms), 2 mM EDTA (blue) 5 mM MgCl₂ and 2 mM EGTA (black) or 5 mM MgCl₂ and 2 mM CaCl₂. Tables show calculated molecular weights for the dominant peaks. Gel filtration was performed on an ÄKTA HPLC using a Superdex 200 10/300 GL analytical gel filtration column and data were processed using the Unicorn software package (GE Healthcare) and Microsoft Excel.

2.1.5 Determination of the calcium ion-binding stoichiometry of CCaMK

Manual analysis of the CCaMK sequence revealed that all three of the EF-hands identified previously (60) contain canonical sequences that would be expected to bind calcium-ions. As EF-hands are always found in pairs (discussed in chapter one section 1.1.4 “the EF-hand”) (26) and all NCS proteins contain four EF-hands, the first of which is inactive (62), it seemed likely that CCaMK contained a fourth EF-hand upstream of the previously reported sites.

Further analysis of the sequence with this in mind revealed a degenerate EF-hand binding loop, which has two substitutions in key positions highlighted in the alignment with the other three

binding loops in Figure 2.9. Although comparison to visinin, which contains four EF-hands has been made previously (60), this degenerate EF-hand has not previously been characterised in CCaMK. Tirichine *et al.* suggested that a fourth EF-hand may be present in CCaMK but this was not analysed further (64). The first substitution occurs in the fifth position, acting as the Z ligand, where an alanine (Ala384) is located. This is likely to have a profound effect on calcium ion-binding as the lack of an oxygen containing side chain, found in this position in canonical sequences (26), means a ligand to the calcium ion is missing. This is likely to reduce the favourability of binding a calcium ion considerably. A second substitution was found in the sixth position where glycine is absolutely conserved in active canonical EF-hands. In the degenerate EF-hand, it is substituted with a threonine residue (Thr385). As this glycine allows the binding loop to undergo a sharp turn of approximately 90° (26), it is likely that the degenerate binding loop is unable to adopt the correct conformation for complete coordination of a calcium-ion. Taken together, these substitutions suggest that the degenerate EF-hand is unlikely to bind calcium-ions. This means its function is likely to be as a structural scaffold to the neighbouring EF-hand and other elements of the protein, as is the case in other proteins containing non-ion-binding EF-hands (26). Analysis of the sequences from other CCaMKs showed that the AT amino acid substitution (residues 384-385) in EF-hand one is conserved, as shown in Figure 2.1, demonstrating that this EF-hand is unlikely to bind calcium ions in all CCaMKs.

Calcium ion-binding was observed experimentally by native page. Both the visinin-like domain and visinin-like domain with autoinhibition constructs migrated slower in excess CaCl₂ than in excess EDTA. As native page can report on shape, size and charge the cause of this shift was not determined (data not shown). This migration was in the opposite direction to gel shifts reported by Takezawa *et al.* for calcium ion-binding to CCaMK; however their experiments were performed using denaturing SDS-PAGE (61). These experiments were not able to inform on the calcium ion-binding stoichiometry. To verify the prediction of three sites made by sequence analysis, the protein was analysed by ESI-MS in the presence of excess calcium or magnesium-ions, EDTA or without additives. The -9 H⁺ state was selected for analysis as it combined the strongest signal for wild-type, shown in Figure 2.10 G, and enough separation between mass to charge (m/z) values for ion-bound states for correct identification. Expected apo masses were calculated by deducing 9 from the theoretical protein mass to account for the loss of 9 protons, then dividing by 9 to attain the correct mass to charge ratio. Masses for the addition of calcium-ions were calculated by deducing two from the mass of calcium (40.1) to account for the loss of two protons from the protein to balance charge, then dividing by 9 as described by Hu *et al.* (125). The same procedure was repeated for sodium to achieve expected differences of 2.4 and 4.2 for sodium and calcium ions, respectively, for the -9 charge state. All theoretical m/z ratios are shown in Table 2.1.

Ligand	X		Y		Z		-Y		-X			-Z
EF-hand one	D	R	D	N	A	T	L	S	E	F	E	E
EF-hand two	D	N	N	R	D	G	T	V	D	M	R	E
EF-hand three	D	T	D	R	S	G	C	I	S	K	E	E
EF-hand four	D	A	N	N	D	G	K	V	T	F	D	E
Consensus	D	-	D	G	D	G	-	I	oxy	-	-	E
			N	K/R N	S/N			V/L				D

Figure. 2.9. Manual alignment of CCaMK EF-hand binding loops. The ligand row shows the calcium ion-chelating positions. The consensus row displays the most common residue in a given position above, and other common residues below, where the most common residue is found in more than 50% of sequences (refer to chapter one section 1.1.4 “The EF-hand” and review by Gifford *et al.* (26)). “oxy” denotes positions of amino acids with oxygen containing side chains, whereas - denotes that a wide range of residues may be located in a given position. Residues shaded in black are found in more than 50% of sequences, grey shading corresponds to other residues found in functional EF-hands and residues that are not found in functional EF-hands are highlighted in red.

This experiment clearly demonstrated that CCaMK binds three calcium-ions. When calcium was not added the mass of the protein corresponded to the monomeric apo form, whereas the addition of calcium acetate gave a major peak corresponding to the three calcium ion-bound state as shown in Figure 2.10. No mass peaks corresponding to four bound ions were observed even though calcium-ions were in 5 fold excess over the protein concentration. Over the course of long injections it was observed that the ratio of the three calcium ion peak to lower occupancy forms decreased (data not shown). This suggests that the ESI-MS was stripping calcium ions from the protein slowly over time and thus the relative abundances may not be truly representative of occupancy in solution. However, this effect did not prevent the formation of a dominant peak for the maximum occupancy; therefore the data appear to be reliable when not assessed quantitatively.

The addition of EDTA removed all peaks corresponding to calcium ion-bound forms; however it gave rise to multiple, sodium-adduct peaks as shown in Figure 2.10 C. Without additives the major peak is the apo protein. However, a small amount of one calcium-ion bound is observed due to calcium ion-contamination in the buffer. Analysis of the visinin-like domain mutants demonstrated that the correct stoichiometries were observed when EF-hands were disabled. This is shown for mutants in EF-hand two, and the two-three double mutant in Figure 2.10 D and E, respectively, which are typical for the single and double mutant spectra.

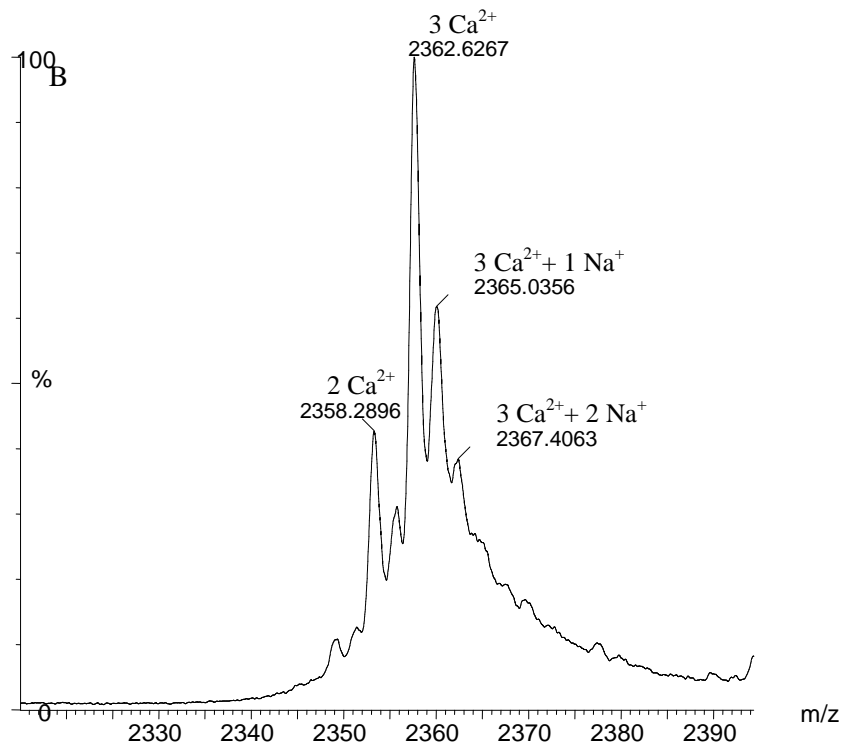
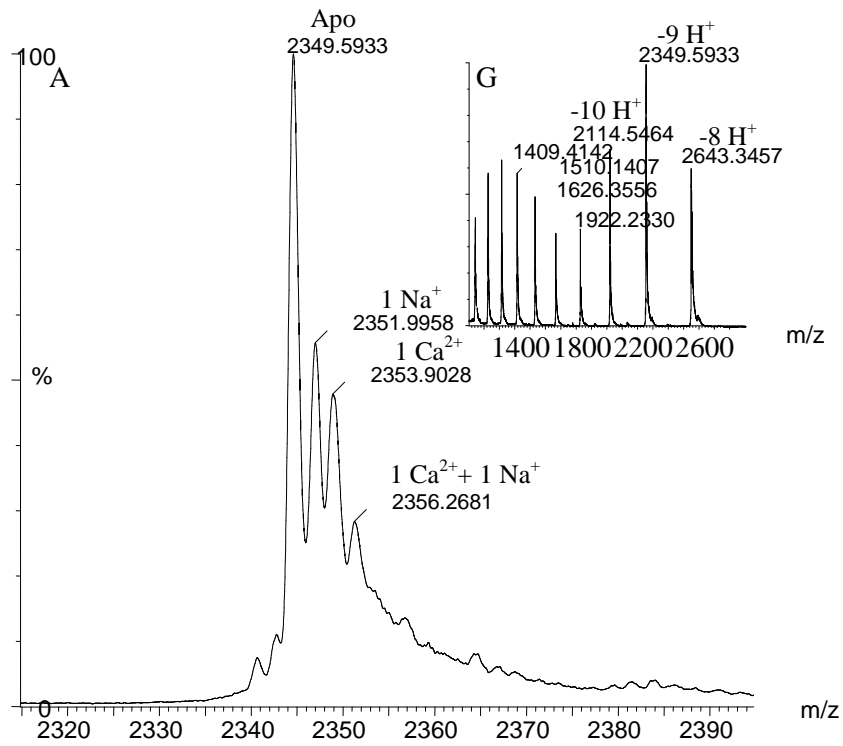
The addition of 500 μ M magnesium acetate demonstrated that magnesium ions also bind to CCaMK (shown in Figure 2.10 F), as is the case for most EF-hand containing proteins (26). As the

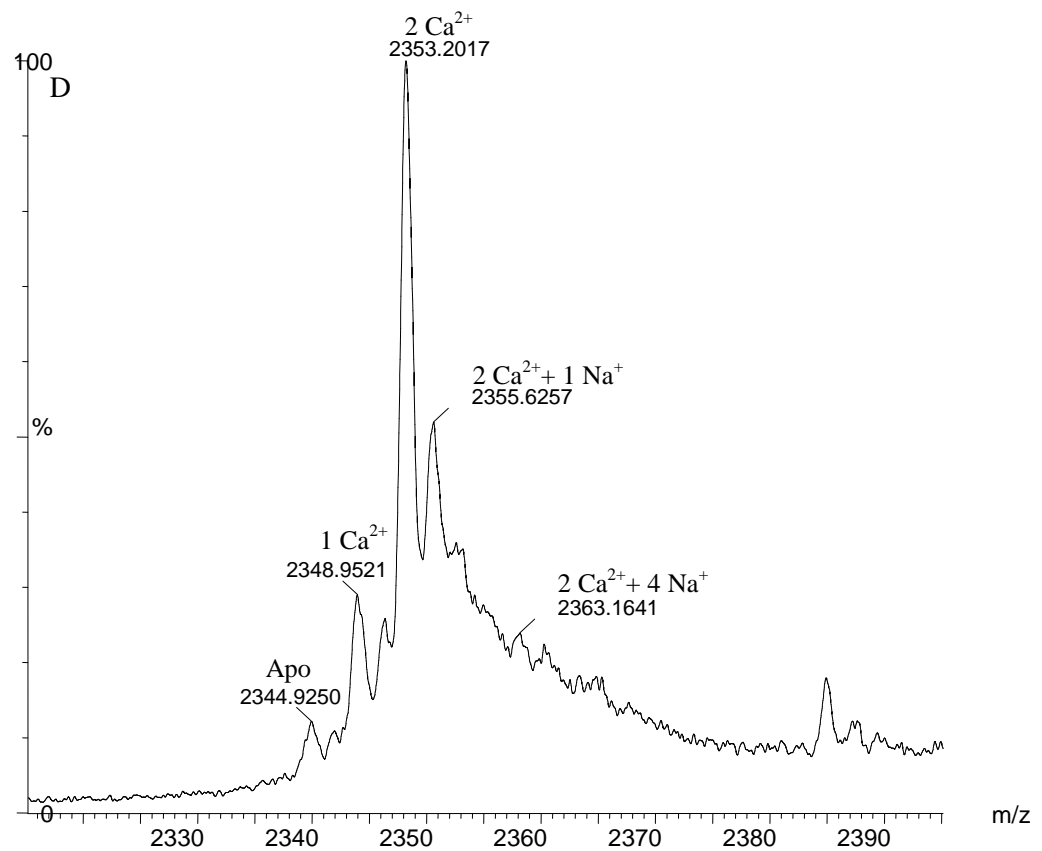
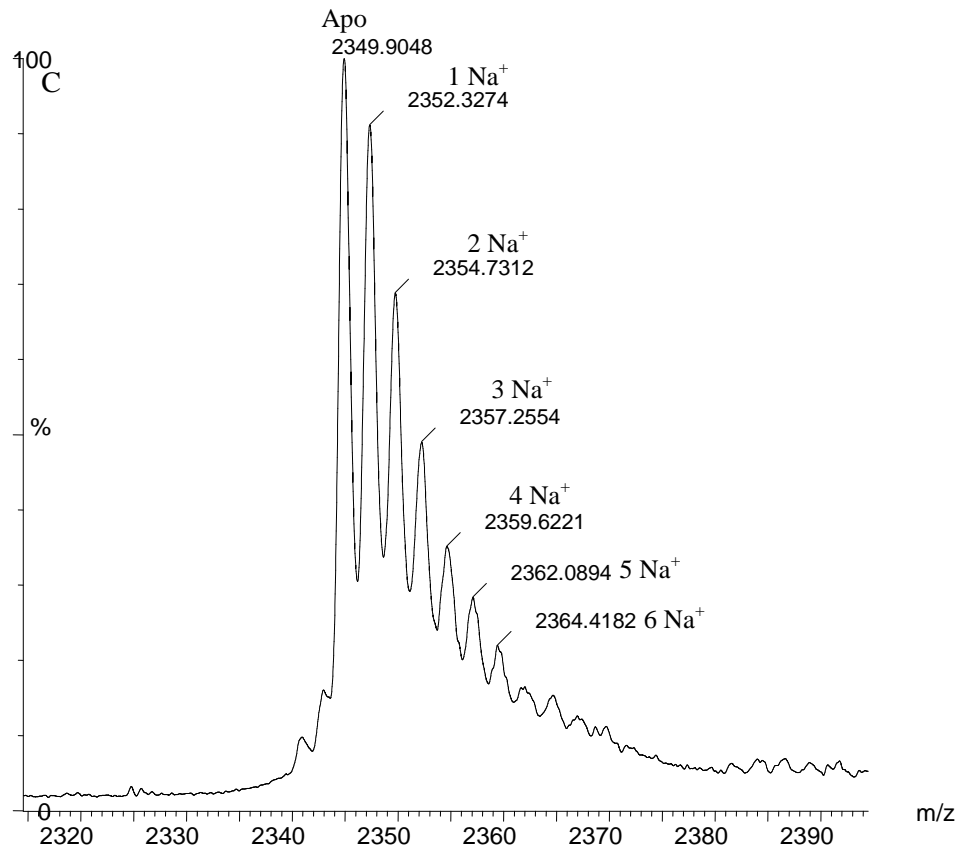
major peak corresponds to the three ion-bound state it is likely that magnesium occupies all three sites. This is supported by the single mutant spectra giving two ion-bound forms as the major peak in a pilot experiment (data not shown). The double mutants were not screened. The remaining peaks may correspond to sodium adducts or magnesium adducts. The two ions cannot be separated in this spectrum as the change in m/z for these ions are very similar at 2.2 and 2.3 for magnesium and sodium respectively. Given the large number of additional peaks, which exceeds that in the calcium acetate spectra, it is likely that there is a combination of sodium and magnesium adducts. It is probable that this affect is observed with the addition of magnesium but not calcium acetate due to the larger excess required. This increased excess was required because of the lower affinity for magnesium in all EF-hands (26).

Protein	Apo	+1 ion	+2 ions	+3 ions	+4 ions
	Apo	+1 Ca ²⁺	+2 Ca ²⁺	+3 Ca ²⁺	+4 Ca ²⁺
WT	2349.7	2353.9	2358.1	2362.4	2366.5
Single mutant	2344.8	2349.0	2353.2	2357.4	-
Double mutant	2339.9	2342.4	2346.6	-	-
	Apo	+1 Mg ²⁺	+2 Mg ²⁺	+3 Mg ²⁺	+4 Mg ²⁺
WT	2349.7	2352.1	2354.6	2357.1	2359.6
Single mutant	2344.8	2344.8	2347.3	2349.7	-

Table. 2.1. Theoretical mass to charge (m/z) ratios for the ESI-MS spectra of CCaMK visinin-like domain.

Values are shown for the -9 H⁺ charge state with calcium or magnesium ions bound. Values for the wild-type, single and, where relevant, double mutants are shown.





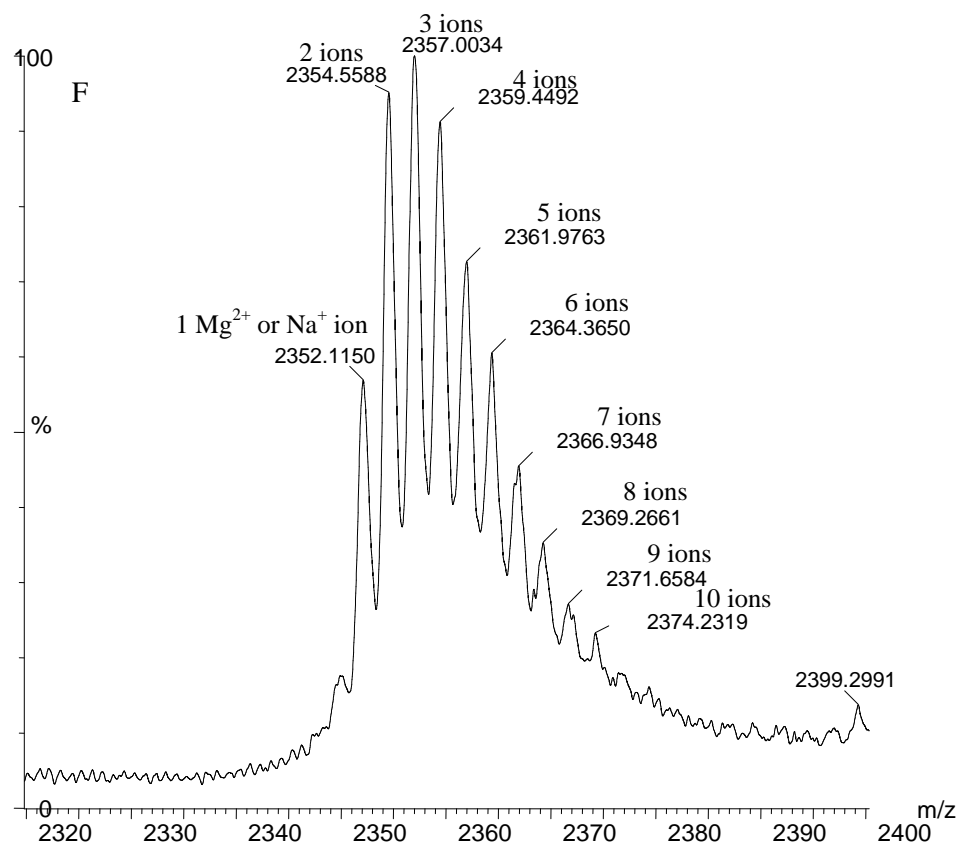
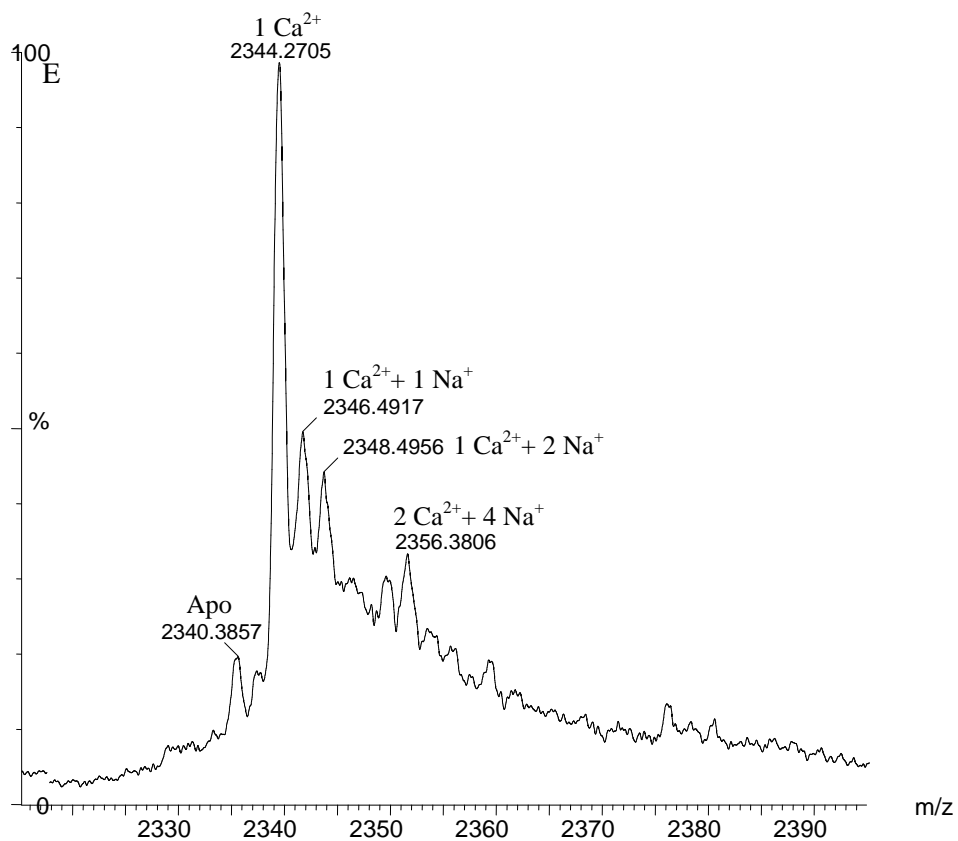


Figure. 2.10. Electrospray ionisation mass spectra of the CCaMK visinin-like domain. A, zoomed $-9 H^+$ peak of the wild-type visinin-like domain without additives. B, zoomed $-9 H^+$ peak in the presence of $100 \mu M$ calcium acetate or C, $100 \mu M$ EDTA. D, visinin-like domain mutant EF-hand two showing a typical spectrum for the single mutants and E, mutant EF-hands two-three showing a typical spectrum for the double mutants in $100 \mu M$ calcium acetate. Masses corresponding to the calcium-ion occupancy and sodium adducts are labelled. F, wild-type visinin-like domain in $500 \mu M$ magnesium acetate, peaks are labelled with “ion” as magnesium and sodium ion-bound peaks cannot be separated. Panel G, shows the full spectrum of the protein without calcium, masses corresponding to the -8 to $-10 H^+$ states are labelled. Theoretical masses are shown in Table 2.1.

2.1.6 Determination of the CCaMK regulatory domain oligomerisation state

As CCaMK was predicted to contain a coiled-coil motif (described in section 2.1.3 prediction of the kinase domain boundary and additional features of CCaMK) that, by analogy with CaMKII may act as a dimerisation interface, it was necessary to determine the oligomerisation state experimentally. The predicted coiled-coil of CCaMK is present in both the visinin-like domain and visinin-like domain with autoinhibition constructs. It was shown by analytical ultracentrifugation that the CCaMK regulatory domains are monomeric in their apo, calcium ion and magnesium ion-bound forms as shown in Table 2.2. This demonstrated that the predicted coiled-coil is not a CCaMK dimerisation interface as seen in CaMKII. However, the full length CCaMK may behave differently and will need to be assessed in future experiments.

Construct	Concentration μM	Condition	Mw by AUC kDa	Theoretical Mw of monomer kDa
visinin-like domain	125	CaCl ₂	20.8 ± 0.1	21.1
		EDTA	24.5 ± 0.1	
		MgCl ₂	24.1 ± 0.2	
visinin-like domain with autoinhibition	50	CaCl ₂	23.7 ± 0.1	23.5
		EDTA	25.3 ± 0.1	
		MgCl ₂	$20.9 \pm 0.2^*$	

Table. 2.2. Analytical ultracentrifugation of CCaMK regulatory domain constructs

*Data are shown for simultaneous fitting to 10 000, 15 000 and 20 000 RPM equilibrium data. Fitting was performed using the 1-component ideal model in the Ultrascan II software package (126). Values highlighted with * indicate “acceptable” fits; all other values correspond to “good” fits as determined in the Ultrascan II fitting report. Concentrations were selected to give 0.5 – 0.6 absorbance units at 280 nm. Errors were estimated by Monte Carlo analysis.*

2.1.7 Determination of the visinin-like and autoinhibitory domains secondary structure

To assess alterations in secondary structure upon calcium ion-binding, the CCaMK regulatory domains were analysed by far-UV CD spectroscopy. The spectra revealed that the visinin-like domain and visinin-like domain with autoinhibition are predominately alpha helical as shown in Table 2.3 and Figure 2.11. The estimated secondary structure content of the visinin-like domain of 60% helix and 4% strand in the calcium ion-bound form is similar to that of the solved crystal structure of calcium ion-bound bovine neurocalcin, which consists of 54% helix and 5% strand (109). This supports the bioinformatic prediction that these proteins are related.

Addition of $MgCl_2$ gave spectra that were almost identical to the apo form suggesting that magnesium ion-binding has no effect on the protein conformation (Table 2.3). This shows that the protein is very likely to be fully folded in its apo form and does not require the binding of magnesium-ions for correct folding as is the case for soybean CaM isoform four (127). When spectra were collected in the presence of $CaCl_2$, the wild-type visinin-like domain spectral maxima shifted from 191.4 to 192.8 nm. A similar shift was also seen in the visinin-like domain with autoinhibition as shown in Figure 2.11 A. This had previously been observed in calbindin D_{28K} and dismissed as noise (128). However, as these spectra are generally reliable above 185 nm, this shift is likely to be a significant effect of calcium ion-binding. Deconvolution of the spectra showed that the binding of either calcium-ions or magnesium-ions had no effect on the helical content, but some changes strand, turn and unordered content were predicted upon calcium ion-binding. This may provide an explanation for the shift in the maxima observed. However, as they were small it cannot be determined which, if any of these changes are significant. A perturbation of the strand conformation is likely to occur upon calcium ion-binding as two residues in each binding loop form an antiparallel β -strand with the corresponding residues in the neighbouring EF-hand (for a more in depth discussion see review by Gifford *et al.*) (26). It has previously been shown by molecular dynamics modelling that the strands are affected by conformational changes upon calcium ion-binding in calbindin D_{9K} (129).

Analysis of the EF-hand mutants, shown in Figure 2.11 B and Table 2.3, demonstrated that the secondary structure content of mutants two, four and the two-four double mutant are very similar to wild-type in the calcium and magnesium ion-bound, and apo forms. The mutant of EF-hand two differed from the wild-type in that the shift in the maximum did not occur upon calcium ion-binding (Figure 2.11 B). This effect was also observed in the EF-hand two-three and two-four double mutants. These data suggest that calcium ion-binding to EF-hand two may initiate different conformational changes to EF-hands three or four.

Mutation of EF-hand three and of two-three gave a reduced signal corresponding to a reduced helical content and increased disorder in the apo and ion-bound forms. This may suggest that mutation of EF-hand three alters the fold slightly or reduced protein stability.

Construct	Condition	Total helix %	Total strand %	Turns %	Unordered %
Visinin-like domain with autoinhibition	EDTA	64	5	11	19
	CaCl ₂	67	5	11	17
	MgCl ₂	63	6	12	18
Visinin-like domain (wild-type)	EDTA	60	11	13	16
	CaCl ₂	60	4	13	21
	MgCl ₂	61	9	13	16
Visinin-like domain Mutant EF-hand two	EDTA	58	11	13	18
	CaCl ₂	59	6	13	22
	MgCl ₂	61	8	14	17
Visinin-like domain Mutant EF-hand three	EDTA	50	13	14	22
	CaCl ₂	51	9	16	23
	MgCl ₂	51	12	14	23
Visinin-like domain Mutant EF-hand four	EDTA	58	9	15	17
	CaCl ₂	56	7	15	22
	EDTA	58	9	14	19
Visinin-like domain Mutant EF-hands two and three	EDTA	47	9	16	27
	CaCl ₂	45	11	16	28
Visinin-like domain Mutant EF-hands two and four	EDTA	65	5	12	18
	CaCl ₂	60	6	11	24

Table 2.3. Secondary structure of CCaMK regulatory domains and EF-hand mutants.

Values for secondary structure elements determined from deconvolution of far-UV CD spectra using the Dichroweb server (130) with the CDSSTR algorithm (131). Values for helix and strand are combined totals from the subtypes of helix (alpha and 3₁₀) and strand (parallel and antiparallel) given by the CDSSTR output. CDSSTR was selected as it provided the lowest RMSD (0.008) values for fitting to the wild-type visinin-like domain data. Fitting with CONTIN and SELCON3 gave RMSD values of 0.07 and 0.24, respectively.

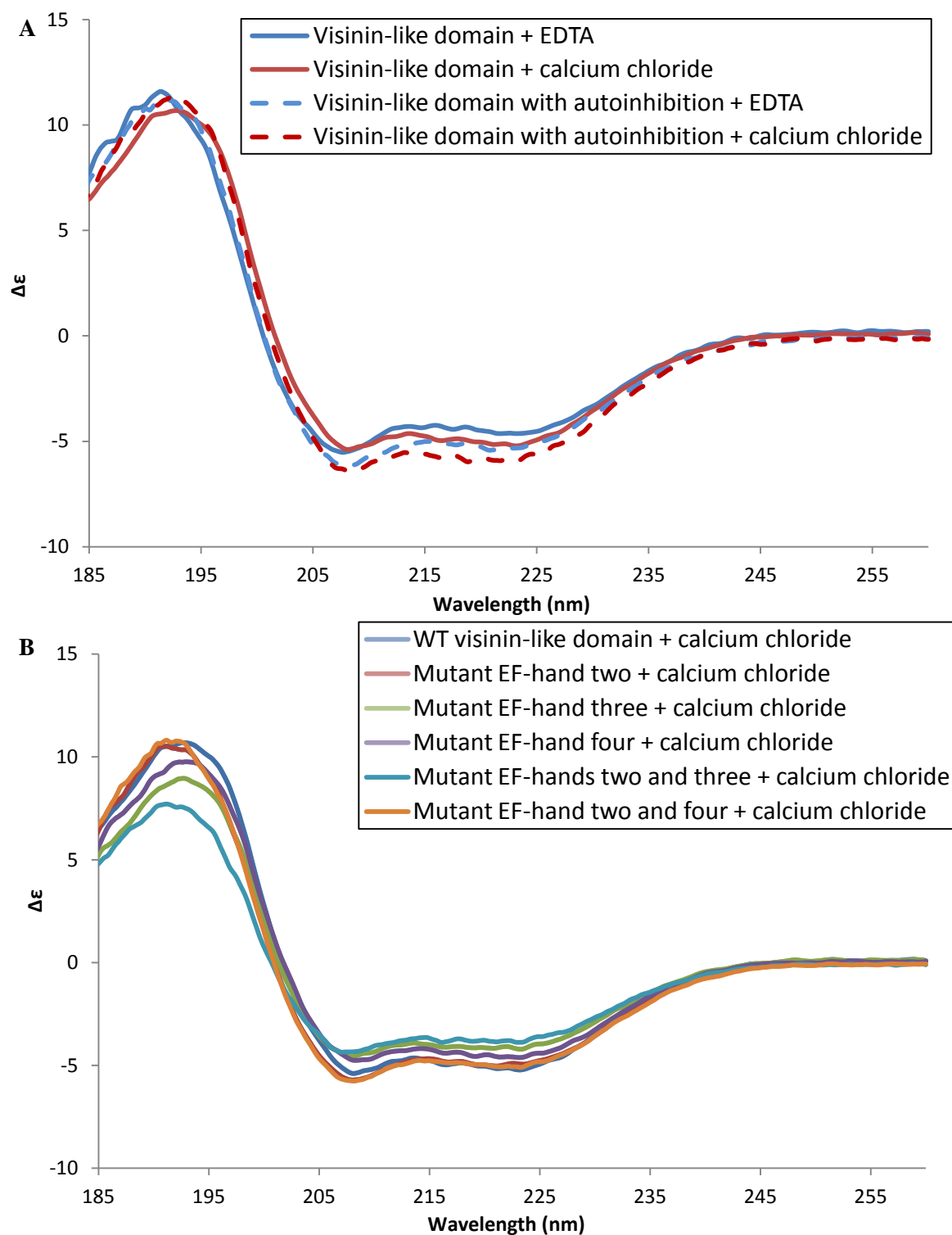


Figure 2.11. Far-UV CD spectra. A, CCaMK visinin-like domain (solid lines) and the visinin-like domain with autoinhibition (dashed lines) in the presence of either 2 mM CaCl₂ (red) or 2 mM EDTA (blue). B, wild-type visinin-like domain (blue lines) and visinin-like domain EF-hand single mutants (two – red, three – green, four – purple, two-three – cyan, two-four – orange) in the presence of 2 mM CaCl₂. The pathlength was 0.1 mm and the protein concentration was 40 μM

Comparison of the visinin-like domain with autoinhibition with the visinin-like domain revealed that the former construct contains a higher alpha helical content, as shown in Table 2.3. By calculating the number of additional residues in an alpha helical conformation, it was possible to predict that the increased alpha helical content corresponds to the autoinhibitory domain. As the visinin-like domain is 184 residues long and 60% corresponds to alpha helix, the visinin-like domain construct contains approximately 110 residues in alpha helical conformation in both excess CaCl_2 and EDTA. The visinin-like domain with autoinhibition is 207 residues in length and was shown to be 64% alpha helical in EDTA corresponding to approximately 132 amino acids, and 67% alpha helical in CaCl_2 corresponding to approximately 139 amino acids. This means that the visinin-like domain with autoinhibition contains approximately 22 and 28 more residues in an alpha helical confirmation in the presence of EDTA and CaCl_2 , respectively, which corresponds well to the additional sequence of 23 residues corresponding to the autoinhibitory domain. It is worth noting that the differences between the two constructs alpha helical content are within accepted errors, which are typically 2-3%. Nevertheless this demonstrates that the autoinhibitory domain from residue 317 to 346 is likely to be alpha helical and supports the prediction that it is analogous to the autoinhibitory domain of CaMKII.

2.1.8 *Evidence of overall conformational changes in CCaMK*

Near-UV circular dichroism of aromatic residues is highly influenced by their local environment, so it was used to monitor conformational changes upon calcium ion-binding. The combination of these spectra with knowledge of the structural elements of CCaMK and visinin-like domain mutants allowed details of the conformational changes that occur upon calcium ion-binding to be determined.

In near-UV CD spectra, aromatic amino acids give signals at the same wavelengths as their UV absorbance. This means that phenylalanine signals range from 250 to 270 nm whilst tyrosine and tryptophan signals range from around 250 to 295 and to 305, respectively. These signals may be either positive or negative and vary in intensity and shape depending on their local environment (132). As shown in Figure 2.12, the spectra of both the visinin-like domain and the visinin-like domain with autoinhibition showed signals for tyrosine and phenylalanine residues. No additional signal was seen for the visinin-like domain with autoinhibition when compared to the visinin-like domain between 270 and 295 nm. As the tryptophan present in the autoinhibitory domain would be expected to absorb strongly in this range, it can be concluded that there is no signal from Trp26 (Trp342 in the full CCaMK sequence) in the spectrum of the visinin-like domain with autoinhibition. As tryptophan has no chiral atoms in its side chain, it only exhibits circular dichroism at 280 nm when in an optically asymmetric environment, which arises from burial in the core of a protein. Consequently an optically symmetrical environment such as the solvent will result in no circular dichroism (for further detail see review on CD spectroscopy by R. Pain) (132). From this it can be concluded that the tryptophan residue is solvent exposed in the visinin-like

domain with autoinhibition and does not interact with the visinin-like domain in this construct. In the apo form spectra of the visinin-like domain and visinin-like domain with autoinhibition differ slightly in the 250-270 nm range. This is likely to be a result of signals from one or both of the additional phenylalanine residues contained within the autoinhibitory domain.

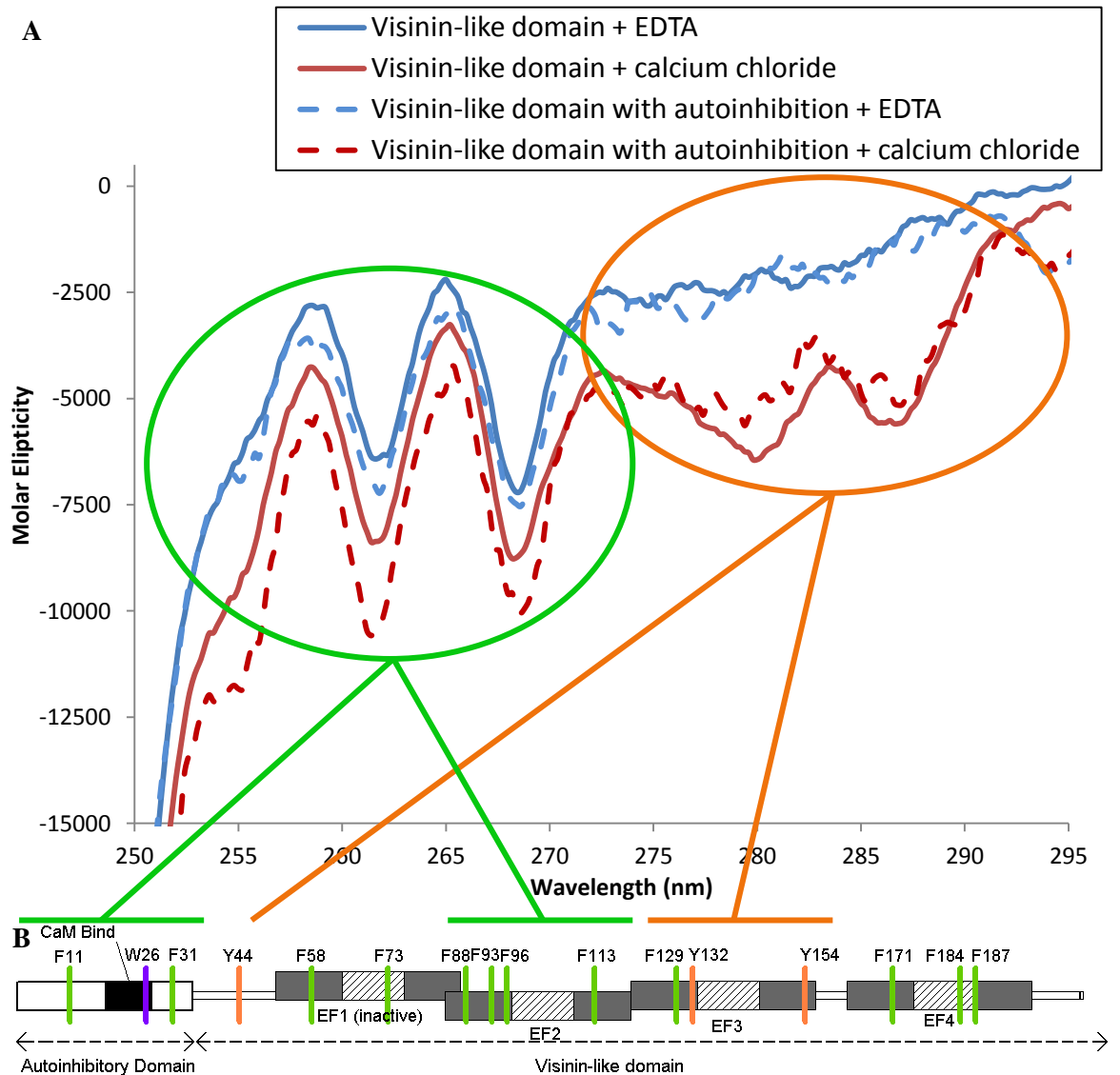


Figure. 2.12. Near-UV CD spectra of the CCaMK regulatory domain constructs. A, spectra of the visinin-like domain (solid lines) and the visinin-like domain with autoinhibition (dashed lines) in the presence of either 2 mM CaCl_2 (red) or 2 mM EDTA (blue). B, illustration of the predicted structural features of the visinin-like domain with autoinhibiton, EF-hands are highlighted in grey with calcium ion-binding loops highlighted with diagonal lines. The autoinhibitory domain is illustrated with a white box and the predicted CaM binding site is highlighted in black. The locations of phenylalanine residues (green), tyrosine residues (orange) and tryptophan residues (purple) are also shown. Circles and lines highlight regions of the protein giving rise to alterations in specific regions of the spectrum upon calcium ion-binding.

Comparison of the apo and the calcium ion-bound forms of both constructs showed that there was an increase in negative signal over the full spectral range upon calcium-ion binding. This result suggests that the environments of both tyrosine and phenylalanine residues have been altered upon calcium ion-binding. As the signal for the visinin-like domain with autoinhibition increased a little more in the 250-270 nm range than that of the visinin-like domain in isolation (probably related to Phe11 and/or 31), it implies that the autoinhibitory domain undergoes conformational changes upon calcium ion-binding.

To further deconvolute the spectra, the visinin-like domain EF-hand mutants were analysed and the data was compared to the wild-type as shown in Figure 2.13. The spectra of the apo forms were similar suggesting that the apo structures are similar. The spectra of the calcium ion-bound forms showed many significant differences. All spectra displayed a less negative signal in the 270-295 nm region, which corresponded to the tyrosine signal. This may be linked to any of the three tyrosine residues. However, comparison of the mutants suggests it is most likely to be associated with Tyr44 (Tyr360 in the full CCaMK sequence) as described below.

The EF-hand two mutant showed an increased phenylalanine signal (250-270 nm) in the calcium ion-bound form when compared to wild-type, which is possibly linked to any of the phenylalanine residues in EF-hand two as illustrated in Figure 2.12. The EF-hand three mutant showed a large decrease in signal throughout probably due to loss of signal from the Tyr132 (Tyr470) adjacent to the third EF-hand binding loop and possibly Tyr 154 (Tyr492) at the end of EF-hand three. The reduction in signal upon calcium ion-binding to the EF-hand three mutant suggests the one of the tyrosine residues outside of EF-hand three, probably Tyr44 (Tyr382), loses signal upon calcium-ion binding. This suggests that there may be alterations in the N-terminal region of the visinin-like domain upon calcium ion-binding to EF-hands two and/or four. This may not be seen in the wild-type as this signal is swamped out by the larger signal relating to EF-hand three. In contrast to EF-hands two and three, the mutant in EF-hand four showed no significant differences in the phenylalanine range. This suggests that phenylalanines within EF-hand four (shown in Figure 2.12) are unlikely to be affected by calcium ion-binding.

Analysis of the double mutants allows further deconvolution of the spectra. The spectrum of the EF-hand two-four double mutant was almost identical to the EF-hand two single mutant supporting the interpretation that calcium ion-binding to EF-hand four does not lead to alterations in the phenylalanine signal. This means that the majority of the alterations in the phenylalanine signal originate from calcium ion-binding to EF-hand two. The EF-hand two and three double mutant showed no change in the spectrum from the apo state. In addition no reduction in tyrosine signal was seen, as was the case for the EF-hand three single mutant. This suggests that a signal from Tyr44 may either be linked to calcium ion-binding to EF-hand two, or a global conformational change, which is abolished in the two-three double mutant.

Taken together, these data show that the majority of the signals seen for calcium ion-binding to both the wild-type visinin-like domain and the visinin-like domain with autoinhibition are due to local rearrangements in EF-hand two and three. Some additional signals appear to give evidence for further global conformational changes and alterations in the interaction of the visinin-like domain with the autoinhibitory domain.

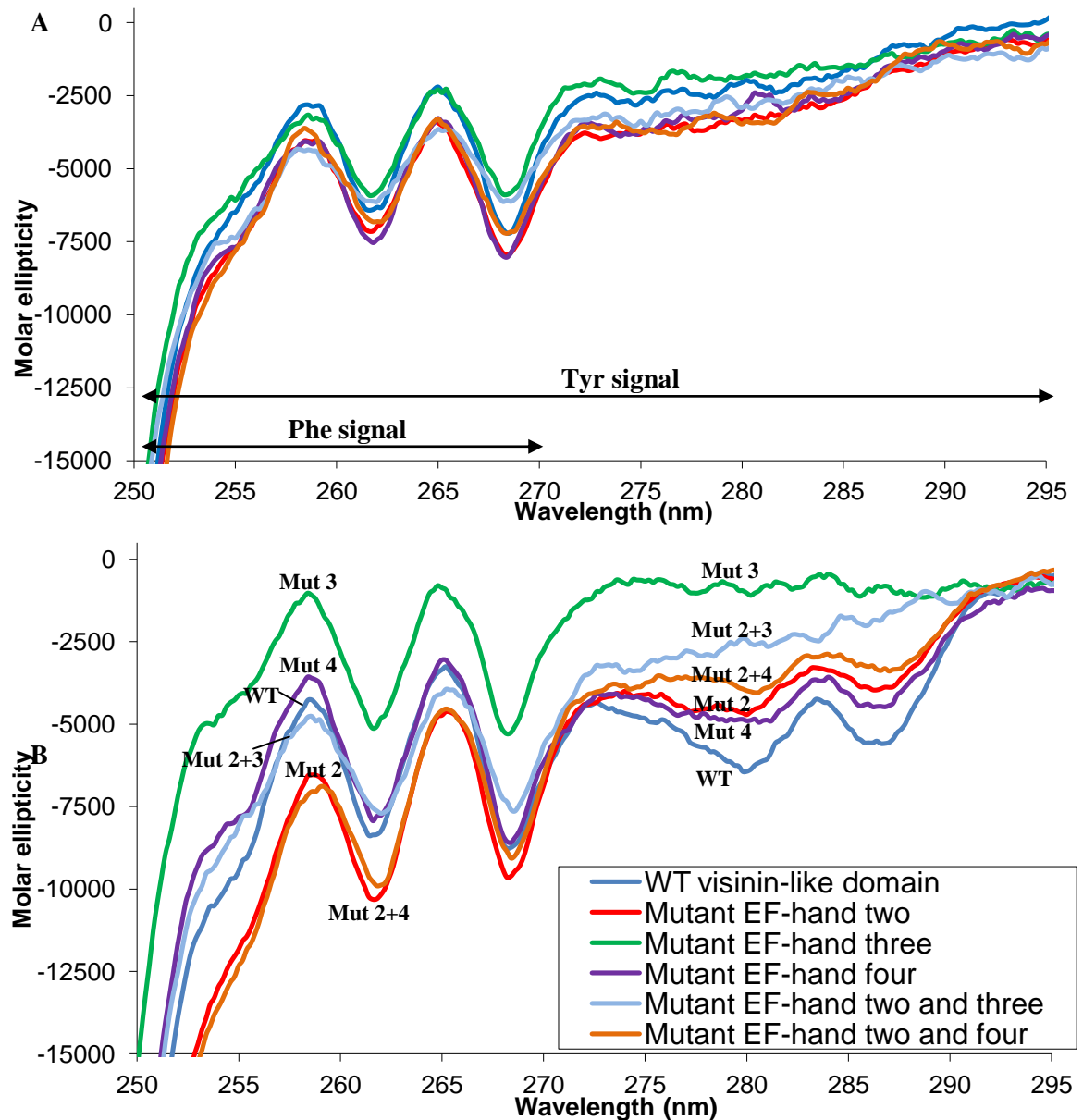
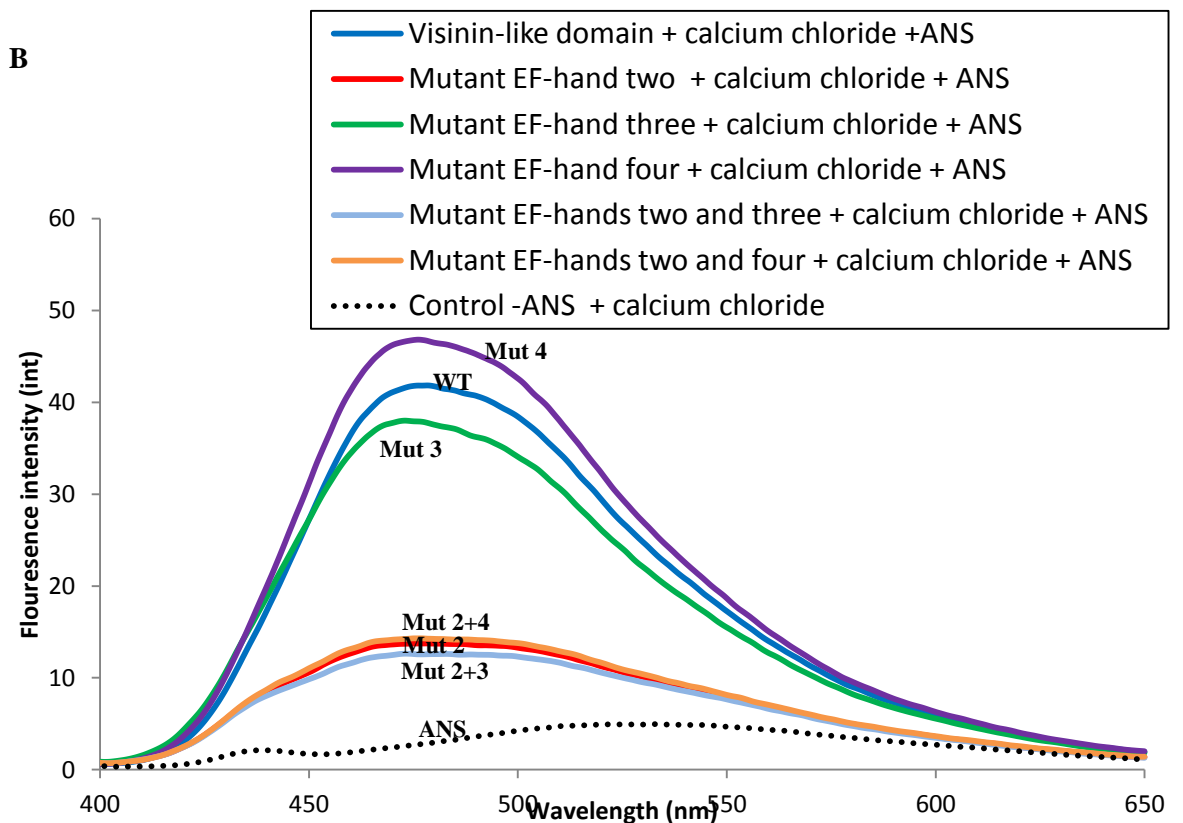
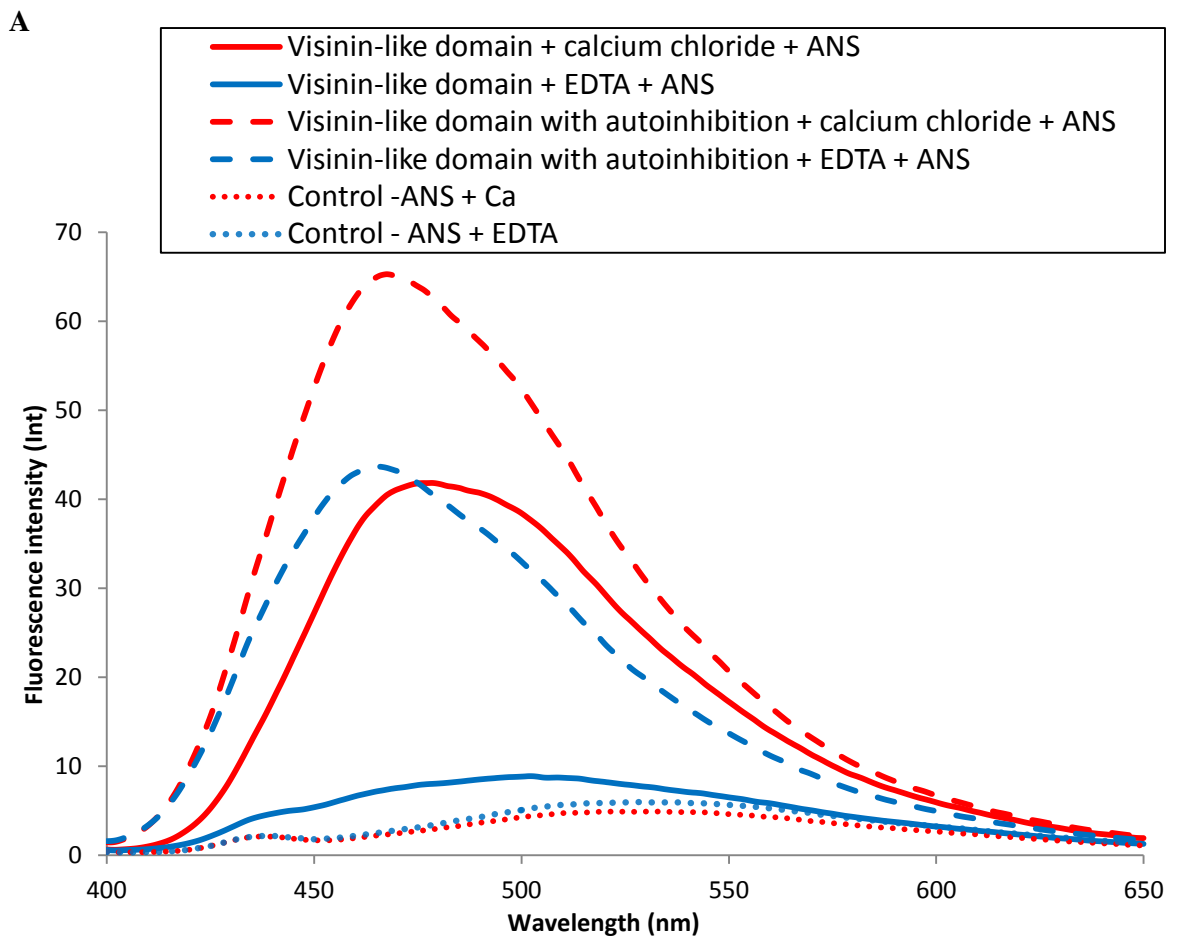


Figure. 2.13. Near-UV CD spectra of the CCaMK visinin-like domain and visinin-like domain EF-hand mutants. A, spectra in the presence of 2 mM EDTA and B, spectra in the presence of 2 mM CaCl₂. Spectra of wild-type visinin-like domain (blue lines) and visinin-like domain EF-hand mutants (two – red, three – green, four – purple, two and three – cyan, two and four orange) are shown. Annotations on A show the regions of the spectrum influenced by Tyr and Phe residues and annotations on B highlight each curve (Abbreviated to “Mut #” for mutants or “WT” for wild-type)



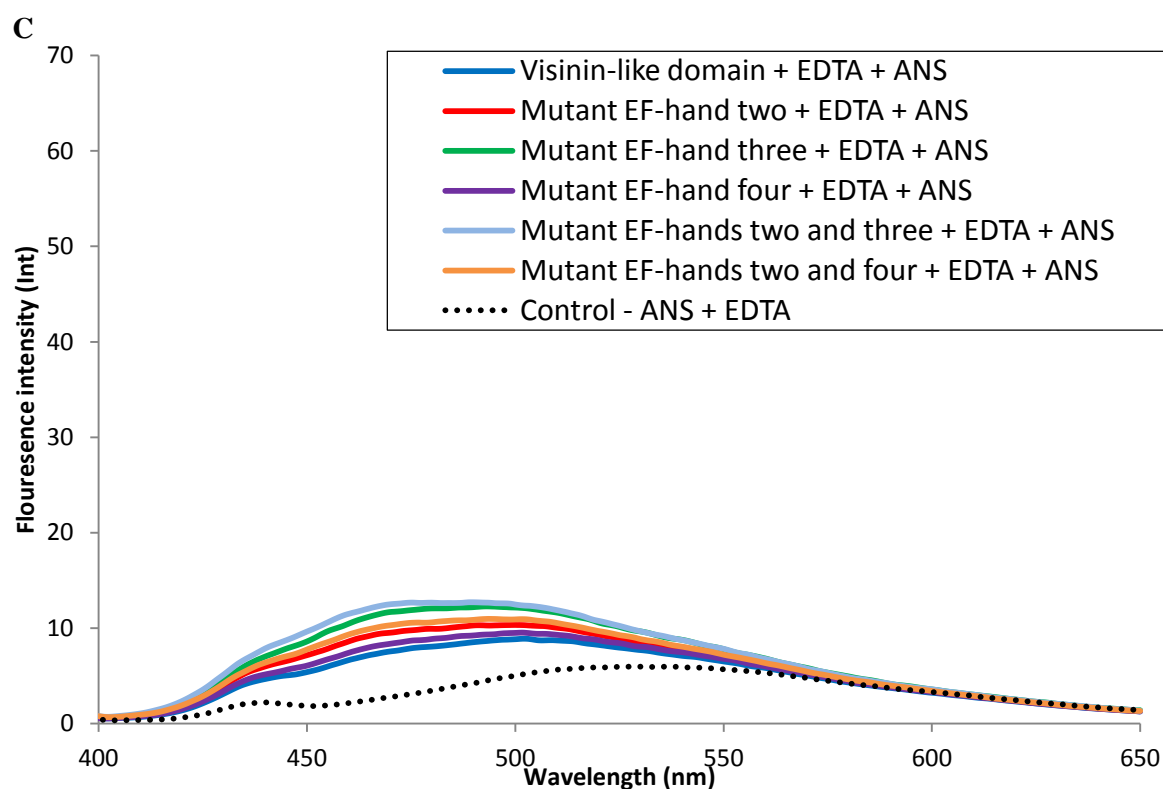


Figure. 2.14. ANS fluorescence spectra. A, fluorescence spectra of the CCaMK visinin-like domain (solid lines), visinin-like domain with autoinhibition (dashed lines) and ANS only controls (dotted lines) in the presence of either 2 mM CaCl_2 (red lines) or 2 mM EDTA (blue). B, spectra in the presence of 2 mM CaCl_2 or C, 2 mM EDTA of visinin-like domain (solid blue line), visinin-like domain EF-hand mutants (two – red, three – green four – purple, two-three – cyan and two-four – orange) and ANS only control (black dotted line). All spectra were collected in the presence of 15 μM ANS using an excitation wavelength of 380 nm. Annotations on B highlight each curve (Abbreviated to “Mut #” for mutants or “WT” for wild-type)

2.1.9 Monitoring of hydrophobic exposure upon calcium ion-binding

ANS is a hydrophobic dye, which increases its fluorescence signal upon binding to hydrophobic regions of proteins. ANS fluorescence spectra of the CCaMK visinin-like domain and visinin-like domain with autoinhibition showed that hydrophobic exposure is increased upon calcium ion-binding as shown in Figure 2.14 A. This has been reported to occur in many calcium ion-binding proteins such as CaM (85) and calcium and integrin-binding protein (an NCS family protein) (133). The visinin-like domain with autoinhibition gave a larger signal than the visinin-like domain in both the calcium ion-bound and apo forms suggesting additional hydrophobicity from the autoinhibitory domain.

Analysis of the EF-hand mutants revealed that inactivation of EF-hand two abolishes the increase in ANS signal, whereas the signal increase still occurred in mutants of EF-hand three and

four as shown in Figure 2.14 B. The same loss in signal was also observed in the EF-hand two-three and two-four double mutants (Figure 2.14 B). This shows that the majority of hydrophobic exposure observed is a property of calcium ion-binding to EF-hand two. All mutants gave a similar signal to wild-type in the presence of excess EDTA (Shown in Figure 2.14 C) suggesting that they are all correctly folded and stable in the apo form.

2.1.10 Low resolution structures of the CCaMK regulatory domains and calmodulin

In order to gather more structural information on the CCaMK visinin-like and autoinhibitory domains, small angle X-ray scattering (SAXS) experiments were performed. Although this technique does not provide high resolution structures, the low resolution molecular envelopes and the associated parameters provide information on the overall shape of the molecule. By analysing the visinin-like domain, visinin-like domain with autoinhibition and visinin-like domain EF-hand mutants in their apo and calcium ion-bound forms the conformational changes, which occur upon calcium ion-binding, could be assessed in terms of the overall shape of the molecule.

Low resolution structures showed that mtCaM1 has a similar structure in solution to the solved atomic structures of potato CaM in its calcium ion-bound form, and *Xenopus* CaM in its apo form as shown in Figure 2.15 A and B. The Kratky plots for the CaM data (shown in Figure 2.15 D) are typical profiles for globular proteins (134) demonstrating that CaM is folded in its apo and calcium-ion bound forms. An unfolded protein gives a Kratky plot, which has a flat rather than a bell-shaped profile between angles of $0.5\text{-}2\text{ nm}^{-1}$ (134).

The logI plots (log intensity vs. angle of scattering in Figure 2.15 E) showed evidence for a conformational change as the curves differed from one another. From the curves the radius of gyration (R_g) was estimated using the Guinier approximation in which the R_g was extrapolated from the linear portion of the raw, buffer subtracted intensity curve at low angles of $S \cdot R_g$ less than 1.3 (see review by H. D. Mertens for a brief description (134)). R_g values for all proteins analysed are shown in Table 2.4. The R_g was determined using the program AutoRg, which also provided a measure of sample quality by assessing linearity at low angles. Deviations from linearity are a sign of weak attractive or repulsive effects between molecules in solution, as well as the presence of aggregates. The linearity of the curve at low angles, the number of data points discarded from the curve and the accuracy of the R_g calculation are considered when assessing quality of the data. This quality is expressed as a percentage as shown in Table 2.4. Usually, quality of above 50% is considered to be acceptable. (135). Both CaM curves were determined to be of high quality showing that CaM was not aggregated. Molecular masses were determined by comparison of the initial scattering intensity with a standard, which was BSA. The Deviations from the expected values indicate the inaccuracy of the concentration measurement (134). For CaM, molecular weights were above the expected value of 17 kDa as shown in Table 2.4. However the molecular weights were close to the theoretical values.

Pair distance distribution $P(r)$ curves are generated from an indirect Fourier transform of the scattering data, the shape of which is related to the shape of the molecule in solution (134). To produce $P(r)$ curves the value for the maximum particle diameter (D_{\max}) must be provided by the user, however autoGNOM analyses outputs from multiple GNOM runs and determines the best value of D_{\max} computationally (135). Analysis of the $P(r)$ curves for CaM (Figure 2.15 C) showed that the conformational change resembles an alteration from a dumbbell shape (signified by a two-peak profile) in the apo form, to a prolate ellipsoid shape (signified by a left skewed single peak) in the calcium-ion bound form (134), which is also evident from the SAXS envelopes (Figure 2.15 A and B). The increase in D_{\max} but not R_g (shown in Table 2.4) suggests that mtCaM1 becomes more elongated upon calcium ion-binding. This is also evident when the crystal structures of apo *Xenopus* CaM and calcium ion-bound potato CaM are compared.

The GNOM outputs were used for *ab initio* modelling of the SAXS data. This was performed in DAMMIF, which uses a sphere of densely packed dummy atoms represented as beads, and searches for the best model to describe the SAXS curves by randomly adding or removing these beads. This method applies several constraints to ensure probable models are produced, for instance disconnected structures are rejected, and the maximum particle size is determined by D_{\max} . DAMMIF produces envelopes, which are inclusive of the solvation shell surrounding the protein. Modelling was also performed in GASBOR, which uses dummy residues to approximate the structure of the protein core. This is achieved searching randomly within a sphere of diameter of D_{\max} with a number of dummy residues that matches the number of amino acids in the protein under investigation. The algorithm contains penalty terms, which reject non-protein-like structures in order to produce the most probable models. This approach also allows GASBOR to fit the data to much higher angles than DAMMIF ($> 10 \text{ nm}^{-1}$ rather than $\sim 2.5 \text{ nm}^{-1}$) as the assumption that electron density is uniform throughout the molecule is not employed, whereas this is applied in DAMMIF. For more detail on *ab initio* modelling see review by Mertens and Svergun (134). As there was variation in the models from each run of DAMMIF or GASBOR, each method was run 10 times, and then averaged models were produced using DAMAVER. This program aligns the models and then removes atoms/residues with low occupancy and loose connections to the rest of the molecule (136). As the approaches of DAMMIF and GASBOR differ, the models they produce are not identical; however, they should be similar and thus complimentary to one another.

SUPCOMB aligns three-dimensional structures by minimising the normalized spatial discrepancy (NSD) between objects. Values of less than one suggest that the two items are highly similar. However when overlaying high and low resolution data values above one are typical as SAXS envelopes also contain the hydration shell, which is not present in atomic level structures (137). Values of approximately 1.1-1.25 are typical for ideally matched crystal and SAXS structures, whilst values of 2.24 are seen when non-related crystal and SAXS structures are aligned.

The NSD values for the CaM alignments are higher than the ideal values. In the case of the calcium ion-bound structures this may be due to flexibility in the molecule. This will be represented in the SAXS structure, but not in the crystal structure of potato CaM. This may mean that the mtCaM1 in solution may adopt a slightly different average conformation to the potato CaM in the crystal. In the case of the alignment with *Xenopus* CaM the differences may arise due to the similarity between the two proteins. As the CaMs are from different organisms, one animal and one plant, the two structures are expected to be slightly different, which will be reflected in the NSD values of the alignments. NSD values were 1.72 and 1.42 for apo *Xenopus* CaM aligned with envelopes of mtCaM1 in EDTA generated with DAMMIF and GASBOR, respectively. The alignments generated with *Xenopus* CaM were mirror images of one another. This is because the fitting methods used by both DAMMIF and GASBOR cannot solve the handedness of the structure. Therefore, when aligning using SUPCOMB it was necessary to allow enantiomorphs in the fitting procedure to provide the best solution by allowing the matching of the handedness of both structures (137). Alignments of calcium ion-bound potato CaM with envelopes of mtCaM1 in CaCl₂ gave NSDs of 1.59 and 1.78, respectively.

The DAMMIF and GASBOR solutions were compared by aligning in SUPCOMB. NSD values were 0.70 and 0.61 for the calcium ion bound and apo models, respectively. This shows that the DAMMIF and GASBOR solutions are similar. The values do not tend towards zero as the models produced are different for the two methods as described above. This means that it is difficult to difficult compare DAMMIF and GASBOR models by alignment.

To compare the envelopes the models of apo CaM were aligned with calcium ion bound CaM. Distances were 0.75 and 0.78 for the DAMMIF and GASBOR models respectively showing that conformational changes had taken place. However these were not large enough to dramatically change the overall shape of the molecule allowing them to be aligned. It should be noted that NSD values would be near zero if no conformational change had occurred as models generated by the same method can be directly compared as they share the same approximations as described above.

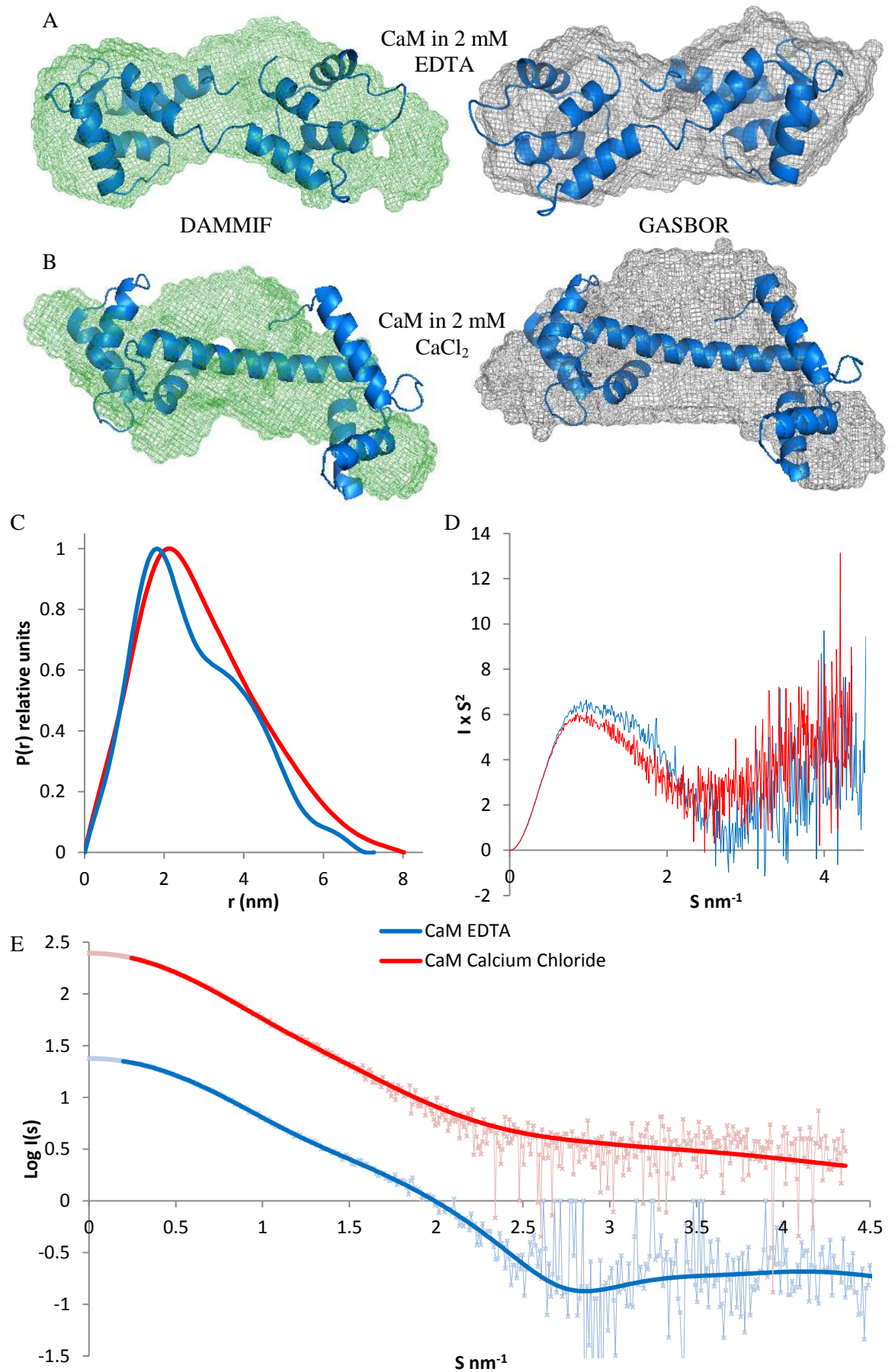


Figure. 2.15. SAXS data for calmodulin in the apo and calcium ion-bound forms. A, apo *Xenopus* CaM (PDB 1CFD) aligned with SAXS envelopes of mtCaM1 in excess EDTA. B, calcium ion-bound potato CaM overlaid with SAXS envelopes of mtCaM1 in excess CaCl₂. Envelopes were generated using either DAMMIF (left) or GASBOR (right) and alignments were generated using SUPCOMB with enantiomorphs enabled. NSDs were 1.72 and 1.43 for apo *Xenopus* CaM overlaid with envelopes of mtCaM1 in EDTA generated with DAMMIF and GASBOR, respectively. NSDs were 1.59 and 1.78, respectively, for alignments of calcium ion-bound potato CaM with mtCaM1 in CaCl₂. C, P(r) plots for mtCaM1 in EDTA or CaCl₂ generated with autoGNOM. Plots have been normalised to a maximum intensity of 1 by dividing all values by the maximum P(r) for each curve. D, kratky plots of the mtCaM1 data. E, plots of Log I (feint scattered lines) and fitted curves generated by autoGNOM (solid lines). The CaCl₂ curve has been offset by 1 for clarity. Blue lines show data for mtCaM1 in 2 mM EDTA, and red lines show data in 2 mM CaCl₂.

SAXS data for the isolated visinin-like domain show that D_{\max} increased upon calcium ion-binding as shown in Table 2.4 and Figure 2.16. This shows that the visinin-like domain becomes more elongated upon calcium-ion binding. Molecular envelopes were generated with DAMMIF and GASBOR. These models show that the protein became elongated upon calcium ion-binding as shown in Figure 2.16. This is similar to the data for CaM. However, the visinin-like domain appeared to have a prolate shape in both the calcium ion-bound and apo forms.

Alignments of the DAMMIF and GASBOR models showed that they were similar giving NSD values of 0.64 and 0.81 for the visinin-like domain in CaCl₂ and EDTA respectively. Alignment of the calcium ion-bound and apo models suggested that the conformational changes had a small effect on the overall shape of the molecule as in CaM. NSD values were 0.72 and 0.67 for the DAMMIF and GASBOR models respectively.

The structure of recoverin could not be aligned with the molecular envelopes of the visinin-like domain. Alignments (with the myristoyl group removed) gave poor NSD values of 2.28 and 1.87 for alignments of calcium ion-bound recoverin with the DAMMIF and GASBOR models respectively. The high NSD values obtained were likely to be a result of the low sequence identity between recoverin and the visinin-like domain, which is likely to mean that the structures of the two proteins differ significantly. The structure of apo recoverin did not align well with the envelopes of the visinin-like domain in EDTA. NSD values were 3.03 and 2.03 for the DAMMIF and GASBOR models respectively. NSDs were significantly improved when docking the calcium ion-bound recoverin into the apo visinin-like domain envelopes. NSDs were 2.29 and 1.51 for the DAMMIF and GASBOR envelopes respectively. However, these alignments were still poor

meaning that calcium ion-bound recoverin is not a suitable structure for comparison to the apo visinin-like domain.

Protein	Condition	Theoretical Mw <i>kDa</i>	Observed Mw <i>kDa</i>	R_g <i>nm</i>	D_{max} <i>nm</i>	Quality %
Visinin-like domain	2 mM CaCl ₂	21	21	2.36 ± 0.09	8.26	82
	0.1 mM EDTA		16	2.27 ± 0.07	6.79	83
Visinin-like domain with autoinhibition	2 mM CaCl ₂	24	25	2.77 ± 0.17	8.83	78
	2 mM EDTA		15	2.27 ± 0.41	6.65	39
Mutant EF-hand two	2 mM CaCl ₂	21	15	2.32 ± 0.14	8.10	70
	2 mM EDTA		17	2.17 ± 0.20	6.63	72
Mutant EF-hand three	2 mM CaCl ₂	21	40		n/d ^a	
	2 mM EDTA		4			
Mutant EF-hand four	2 mM CaCl ₂	21	20	2.26 ± 0.09	7.56	79
Mutant EF-hand two-four	2 mM CaCl ₂		19	2.18 ± 0.13	7.60	81
	2 mM EDTA	21	14	2.11 ± 0.17	7.39	74
Calmodulin	2 mM CaCl ₂	17	24	2.29 ± 0.05	8.02	82
	2 mM EDTA		23	2.12 ± 0.04	7.27	87

Table. 2.4. Fitted parameters from SAXS data curves

Table showing the calculated values for the molecular weight (M_w), radius of gyration (R_g), maximum particle size (D_{max}) and quality for the SAXS data. Errors in R_g have been converted from % errors reported by AutoRg. Data with an observed M_w within 10 kDa of the theoretical value was processed. Quality above 50% indicates that curves are appropriate for further processing; values below this suggest that limitations may exist in the values obtained.

^a not determined

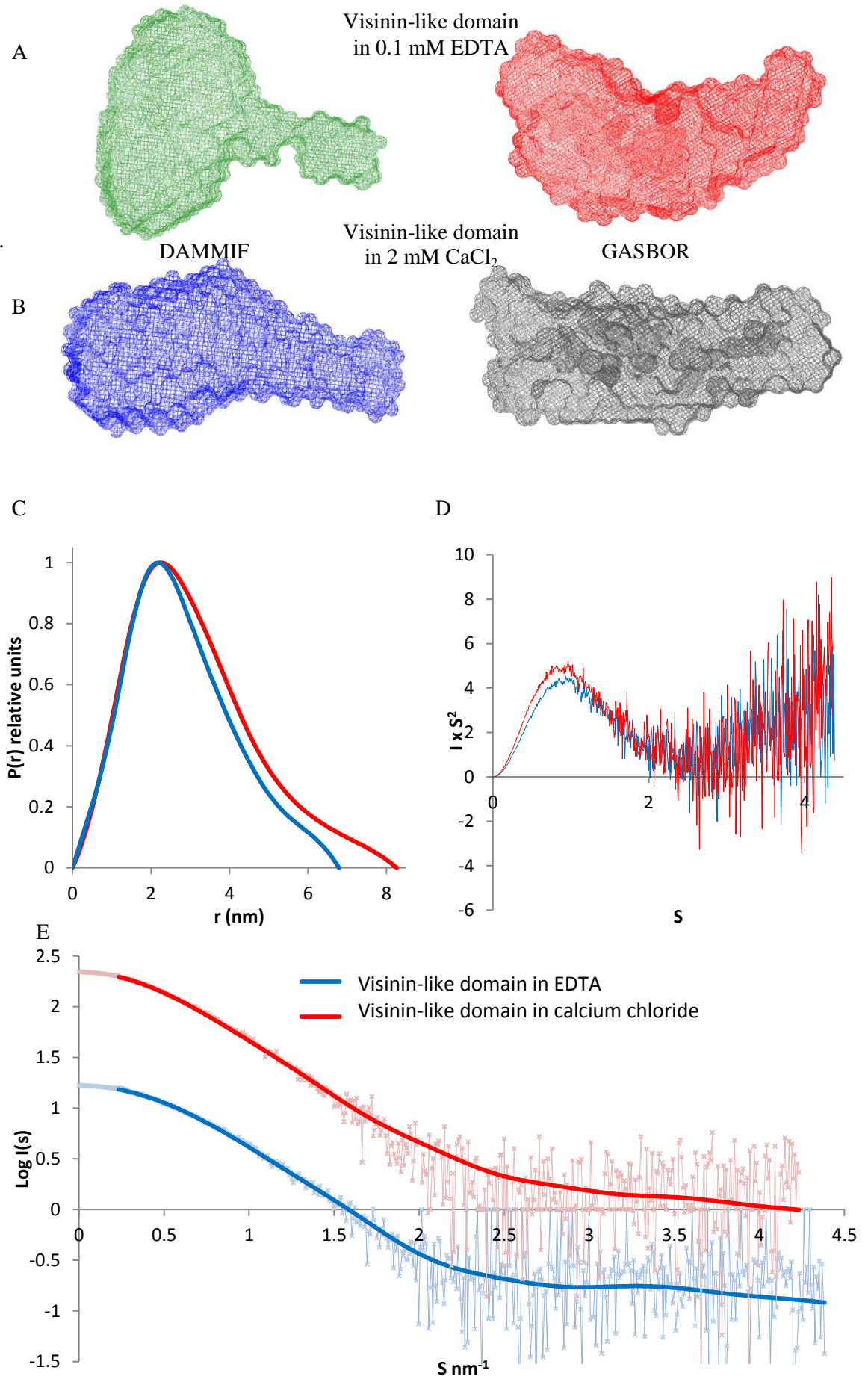


Figure. 2.16. SAXS data for the visinin-like domain in the apo and calcium ion-bound forms. A, SAXS envelopes of the visinin-like domain in excess EDTA. B, SAXS envelopes of the visinin-like domain in excess CaCl₂. Envelopes were generated with either DAMMIF (left) or GASBOR (right). Molecules were oriented according to alignments with SUPCOMB. C, P(r) plots for the visinin-like domain in EDTA or CaCl₂ generated with autoGNOM. Plots have been normalised to a maximum intensity of 1. D, kratky plots of the visinin-like domain data. E, plots of Log I (feint scattered lines) and fitted curves generated by autoGNOM (solid lines). The CaCl₂ curve has been offset by 1. Blue lines show data in 0.1 mM EDTA, and red lines show data in 2 mM CaCl₂.

Although the quality of the curve for the visinin-like domain with autoinhibition in EDTA was low (shown in Table 2.4), all other parameters were acceptable and the data set was processed. However, due to the limitations this imposes, analysis of these data was undertaken with care and using comparisons to the isolated visinin-like domain to support any conclusions. Comparison of the data for the visinin-like domain and the visinin-like domain with autoinhibition revealed their sizes and structures were similar in the presence of EDTA. This is shown in Figure 2.17 and by the similarity in R_g and D_{max} values in Table 2.4. In addition the similarity of the overlaid GASBOR structures (Figure 2.17 A) and the similarity of the P(r) curves in excess EDTA (Figure 2.17 D) support this conclusion. The differences seen in the DAMMIF models of the two constructs were more significant. These are likely to arise from ambiguity in the models for the visinin-like domain in EDTA. The protrusion is seen in multiple locations in the individual models before averaging. This ambiguity may artificially increase the size of the model when averaging, which in turn leads to significant differences between the models of the two constructs. These data could suggest that the His-tag was highly flexible and exposed to the solution in excess EDTA. Nevertheless the shapes both show a ball and stick shape.

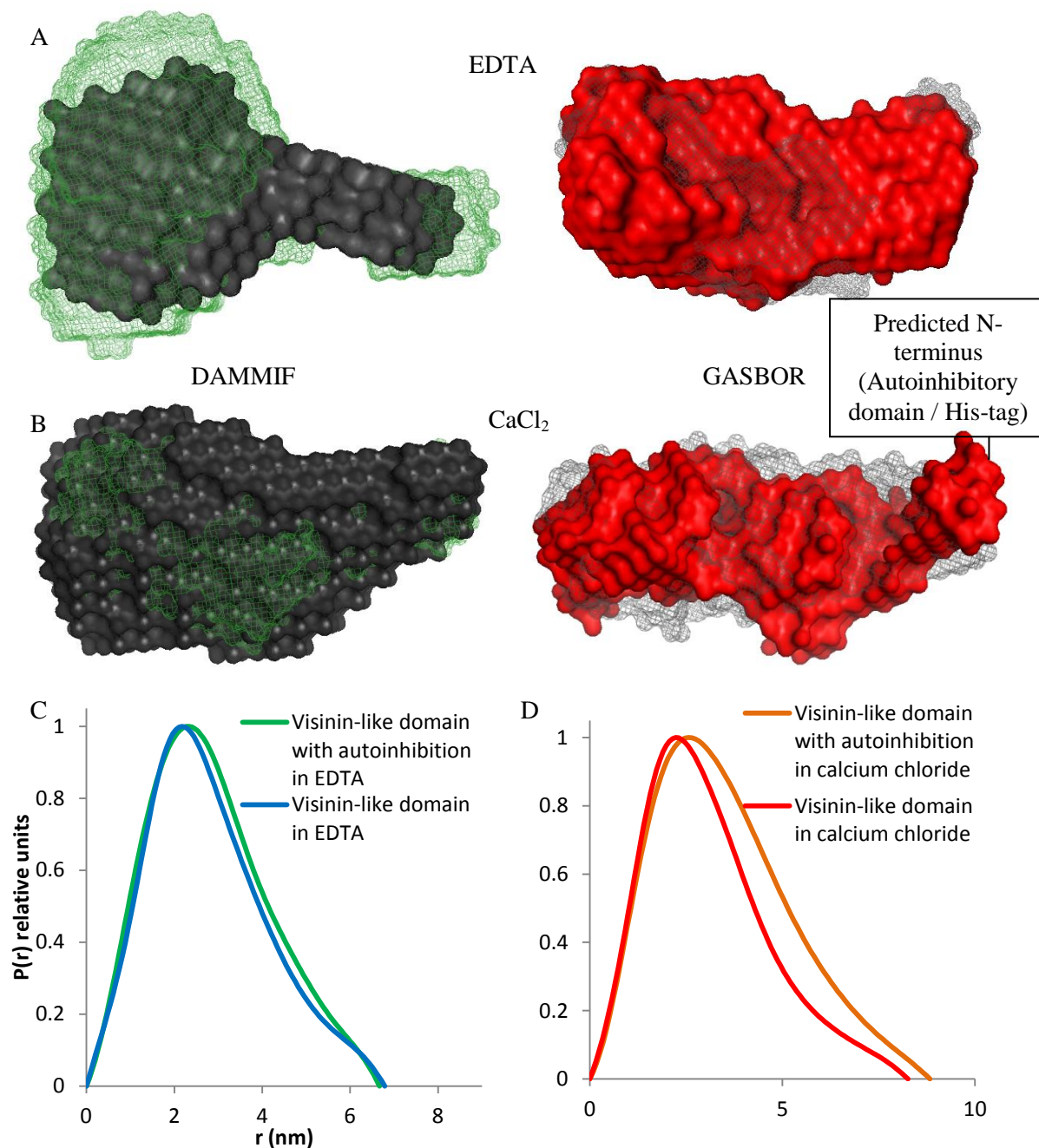


Figure. 2.17. Comparison of SAXS data for the visinin-like domain and visinin-like domain with autoinhibition. A, models of the apo visinin-like domain with autoinhibition (solid surface representation) aligned with the visinin-like domain (mesh). Models have been flipped to the same orientation as the CaCl₂ models. B, models of visinin-like domain with autoinhibition aligned with the visinin-like domain in excess CaCl₂. Envelopes were generated with either DAMMIF (left) or GASBOR (right) and alignments were generated using SUPCOMB with enantiomorphs enabled. NSD values were 0.690 and 0.686 for the EDTA envelopes generated with DAMMIF and GASBOR respectively. NSD values were 0.629 and 0.682 for alignments of calcium ion-bound envelopes. C, P(r) curves in EDTA (blue – visinin-like domain, green – visinin-like domain with autoinhibition) or D, CaCl₂ (red – visinin-like domain, orange – visinin-like domain with autoinhibition) generated with autoGNOM and normalised to a maximum intensity of 1.

Close analysis of the calcium ion-bound envelopes suggested that there are subtle differences between structures of the two constructs. Differences in the region corresponding to the N-terminus would be expected to correspond to the addition of the autoinhibitory domain in place of the His-tag. Comparison of the envelopes showed that there was no significant additional length despite the autoinhibitory domain adding 23 residues over the visinin-like domain (including 6 residue His-tag). This may be due to the His-tag being disordered and flexible thus representing more space than its size would suggest. In contrast the autoinhibitory domain is likely to be well folded, and in a more fixed position. Evidence consistent with this was seen in the GASBOR model of the visinin-like domain with autoinhibition (Figure 2.17 B, right) where the left hand side forms a more extended structure. This was not observed in the visinin-like domain model suggesting that this extended structure may be the autoinhibitory domain as this is the largest difference between the two constructs. However, as the resolution is only 1.5-2 nm, the differences observed are not sufficient to unambiguously assign the N-termini. Comparison of the GASBOR models in EDTA (Figure 2.17 A, right) with the calcium ion-bound protein showed evidence for elongation of the molecule when calcium ions bind. The DAMMIF models (Figure 2.17 A and B, left) were more difficult to interpret in the same way. The EDTA structure showed an elongated rod-like structure, which was less clear in the calcium ion-saturated protein. In agreement with the GASBOR models, and the visinin-like domain in isolation, the molecule did appear to become elongated overall upon calcium ion-binding.

Data were also collected for the visinin-like domain EF-hand mutants to study the roles of each EF-hand in the conformational changes. Datasets for mutant EF-hand three in EDTA and CaCl_2 were rejected as estimated molecular weights deviated significantly from the expected value of 21 kDa at 4 and 40 kDa respectively. Mutant EF-hand two-three was not analysed in either condition and mutant EF-hand four was not analysed in EDTA due to insufficient quantities of sample.

These data show that the mutants of EF-hand two and two-four were similar to the wild-type visinin-like domain in EDTA (shown in Figure 2.18 A and values in Table 2.4). In the presence of excess CaCl_2 the mutants of EF-hand two, four and two-four differed only slightly from the wild-type protein (Figure 2.18 B and Table 2.4). However these differences are unlikely to be significant. This therefore suggests that calcium ion-binding to EF-hand three is responsible for most of the elongation observed. However, without reliable data for the mutant EF-hand three this could not be conformed using these data.

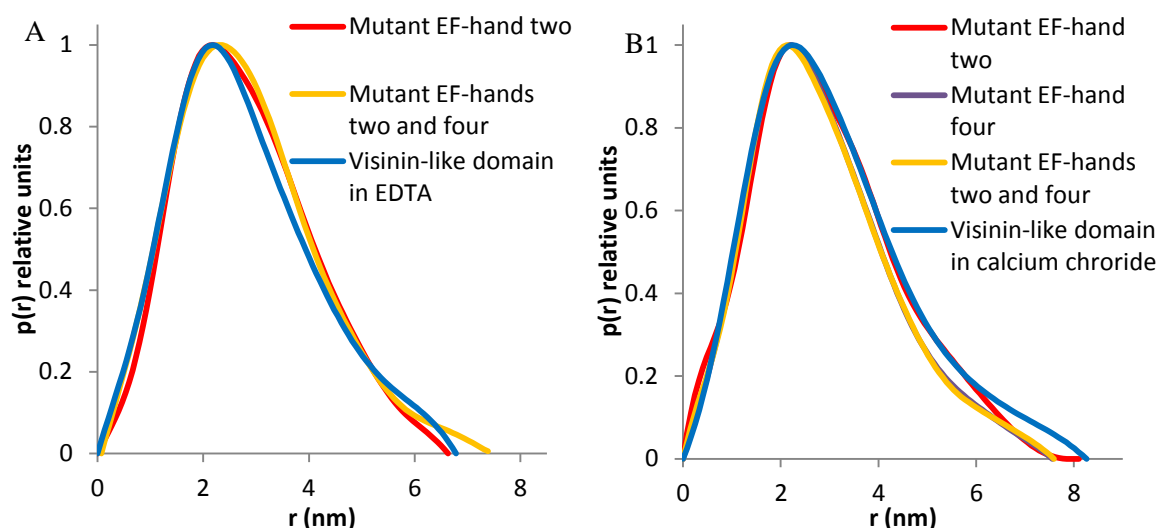


Figure. 2.18. Comparison of SAXS $P(r)$ curves for the visinin-like domain EF-hand mutants. $P(r)$ curves generated in the presence of A, EDTA or B, CaCl_2 . Data for the wild-type visinin-like domain (blue) and EF-hand mutants (two – red, four – purple and two-four – orange) are shown. All curves have been normalised to a maximum intensity of 1.

2.2 DISCUSSION

Although role and general organisation of the individual domains of CCaMK have previously been reported, the exact boundaries between these domains have not been identified. In addition, in-depth sequence analysis of the individual domains has not been performed beyond automated methods.

In this work it has been identified that the boundary between the autoinhibitory domain and visinin-like domain lies in the region of residue 350. The boundary between the autoinhibitory and kinase domains was more difficult to define as there is no distinct boundary as the domains overlap. Additionally the autoinhibitory and CaM-binding domains cannot be separated as they completely overlap in CCaMK. This suggests that these are one and the same domain, as is the case in CaMKII (91). Given the homology of CCaMK to the CaM kinases, and evidence for a similar arrangement of the kinase and autoinhibitory domains, it is likely that autoinhibition relief by CaM binding occurs by a similar mechanism to that of CaMKII. In this mechanism CaM binding causes rearrangement of the autoinhibitory domain. This removes steric hindrance of the active site and rearranges the ATP binding site to activate the enzyme (138). For a more detailed description see Chapter 1 Section 1.5 “Calmodulin dependent protein kinase II”.

As a lack of structural information exists on CCaMK and the full length protein was unsuitable for the biochemical studies described above, a divide and conquer approach was utilised. This approach offered multiple advantages. Firstly it provided constructs, which were amenable to biochemical studies requiring large quantities of stable, monodisperse protein. Secondly, separation

of the domains and their functions allowed for detailed characterisation of properties of each domain without interference from the rest of the protein. This means that the regions of interest were more amenable to characterisation, and studies of isolated domains could be compared to the full-length protein or multi-domain constructs in future studies using a top-down approach.

In-depth analysis of the kinase and autoinhibitory domains by combining data from disorder prediction, coiled-coil prediction and the threaded model allowed some hypotheses to be made regarding the mechanism and function of autophosphorylation. The prediction of a loop around the autophosphorylated Thr271 is interesting as this would allow it to be presented as an ideal substrate for efficient phosphorylation. The threaded model suggests that its position, adjacent to the beginning of the autoinhibitory helix, may allow it to affect the autoinhibitory domain in a phosphorylation-dependent manner, as is evident from the fact that autophosphorylation enhances the affinity of the CaM binding site in this domain (72). This position also suggests that autophosphorylation of Thr271 will occur through an inter-oligomer mechanism as the kinase domain of CCaMK cannot access its own Thr271.

The prediction that the N-terminal amino acids of CCaMK are unfolded may be relevant to the stability of the protein. It is possible that some of this region is unfolded given that the threaded model of CCaMK begins at Ser42 suggesting that the equivalent N-terminal region of CaMKII is disordered or flexible. However the extent of unfolded protein is unlikely to extend much beyond this point as it would lead to disorder in core regions of the kinase domain. The predicted coiled-coil in this region could be of importance for complex formation or substrate interactions as it is ideally located to allow specific interactions with the kinase domain. However, the two reported substrates of CCaMK to date have been shown not to interact with this portion of the protein. IPD3 (CYCLOPS) has been shown to interact with active full length kinase-domain constructs of CCaMK but not with the autoinhibitory or visinin-like domains in yeast two hybrid experiments (66). CIP73 was shown to interact with CCaMK constructs containing the first amino acids 60-180, which are located in the kinase domain, by yeast two hybrid experiments (51).

As attempts to crystallise the CCaMK visinin-like domain and visinin-like domain with autoinhibition failed, and expression levels were approximately ten-fold too low for structure determination by NMR to be viable, the structural properties of these constructs were analysed by a variety of low-resolution techniques. Manual sequence analysis revealed that an inactive EF-hand lies upstream of the three predicted by Patil *et al* (60), which makes the CCaMK visinin-like domain consistent with the animal NCS and plant CBLs (62, 114). To conform to the nomenclature for these protein families, the EF-hands of CCaMK should be named EF-hands one to four according to their order in the sequence. This means that the previously named EF-hand one becomes EF-hand two, and EF-hands two and three become three and four, respectively, under this system. Manual analysis of the inactive EF-hand showed a conserved AT amino acid substitution in positions five and six within the binding loop (384-385 in full CCaMK sequence), which is

conserved in all CCaMKs (shown in Figure 2.1). This differs from the animal NCS, which contain a CP substitution in positions three and four in their first inactive EF-hands (amino acids 37-38 in frequenin and NCS-1). In addition the experimental confirmation that three calcium ions bind shows that CCaMK's visinin-like domain differs from a subgroup of the NCS, which also contain an inactive EF-hand in the fourth position (62). The CBL EF-hand one differs from both CCaMK and the NCS as it is inactivated by substitution of the first and/or third positions in the binding-loop. In addition CBLs may contain one or two additional inactivated EF-hands (114). This suggests that the CCaMK visinin-like domain is distinct from these proteins and may have originated early in the evolution of this protein family. An additional important difference is that the NCS and CBLs exist as single domain proteins, often modified by myristoylation at the N-terminus (62, 114). In CCaMK the visinin-like domain is fused to the autoinhibitory domain at its N-terminus and thus cannot be modified by myristoylation. However, the mechanisms to adapt the interaction of the protein with its N-terminal region, for example by a flip-out mechanism as found in recoverin (117), and conformational changes allowing interactions with target proteins are perhaps likely to occur in a similar manner upon calcium ion-binding.

The results demonstrate that the CCaMK visinin-like domain undergoes conformational changes, which do not occur significantly at either the secondary or quaternary structural level. By contrast, alterations in the tertiary structure upon calcium ion-binding are significant. There is a large increase in hydrophobic exposure that occurs upon calcium ion-binding to EF-hand two. This may be important for the calcium ion-dependent interactions with other proteins, as is the case for many EF-hand-containing proteins including CaM (26), or the CCaMK kinase domain. This hydrophobic exposure is unlikely to be a mechanism by which the autoinhibitory domain can be bound by the visinin-like domain as a similar increase in hydrophobic exposure was observed in the two constructs. These structural changes lead to an overall elongation of the molecule.

Together the structural data suggest that each EF-hand plays a distinct role in the overall conformational change of the molecule when calcium ions bind. The SAXS data suggest that the elongation of the molecule is driven primarily by calcium ion-binding to EF-hand three. The data also show that the conformational changes in the visinin-like domain upon calcium ion-binding are more subtle changes than in recoverin. These data, along with the peak shift in the CCaMK far-UV CD spectra that takes place upon calcium ion-binding to EF-hand two, indicate that significant conformational changes in the visinin-like domain correlate with calcium ion-binding to EF-hand two. However these have little effect on the overall shape of the molecule within the limits of this analysis. The role of EF-hand four is less clear from these data as no major role in the conformational changes have been correlated to this site. This suggests that the role of EF-hand four is subtle and may only be relevant in the context of calcium ion-binding to the other two sites. As CCaMK lacks the conserved glycine residue in EF-hand one, which facilitates the “swing-out”

of the myristoyl group in recoverin by acting as a hinge, the N-terminal region would be expected to be less flexible in the CCaMK visinin-like domain.

The NCS proteins contain another conserved glycine residue between EF-hands two and three (found at position 94 in recoverin), which acts as a hinge point allowing a 45° rotation of the two sub-domains relative to one another (117). Sequence alignments show that a glycine residue is present at a similar position in CCaMK (highlighted in green in Figure 2.2). This suggests that the inter EF-hand-pair rotation upon calcium ion-binding may occur in the CCaMK visinin-like domain. In addition the finding that EF-hand four plays a less significant role correlates well to recoverin in which this site is inactive (62).

The finding that the predicted coiled-coil in the visinin-like domain N-terminal region does not lead to dimerisation shows that CCaMK may be different to CaMKII in its oligomerisation state. However, it has been demonstrated that CaMKII constructs lacking the association domain to drive dodecomer formation only interact at concentrations above 100 μM . As CaMKII forms dodecomeric complexes via its association domain, which places the autoinhibitory of neighbouring CaMKII monomers in close proximity, the CaMKII coiled-coil interaction is physiologically relevant. This leads to secondary interactions of the autoinhibited kinases within the CaMKII dodecomer via coiled coil formation between the autoinhibitory domains (91). This means that a role for self association via this predicted coiled-coil cannot be discounted in CCaMK if the full-length protein is found to form homo-complexes. Alternatively the predicted coiled-coil may be important for interactions with other proteins.

Figure 2.19 shows a cartoon representation of the CCaMK visinin-like domain where the autoinhibitory domain is partially obscured in the apo form. Upon calcium ion-binding the autoinhibitory domain is exposed to the solvent possibly allowing calmodulin to bind or altering interactions with the kinase domain. However, to fully understand the observations made, an atomic level structure of CCaMK, particularly of the constructs analysed here, is required.

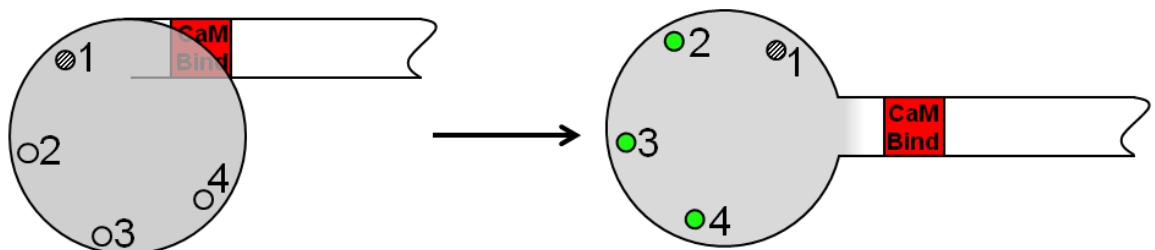


Figure. 2.19. Model of CCaMK regulatory domain rearrangements upon calcium binding.

Cartoon representation of CCaMK visinin-like (grey) and autoinhibitory (white) domains in the apo form (left) and the calcium ion-bound form (right). The inactive EF-hand one is filled with diagonal lines and the active EF-hands are filled either in grey (apo) or green (calcium ion-bound). Tertiary level structural rearrangements driven by calcium ion-binding lead to an altered interaction between the two domains.

2.3 MATERIALS AND METHODS

2.3.1 *BLAST analysis*

Sequences of mtCCaMK full length and the visinin-like domain (residues 330-523) were aligned against entries in the non-redundant protein sequences database with the blastp algorithm using the NCBI blast tool (<http://blast.ncbi.nlm.nih.gov>). Additionally the full CCaMK sequence was aligned against entries in the PDB using the PDB search tool in BLAST mode (<http://www.pdb.org/pdb/search/advSearch.do?st=SequenceQuery>). Multiple alignments were produced using the ClustalW server (<http://www.ebi.ac.uk/Tools/msa/clustalw2/>), combined with the T-Coffee combine tool (139) (<http://tcoffee.crg.cat/apps/tcoffee/play?name=combine>) and formatted using the box shade server (http://www.ch.embnet.org/software/BOX_form.html).

2.3.2 *Disorder prediction*

Disorder prediction was performed on the full CCaMK sequence using the foldindex server (<http://bip.weizmann.ac.il/fldbin/findex>) (119).

2.3.3 *Coiled-coil prediction*

Coiled-coil prediction was performed on the full CCaMK sequence using the coils server (http://www.ch.embnet.org/software/COILS_form.html) (120).

2.3.4 *Experimental determination of the visinin-like domain boundary*

A solution of the visinin-like domain with autoinhibition was incubated at 4 °C for two weeks in 10 mM Tris-HCl pH 7.5 containing 150 mM NaCl, 1 mM tris(2-carboxyethyl)phosphine (TCEP) and 0.005% v/v tween 20. Sample masses were analysed by SDS-PAGE and MADLI-MS. MALDI-MS was performed using protein samples at a concentration of around 0.5 µg µl⁻¹ that were acidified with trifluoroacetic acid (TFA) (Rathburn Chemicals), mixed 1:1 with 2 mg ml⁻¹ sinapic acid (Sigma) in 90% acetonitrile/10% of 0.1% TFA, and spotted onto an AnchorChipTM MALDI steel target plate (Bruker Daltonics). The spots were washed and re-crystallised if necessary. Ubiquitin and trypsinogen (Sigma) were spotted in the same way and used as standards for mass calibration. After drying, the samples were analysed by MALDI-TOF on a Bruker Ultraflex TOF/TOF using a method optimised for the mass range around 12 kDa in linear mode. Data were processed in FlexAnalysis (Bruker).

Limited proteolysis was performed in 50 mM Tris-HCl pH 7.5 containing 100 mM NaCl and 1 mM DTT. CCaMK visinin-like domain with autoinhibition at 1 mg ml⁻¹ was incubated for 1 h at 25 °C with 0.1-15 µg ml⁻¹ trypsin in either 2 mM CaCl₂ or 2 mM EDTA. Reactions were quenched by the addition of 240 µg ml⁻¹ soybean trypsin inhibitor and analysed by SDS-PAGE and MALDI-MS as described above, or quenched by the addition of 10% TFA followed by reflection in-source decay (rISD) sequencing by modifying the method used by Belfield *et al.* (140) as follows: A solution of the protein was prepared in 20 mg/ml 2,5-dihydroxybenzoic acid in 30% acetonitrile, 0.1% TFA, then mixed 1:1 with sample and spotted onto a stainless steel target. Spectra were

collected using an UltraFlex MALDI-ToF/ToF in reflection mode. Laser power was set to 40% and masses were determined by calibration with pre-spotted standards.

2.3.5 Threaded model of CCaMK kinase and autoinhibitory domains

A threaded model of the CCaMK kinase domain was produced in Swiss-PDB viewer (<http://spdbv.vital-it.ch/>) by aligning the CCaMK sequence with the crystal structure of bovine CaMKII (PDB 2bdw), which was selected using the “find appropriate ExPDB templates tool”.

Name	Length	Oligo Sequence
	<i>bp</i>	
Cloning forward primers:		
Start N-terminus	26	CACCATGGGCTATGGTACACGTAAC
Start 317	25	CACCATGCCGAAATTGTGTCTCG
Start His-tag+317	43	CACCATGCATCACCATCACCATCA ⁺ CCCGAAATTGTGTCTCG
Start His tag+346	44	CACCATGCATCACCATCACCATCA ⁺ CTTCCTGCGCACCAAAAAAC
Cloning reverse Primers:		
End 306+His-tag	39	CTAGTGATGGTGGTGGTGGTAA ⁺ ACCCACGGGTCGCTCAG
End 323+His-tag	39	CTAGTGATGGTGGTGGTGGTGG ⁺ GCGAGACACAATTTCCGG
End 353+His-tag	22	CTACAGTTTTTTGGTGCGCAGG
End c-terminus	22	CTACGGGCGGATTGACGACAGA
Mutagenesis primers (forward only)		
Mutant EF-hand two	36	CGCATTTTCGATCTGTTTCGCTAATAATCGCGACGGT
Mutant EF-hand three	36	TGCTTTCAAATGTATGCTACCGACCGTTCGGGTTGC
Mutant EF-hand four	36	GAAATTTTCGATCTGATGGCTGCCAACAATGATGGC

Key to mismatched sequence: CACC Directional TOPO overhang

Start Codon
Stop Codon
His-tag
Base change

Table. 2.5. PCR primers for TOPO cloning and Quick-Change mutagenesis.

Mismatched sequence is highlighted according to the key below. All other sequence is complimentary to the target. Mutagenesis primers were produced with the sequences shown. The reverse compliments of the mutagenesis primers have been omitted from the table.

2.3.6 Cloning of mtCaM1, mtCCaMK and CCaMK-constructs

mtCaM1 (UniProtKB ID Q71JC6) and full length CCaMK (UniProtKB ID Q6RET7) were synthesised with optimised codon usage for *E. coli* expression and sub cloned into pET21(a)+ (Novagen) by Genscript USA.

Plasmids containing *E. coli*-optimised sequences for either CCaMK residues 1-306 (short kinase) or 1-323 (long kinase) with a C-terminal 6 × His-tag, 1-353 (kinase with autoinhibition) or 317-523 (visinin-like domain with autoinhibition) without affinity tags, or 346-523 (visinin-like domain) with N-terminal 6 × His-tag were produced using the pET101/D-TOPO kit (Invitrogen). PCR primers for the production of gene fragments are listed in Table 2.5. Mutants of the EF-hands were produced in the visinin-like domain construct using the Quickchange® Lightning Site-Directed Mutagenesis Kit (Stratagene). Primers (listed in Table 2.4) were designed to mutate the Asp codon (GAT) to Ala (GCT) to produce the following visinin-like domain variants: D70A (EF-hand two), D106A (EF-hand three), D148A (EF-hand four), D70A + D106A (EF-hands two and three), D70A + D148A (EF-hands two and four) and D106A + D148A (EF-hands three and four). All EF-hand mutants were expressed and purified as described for the wild-type CCaMK visinin-like domain construct.

2.3.7 Expression and purification of CaM1, CCaMK and CCaMK constructs

CaM1 was expressed in *E. coli* BL21*(DE3) cells by growing at 37 °C until the OD₆₀₀ reached 0.5 before inducing with 1 mM IPTG and growing for a further 3 h. Cells were harvested by centrifugation for 10 min at 5 000 × g and resuspended in 50 mM Tris-HCl pH 7.5 containing 1 mM CaCl₂, DNase I and Roche protease inhibitor tablets. Cells were lysed using a Constant systems cell disruptor at 25 kPSI and spun at 20 000 × g for 30 min. Pellets were discarded and the lysate was heated to 90 °C for 3 min, incubated on ice for 5 min and spun again at 20 000 × g for 30 min. The remaining purification steps were performed on an ÄKTA FPLC using a 5 ml HiTrap Phenyl Sepharose FF column (GE Healthcare) as described by Fromm & Chua (141). Final enrichment was achieved by gel filtration using a Superdex 75 16/60 column (GE Healthcare) pre-equilibrated with 50 mM Tris-HCl pH 7.5 containing 100 mM NaCl and 1 mM DTT.

Full length CCaMK was expressed in *E. coli* BL21 (DE3) pLysS cells by growing at 37 °C until the OD₆₀₀ reached 0.5. Expression was induced by the addition of 1 mM IPTG and cells were grown at 18 °C overnight. Cells were harvested by centrifugation at 5 000 × g and resuspended in 50 mM Tris-HCl pH 7.5 containing 1 M NaCl, 2 mM CaCl₂, protease inhibitor cocktail and DNaseI. Cells were lysed by passing through a French press twice at 1 000 kPa and the lysate was clarified by centrifugation at 20 000 × g for 30 min. Purification of CCaMK was performed using an adapted method by Takezawa *et al.* (61). Lysate was applied to a 10 ml calmodulin Sepharose 4B column (GE Healthcare) pre equilibrated with 10 mM Tris-HCl pH 7.5, 1 M NaCl, 2 mM CaCl₂. Unbound sample was washed out over 3.5 column volumes in the same buffer. Bound CCaMK was eluted by washing with 50 mM Tris-HCl pH 7.5 containing 2 mM EDTA.

The visinin-like domain with autoinhibition was expressed in *E. coli* BL21*(DE3) cells in auto-induction media (142) by growing at 37 °C for 2 h followed by 20 °C for 20 h. Cells were processed using the same method as full length CCaMK with the following alterations: cells were resuspended in 50 mM Tris-HCl pH 7.5 containing 1 M NaCl, 1 mM CaCl₂, 1 mM DTT, DNase I

and Roche protease inhibitor tablets. Cells were lysed using a constant systems cell disruptor at 25 kPSI. The equilibration/wash buffer was 50 mM Tris-HCl pH 7.5 containing 1 M NaCl, 2 mM CaCl₂ and 1 mM DTT. The elution buffer was 50 mM Tris-HCl pH 7.5 containing 2 mM EDTA and 1 mM DTT. The wash step after loading was extended to 5.5 column volumes and additional purification was achieved by gel filtration as described for CaM1.

The visinin-like domain was expressed, and the cells were harvested, as described for the visinin-like domain with autoinhibition. Cells were resuspended in 50 mM Tris-HCl pH 7.5 containing 300 mM NaCl, 10 mM imadazole, DNase I and Roche protease inhibitor tablets. Cells were lysed using a constant systems cell disruptor at 25 kPSI followed by centrifugation at 20 000 × g for 30 min. Clarified lysate was applied to a 1 ml His-trap FF column (GE Healthcare) pre equilibrated with 50 mM Tris-HCl pH 7.5 containing 300 mM NaCl and 10 mM imadazole. Unbound sample was washed out with 5 column volumes of the same buffer. The visinin-like domain was eluted by washing with 50 mM Tris-HCl pH 7.5 containing 300 mM NaCl and 500 mM imadazole. Further purification was achieved by gel filtration as described for CaM1.

Small scale expression trials were performed for the kinase domain with autoinhibition construct as described for full length CCaMK but without gel filtration. The short and long kinase domains were purified using 0.1 ml gravity flow His-trap columns as described for the visinin-like domain except lysis was performed by sonication for 2 min and gel filtration was omitted.

Products from all purifications were analysed by SDS PAGE and protein identities were confirmed by MALDI-MS mass fingerprinting by washing gel pieces, treating with trypsin, and extracting according to standard procedures. The peptide solution resulting from the digests were spotted onto a PAC plate (Prespotted AnchorChipTM MALDI target plate, Bruker Daltonics) and the spots were briefly washed with 10 mM ammonium phosphate, 0.1% TFA according to the manufacturer guidelines. After drying, the samples were analysed by MALDI-TOF on a Bruker Ultraflex TOF/TOF. The instrument was calibrated using the pre-spotted standards (ca. 200 laser shots). Samples were analysed using a laser power of approximately 25% and spectra were summed from about 30 × 15 laser shots. Data were processed in FlexAnalysis (Bruker) and submitted for a database search using an in-house Mascot Server (Matrixscience).

	1	2	3	4	5	6	7	8	9	10	11	12
A	Citric acid pH 4	NaAc pH4.5	Phosphate pH5	citrate pH5.5	Bis-Tris pH6	Bis-Tris propane pH6.5	Phosphate pH7	Tris pH7.5	EPPS pH8	Tris pH8.5	CHES pH9	CHES pH9.5
B	Citric acid pH 4	NaAc pH4.5	Phosphate pH5	citrate pH5.5	Bis-Tris pH6	Bis-Tris propane pH6.5	Phosphate pH7	Tris pH7.5	EPPS pH8	Tris pH8.5	CHES pH9	CHES pH9.5
C	Citric acid pH 4	NaAc pH4.5	Phosphate pH5	citrate pH5.5	Bis-Tris pH6	Bis-Tris propane pH6.5	Phosphate pH7	Tris pH7.5	EPPS pH8	Tris pH8.5	CHES pH9	CHES pH9.5
D	Citric acid pH 4	NaAc pH4.5	Phosphate pH5	citrate pH5.5	Bis-Tris pH6	Bis-Tris propane pH6.5	Phosphate pH7	Tris pH7.5	EPPS pH8	Tris pH8.5	CHES pH9	CHES pH9.5
E	2 mM AMP	2 mM ADP	2 mM ATP	-	-	2 mM AMP-PNP	-	-	-	-	-	-
F	-	-	-	-	-	-	1% glycerol	5% glycerol	10% Glycerol	20% Glycerol	1mM DTT	5mM DTT
G	10 mM CaCl ₂	10 mM MgCl ₂	-	-	10 mM FeCl	100 mM KCl	-	-	-	Water	3% DMSO	-
H	100 mM Gly	-	10 mM Urea	5% PEG 400	-	-	10 mM Ala	-	10 mM Ser	10 mM Arg	-	-

Table 2.6. Map of the 96 conditions screened in the thermofluor assay

Empty wells are marked with -. The top half of the plate contains a variation of buffers from low to high pH, and each row contains a salt concentration from 0 – 500 mM NaCl. The lower half of the plate contains a range of additives in MilliQ H₂O.

2.3.8 *Determination of extinction coefficients*

Extinction coefficients at 280 nm for the full length CCaMK and the visinin-like domain with autoinhibition were predicted using the ExPASy ProtParam server (<http://expasy.org/tools/protparam.html>) (143). Extinction coefficients were determined for the visinin-like domain and CaM1 in 10 mM Tris-HCl pH 7.5 containing 50 mM NaCl and 1 mM TCEP. UV/vis spectra were collected over 240-340 nm on a Perkin Elmer Lambda18 UV/vis spectrophotometer at 298 K in 10 mm, 0.5 ml quartz cuvettes. Exact concentrations of the protein solutions were determined by amino acid analysis at the University of Cambridge Protein and Nucleic Acid Chemistry Facility. The extinction coefficients ($M^{-1} cm^{-1}$) were calculated using the formula $\epsilon = \frac{A}{c.l}$ where A is the absorbance, C is the concentration and l is the path length of the cell in cm.

2.3.9 *Screening of buffer conditions for the full length protein*

The thermofluor method was used to screen for suitable buffers as described by Nettleship *et al.* (122) using a Biorad Opticon 2 qPCR thermo cycler and a CCaMK stock concentration of 0.6 mg ml^{-1} . The conditions screened are displayed in Table 2.6. A filter based assay published by Bondos and Bicknell (144) was also used to screen 0.15 M $(NH_4)_2SO_4$, 0.4 M RbCl, 1 % w/v glycine, 10% v/v glycerol, 0.1% v/v triton-X 100 and 5 mM DTT. Further screening was performed by analytical gel filtration on a Superdex 200 10/300 GL column (GE Healthcare) in a range of buffers.

2.3.10 *Analytical gel filtration of visinin-like domain and visinin-like domain with autoinhibition*

A volume of 200 μl of 55 μM visinin-like domain, visinin-like domain with autoinhibition or soybean trypsin inhibitor was injected onto a Superdex 200 10/300 GL column (GE Healthcare) pre-equilibrated with 10 mM HEPES pH 7.5 containing 50 mM NaCl, 1 mM TCEP and either 2 mM EDTA, 2 mM $CaCl_2$ or 5 mM $MgCl_2$ + 2 mM EGTA. The column was calibrated using a molecular weight marker kit, 12 000-200 000 molecular weight range (Sigma), which consists of blue dextran (2 000 kDa, elution in the void volume), β amylase (200 kDa), alcohol dehydrogenase (150 kDa), albumin (66 kDa), carbonic anhydrase (29 kDa) and cytochrome c (12 kDa). The calibration buffer was 10 mM HEPES pH 7.5 containing 2 mM EDTA and 1 mM TCEP.

2.3.11 *Electrospray ionisation mass spectrometry*

The Electrospray ionisation mass spectrometry (ESI-MS) experiments were based upon studies by Hu *et al.* (125) and Shirran *et al.* (145). Visinin-like domain and visinin-like domain EF-hand mutants were exchanged 1 000-fold into 10 mM ammonium acetate pH 7.5 using Vivaspin centrifugal concentrators (Sartorius). Samples of 20 μM protein in 25% acetonitrile containing either 100 μM EDTA, 100 μM calcium acetate, 100 μM EGTA together with 500 μM magnesium acetate or no additives were analysed by ESI-MS in negative ion-mode on a Q-Tof-2 mass spectrometer (Walters/Micromass UK). Samples were applied to the mass spectrometer via an

electrospray ionisation interface with a flow rate of $5 \mu\text{l min}^{-1}$, a desolvation temperature of $150 \text{ }^\circ\text{C}$, a desolvation gas flow of 6.7 L min^{-1} , and a capillary spray voltage of 2.3 kV . The cone voltage was set to 65 V and the source temperature to $80 \text{ }^\circ\text{C}$. Calibration was performed using an $8 \mu\text{M}$ myoglobin (Sigma-Aldrich) solution in 50% acetonitrile, 0.1% NH_4OH . Scans were acquired in the mass range of $m/z = 1\ 000$ to $4\ 000$. Data were acquired and processed using MassLynx 4.1 (Waters). Final spectra were generated by combining a number of scans, and applying background removal and a Savitzky–Golay smoothing method.

2.3.12 Analytical ultracentrifugation

CCaMK visinin-like domain and visinin-like domain with autoinhibition constructs were dialysed into $10 \text{ mM HEPES pH } 7.5$ containing 50 mM NaCl and 1 mM TCEP . Solutions of $115 \mu\text{M}$ visinin-like domain, or $50 \mu\text{M}$ visinin-like domain with autoinhibition were prepared in either 2 mM CaCl_2 , 2 mM EDTA , $5 \text{ mM MgCl}_2 + 2 \text{ mM EGTA}$, or $5 \text{ mM MgCl}_2 + 2 \text{ mM CaCl}_2$. Samples spun in a Beckman Optima XL-I analytical ultracentrifuge (High Wycombe, United Kingdom) equipped with absorbance optics and an An-50 Ti rotor. Equilibrium experiments were performed at $10\ 000$, $15\ 000$ and $20\ 000 \text{ RPM}$ and absorbance profiles were measured at 280 nm every 4 h after equilibrium had been reached. Five scans were collected per velocity. Data were analysed using Ultrascan II software (126) using the 1-component, ideal model. Errors were estimated with the Monte Carlo analysis module with default settings except “ignore runs with variance above”, which was set to $2\text{e-}4$ (default $1\text{e-}4$). Buffer density and protein v_{bar} values were calculated using Sednterp (<http://www.jphilo.mailway.com/download.htm>).

2.3.13 Circular dichroism spectroscopy

CCaMK visinin-like domain with autoinhibition, visinin-like domain and visinin-like domain EF-hand mutants were dialysed into $10 \text{ mM HEPES pH } 7.5$ and prepared at $40 \mu\text{M}$ in either 2 mM EDTA , 2 mM CaCl_2 or $5 \text{ mM MgCl}_2 + 2 \text{ mM EGTA}$. Spectra were collected on a Jasco J-710 spectropolarimeter. Near-UV spectra were collected using a 10 mm quartz cuvette and scanning between 330 and 250 nm . Far-UV spectra were collected using a 0.1 mm quartz cuvette and scanning between 260 and 180 nm . All spectra were collected with a sensitivity of 100 mdeg , 0.2 nm data pitch, 4 s response time and a 1.0 nm bandwidth at a scan speed of 20 nm min^{-1} . Final spectra were produced by averaging four scans and subtraction of a buffer only measurement. Far-UV spectra were smoothed using the Savitzky-Golay method with a factor of 5 using the Jasco CD spectrophotometer software.

Near UV spectra were converted to units of molar ellipticity ($\text{deg cm}^2 \text{ dmol}^{-1}$) using the formula: $[\theta] = \frac{\theta}{10 \cdot C \cdot l}$ (146) where θ is the ellipticity in mdeg, C is the concentration and l is the path length of the cell in cm. Far UV-CD spectra were converted to units of $\Delta\epsilon$ ($\text{mdeg M}^{-1} \text{ cm}^{-1} \text{ residue}^{-1}$) using the formula: $\Delta\epsilon = \frac{\theta}{n \cdot C \cdot l \cdot 3298}$ where n is the number of residues. The remaining symbols are described above. Far-UV spectra were deconvoluted on the Dichroweb server

(<http://dichroweb.cryst.bbk.ac.uk/html/home.shtml>) (130) using the CDSSTR algorithm and reference set 6 (131).

2.3.14 *ANS fluorescence spectroscopy*

This method is based upon the use of 8-anilino-1-naphthalenesulfonic acid (ANS) to monitor hydrophobic exposure upon calcium ion-binding to CaM (85). CCaMK visinin-like domain with autoinhibition, visinin-like domain and visinin-like domain EF-hand mutants were exchanged 1 000-fold into 10 mM Tris-HCl pH 7.5 containing 50 mM NaCl and 1 mM TCEP using Vivaspin centrifugal concentrators (Sartorius). Fluorescence spectra of solutions containing 5 μ M protein, 15 μ M ANS and either 2 mM CaCl₂, 2 mM EDTA or 5 mM MgCl₂ + 2 mM EGTA were collected between 400 and 650 nm on a Perkin Elmer LS55 luminescence spectrometer. The excitation wavelength was 380 nm with 10 nm slits and the scan speed was 500 nm min⁻¹.

2.3.15 *Shape determination by small angle X-ray scattering (SAXS)*

SAXS curves for the CCaMK visinin-like domain, visinin-like domain with autoinhibition and visinin-like domain EF-hand mutants were collected in both excess EDTA and CaCl₂. Data were collected at the X33 beam line on the DORIS synchrotron at EMBL, DESY in Hamburg, Germany.

Samples were dialysed into 10 mM Tris-HCl pH 7.5 containing 50 mM NaCl and either 0.1 mM EDTA, 2 mM EDTA or 2 mM CaCl₂. All samples were centrifuged at 13 400 RPM in a bench-top micro-centrifuge for 10 – 15 min to remove aggregated protein. Scattering curves were collected for the dialysis buffer, followed by the protein solution then a second buffer blank. Data were collected for solutions containing 1.46 mg ml⁻¹ visinin-like domain, 0.87 mg ml⁻¹ mutant EF-hand two, 1.18 mg ml⁻¹ mutant EF-hand three, 1.54 mg ml⁻¹ mutant EF-hand four, 1.11 mg ml⁻¹ mutant EF-hands two-four, 0.81 mg ml⁻¹ visinin-like domain with autoinhibition and 2.13 mg ml⁻¹ CaM in 2 mM CaCl₂. Data were also collected for solutions of 1.88 mg ml⁻¹ visinin-like domain in 0.1 mM EDTA, and solutions of 0.59 mg ml⁻¹ mutant EF-hand two, 1.03 mg ml⁻¹ mutant EF-hand three, 0.5 mg ml⁻¹ mutant EF-hands two-four, 0.74 mg ml⁻¹ visinin-like domain with autoinhibition and 1.82 mg ml⁻¹ CaM in 2 mM EDTA. All data were collected at 10 °C by averaging 8 × 15 s frames.

All GNOM output files and values for R_g and Mw were generated by the automated pipeline, which consists of programs Autopilatus/Automar, AutoSub, AutoRg and AutoGNOM (135). EF-hand mutant three in CaCl₂ was manually processed. For manual processing blank subtraction was performed in PRIMUS, molecular weight was estimated using autoprod and GNOM outputs were generated with autoGNOM in the ATSAS 2.4 software package (135). Samples with predicted molecular weights that differ from the theoretical mass by more than 10 kDa were rejected. Molecular envelopes were generated for each curve by running either DAMMIF (147) or GASBOR in reciprocal space (148) ten times followed by generating the most probable model by averaging with DAMAVER (136).

Comparison of the models was made by generating three dimensional alignments using SUPCOMB (137). Selected models were also aligned with structures of recoverin in the Apo (PDB

entry 1IKU (149)) or calcium ion-bound (PDB entry 1JSA (117)) forms. As the complete NMR structures could not be aligned in SUPCOMB, only the first structure in the PDB file was aligned. This was selected as all models were very similar, except for the N-terminus of the calcium-ion bound form, which was flexible. In addition the myristoyl group was removed as the CCaMK visinin-like domain does not have this modification. The CaM envelopes were aligned with the crystal structure of calcium ion-bound potato CaM (PCM6) (PDB entry 1RFJ (27)) or the average NMR structure of apo *Xenopus* CaM (PDB entry 1CFD (150)).

3. Chapter three – Affinity and thermodynamics of calcium ion-binding to CCaMK EF-hands

In order to understand the role of CCaMK in calcium spiking the concentration ranges over which calcium ions bind must be understood. By measuring the affinity of the CCaMK EF-hands for calcium ions the behaviour of CCaMK can be related to the physiological concentrations observed during calcium spiking. To this end, the equilibrium binding and affinity of calcium ions to the CCaMK visinin-like domain has been studied using electrospray ionisation mass spectrometry, fluorescence spectroscopy and isothermal titration calorimetry. It was discovered that the visinin-like domain of CCaMK binds calcium to one high affinity site with a K_D of less than 200 nM and two low affinity sites with an average K_D of 200 nM. It was also discovered that these sites are independent and non-interacting, and that each site has a specific set of thermodynamic parameters.

3.1 RESULTS

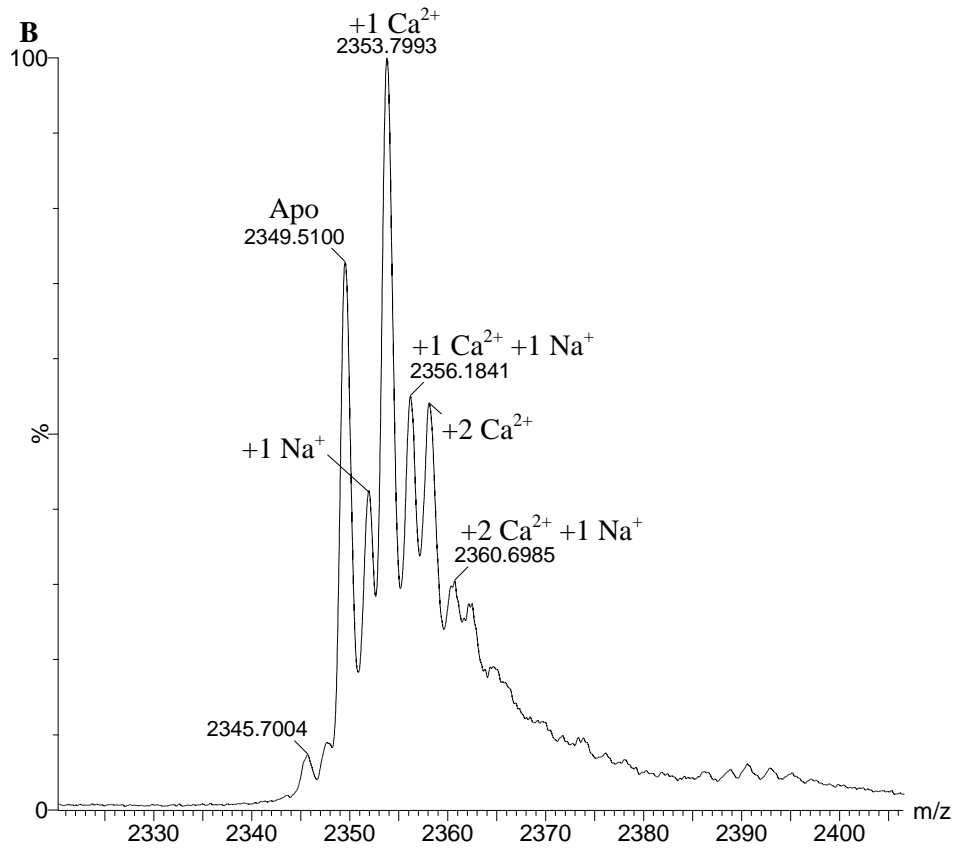
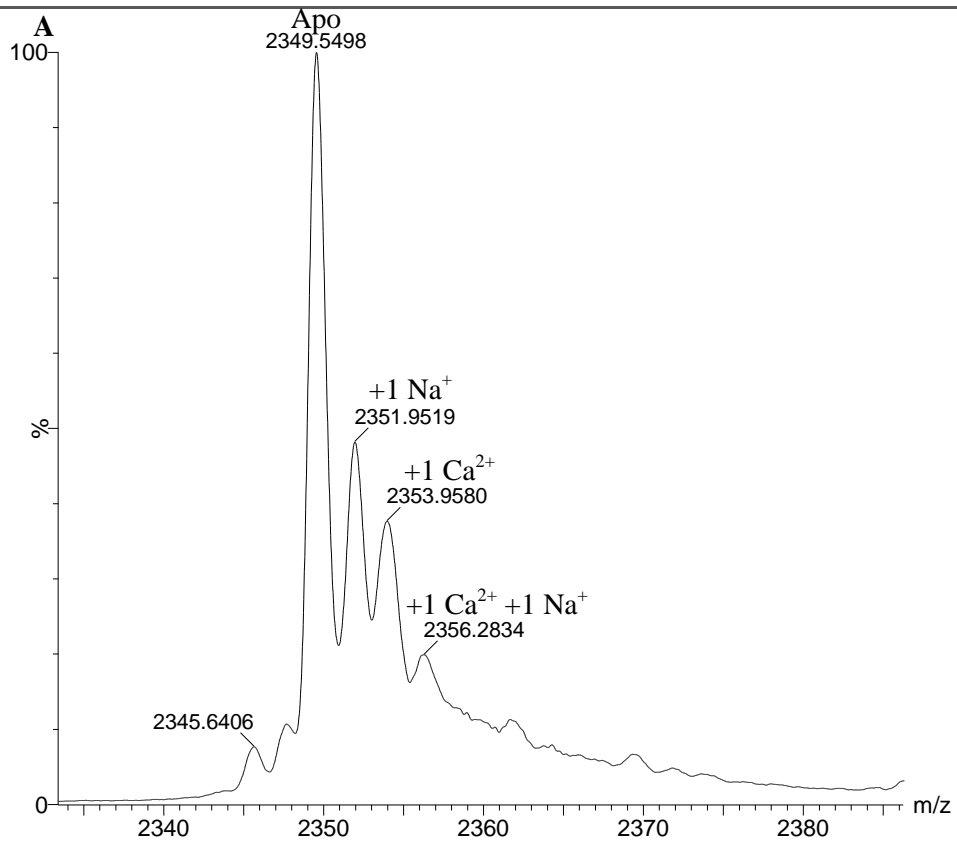
3.1.1 Determination that the CCaMK EF-hands are independent and non-interacting

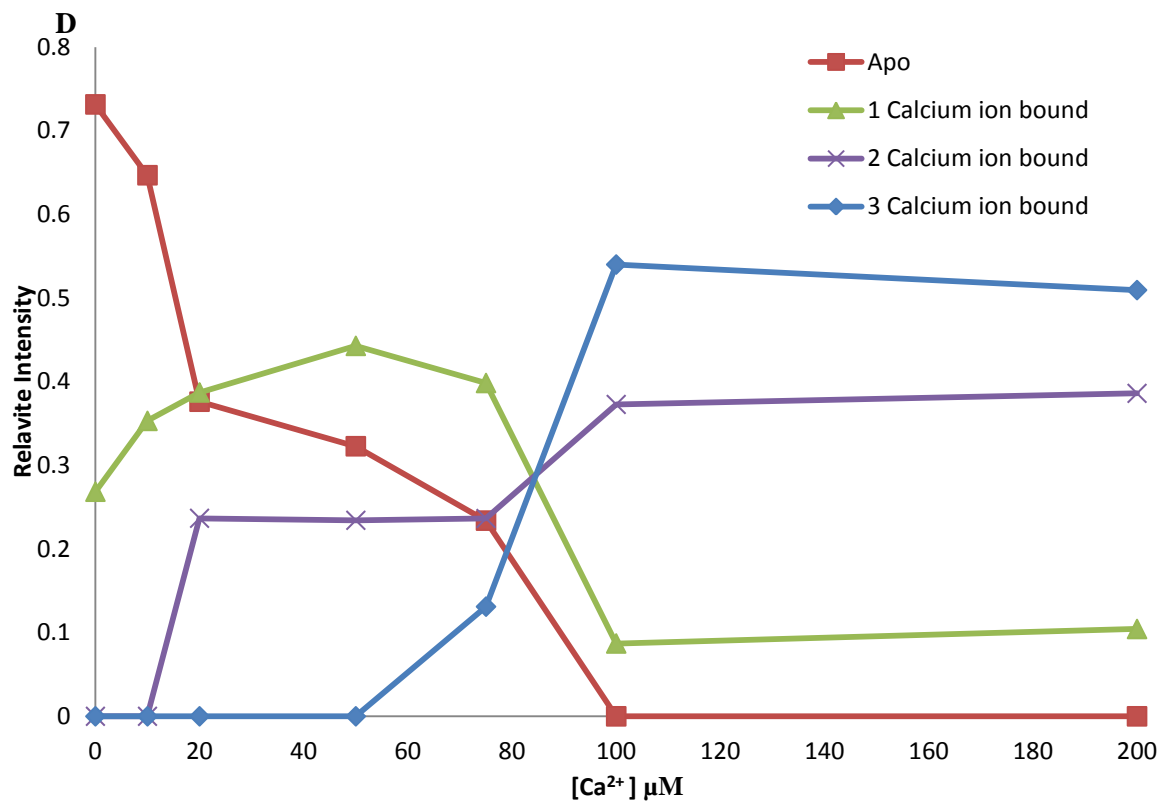
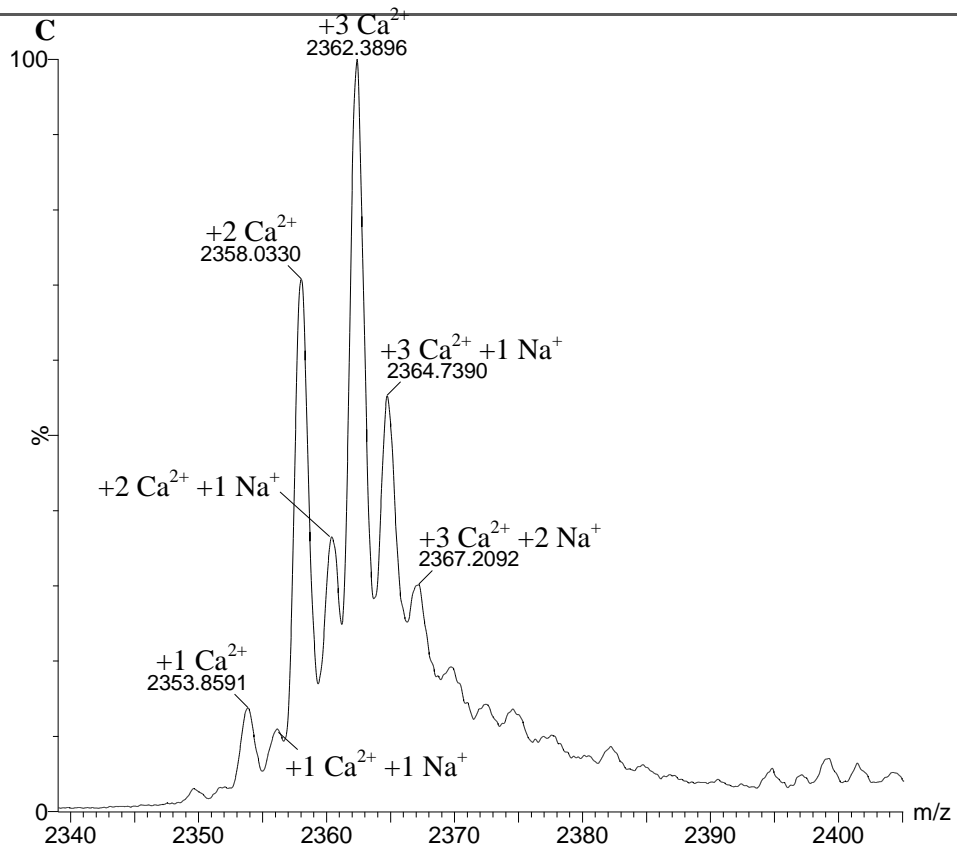
As methods such as ITC and fluorescence (described below) could not monitor net occupancies of each EF-hand, it was necessary to use ESI-MS to monitor the formation of the single, double and triple calcium ion-bound visinin-like domain. In this experiment, solutions of the CCaMK visinin-like domain were prepared in calcium acetate at concentrations that cover a range at which one, two or three sites would be expected to be filled if they were independent and non-interacting. In a cooperative system it would be expected that higher occupancy forms will be produced more readily than the mid occupancy forms. This is because ligand binding to one site significantly enhances the affinity for another site. This effect is observed in *Bovine* CaM which is known to bind calcium ions cooperatively. ESI-MS of Ca^{2+} binding to CaM by Shirran *et al.* demonstrated that the four calcium ion-bound form was observed at the same concentrations as the three ion-bound forms. This demonstrates that cooperatively is occurring to produce the four calcium ion bound form (145). This gave a profile whereby the saturated protein forms even at low concentrations of calcium ions rather than being produced only when the concentrations of the lower occupancy species became significant.

In an independent system, each species would be sequentially formed as the calcium ion-concentration increases. This is because there is no affinity enhancement of other sites when a ligand binds. This means that proteins are filled according to the affinities of the individual sites and with an even distribution of occupancies being most probable at a given ligand concentration. This type of binding was observed for magnesium ion-binding to *Bovine* CaM (145).

ESI-MS spectra of the CCaMK visinin-like domain construct gave masses for each level of occupancy as the calcium ion-concentration was increased. ESI-MS spectra for the visinin-like domain in buffer (contamination leads to a small amount of the one calcium ion-bound state), 50 μM (0.8:1 Ca^{2+} to binding site ratio) and 100 μM (1.7:1 ratio) calcium acetate are shown in Figure 3.1 A, B and C, respectively. From these data it was observed that the one calcium ion-bound protein forms at low calcium ion-concentrations, the two calcium ion-bound form is produced at moderate concentrations and finally the saturated form is produced at high calcium ion concentrations. This is clear when the proportions of each species are plotted against the calcium ion-concentration as shown in Figure 3.1 D. These data suggest that the EF-hands of the CCaMK visinin-like domain are unlikely to be cooperative.

As the calcium ions were being stripped from the protein over time, as discussed in Chapter two section 2.1.5 “Determination of the calcium ion stoichiometry of CCaMK”, the data may not be representative of the calcium ion bound-states in solution. This stripping is likely to be the reason why the maximum occupancy appears to be 2.5 of the 3 sites as shown in Figure 3.1 E. It is also likely to be the reason why the apo form could be detected in these experiments whereas it could not be detected by ITC and fluorescence (Discussed below). Furthermore significant overlap between specific calcium ion-bound peaks and sodium adducts meant that the peaks could not be reliably integrated to give accurate quantification of each species. Together these limitations meant that the data could only be assessed qualitatively meaning that it was inappropriate to fit the data to binding models to determine the K_D values of the sites.





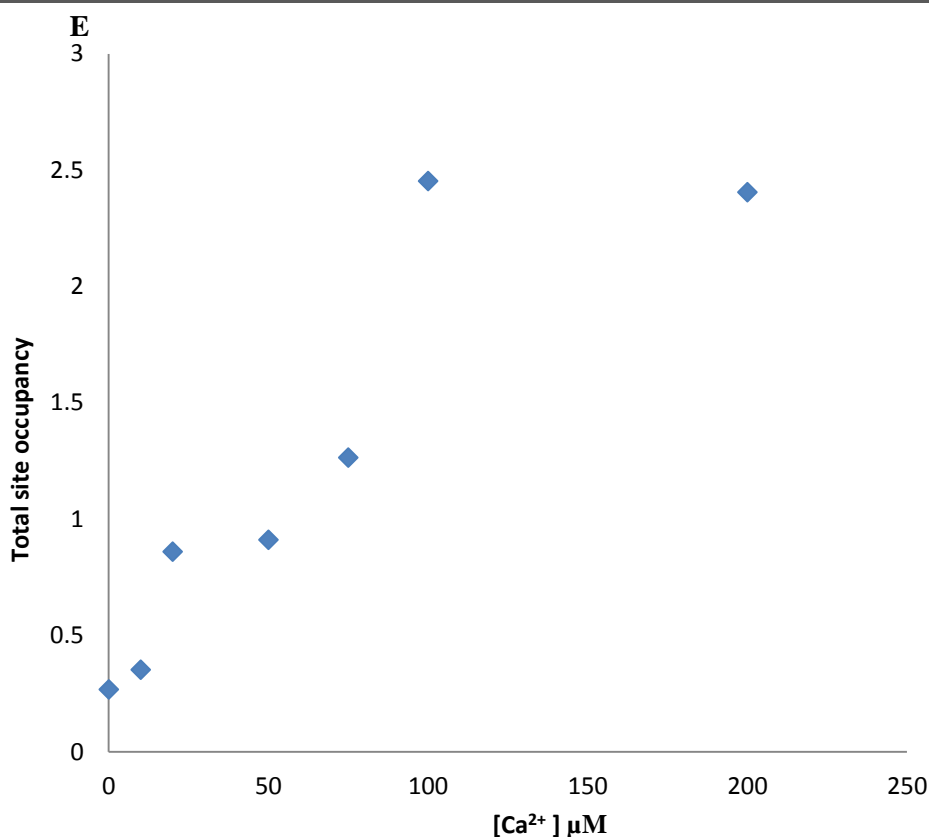


Figure 3.1. Calcium ion titration monitored by ESI-MS. ESI-MS spectra of 20 μM CCaMK visinin-like domain with the addition of A, 0, B, 50 and C, 100 μM calcium acetate. Peaks have been annotated with the corresponding bound ions. Expected masses are displayed in Chapter two, Table 3.1. D, graph of abundances of each species calculated from the intensity of peaks of the species of interest and associated single sodium adducts. Values have been normalised to fractions of the total observed. E, graph showing total number of sites occupied at each calcium ion-concentration.

3.1.2 Determination of the calcium ion-affinity of the CCaMK visinin-like domain

The affinity of the CCaMK visinin-like domain EF-hands for calcium ions was determined using isothermal titration calorimetry (ITC). As ligand was titrated and sites were filled, the heat changes for each injection were recorded. Initial injections gave maximal signal as the binding site concentration exceeded the ligand concentration meaning all of the ligand was bound. As the sites were filled, the signal per injection was reduced until the protein was saturated, when only the enthalpy of mixing the solutions was recorded. Integration of the peaks for each injection allowed the heat change per injection to be plotted; typically this yielded a sigmoid curve. These plots could be fitted to various models to determine the association constant (K_A), enthalpy of binding (ΔH) and the number of binding sites (n). For a protein containing a single binding site or identical non-interacting binding sites the K_A was related to the gradient of the curve at its steepest point (note that this is also influenced by the protein concentration). The ΔH was determined by integration of

the area above or below the fitted curve and n was determined from the inflection point. In more complex systems, i.e. those with multiple K_D s or cooperative binding, the curves are more complex and can adopt a range of non-sigmoid shapes. From the fitted parameters it was also possible to calculate the dissociation constant (K_D), Standard Gibbs free energy of binding (ΔG°) and the entropy (ΔS) meaning that the thermodynamics of binding could also be characterised from a single experiment.

The ability of this method to accurately measure K_A values when the protein concentration is considerably higher than the K_D was particularly advantageous. As other methods capable of detecting calcium-ion binding to the visinin-like domain construct require concentrations of tens of μM , such as CD spectroscopy (discussed in Chapter two) and fluorescence (described below), optimisation of conditions and fitting of the data can be challenging as the curves are not simple binding curves that can be assessed with Equation 1.

$$\text{Occ} = \frac{[\text{L}]}{K_D + [\text{L}]} \quad \text{Where Occ is the proportion of protein with ligand bound, } [\text{L}] \text{ is the ligand concentration and } K_D \text{ is the dissociation constant.} \quad (1)$$

At the high protein concentrations used in these experiments the effect of binding ligand to the protein has a significant effect on the free ligand concentration. This is because the amount of ligand bound to the protein will be a large proportion of the total. This means that the concentration of free ligand, required in Equation 1, cannot simply be assumed to be the total ligand concentration. For this assumption to be valid, the protein concentration must be at least 10 fold lower than the K_D . However 100 or 1000 fold lower than K_D is considered ideal. Under these conditions the effect of the protein concentration on the free ligand concentration can be considered to be insignificant and it can be removed from equations to simplify the calculation of the K_D .

Another issue was the calcium ion-contamination of the samples. Should a method be identified where the calcium ion-bound state of the CCaMK visinin-like domain could be monitored at nM concentrations of protein, it is likely that the protein will be saturated at the beginning of the titration as the calcium ion concentration in the buffer was determined to be 1.5 μM as discussed below. This would mean that a binding curve could not be collected.

Another advantage of ITC is that binding to all sites can be observed in a single measurement, which greatly simplifies the fitting procedure for the data. In methods such as CD and fluorescence spectroscopy, each binding site can report with a different signal, or some sites may not report at all, which makes fitting complex. This will be discussed in more detail later in this chapter. By contrast the models used in ITC to fit the data are well established and accepted as being comparable to data fitted with simple binding curves. A final advantage of ITC is that thermodynamic parameters can be determined for the binding of a ligand to the protein. When combined with other data, these values can provide insights to the mechanisms involved in binding.

In order to monitor calcium ion-binding to the CCaMK visinin-like domain, contaminating calcium ions had to be removed from the protein solutions as dialysis against decalcified buffers was not adequate. ITC of a dialysed sample suggested there were less than 0.5 sites remaining free of calcium (data not shown). The addition of EDTA followed by dialysis was also not suitable. EDTA-treated samples provided ITC data suggesting that there were approximately 12 binding sites (data not shown). Additional experiments revealed that this effect was due to contamination of the samples with EDTA. To overcome these issues an immobilised chelator was used. This had the advantage of being able to remove calcium ions without leading to contamination of the samples with chelator. Commercial chelating resins use either iminodiacetic acid (IDA) or nitrilotriacetic acid (NTA) as the chelating group. IDA is found in resins such as Chelex (Biorad) or Chelating HP (GE healthcare). NTA is most commonly utilised in nickel affinity resins such as those used in HisTrap FF columns (GE healthcare). As NTA contains four chelating groups whereas IDA contains three, NTA was considered to be most appropriate for calcium ion-removal from protein samples due to its higher affinity for calcium ions. Calcium ion removal was performed using a 1 ml His-trap FF column (GE healthcare). As residual EDTA led to contamination of the samples when used to remove calcium ions from the column (data not shown), a method relying on 1 M HCl was developed. The resin was stripped of all ions by washing with 1 M HCl, which protonates all acidic groups and reduces the resins affinity for metal ions by several orders of magnitude. The column was then washed with water to remove residual acid and equilibrated with the experimental buffer (10 mM Tris-HCl pH 7.5 containing 50 mM NaCl and 1 mM TCEP). It was found that 15 column volumes were required before the pH of the column eluant was stabilised at pH 7.5. Once the column was equilibrated the protein solution was concentrated and flowed over the resin. This method was repeated three times to maximise the calcium ion removal. As samples treated by this method gave approximately two sites by ITC for the wild-type protein (described below), it was considered to provide suitable samples for the detailed analysis of the calcium ion-affinity of the low affinity EF-hands of CCaMK.

In the present work, the CCaMK visinin-like domain construct was assessed at a concentration of 15 μM . A 275 μM solution of CaCl_2 was titrated into the protein solution to a molar ratio of 4:1 CaCl_2 to protein as shown in Figure 3.2 A. As the curve fitted well to the one set of sites model, this was deemed to be the most appropriate supporting the conclusion that the binding sites are independent and non-interacting as suggested by the mass spectrometry data. This meant that the binding of calcium ions to the individual sites could not be resolved and thus the K_D obtained is likely to be an average for the observed sites. Analysis of the data (shown in Table 3.1) revealed that the K_D for calcium ions was 200 nM. This value is ideal for the decoding of calcium spiking, which has a range of 5 - 800 nM (8). This means that the protein will be able to respond to the *in vivo* calcium spiking signal by adopting a low occupancy state at basal calcium ion-concentrations, rapidly rising to high occupancy during a calcium spike. The error of the K_D value is higher than

ideal (> 10 %). This is likely to be a result of the weak signal caused by the use of a low protein concentration. Higher protein concentrations were found to give very steep curves with few data points on the curve, which also produced large errors. A protein concentration of 15 μM provided the best compromise between curve shape and signal. It was also revealed that both the ΔH and ΔS of binding were favourable at $-33.1 \text{ kJ mol}^{-1}$ and $24.3 \text{ J mol}^{-1} \text{ K}^{-1}$, respectively. This gave a ΔG° of $-40.3 \text{ kJ mol}^{-1}$ at 25 $^\circ\text{C}$. The number of sites observed was 1.79, which was below the expected value of three. It was suspected that this was due to some remaining calcium-ion contamination in the samples.

To determine the level of calcium ion-contamination experimentally the buffers and protein samples were analysed by inductively coupled plasma optical emission spectrometry (ICP-OES). This technique allows the metal ion-concentrations in a given solution to be measured. The calcium ion-concentration was 13.21 μM for a 15 μM solution of the visinin-like domain construct. From this analysis the concentration of free EF-hands was calculated by deducting the calcium ion-concentration from the protein concentration multiplied by the number of binding sites (15×3 for wild-type to give 45 μM binding sites, minus 13.21 to leave 31.8 μM sites free). From this the number of free sites was determined by dividing this value by the expected binding site concentration and multiplying by the expected number of sites (for wild-type, 31.8 divided by 45 to give 71% free, multiplied by 3 to give 2.2 free sites). All calculated parameters are displayed in Table 3.1. The data from the ICP analysis also showed that the calcium ion-contamination in the buffer was 1.5 μM . This demonstrated that the majority of the calcium ion-contamination was in the protein solutions. This finding suggests that a high affinity for calcium-ions led to the accumulation of calcium ion contamination in the protein samples during sample preparation.

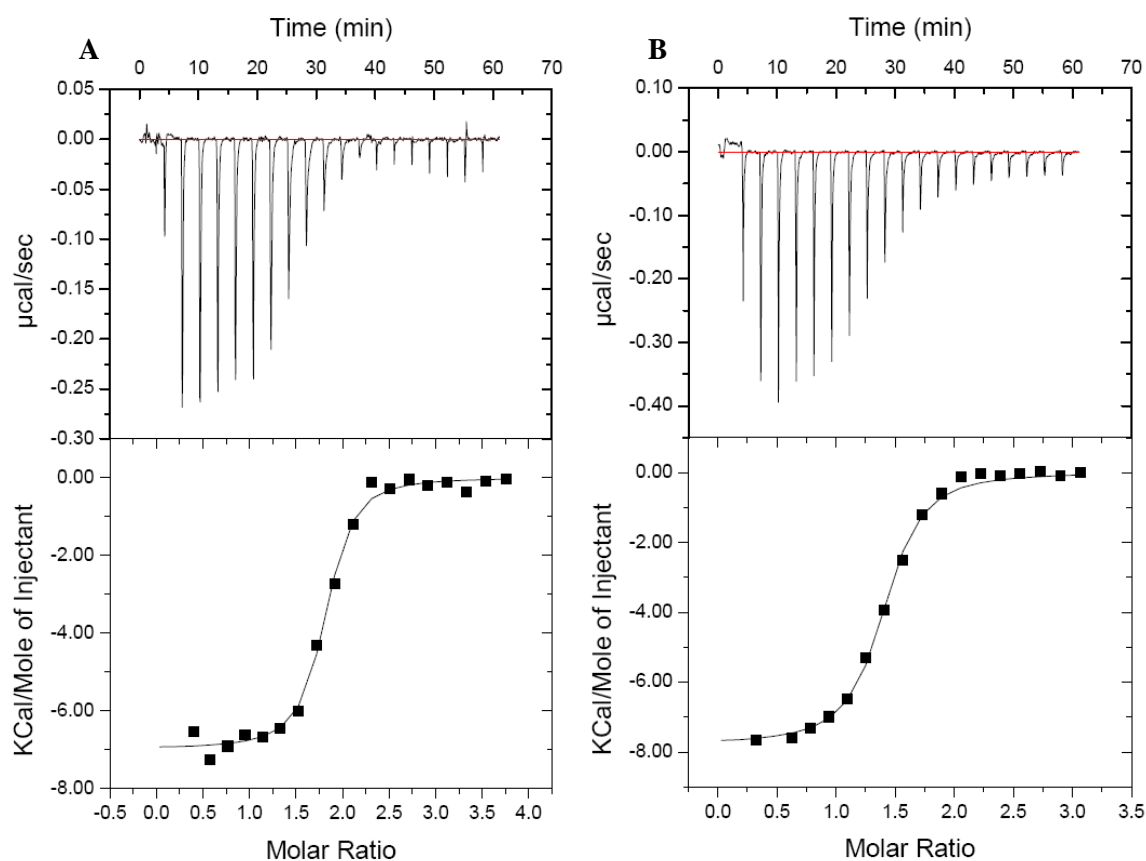


Figure. 3.2. Isothermal titration calorimetry of calcium ion-binding to the CCaMK visinin-like domain. A. isotherm of calcium ion-binding to the CCaMK visinin-like domain (top) and a plot of the integrated peak values fitted with the one set of sites model (lower). The K_D was estimated to be 200 ± 46 nM and the number of sites observed was 1.79. B, calcium ion-binding to the CCaMK visinin-like domain in excess $MgCl_2$. The K_D value obtained was 300 ± 56 nM and the number of observed sites was 1.27. The protein concentration was $15 \mu M$ and the temperature was $25^\circ C$.

Although the number of binding sites determined by ICP-OES and ITC do not match exactly, both demonstrate that approximately two sites are free of calcium-ions in the wild-type protein solutions. The differences between the two measurements may have arisen from the additional processing of the ITC samples allowing an increase in the calcium ion-contamination or additional calcium contamination in the $CaCl_2$ solutions leading to inaccurate measurement of the ITC titrant.

Taken together these data showed that two binding sites measured in the visinin-like domain construct have an average K_D of 200 nM and the third site has a K_D of less than 200 nM, which could not be measured.

Construct	Sites expected	Sites ITC	Sites ICP	K_D	ΔH	ΔS	ΔG°
				<i>nM</i>	<i>kJ mol⁻¹</i>	<i>J mol⁻¹ Deg⁻¹</i>	<i>kJ mol⁻¹</i>
Visinin-like domain	3	1.79 ± 0.02	2.1	200 ± 46	-33.1 ± 0.6	24.3	-40.3
Mutant EF-hand two	2	1.07 ± 0.01	1.2	325 ± 58	-37.7 ± 0.7	-2.4	-37.0
Mutant EF-hand three	2	0.80 ± 0.01	1.5	5 800 ± 577	-22.2 ± 0.6	25.4	-29.9
Mutant EF-hand four	2	1.66 ± 0.03	1.6	700 ± 122	-29.6 ± 0.7	18.9	-35.3

Table. 3.1. ITC and ICP-OES data for calcium ion-binding to the CCaMK visinin-like domain.

Values for Sites ITC and ΔH were determined directly in the ITC fitting process. K_D was determined from the inverse of the fitted association constant (K_A). The sites for ICP were calculated by deduction of the measured calcium ion-concentration in the protein samples from the expected binding site concentration, then dividing by the binding site concentration and finally multiplying by the number of sites. Values for ΔG° were calculated using the formula $\Delta G^\circ = -RT \ln K$ where R is the gas constant (8.314), T is the temperature in Kelvin and K is the K_A . Values for ΔS were calculated using the formula $\Delta S = -\frac{\Delta G - \Delta H}{T}$. The temperature was 25 °C (273 K) for all datasets.

Although the number of binding sites determined by ICP-OES and ITC do not match exactly, both demonstrate that approximately two sites are free of calcium-ions in the wild-type protein solutions. The differences between the two measurements may have arisen from the additional processing of the ITC samples allowing an increase in the calcium ion-contamination or additional calcium contamination in the CaCl₂ solutions leading to inaccurate measurement of the ITC titrant.

Taken together these data showed that two binding sites measured in the visinin-like domain construct have an average K_D of 200 nM and the third site has a K_D of less than 200 nM, which could not be measured.

As magnesium ions are likely to bind to the CCaMK EF-hands, as determined by mass spectrometry in Chapter two section 2.1.5 “Determination of the calcium ion-binding stoichiometry of CCaMK” it was necessary to test whether magnesium ions could act as a competitive inhibitor of calcium ion-binding. It is known that magnesium ions are present at high concentrations *in vivo* but the magnesium ion-concentration in a root hair cell nucleus is currently not known. However, values 0.4 mM have been reported as a typical free magnesium ion-concentration for plant cells (151). The effect of magnesium ions was analysed by repeating the ITC calcium ion-binding

experiment to the wild-type visinin-like domain construct with the addition of MgCl_2 to a final concentration of 5 mM. This magnesium ion-concentration was selected as it would provide an excess that would exceed the maximum expected concentration within the cell. This was added after the removal of calcium-ions from the protein as the NTA column was not effective when MgCl_2 was in the dialysis buffer (data not shown). This experiment demonstrated that MgCl_2 had a small effect of calcium ion-binding to the CCaMK visinin-like domain. The K_D for the observed sites was 300 ± 26 nM, a 1.5 fold increase over the protein in the absence of MgCl_2 . The number of sites observed was also reduced slightly to 1.27. These reductions may be due to additional calcium ion-contamination from the added MgCl_2 . This additional contamination may reduce the amount of the curve seen by removal of signal from the higher affinity sites as a higher proportion of them will be calcium ion-bound, meaning the majority of the curve corresponded to the lowest affinity site. Overall these data demonstrated that magnesium ions are not potent competitive inhibitors of calcium ion-binding.

Calcium ion-binding was also monitored by tyrosine fluorescence spectroscopy. It was observed that the tyrosine fluorescence emission at 305 nm was quenched upon calcium ion-binding as shown in Figure 3.3 A. As this signal reported directly on calcium ion-binding, it could be monitored throughout a titration of CaCl_2 to collect a binding curve, as shown in Figure 3.3B. As the protein concentration was much higher than the K_D obtained by ITC at 10 μM , fitting by the standard equation (shown in Equation 1) was not appropriate as the requirement for a low protein concentration is was not met as discussed above. To overcome this issue the data were fitted with Equations 11 and 12. To simplify the model, the three binding sites were accounted for by using binding site concentration ($[\text{P}] \times 3$) instead of deriving an equation to account for multiple sites. This assumption requires that the binding sites are independent and non-interacting as suggested by the ITC and ESI-MS data above.

As the concentration of binding sites ($[\text{B}]$) and ligand ($[\text{L}]$) is influenced by the amount of complex formed, their free concentrations ($[\text{B}]$ and $[\text{L}]$) are defined by the total concentration ($[\text{B}]_0$ and $[\text{L}]_0$) minus the concentration of the complex ($[\text{BL}]$) as shown in Equations 3 and 4.

The concentration of ligand bound protein is related to the K_D according to Equation 2.

$$K_D = \frac{[\text{B}][\text{L}]}{[\text{BL}]} \quad (2)$$

Exact concentrations of free ligand and free binding sites can be calculated using Equations 3 and 4.

$$[\text{B}] = [\text{B}]_0 - [\text{BL}] \quad (3)$$

$$[L] = [L]_0 - [BL] \quad (4)$$

Rearrangement of Equation 2 in terms of [BL] gives equation 5.

$$[BL] = \frac{[B][L]}{K_D} \quad (5)$$

The formulae for the free binding site and ligand concentrations in Equations 3 and 4 can be substituted into Equation 5 to give Equation 6.

$$[BL] = \frac{([B]_0 - [BL]) \times ([L]_0 - [BL])}{K_D} \quad (6)$$

Expansion of Equation 6 gives Equation 7.

$$[BL] = \frac{[BL]^2 - [B]_0[BL] - [L]_0[BL] + [B]_0 [L]_0}{K_D} \quad (7)$$

Equation 7 can be rearranged to equal 0 as shown in Equation 8.

$$0 = [BL]^2 - [BL](K_D + [B]_0 + [L]_0) + [B]_0 [L]_0 \quad (8)$$

As equation 8 is a quadratic formula, it can be solved using the quadratic formula in Equation 9

$$x = \frac{-b \pm \sqrt{b^2 - 4ac}}{2a} \quad (9)$$

Substitution of Equation 8 into Equation 9 yields Equation 10 to calculate the concentration of occupied binding sites ([BL]).

$$[BL] = \frac{(K_D + [B]_0 + [L]_0) \pm \sqrt{(K_D + [B]_0 + [L]_0)^2 - 4 [B]_0 [L]_0}}{2} \quad (10)$$

The theoretical fluorescence (F) was calculated by multiplying the calculated $[BL]$ by the molar fluorescence of an occupied site (F_{occ}). This value was added to the free binding site concentration $[B]$ (calculated in Equation 3) minus the concentration of complex multiplied by the fluorescence of the apo protein (F_{apo}). This gave Equation 11.

$$F = ([BL] \times F_{occ}) + ([B]_0 - [BL]) \times F_{apo} \quad (11)$$

Equations 10 and 11 were used to calculate the K_D , n , F_{apo} and F_{occ} using non-linear least squares fitting methods. The model was fitted to the fluorescence data by minimising χ^2 between the fitted and observed data points. This was achieved using the solver module in Microsoft Excel. Dilution of the protein and ligand was accounted for by recalculating all concentrations for each data point. This means that the slope seen after saturation (due to loss of signal by dilution as shown in Figure 3.3 B) is also fitted directly.

The calcium ion-contamination in the visinin-like domain solution was determined to be $10 \mu\text{M}$ by ICP-OES. To improve fitting the calcium ion-concentrations for each data point were updated to account for the initial concentration. Fitting of the data gave values of 6.51×10^3 and 7.80×10^3 fluorescence M^{-1} for F_{apo} and F_{occ} , respectively. The number of sites was calculated as 3.0 after correction for calcium ion-contamination (2.0 sites were observed) and the K_D was $2.12 \mu\text{M}$. The number of sites determined from this analysis was as expected. However, the value for K_D is ten-fold higher than the value obtained by ITC. The reason why the affinities are significantly different may be due to limitations in the fitting of the fluorescence data. As mentioned above, it is assumed that all sites are identical and independent and non-interacting. Non-identical interacting sites would provide a non-ideal fit to the model and thus give an incorrect value for K_D . However, the data presented within this chapter suggest that this assumption is most likely to be valid.

Another assumption is that all sites report equally upon calcium ion-binding meaning that the signal corresponds to all binding events. As the aromatic residues of each binding site were shown to respond differently upon calcium ion-binding by near-UV CD spectroscopy in Chapter two section 2.1.8 “Evidence of overall conformational changes in CCaMK”, this assumption is unlikely to be valid. As tyrosine residues were being monitored during the titration and the near-UV CD spectra demonstrate that the largest alteration in tyrosine environments occur upon calcium ion-binding to EF-hand three, it is likely that the majority of the signal in the curve is due to calcium ion-binding to EF-hand three. This means that the signal from EF-hands two and four is not correctly accounted for in the fitting, which in turn leads to errors in the calculated K_D . As there is no method by which the spectra can be deconvoluted, and models involving three sites are too complex, a more appropriate model cannot be applied to these data. Together this means that the K_D by ITC should be taken as the most reliable.

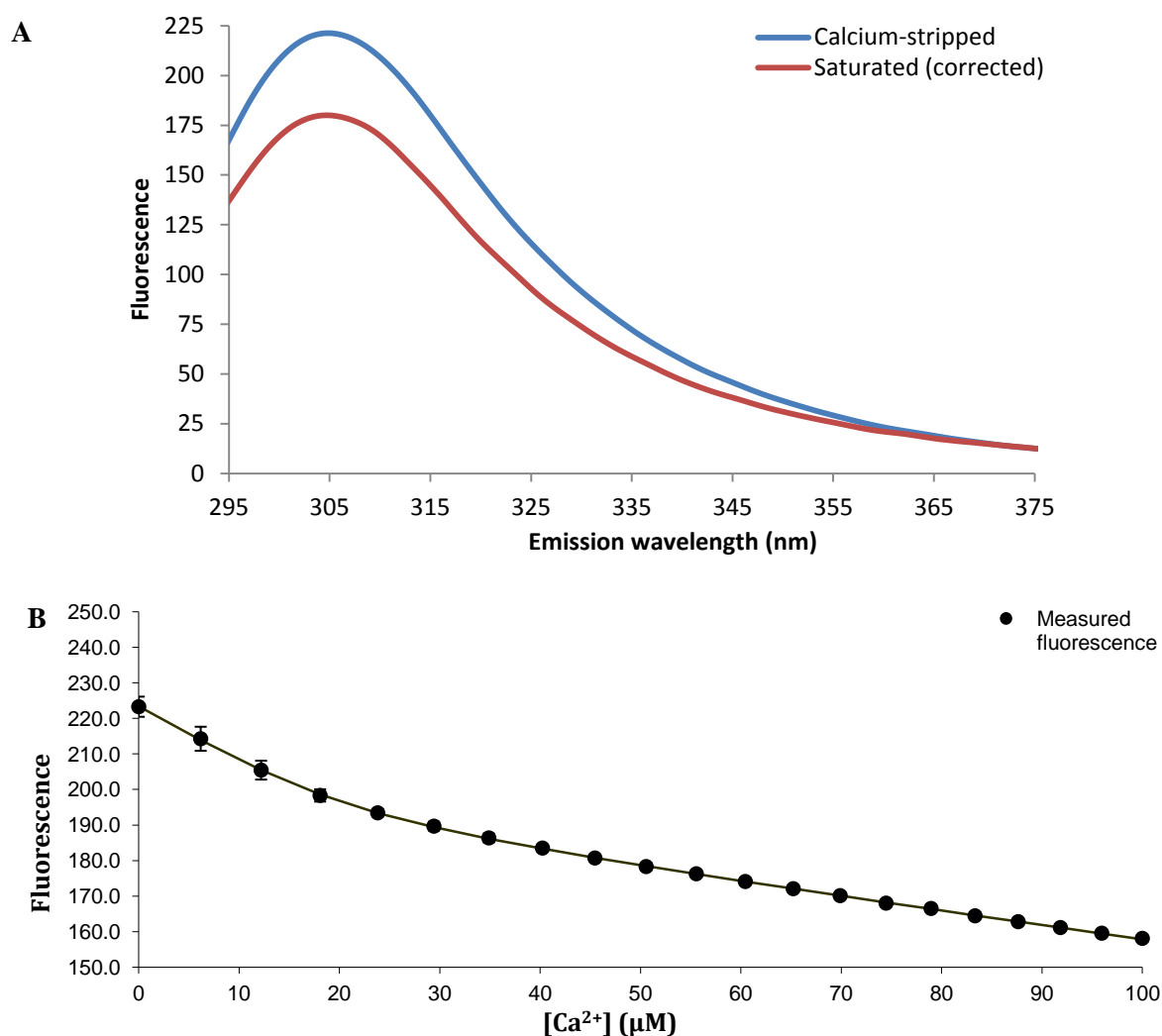


Figure 3.3. Titration of CaCl₂ into the CCaMK visinin-like domain monitored by tyrosine fluorescence. A, fluorescence spectra of the visinin-like domain after removal of calcium ions (calcium ion-concentration was 10 μM corresponding to one site occupied) using the NTA column (blue) and after calcium ion-saturation at the end of the titration (red). The calcium ion-saturated spectrum was corrected for dilution by multiplying values by 1.25. The excitation wavelength was 276 nm, slit widths were 10 nm and the scan speed was 500 nm min⁻¹. B, curve showing fluorescence of the CCaMK visinin-like domain construct at 305 nm over a titration of CaCl₂. Dots show the raw data and the line shows the data fitted with Equations 10 and 11, which were used to determine K_D , n and fluorescence per mol of apo (F_{apo}) and calcium ion-bound protein (F_{occ}) by non-linear least squares fitting. The initial protein concentration was 10 μM and 20 × 10 μl injections of 0.5 mM CaCl₂ were added with a new reading after each. Data were collected in triplicate and averaged. Error bars are ± standard errors for each value. The excitation wavelength was 276 nm, slit widths were 10 nm and the integration time was 0.5 s. Data fitting was performed in Microsoft Excel using the solver plug-in.

3.1.3 *Effect of EF-hand mutation on the calcium ion-affinity*

In order to assess the properties of each EF-hand, EF-hand mutants of the visinin-like domain construct were analysed by ITC. Comparison of these data with the wild-type allowed for some separation of the sites properties and their influences on the overall affinity of the visinin-like domain for calcium ions. Only the single EF-hand mutants were assessed in these experiments.

Mutation of EF-hand four lead to a three-fold reduction in the calcium ion-affinity. The K_D was 700 ± 122 nM. Values for ΔH , ΔG° and ΔS were very similar to the wild-type suggesting that calcium ion-binding to the observed sites was only slightly disrupted by this mutation as shown in Figure 3.4 C and Table 3.1. The largest difference was in the number of sites observed when compared to the wild-type data. A total of 1.6 of the two expected sites were determined to be free of calcium ions by both ITC and ICP-OES analysis. This suggests that the values determined for the EF-hand four mutant corresponded to both functional EF-hands. These data therefore demonstrated that EF-hand four is likely to be the high affinity site, which was pre-saturated with calcium ions in the wild-type protein.

Mutation of EF-hand two also had a small effect on the affinity for calcium ions. The K_D was determined to be 325 ± 58 nM, a 1.6 fold reduction when compared to the wild-type. The values for ΔH and ΔG° were also similar to the wild-type shown in Figure 3.4 A and Table 3.1. The number of sites observed by both ITC and ICP-OES was one of the two expected demonstrating that the high affinity site was still present in this mutant. This meant that the data collected were most probably associated with calcium ion-binding to EF-hand three only. The most profound change was in the ΔS , which was negligible at $-2.4 \text{ J mol}^{-1} \text{ deg}^{-1}$. This suggests that the favourable entropy of calcium ion-binding in the wild-type is caused by binding to EF-hand two. This means that calcium ion-binding to EF-hand three is driven by enthalpy. The entropic contribution of binding to EF-hand two may be due to a conformational change, which was abolished in the mutant. These conformational changes must give a larger positive entropy change then the loss of entropy through hydrophobic exposure, which was linked to EF-hand two in chapter two section 2.1.9 “Monitoring hydrophobic exposure upon calcium ion-binding”.

Mutation of EF-hand three had the largest effect on the affinity for calcium ions. The K_D was determined to be $5\,800 \pm 577$ nM, 30-fold lower than the wild-type shown in Figure 3.4 B and Table 3.1. Consequently the ΔG° was also less negative than that of the wild-type. The ΔH was significantly less negative whereas the ΔS was similar to the wild-type showing that the mutation of EF-hand three predominantly affects the enthalpy of binding. This reduction in affinity may be due to a reduction in protein stability; discussed in Chapter two section 2.1.7 “Determination of the visinin-like and autoinhibitory domains secondary structure”. Alternatively this could be due to the loss of a conformational change linked to EF-hand three. The values for the number of sites differed in the ICP-OES and ITC analysis. ITC suggested that only 0.8 sites were free of calcium ions, whereas ICP-OES suggested that this value was 1.5. It may be that some of the protein was

not active meaning fewer sites were seen by ITC than expected. Nevertheless it is clear from the data that mutation of the third EF-hand had the most profound effect on the calcium ion-affinity to the visinin-like domain of CCaMK.

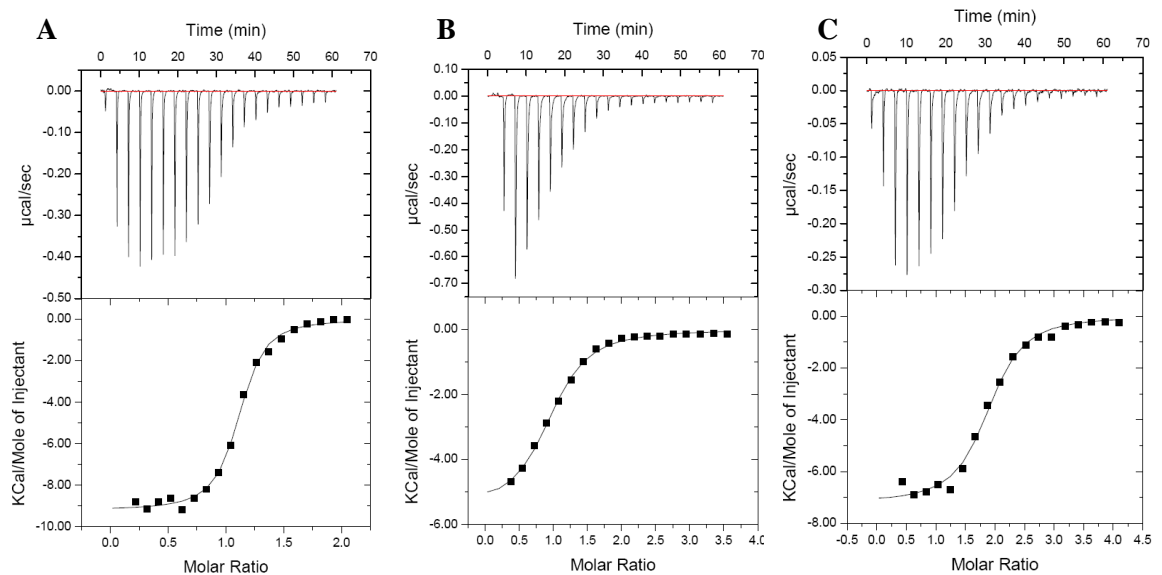


Figure. 3.4. Isothermal titration calorimetry of calcium ion-binding to the CCaMK visinin-like domain mutants. Isotherms of calcium ion-binding to the CCaMK visinin-like domain mutants A, EF-hand two, B, EF-hand three and C, EF-hand four. Isotherms are shown in the top panels and fitting to the integrated peaks with the one set of sites model is shown in the lower panels. Values for K_D , ΔH , ΔS , ΔG° and the numbers of observed sites are shown in Table 3.1.

3.2 DISCUSSION

The 200 nM K_D determined for the EF-hands is ideal for the interpretation of calcium spikes generated in *M. truncatula* root hair nuclei upon Nod factor stimulation, which has previously been measured at 5-800 nM *in vivo* (8). Although the protein does not appear to bind calcium ions cooperatively, the occupancy of the EF-hands would be expected to rise rapidly in accordance with the calcium spike provided the association rate is rapid (this will be discussed in detail in chapter 4 discussion [section 4.2]). Assuming all sites have a 200 nM K_D for simplicity, the proportion of protein bound with calcium ions at a particular calcium-ion concentration could be predicted using Equation 11. In this model the K_D was set to 200 nM and the calcium ion-concentration ($[L]$) was modelled over a range of 0 – 800 nM. To simplify the model the binding site concentration ($[B]$) was set to 10 nM. The simulated binding curve is shown in Figure 3.5. Note that this model will not be accurate should future experiments show that the CCaMK concentration exceeds 3.3 nM (10 nM binding sites) *in vivo*. This model showed that at 5 nM Ca^{2+} the occupancy of the EF-hands would be 2%. This rose to 5 and 9% at 10 and 20 nM calcium ions respectively. This shows that

occupancy is expected to be low at the basal concentrations. Additionally, as the occupancy is likely to be spread evenly over CCaMK molecules, the majority of CCaMKs will probably be in the apo form, or have a single calcium ion-bound. At a calcium ion concentration of 800 nM the predicted occupancy is 80% suggesting that an average of 2.4 sites per CCaMK will be occupied. This suggests that the majority of CCaMK will be in the double or triple ion-bound state at calcium ion concentrations corresponding to the top of a calcium spike. This demonstrates that the *in vivo* calcium ion-concentrations can be converted into a wide occupancy range of the CCaMK EF-hands under equilibrium conditions. The physiological relevance of these data is dependent on the rate constants of calcium ion-association and dissociation relative to calcium spiking. This will be discussed in chapter four “The kinetics of calcium ion-dissociation from the EF-hands”.

The binding data demonstrate that the EF-hands are unlikely to be cooperative. When combined with the ITC and ICP-OES data, these analyses showed that there are likely to be one high affinity site and two low affinity sites, which are independent and non-interacting. Analysis of the EF-hand mutants showed that EF-hand four is probably the high affinity site with a K_D of < 200 nM. This means that this site is likely to be occupied in a proportion of CCaMK molecules at basal calcium ion-concentrations. A similar situation was observed for the protein calcium- and integrin-binding protein, which contains two active EF-hands in position three and four. In this protein the affinity of EF-hand four is 3.5 times higher than EF-hand three at 0.54 and 1.9 μM , respectively (133).

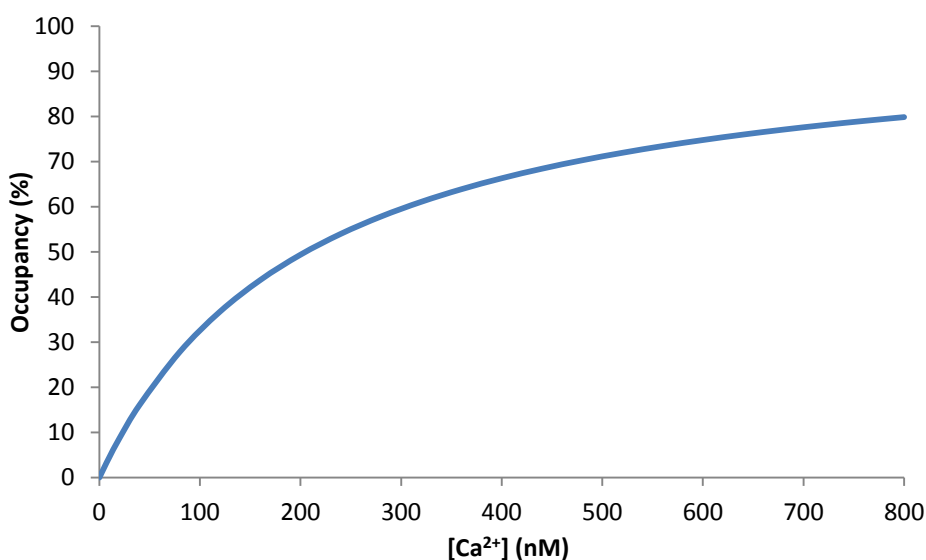


Figure 3.5. Predicted calcium ion-occupancy of CCaMK over the measured concentration range of a calcium spike. The predicted curve has been produced using Equation 11 to calculate the concentration of calcium ion-bound sites at a given calcium-ion concentration. The binding site concentration ($[B]$) was 10 nM and the K_D was 200 nM. A calcium ion-range of up to 800 nM is

based on *in vitro* measurements of nuclear calcium spiking in *M. truncatula* stimulated with Nod factor by (8).

Calcium ion-binding frequently leads to conformational changes in proteins (discussed in the introductory chapter section 1.1.4 “The EF-hand” and reviewed by Gifford et al) (26). These conformational changes are driven by calcium ion-binding, which allows the protein to adopt a more favourable conformation through the rearrangement of the EF-hand to accommodate the calcium ion. This process provides an overall favourable ΔG° value for binding. As the conformational changes in EF-hands are varied, the precise mechanisms leading to the values obtained in the ITC experiments cannot be determined in the absence of atomic resolution structural data. However, the values do provide insights on the enthalpic and entropic contributions of calcium binding, which drive the conformational changes discussed in chapter two.

Analysis of EF-hand mutants two and three revealed that the binding of calcium ions to the remaining two sites were driven differently. EF-hand two was linked to a change in entropy upon calcium ion-binding, which was lost when it was mutated. EF-hand two was previously linked to exposure of hydrophobic residues by ANS fluorescence described in chapter two section 2.1.9 “Monitoring hydrophobic exposure upon calcium ion-binding”. This would suggest that the entropy of conformational changes induced by calcium ion-binding to EF-hand two are able to exceed the unfavourable entropy of exposure of hydrophobic residues (152) leading to favourable entropy overall. Calcium ion-binding to EF-hand three was also shown to lead to conformational changes in Chapter two section 2.1.8 “Evidence of overall conformational changes in CCaMK” and section 2.1.10 “Low resolution structure of the CCaMK regulatory domains and calmodulin”. Together with the finding that calcium ion-binding to this site is favourable for both entropy and enthalpy, these data suggest that these conformational changes are linked to the favourable energy of calcium ion-binding to EF-hand three.

These data suggest a model where calcium ions bind to EF-hand four at basal concentrations. When the calcium ion-concentration increases, calcium ion binding to EF-hands two and three invokes conformational changes, which in turn allow the calcium ion-bound CCaMK to trigger downstream processes.

3.3 EXPERIMENTAL PROCEDURES

3.3.1 *Removal of calcium ions from protein samples*

All proteins were dialysed into 10 mM Tris-HCl pH 7.5 containing 50 mM NaCl and 1 mM TCEP. To minimise calcium ion-contamination all solutions were prepared in plasticware, which was washed with 1 M HCl and rinsed thoroughly with MilliQ water. All chemicals were $\geq 98\%$ purity. The chemicals used were Tris $\geq 99\%$ (Fomedium), NaCl $\geq 99.8\%$ (Sigma) and TCEP $\geq 98\%$ (Sigma). To remove calcium ions from the buffer, it was passed three times through a 40 ml Chelex

100 (BioRad) column. The resin was stripped of all ions by washing with 2 column volumes 1 M HCl followed by 2.5 column volumes of MilliQ water. To restore the pH of the column it was washed with 2 column volumes of 1 M Tris-HCl pH 7.5 followed by 100 ml MilliQ water. The buffer was then passed through as a 2-fold concentrate and diluted to the final volume (1 L) after three passes through the column.

Calcium ions were removed from the protein using a modified HisTrap FF column (GE Healthcare). All metal ions were stripped from the column by washing with 2 column volumes of 1 M HCl followed by 5 column volumes of MilliQ water. The column was then equilibrated with 15 column volumes of buffer. To decalcify the protein, samples were concentrated to 0.5 ml using a sartorius vivaspin 4 ml, 10 000 molecular weight cut-off centrifugal filter pre-washed with MilliQ water. Samples concentrated to 0.5 ml were injected onto the column and the flow-through was collected over 15 column volumes. Protein-containing fractions were retained and all other fractions were discarded. This process was performed three times to ensure calcium ion-removal was optimal.

Calcium ion-concentrations of samples were determined by ICP-OES as a service provided at the school of environmental sciences, UEA, Norwich.

3.3.2 *Electrospray ionisation mass spectrometry*

The method used was as described in Chapter two, experimental procedures, section 2.4.11 “Electrospray ionisation mass spectrometry” with the following amendments:

Samples were prepared in buffer, or 10, 20, 50, 75, 100 and 200 μM calcium acetate. Samples were not prepared in solutions containing magnesium acetate or EDTA.

3.3.3 *Isothermal titration calorimetry of calcium ion-binding to the CCaMK visinin-like domain.*

ITC experiments were performed with samples after calcium ion-removal as described above in “removal of calcium ions from proteins”, section 1.1.1. These experiments were performed on an iTC200 isothermal titration calorimeter (Microcal/GE healthcare). The CCaMK visinin-like domain and visinin-like domain mutants in EF-hands two and four were in the cell at a concentration of 15 μM , and mutant EF-hand three was at 75 μM . CaCl_2 was titrated over 20 injections ($1 \times 0.4 \mu\text{l}$ followed by $19 \times 2 \mu\text{l}$). CaCl_2 solutions were prepared using 99.99 % ultradry CaCl_2 (sigma) to ensure concentrations were accurate. CaCl_2 concentrations were 275 μM for wild-type, 250 μM Mutant EF-hand two, 1.3 mM Mutant EF-hand three and 300 μM for mutant EF-hand four. The wild-type protein was also assessed with the addition of 5 mM MgCl_2 , which was added to all solutions after calcium ion removal from the protein. In this experiment the protein concentration was 15 μM and the CaCl_2 concentration was 225 μM . All ITC experiments were performed at 25 °C. Data were processed using the Origin software package with the iTC 200 plugin provided by microcal.

3.3.4 *Titration of CaCl₂ into the visinin-like domain monitored by tyrosine fluorescence.*

Fluorescence experiments were performed on a Perkin Elmer LS55 luminescence spectrometer. Protein samples were prepared as described above in the “removal of calcium ions from proteins”, section 3.3.1. A 0.8 ml solution containing 10 μ M visinin-like domain was placed into a reduced volume (0.8-1.5 ml) clear quartz fluorescence cuvette and an initial reading was collected. Twenty 10 μ l injections of 500 μ M CaCl₂ were added to the protein solution with readings collected after each. Readings were collected by exciting at 276 nm and monitoring emission at 305 nm. The slit widths were 10 nm and the integration time was 0.5 s. Emission spectra were collected for an additional data set between 290 and 400 nm using an excitation wavelength of 276 nm, slit widths of 10 nm and a scan speed of 500 nm min⁻¹. All fluorescence experiments were performed at 25 °C. All CaCl₂ solutions were prepared with 99.99% ultradry CaCl₂ (Sigma).

4. Chapter Four – The kinetics of calcium ion-dissociation from the CCaMK EF-hands

In order to understand calcium ion-binding in the context of a calcium spiking signal, the kinetics of calcium ion-binding and dissociation must be known. As these values cannot be predicted using current knowledge of CCaMK or by analogy to other proteins or systems these rate constants had to be determined experimentally. In this chapter the determination of the calcium ion-dissociation rate constants for the visinin-like domain and visinin-like domain with autoinhibition will be described. It was determined that the third EF-hand has the fastest dissociation rate, with EF-hands two and four releasing calcium ions at a slower rate observable on the second time scale. The data will then be placed in the context of calcium spiking using a simple model to show that the calcium ion-bound CCaMK concentration is likely to oscillate with a similar pattern to the calcium spikes that are being interpreted.

4.1 RESULTS

4.1.1 *Calcium ion-dissociation rate constants from the visinin-like domain and visinin-like domain with autoinhibition*

In these experiments the dissociation rate constants of calcium ions from CCaMK were determined by stopped-flow using the calcium ion-sensitive dye Quin-2. Quin-2 is a chelator of calcium ions, similar to EGTA. However, unlike EGTA, it is able to report of whether calcium ions are bound by altering its absorbance (figure 4.2 A) and fluorescence spectra (not shown). Other dyes, which report on their calcium ion-occupancy, include BAPTA, Fura-2 and Rhod. In these experiments Quin-2 performed two major roles: First it was able to bind calcium ions as soon as they dissociated from the EF-hands of the CCaMK constructs. Secondly, the dye was able to report on its state of calcium ion-binding by alterations in their absorbance or fluorescence spectra. Together these properties allowed the indirect measurement of calcium ion-dissociation in real-time under stopped-flow conditions. The stopped-flow experiments involved the rapid mixing of protein solutions with solutions containing Quin-2 and monitoring changes in absorbance or fluorescence on the millisecond timescale. These experiments were designed to give a final Quin-2 concentration that greatly exceeded the concentration of calcium ion-binding sites in the protein. Under these conditions competition between the protein and Quin-2 for calcium ions is minimised by driving the equilibrium towards calcium ion-bound Quin-2. The effect of this is that the rates measured are not limited by the time required to reach equilibrium between calcium ion-bound protein and calcium ion-bound dye. Additionally, the calcium ion-association rate to the dye was much faster than the release rate from the EF-hands (described in the control experiments below). Together these properties allow the assumption that the rates observed are exclusively due to

calcium ion-dissociation from the protein. This allowed the reaction to be treated as first order greatly simplifying the data analysis.

In preliminary experiments the calcium ion-bound state of Quin-2 was monitored by fluorescence. When Quin-2 binds calcium ions, the fluorescence at 495 nm is reduced. This means that as Quin-2 binds calcium ions a reduction in the signal is observed and an increase is observed when calcium ions dissociate.

Control experiments showed that the rate constant of calcium ion-dissociation from 50 μM calcium ion-saturated Quin-2 when mixed with an excess of 10 mM EDTA at 25 °C was $61.2 \pm 0.2 \text{ s}^{-1}$ (shown in Figure 4.1 by the brown trace). This value agrees with the value of 61.2 s^{-1} published by Bayley *et al.* This result demonstrates that the experimental setup is able to produce reliable data, which can be compared to previously reported calcium ion-dissociation experiments on CaM (85). It was shown in a separate experiment that mixing buffer with Quin-2 which gave a higher signal than when dye was mixed with calcium as expected. (shown in Figure 4.2 by the black trace). Note that the absolute fluorescence values differed between the two experiments as the arc lamp power was reduced to approximately 75% in the longer time courses to reduce the effects of bleaching.

The association of calcium ions to Quin-2 occurred within the 1 ms dead-time of the instrument (shown in Figure 4.1 by the red trace). Although no binding curve was seen, comparison of this curve with the data for calcium ion-saturated Quin-2 mixed with excess EDTA demonstrated that the calcium ion-saturated protein had been formed. Given the very rapid rate of calcium ion-dissociation from Quin-2, it was clear that the dye in this experiment was calcium ion-bound after 1 ms. This demonstrates that any observed calcium ion-binding events when Quin-2 was mixed with calcium ion-saturated protein were a result of calcium ion-dissociation from the EF-hands, which would be rate limiting.

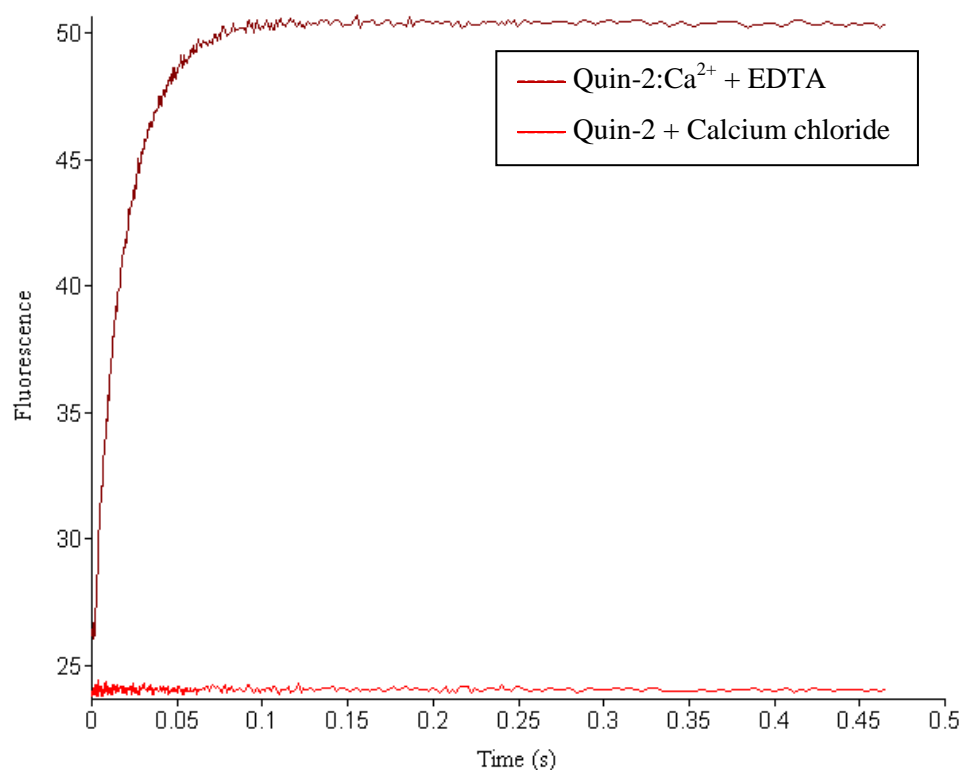


Figure 4.1. Calcium ion-binding and dissociation data for Quin-2. Time-course of Quin-2 binding calcium ions is shown in red (final concentrations 50 μM Quin-2 and 1 mM CaCl_2). Calcium ions were bound by Quin-2 within the 1 ms dead time of the stopped-flow spectrophotometer. Calcium ion-dissociation is shown in brown (final concentrations 50 μM Quin-2, 100 μM CaCl_2 and 10 mM EDTA); the k_d was $61.2 \pm 0.2 \text{ s}^{-1}$. Data were collected at 25 $^\circ\text{C}$ in 10 mM Tris-HCl pH 7.5 containing 50 mM NaCl and 1 mM TCEP. The excitation wavelength was 365 nm and emission was monitored above 450 nm. Both curves are the averages of three time courses.

Preliminary experiments using Quin-2 fluorescence clearly showed that the experimental conditions were able to provide time-courses for calcium ion-dissociation as shown in Figure 4.2 A (red). In order to ensure that there were no undesired background effects and allow the calcium-ion concentration to be estimated, two control experiments were performed. These involved mixing either buffer or buffer supplemented with 20 μM CaCl_2 , with Quin-2 (shown in Figure 4.2 A in the black and grey curves, final concentrations were 50 μM Quin-2 and 0 or 10 μM CaCl_2 , respectively). The end points of these controls allow the baseline signal and the signal corresponding to 20 μM calcium ions to be determined. From these controls the calcium ion-concentration within the protein samples could be estimated. As an EDTA control was not performed for these fluorescence data, the level of calcium ion-contamination in the buffer was not determined in this case.

In these experiments, it was initially assumed that the EF-hands of the visinin-like domain were fully saturated with calcium ions after dialysis as indicated by the requirement to remove calcium ions for the affinity studies discussed in chapter three. This was confirmed by the data showing that the protein solution gave a final signal, which corresponded to a total calcium ion concentration exceeding the 10 μM binding site concentration at 13.5 μM (shown in Figure 4.2 A). The dissociation rate constant obtained was $4.86 \pm 0.06 \text{ s}^{-1}$ for 33.3 μM visinin-like domain mixed with 100 μM Quin-2 (fit is shown in Figure 4.2B). A major problem in the preliminary experiments was that Quin-2 was bleaching over the experimental period as shown in Figure 4.2 A, which is the cause of the slope in the trace after the end-point of the reaction. The signal for the buffer control reduced by 2.7 and the signal for the 20 μM CaCl_2 control reduced by 1.1 corresponding to a loss of 7 and 4% respectively over the 20 s time period. This was a significant loss of signal as the calcium ion-dissociation curve gave a signal of 3.5 fluorescence units after subtraction of the 20 μM CaCl_2 control. As the calcium ion-bound and apo forms of Quin-2 may bleach at different rates, as the controls suggested, it was not possible to remove the effect of this from the rate data, which may have lead to inaccuracies.

To reduce bleaching the light level would need to be reduced further. However this would have significantly reduced the signal leading to difficulty in fitting the data. To overcome these issues the logical step would have been to increase the protein concentration to increase the signal. This would require an increase in the concentration of Quin-2 to maintain the excess. However, the Quin-2 concentration could not be increased in a way that was compatible with fluorescence at 365 nm. This was because the absorbance was already close to the inner filtering limit of 0.1 absorbance units at a concentration of 50 μM in the calcium ion-free form (shown in Figure 4.3 A). When absorbance is above 0.1 absorbance units at the excitation wavelength, signal is lost due to re-absorption of emitted light. It was also inappropriate to alter the excitation wavelength as 365 nm was the only suitable output line of the Hg arc lamp for Quin-2. This is because absorbance at 330 nm was too strong, and the absorbances at 405 nm were very similar in the calcium ion-bound and apo forms meaning there would be little or no signal corresponding to calcium ion-binding. In addition, Fura-2 and Rhod could not be used as their extinction coefficients were higher than that of Quin-2 at appropriate wavelengths (Figure 4.3 B and C). Finally, it was not possible to switch to the use of the Xe arc lamp, for which any wavelength in the absorbance range of the chelators can be used, as its output is orders of magnitude less meaning the signal would be too weak for the detector.

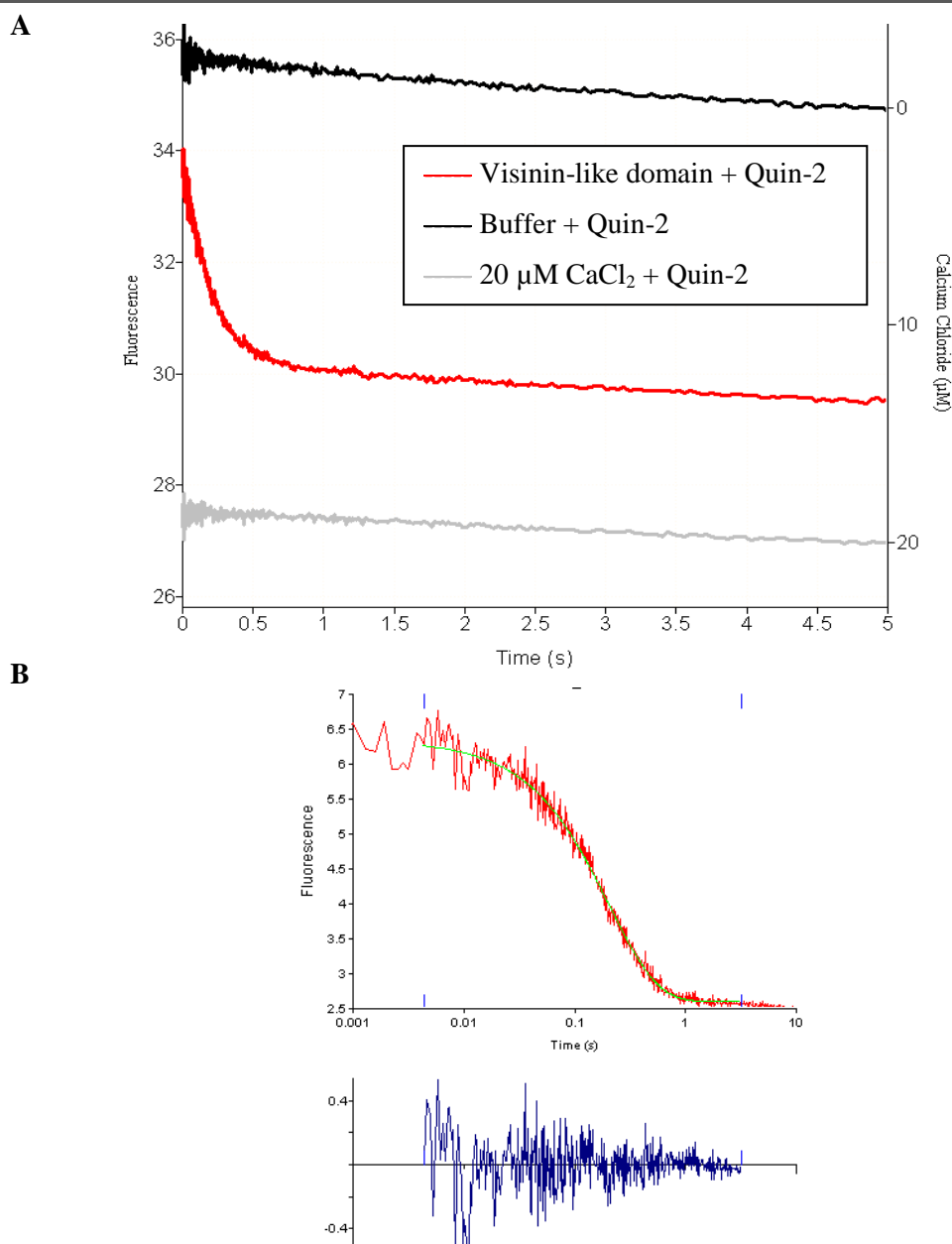


Figure 4.2. Calcium ion-dissociation from the visinin-like domain construct monitored by Quin-2 fluorescence. A, curve showing calcium ion-dissociation from the visinin-like domain (red line). Final concentrations were 50 μM Quin-2 and 3.33 μM visinin-like domain. The black and grey lines show controls of Quin-2 vs. buffer or Quin-2 vs. 20 μM CaCl_2 respectively (final concentrations were 50 μM Quin-2 and 0 or 10 μM CaCl_2 respectively). The gradient in the line after the end-point of each reaction is due to photo-bleaching of Quin-2. A second axis has been added to indicate the levels of calcium indicated by the controls. Data are shown on a linear time scale zoomed to the first five seconds and the temperature was 23 $^\circ\text{C}$. B, fitting to the visinin-like domain calcium ion-dissociation curve after subtraction of the 20 μM CaCl_2 control. The rate constant determined was $4.86 \pm 0.06, \text{s}^{-1}$. Data are shown on a logarithmic time scale. For all curves the excitation wavelength was 365 nm and emission was monitored above 450 nm. All curves are the averages of three time courses.

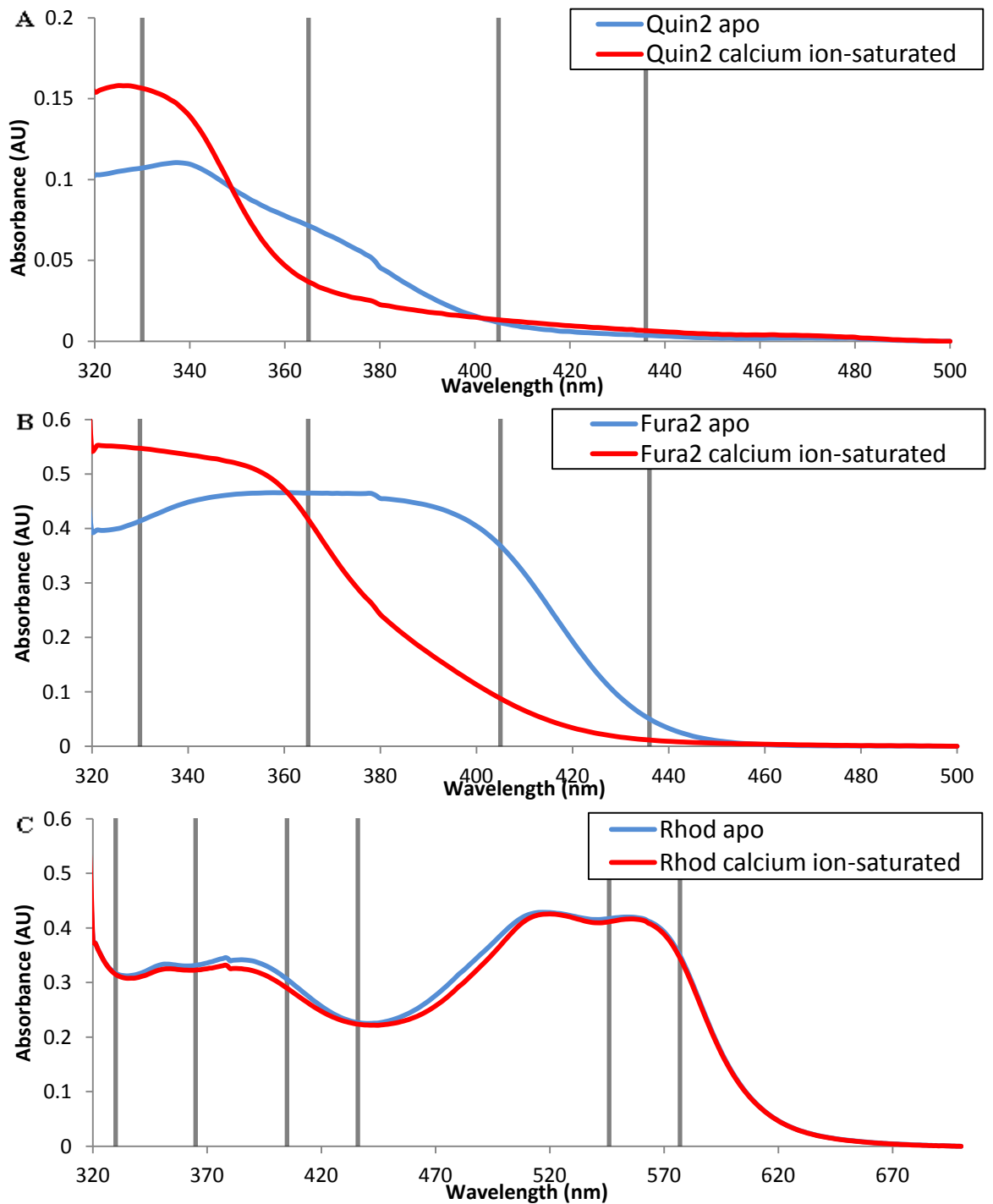


Figure 4.3. UV/Vis spectra of ion-calcium sensitive dyes. Spectra of A, Quin-2, B, Fura-2 and C, Rhod. All dyes were at a concentration of 50 μM in the apo form (spectra shown in blue lines), and 45.45 μM in the calcium ion-saturated form (red lines), which have been scaled to account for the dilution. Vertical lines correspond to the maximum intensity peaks in the output profile of the Hg arc lamp, which are at 313, 330, 365, 405, 436, 546 and 577 nm. Typical excitation wavelengths are 265, 370 and 552 and emission wavelengths are 506, 476 and 581 for Quin-2, Fura-2 and Rhod respectively.

To overcome the problems encountered using fluorescence, calcium ion-binding to Quin-2 was monitored by absorbance. This had many advantages. First, the Xe arc lamp could be used, which has an even output spectrum allowing any wavelength in the appropriate region in the Quin-2 absorbance spectrum to be selected. In addition the absorbance limit was only set by the linear range of the detector (quoted at 2.2 absorbance units) allowing much higher concentrations of Quin-2 and thus a larger excess to be used. Finally, due to the weaker light source, bleaching of the Quin-2 did not occur.

It was shown that the calcium ion-dissociation rate constant was dependent on temperature, as expected. Rate constants of 2.33 ± 0.02 , 2.91 ± 0.02 and 5.74 ± 0.02 s⁻¹ were determined for 15, 20 and 25 °C respectively. This same effect was observed by Bayley *et al.* on the dissociation rate constant of calcium ions from calmodulin (85). The similarity of the rate constants at 25 °C and at 23 °C by fluorescence showed that the data are comparable between the two methods. This also indicates that the increase in Quin-2 excess had little effect on the observed rate constant of calcium ion-dissociation from the EF-hands. As the slower rate constants allow a larger proportion of the curve to be observed within the experimental period due to less of the process occurring within the dead-time, all further experiments were conducted at 15 °C.

To optimise the signal and Quin-2 excess, final concentrations of 100 μM binding sites (33.3 μM wild-type proteins, 50 μM of the single mutants and 100 μM of the double mutants) and 2 mM Quin-2 were selected. To ensure that the protein was in excess calcium ions the protein solutions were supplemented with 100 μM CaCl₂. A wavelength of 390 nm was selected to give an absorbance of approximately 1 absorbance units in a region of the Quin-2 spectrum that provides a significant absorbance change upon calcium ion-binding. This ensured a strong absorbance signal within the linear range of the detector to give the best compromise between signal and noise.

As described for the fluorescence data, control experiments using solutions of known calcium ion concentrations (100 or 200 μM to give 50 or 100 μM final) were used to calibrate the signal and estimate the amount of calcium observed in the dissociation curves (Data not shown). An EDTA control was also performed to chelate all calcium from the buffer (Data not shown). Comparison of the end-point of the EDTA control with the known calcium ion-concentration controls allowed the calcium ion-contamination to be estimated at approximately 10 μM. As the level of calcium ion-contamination was much lower than the chelator concentration it was not considered significant. Comparison of the signal for calcium ion-dissociation from the wild-type visinin-like domain with the controls demonstrated that the signal seen was approximately 50% of the total expected (shown in Figure 4.4 A). This means that calcium ion-dissociation from 1.5 sites was observed within the experimental period, demonstrating that at least one site released its calcium ion within the 1 ms dead time of the instrument. The rate data for the observed phase were fitted to a single exponential and gave a value of 2.11 ± 0.01 s⁻¹ at 15 °C as shown in Figure 4.4 A

in the blue trace, Figure 4.4 B and Table 4.1. A similar slow rate constant was obtained when fitting with two exponentials, which gave rate constants of 19 ± 1 and $1.99 \pm 0.01 \text{ s}^{-1}$ and amplitudes of 0.0043 and 0.059, respectively. As the amplitude of the fast rate was only 7% of the overall signal, which does not correlate to the number of expected sites, the single exponential model was deemed most appropriate. Taken together these data show that the visinin-like domain undergoes biphasic kinetics where at least one calcium ion was released within 1 ms (rate constant $> 700 \text{ s}^{-1}$) and the remaining calcium ions dissociate with a half life of 0.33 s. This is likely to be an average rate constant for the slow release sites, which could not be resolved.

The control experiments showed fluctuations in the Quin-2 signal at the beginning of the experimental period with amplitude of 0.006 over approximately 0.1s (shown in Figure 4.4 A in the black and grey traces). This corresponded to 5% of the expected signal of 0.11 for 50 μM calcium ions and 10% of the 0.06 amplitude of the observed visinin-like domain dissociation curve. The rate constant obtained for the visinin-like domain after deduction of the 100 μM CaCl_2 control (Figure 4.4 C) was 2.04 ± 0.03 , which was an decrease of 0.07 (3%) over the fit to the raw data. In addition, noise levels were increased after the subtraction, meaning a reduced time range of 0.07-4.26 could be fitted reliably. This was predominantly due to deviation from the single exponential model at the beginning and end of the curve. A range of 0.008 – 8.7 s could be used to fit the raw data. Deduction of the 200 μM control (Figure 4.4 D) improved fitting allowing a range of 0.006 – 11 s to be used to yield a rate constant of 2.001 ± 0.001 . However this only corresponds to a decrease of 0.11 (5%) when compared to the raw data. As the effect of background deduction was insignificant it was concluded that background deduction was not required. In addition the inconsistency of the background deduction makes direct comparison of data more difficult. From this it should be noted that the background effects may have lead to errors in the fitting, which should be accounted for in any conclusions made. The background corrected data suggests that this error was approximately 5%.

Analysis of the visinin-like domain with autoinhibition also showed that one site released its calcium ion within 1 ms. The remainder of the curve corresponded to two complete sites (shown in Figure 4.4 A by the green curve) with a best fit to the two exponential model giving rate constants of 4.0 ± 0.2 and $0.57 \pm 0.01 \text{ s}^{-1}$ with amplitudes of 0.012 (25%) and 0.039 (75%) respectively (shown in Figure 4.4 C and Table 4.1) These values do not correspond to the expected 1:1 ratio. This may be due to the similarity between them meaning that they cannot be completely resolved. Attempts to fit the data to a single exponential model did not yield an acceptable fit as the residuals were too large (data not shown). Comparison of the data for the visinin-like domain and visinin-like domain with autoinhibition suggests that interactions between the regulatory domains have a small effect on the calcium ion-binding properties. The slowing of the rate may be the reason why two rate constants can be determined in the visinin-like domain with autoinhibitor data whereas only one can be determined for the visinin-like domain. This is because a slower rate provides

more observable data that can be fitted. In addition the slowing of the rate constants may not be equal for all sites separating them enough to be resolved.

Taken together these data show that the calcium ion-binding sites differ in their dissociation kinetics. This conclusion is based upon the fast unobserved rate constant, which must be $>700 \text{ s}^{-1}$, and the rate constants for the remaining two slow sites of the visinin-like domain with autoinhibition, which were similar.

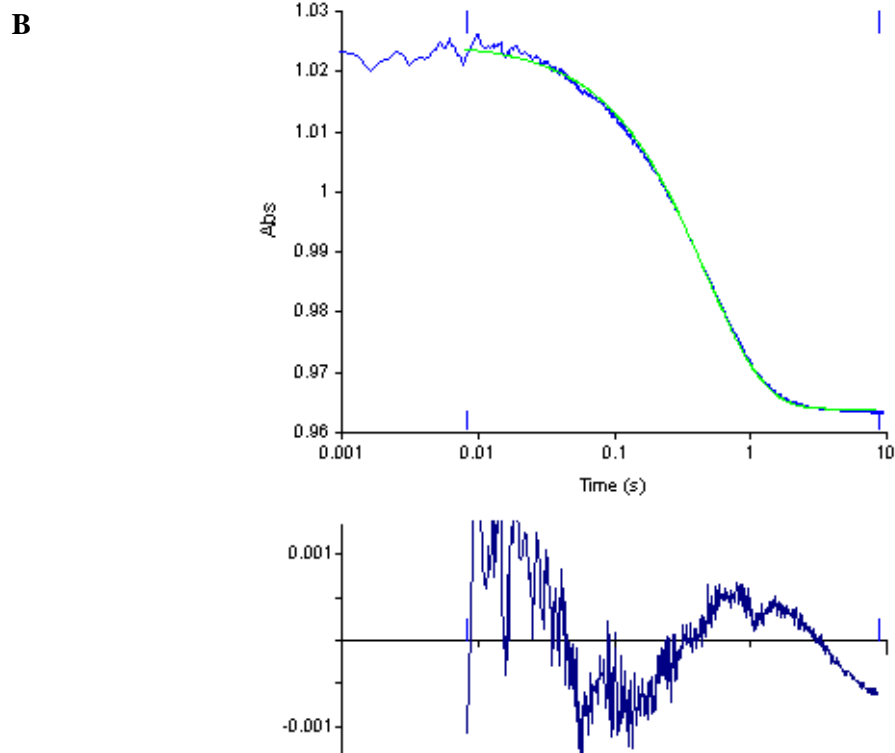
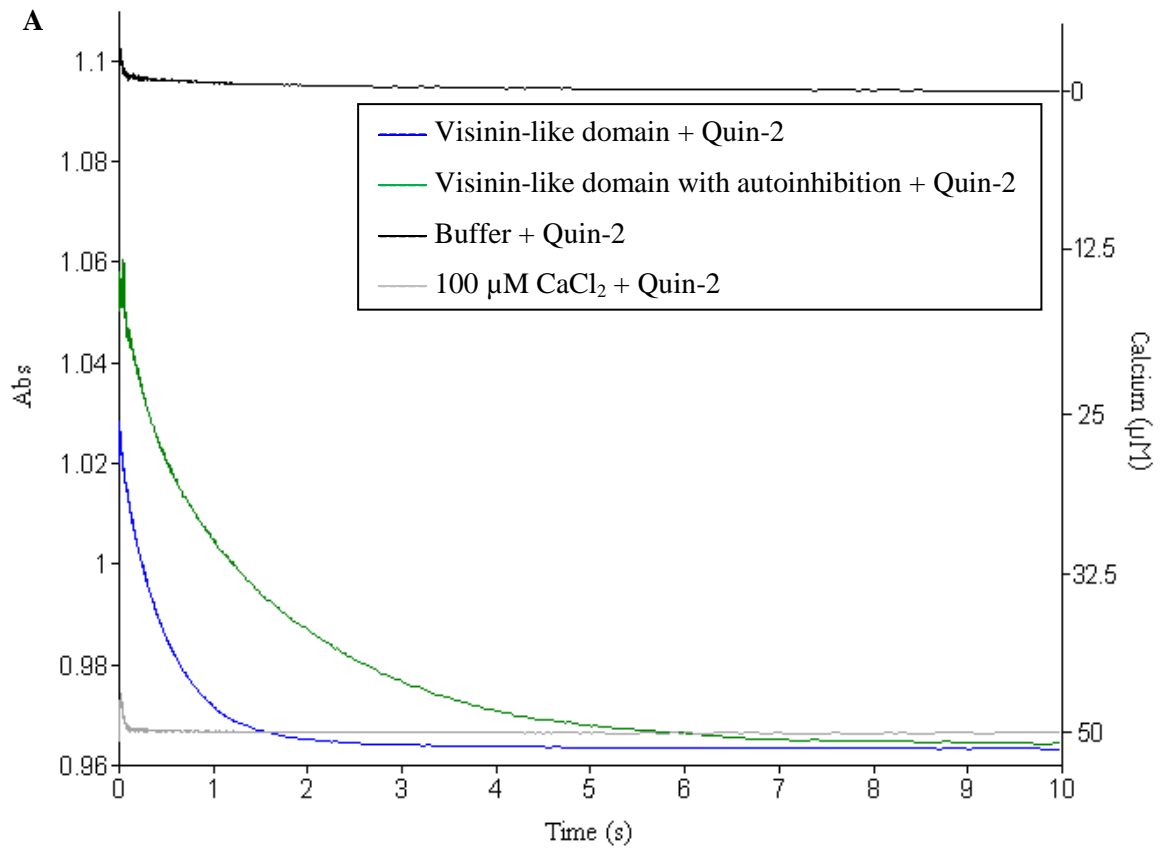
Protein	Sites ^a	k_d		$t^{1/2}$		k_a (calculated)		K_D
		Fast	Slow	Fast	Slow	Fast	Slow	
		s^{-1}		s		$M^{-1} s^{-1}$		nM
Visinin-like domain	1.5	n/d ^b	2.11 ± 0.01	n/d ^b	0.33	n/d ^b	1.05 × 10 ⁷	200 ± 46
Visinin-like domain with autoinhibition	2	4.0 ± 0.2	0.57 ± 0.01	0.17	1.19	n/d ^b	n/d ^b	n/d ^b
Visinin-like domain Mutant EF-hand two	1	12.8 ± 0.2	1.55 ± 0.02	0.05	0.45	3.93 × 10 ⁷	4.77 × 10 ⁶	325 ± 58
Visinin-like domain Mutant EF-hand three	1	15.2 ± 0.3	2.55 ± 0.06	0.05	0.27	2.60 × 10 ⁶	4.37 × 10 ⁵	5800 ± 580
Visinin-like domain Mutant EF-hand four	1	n/d ^b	5.03 ± 0.03	n/d ^b	0.13	n/d ^b	7.58 × 10 ⁶	660 ± 120
Visinin-like domain Mutant EF-Hands two-three	1				n/d ^b			
Visinin-like domain Mutant EF-Hands two-four	0				n/d ^b			

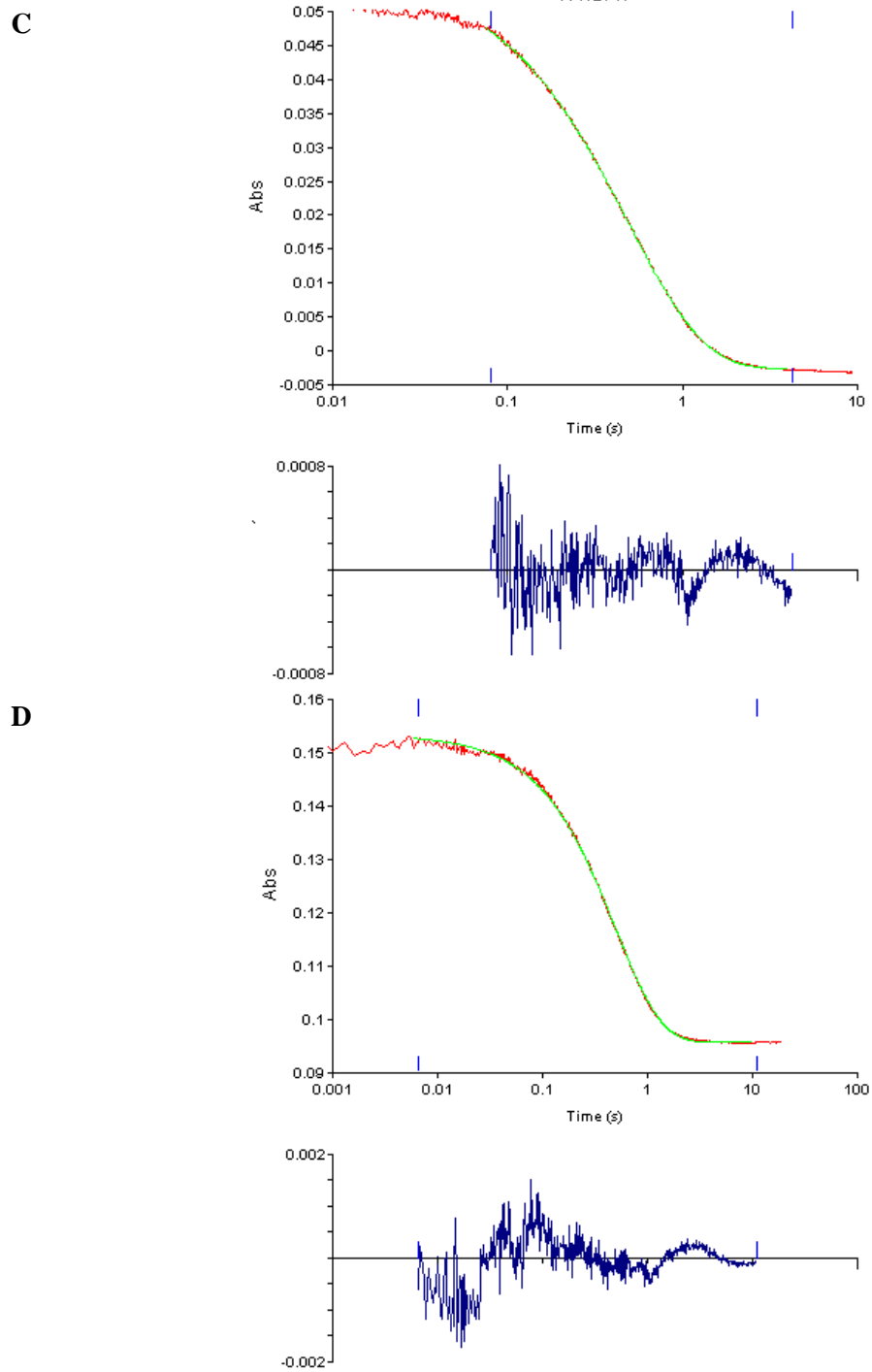
Table. 4.1. Kinetics of calcium ion binding to CCaMK

Measured calcium ion-dissociation rate constants for the visinin-like domain, the visinin-like domain with autoinhibition and the visinin-like domain EF-hand mutants. $t^{1/2}$ Values were calculated from the rate constant data using the formula $t^{1/2} = \frac{1}{k} \times 0.693$. Association rate constants were calculated with the formula $k_a = \frac{k_d}{K_D}$ using the k_d values below and K_D values determined in chapter three. It was assumed that the K_D s are identical for each site.

^a number of EF-hands for which a rate was observable

^b not determined





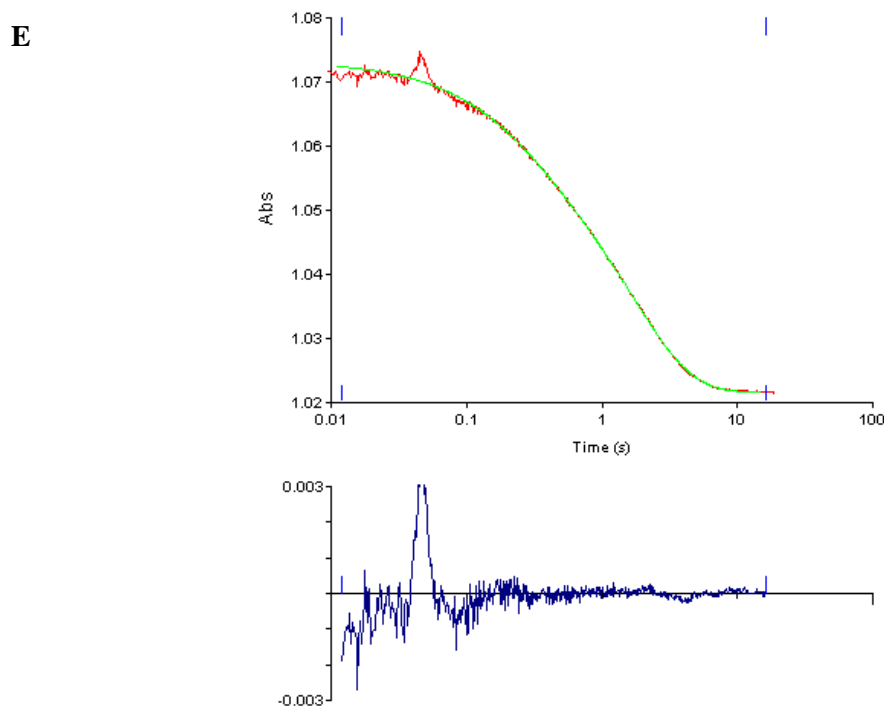


Figure. 4.4. Stopped-flow spectrophotometry time courses of calcium ion-dissociation from the visinin-like domain and visinin-like domain with autoinhibition. A, calcium ion-dissociation curves for the visinin-like domain (blue line) and the visinin-like domain with autoinhibition (green). Controls of buffer only (black) and 100 μM (50 μM final) CaCl_2 (grey) show the expected range for calcium ion-release from the EF-hands. For illustrative purposes, the trace for the visinin-like domain with autoinhibition has been scaled according to the expected range from its associated controls. B, fit to the trace for the visinin-like domain using the single exponential model. C, single exponential fit to the trace for the visinin-like domain after deduction of the 100 μM or D, 200 μM controls. E, fit to the trace for the visinin-like domain with autoinhibition using the two exponential model. The best fit is shown in the top panel in green overlaying the raw data in blue. The lower panel shows the residuals of the fit. Data were collected by Quin-2 absorbance at 390 nm Protein concentrations were 33.3 μM to give a 100 μM binding site concentration (final protein concentration 16.65 μM , 50 μM binding sites) and supplemented with 100 μM CaCl_2 (50 μM CaCl_2 final). All solutions were prepared in 10 mM tris-HCl pH 7.5 containing 50 mM NaCl and 1 mM TCEP.

4.1.2 Dissection of the calcium ion-dissociation from the individual EF-Hands

In order to determine the contribution of each individual EF-hand to the overall dissociation curves, the single and double EF-hand mutants of the visinin-like domain were analysed. The single mutants all gave curves with an amplitude corresponding to the release of a single calcium ion, suggesting that each protein contained one fast and one slow site as shown in Figure 4.5 A. However, the best fits were obtained with the two exponent model for mutants of EF-hands two or

three. The amplitudes for each rate constant were similar (mutant EF-hand two – 0.022 fast and 0.026 slow, mutant EF-hand three 0.028 fast and 0.021 slow) suggest that both may be significant. The two rate constants may have arisen from additional rate limiting steps, such as conformational changes, which were not as evident in the wild-type rate data. Analysis of the EF-hand two or three single mutants showed that their slow dissociation rate constants corresponded well to the wild-type protein as shown in Table 4.1. However the fast rate constant did not correspond to the data for the wild-type. This suggests that dissociation of one calcium ion is being observed with non-ideal kinetics. As the ESI-MS data discussed in chapter two clearly shows that the single mutants contain two active EF-hands, this result was unexpected. This is because by analogy to the rate data for the wild-type visinin-like domain, one mutant was expected to contain two slow sites and the other two single mutants were expected to contain one slow site and one fast site. This unexpected result may be because mutation of one EF-hand could affect the properties of the other sites by affecting a conformational change or protein stability. The rate constant for the EF-hand four mutant was approximately double that of the wild-type, which may suggest that EF-hand four releases its calcium ion slower than EF-hand two suggesting that EF-hand four may have been associated with the slower rate constant for the wild-type visinin-like domain.

The data in Figure 4.5 B show that the EF-hand two-three double mutant gave a signal corresponding to one site accounting for the single active EF-hand but could not be fitted to any kinetic models. This may be because the two-three double mutation has further impaired the protein stability or the conformational change leading to complex kinetics for the fourth EF-hand, which could not be analysed. The two-four double mutant on the other hand gave no visible curve, but was at a level corresponding to the maximum expected calcium ion-concentration showing that the protein contained the expected concentration of calcium ions. This shows that the calcium ion bound to EF-hand three dissociated within the 1 ms dead time. Taken together these data show that EF-hand three is the fast dissociation site and dissociation from EF-hands two and four occurs at a slower rate constant, which is observable on the second timescale. The data for the single mutants suggests that EF-hand four releases calcium at a slower rate than EF-hand two but as they are similar, they are difficult to separate into two distinct events.

Combination of this conclusion with the mutant data suggests that calcium is released from EF-hand three first due to its fast dissociation rate constant, then from EF-hands four two, which are the slow release sites.

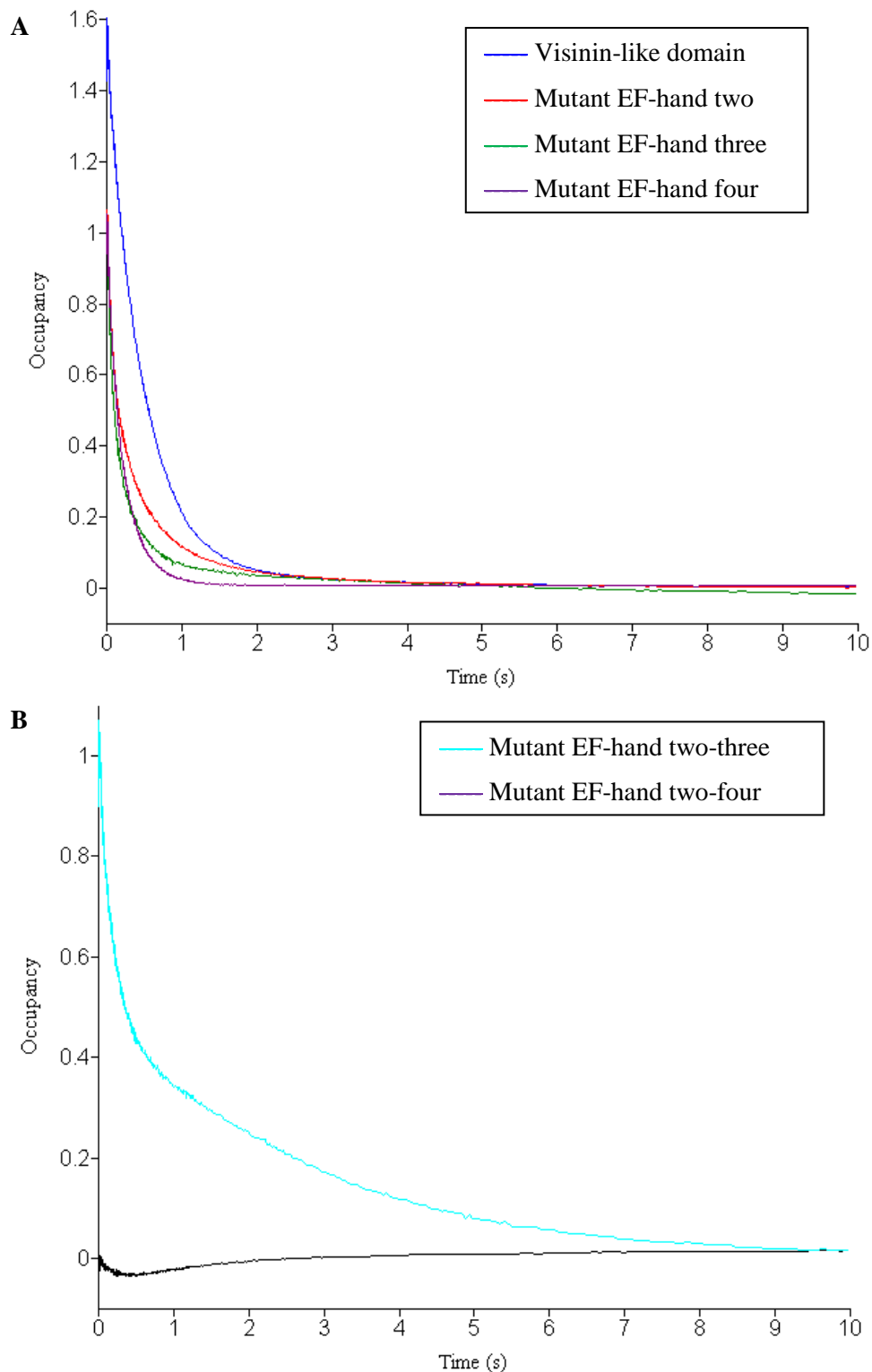


Figure 4.5. Stopped-flow traces of calcium ion-dissociation from the visinin-like domain EF-hand mutants. A, calcium ion-dissociation curves for the wild-type visinin-like domain (blue line) and the single EF-hand mutants (two – red, three – green and four – purple). B, traces for EF-hand double mutants two-three (cyan) and two-four (black). All traces have been scaled according to the occupancy calculated using control experiments.

4.1.3 Calculation of the calcium ion-association rate constants

Using the data presented in this chapter, and the affinities for the visinin-like domain and single EF-hand mutants presented in chapter three, estimates for the calcium ion-association rate constants were calculated. This was achieved by rearranging the formula $K_D = \frac{k_a}{k_d}$ to $k_a = \frac{k_d}{K_D}$. These estimates rested on some assumptions. The major assumption is that the K_D values are identical for all sites; however the K_D for EF-hand four is likely to be higher than the values determined, and the K_D of 200 nM is likely to be an average for the second and third sites as discussed in chapter three. Additionally, it is assumed that the dissociation rate constants calculated are distinct for each site rather than averages for multiple sites. These assumptions mean that matching of appropriate rate constants and K_D s cannot be undertaken to give accurate rate constants for each site, therefore the estimated k_a s are estimations of actual association rate constants (Table 4.1). These data show that calcium ion-association to the wild-type protein for the observed sites was rapid at $1 \times 10^7 \text{ M}^{-1} \text{ s}^{-1}$ meaning that the process is diffusion rate limited. Using the same assumptions the maximum k_a for the fast dissociation site also estimated. It was assumed that the K_D for this site was at most 200 nM and the off rate constant was at least 700 s^{-1} . These parameters yielded k_a of $3.5 \times 10^9 \text{ M}^{-1} \text{ s}^{-1}$. The diffusion rate limit of binding appears to remain when EF-hand two and four are disabled. The mutant in EF-hand three shows a significant reduction of 24-fold in the calcium ion-association rate constant when compared to wild-type but this is still rapid. Taken together these data suggest that the alterations in affinity seen for the EF-hand mutants in chapter three were a result of alterations in both the association and dissociation rate constants. These data also demonstrate that even the slowest association rate constants are close to diffusion rate limitation.

4.2 DISCUSSION

The CCaMK EF-hands display multi-phase dissociation kinetics, with each EF-hand apparently releasing its calcium ion at a different rate. From the present data the magnitude of the difference between the dissociation rate constants cannot be determined exactly. However, the data do allow basic modelling to aid understanding of how the CCaMK EF-hands respond to calcium spiking *in vivo*.

As the association rate constants appear to be essentially diffusion rate limited at $1 \times 10^7 \text{ M}^{-1} \text{ s}^{-1}$ and $3.5 \times 10^9 \text{ M}^{-1} \text{ s}^{-1}$, the EF-hands would be expected to bind calcium ions rapidly mimicking the upward phase of the calcium spike, which has a duration of approximately 10 s (30). This also shows that limitations in the estimates of the association rate constants do not compromise the data sufficiently to alter the conclusion made. Some of the dissociation rate constants also appear to be rapid, although 1.5 – 2 EF hands release calcium ions at a rate that can be observed on the second timescale. The rate constants obtained show that the process of calcium ion-release is rapid and significantly faster than the calcium spiking interval of approximately 90 s in *M. truncatula* root

hair cells stimulated with Nod factor (36). This means that calcium ions would be expected to be released from the EF-hands at a rate that closely resembles the downward phase of a calcium spike, which has duration of approximately 51 s (30). In addition, the difference between the observed dissociation rate constants, and *in vivo* calcium spiking frequency is too large for conclusions to be affected by the limitations caused by the small background signal in the dissociation curves, which was evident from the buffer and calcium only controls. Together these conclusions suggest that the concentration of calcium ion-bound CCaMK could oscillate in a pattern similar to that of calcium spiking.

Models of calcium ion-occupancy of the CCaMK EF-hands in response to calcium oscillations were produced using the Copasi software package (153) as shown in Figure 4.6. Calcium spiking was simulated to give a similar profile to the calcium spiking observed in *M. truncatula* as described in the experimental procedures. This calcium spiking simulation was used to predict the behaviour of the of calcium ion-bound CCaMK during spiking. To simplify the model only a single site was considered with the measured k_d and calculated k_a of the slowest dissociation site. These values were $2.11 \pm 0.01 \text{ s}^{-1}$ and $1 \times 10^7 \text{ M}^{-1} \text{ s}^{-1}$, respectively for the visinin-like domain. The k_d for the visinin-like domain with autoinhibition was $0.57 \pm 0.01 \text{ s}^{-1}$ and the k_a was assumed to be identical to the visinin-like domain as it could not be calculated for this construct. As the slowest site will determine the slowest rate at which calcium ion-bound CCaMK will decay, the behaviour of a more complex model, which accounts for all rate constants, is likely to be very similar. In addition the slower association rate constants of the unobserved sites in the stopped flow ($3.5 \times 10^9 \text{ M}^{-1} \text{ s}^{-1}$) were unlikely to influence the behaviour as association is still too rapid to significantly delay the binding phase. It was also not appropriate to consider additional sites because the role of each site and/or required occupancy for downstream processes is unknown. As the concentration of CCaMK in the cell is not known, a concentration of 10 nM was selected. This protein concentration minimised the effect on the free calcium ion-concentration maintaining simplicity in the model by keeping encoding and decoding effectively independent. This was because the calcium ion-concentration is in excess of the protein concentration for the majority of each spike. Testing of the model for the visinin-like domain construct by adjusting the protein concentration showed that the behaviour remains very similar up to approximately 200 nM. Above this value accumulation of the calcium ion-bound protein occurred with each spike. However this pattern was not physiologically relevant as the simulated calcium ion concentration was depleted through most of it binding to the protein. The concentrations in this model differ from concentrations used in a recent CaMKII/CaM model produced by Pepke *et al.* in which CaMKII was set to 80 μM and CaM was 30 μM . However the calcium ion-concentration was also higher at 10 μM in their system (107). The simulations (shown in Figure 4.6) suggested that calcium ion-bound CCaMK will not accumulate to reach a pseudo-steady-state in which the level of activated protein accumulates with each spike as described for CaMKII in the introduction. Despite the differences in the concentrations in this

model to those used by Pepke *et al.* the predicted oscillation of the calcium ion-bound CCaMK is similar to the oscillations in calcium ion-bound calmodulin bound to CaM kinase model at a low frequency (2 s^{-1} intervals, 0.5 Hz) indicating that the behaviours of the models are comparable.

As well as the oscillating pattern, the simulations show that the concentration of calcium ion-bound visinin-like domain and visinin-like domain with autoinhibition never reaches zero. This is due to the high affinity of CCaMK for calcium ions meaning that a small proportion of CCaMK remains in the calcium ion-bound state at basal calcium ion concentration of 5 nM in the model. This differs from the Pepke *et al.* model as they allowed the calcium ion-concentration to fall to zero (107). The dissociation phase for the visinin-like domain with autoinhibition is slightly slower than the visinin-like domain in the model as expected from the slower rate observed in the stopped-flow.

Although calcium ion-binding to the EF-hands in the model did not lead to the pseudo steady-state accumulation of activated CCaMK that could be the major mechanism for the decoding of calcium spikes, the oscillations are still likely to be significant in the overall decoding mechanism. This pattern of oscillating calcium ion-bound CCaMK concentrations will allow for periods within which CaM binding and autophosphorylation of CCaMK can occur.

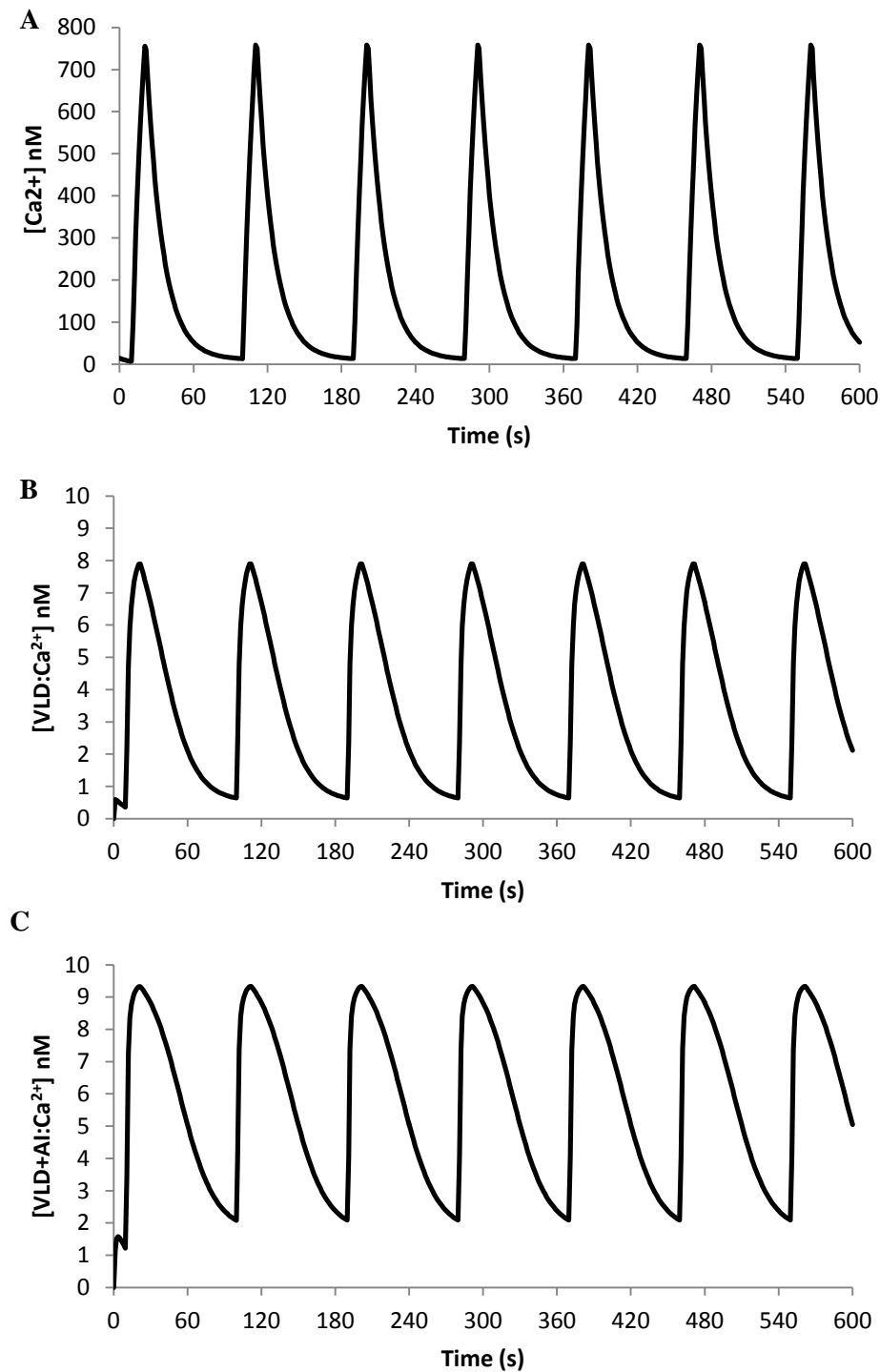


Figure 4.6. Simulation of calcium spiking and calcium ion-bound protein oscillations. A, simulated calcium spiking consisting of eight spikes over a ten minute period based upon previous reports of the calcium spikes observed in *M. truncatula*. B, simulated calcium ion-bound visinin-like domain [VLD:Ca²⁺] concentrations and C, calcium ion-bound visinin-like domain with autoinhibition [VLA+AI:Ca²⁺] concentrations using kinetics for the slowest observed site. Protein concentrations were 10 nM, k_a was $1.05 \times 10^7 \text{ M}^{-1} \text{ s}^{-1}$ and the k_d s were 2.11 s^{-1} and 0.57 s^{-1} for the visinin-like domain and visinin-like domain with autoinhibition respectively.

4.3 EXPERIMENTAL PROCEDURES

4.3.1 *Calcium ion-dissociation monitored by Quin-2 fluorescence*

The method used in this experiment is based upon an experimental procedure published by Bayley *et al.* to determine the kinetics of calcium ion-dissociation from CaM (85). Stopped-flow experiments were performed in a Hi-Tech Scientific SF61 DX2 Double Mixing Stopped-Flow System in fluorescence mode. CCaMK visinin-like domain was prepared by extensive dialysis into 10 mM Tris-HCl pH 7.5 containing 50 mM NaCl and 1 mM TCEP. All other solutions were prepared in the same buffer. Stock solutions of 6.66 μM visinin-like domain, and visinin-like domain supplemented with 10 or 20 μM CaCl_2 were prepared. These were mixed at 23 °C with 100 μM Quin-2 (Sigma) in a 1:1 ratio in the stopped-flow. Final concentrations were 3.33 μM CCaMK visinin-like domain (containing 10 μM calcium ion-binding sites), 5 or 10 μM CaCl_2 and 50 μM Quin-2. Fluorescence was monitored by excitation at 365 nm using a 100 W Hg arc lamp running at 75 W, and emission was monitored above 450 nm by using a > 450 nm filter fitted to the emission photomultiplier. Data were collected over a period of 10 s using a logarithmic time base.

Control experiments were performed by mixing 100 μM Quin-2 with 2 mM CaCl_2 (to give final concentrations of 50 μM Quin-2 and 1 mM CaCl_2). Additional controls involved mixing a solution containing 100 μM Quin-2 and 200 μM CaCl_2 with solutions containing either 5 or 20 mM EDTA (50 μM Quin-2 and 2.5 or 10 mM EDTA final concentrations) at 15, 20 or 25 °C with the arc lamp power at 75 W. All data were analysed in the Hi-Tech Scientific KinetAssist3 software package using the single exponent model.

4.3.2 *Calcium ion-dissociation monitored by Quin-2 absorbance*

Dissociation of calcium was also monitored by Quin-2 absorbance at 390 nm. The stopped-flow spectrophotometer was configured in absorbance mode and equipped with a 75 W Xe arc lamp. All proteins were dialysed extensively into 10 mM Tris-HCl pH 7.5 containing 50 mM NaCl and 1 mM TCEP. All other solutions were prepared in the same buffer. Stock solutions of visinin-like domain, visinin-like domain with autoinhibition or visinin-like domain double EF-hand mutant three-four were prepared at 33.3 μM . Mutants in EF-hand two, three and four were prepared at 50 μM , and EF-hand double mutant two-four was prepared at 100 μM . All protein solutions contained a calcium ion-binding site concentration of 100 μM except the two-three double mutant, which had a 33.3 μM binding site concentration due to limited quantities of the protein. All protein solutions were supplemented with an additional 100 μM CaCl_2 . These were mixed in a 1:1 ratio in the stopped-flow with solutions of 2 mM Quin-2 and the absorbance at 390 nm was monitored over a period of 20 s using a logarithmic time base. This gave final concentrations of 50 μM binding sites (or 17 μM for the two-three double mutant), 50 μM CaCl_2 and 1 mM Quin-2.

Control experiments were performed by mixing 2 mM Quin-2 with 40 mM EDTA, buffer only, 50 μM CaCl_2 or 100 μM CaCl_2 (final concentrations: 1 mM Quin-2, 10 mM EDTA, or 25 or 50 μM CaCl_2). An additional control involved mixing a solution of 2 mM Quin-2 containing 100 μM

CaCl₂ with 40 mM EDTA (final concentrations: 1 mM Quin-2, 50 μM CaCl₂ and 20 mM EDTA). The above experiments were performed at 15 °C except for the visinin-like domain wild-type, which was also analysed at 20 and 25 °C. All data were analysed in the Hi-Tech Scientific KinetAssist3 software package using the single exponential or two exponential models.

4.3.3 *UV/Vis spectroscopy of calcium ion-sensitive dyes*

Solutions of Quin-2, dextran linked Fura-2 (Invitrogen), or dextran-linked Rhod (Invitrogen) were prepared at a concentration of 50 μM in milli-Q water. A volume of 100 μl of each solution was transferred into an Eppendorf UVette and absorbance spectra were collected between 250 and 500 nm. Ten × 1 μl injections of 500 μM CaCl₂ were added to each solution, with spectra recorded after each injection.

4.3.4 *Simulation of calcium spiking and CCaMK calcium ion-binding in silico*

Calcium spiking was simulated using a dummy association reaction between ‘receptor’ and ‘ligand’ in the Copasi 4.6.33 software package (153). Parameters for the simulation were set according to previous publications. The spike frequency was 90 s (36), the calcium ion concentration was 5 – 800 nM (8) and a spike duration was approximately 70 s (with initiation after 9 s) (30). The spikes were asymmetrical with 16% of the duration in the upward phase, and 84% in the downward phase (30). This was achieved by setting the dummy reaction of ‘ligand + receptor = Ca’ to have a k_a of 100 M⁻¹ s⁻¹ and a k_d of 0.075 s⁻¹. The receptor concentration was 11 μM and the ligand concentration was initially 0, stepping to 100 μM at 10 s for duration of 11 s. This sequence was repeated eight times at 90 s intervals using the ‘events’ function. The dummy reaction was a simple method to mimic the calcium spiking pattern and is not related to the spike generation mechanism *in vivo*. The kinetics of calcium ion-binding to the CCaMK constructs were modelled using a reaction between ‘P’ (protein) at a concentration of 10 nM and Ca, the concentration of which was defined by the spiking simulation. The parameters of the P + Ca = PCa reaction were set according to slowest experimentally determined dissociation rate constant, and the calculated association rate constant of 1.05 × 10⁷ M⁻¹ s⁻¹. This calculated association rate constant was used for both the visinin-like domain and the visinin-like domain with autoinhibition. Outputs from the model were generated using the ‘time course’ task over duration of 600 s, with 125 intervals spaced by 4.8 s.

5. Chapter five – Characterisation of CaM binding to the CCaMK visinin-like domain with autoinhibition

As CaM binding is known to be required for the activation of CCaMK (72) the binding and kinetics of CaM must be understood in order to understand CCaMK activation in the context of a calcium spiking signal.

The data presented in this chapter begin to define the interaction between CCaMK and CaM, and of calcium ions within the protein complex. It was determined that calcium ion-dissociation occurs from CaM at the same rate as CaM dissociates from CCaMK. It was also shown that CaM dissociation is biphasic with the N-terminal lobe likely to dissociate from CCaMK before the C-terminal lobe. CaM has a high affinity for CCaMK of approximately 46 nM, which is similar to previously published values for both potato CaM binding to lily CCaMK and bovine CaM binding to rat CaMKII of 55 nm and 14.5 nm, respectively (72, 100).

5.1 RESULTS

5.1.1 Conformation of complex formation between the CCaMK visinin-like domain with autoinhibition and CaM.

It has previously been reported that CCaMK is able to interact with potato CaM (72). From the work described in chapter two section 2.1.4 “Cloning, expression and purification of CCaMK and CCaMK constructs”, purification of this construct with bovine CaM Sepharose 4B (GE Healthcare) demonstrated that bovine CaM interacts the CCaMK visinin-like domain with autoinhibition. However, an interaction with *M. truncatula* CaM has not been demonstrated. To this end the visinin-like domain with autoinhibition construct and *M. truncatula* CaM were analysed both individually and when mixed together by analytical gel filtration as shown in Figure 5.1. This experiment demonstrated that the proteins interact as the elution volume reduced corresponding to a complex of higher mass when they were mixed in the presence of excess CaCl₂. As the proteins give higher than expected masses, the exact mass of the complex could not be determined in this experiment. However, the addition of the monomer masses is roughly equal to the complex mass suggesting that a 1:1 complex had formed. The masses obtained were 33.4, 44.0 and 72.2 kDa for the visinin-like domain with autoinhibition, CaM and the complex, respectively. Expected masses were 23.5, 16.7 and 40.2 kDa, respectively. These large masses may be due to the elongated shape of the molecules as determined in chapter two section 2.1.10 “Low resolution structures of the CCaMK regulatory domains and calmodulin”.

To determine the mass of the complex, the proteins were analysed by analytical ultracentrifugation. Although the masses for the proteins analysed were all below the expected values, the data clearly show that the complex mass is consistent with a 1:1 interaction (shown in

Table 5.1). This was expected due to the presence of a single CaM binding site in the autoinhibitory domain identified by Takezawa *et al.* (61) described in chapter one section 1.3.4 “Proposed mechanism of CCaMK activation”. This remains the case when the visinin-like domain with autoinhibition is in excess over CaM demonstrating that CaM cannot interact with multiple binding sites simultaneously as was suggested in fluorescence experiments (discussed below).

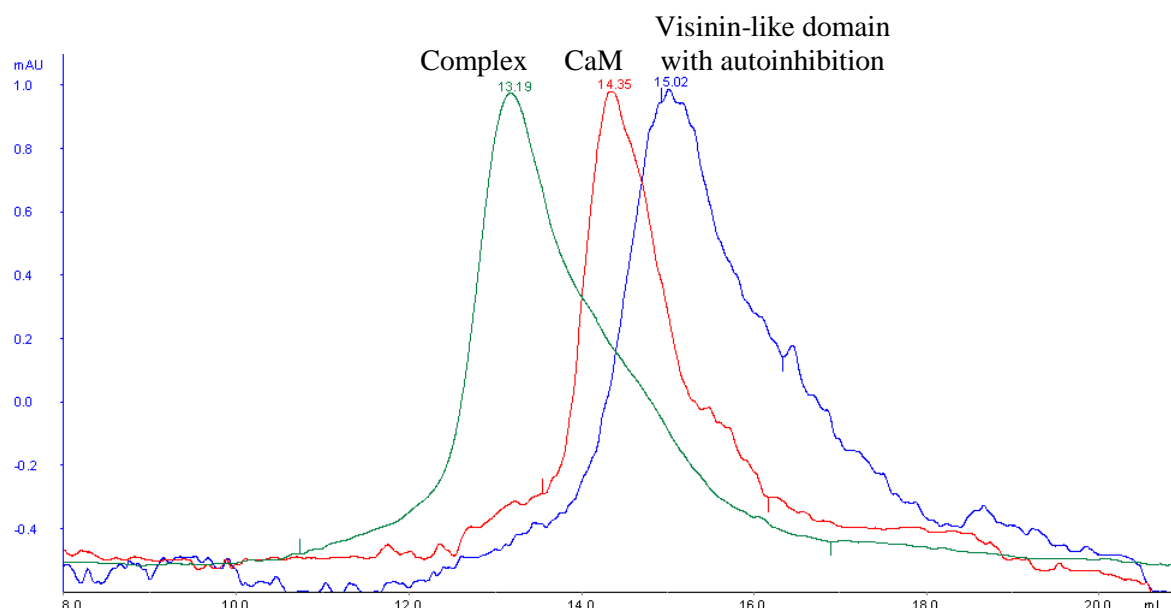


Figure. 5.1. Analytical gel filtration of the CCaMK visinin-like domain with autoinhibition, CaM and the visinin-like domain with autoinhibition/CaM complex. Chromatograms show elution profiles for the CCaMK visinin-like domain with autoinhibition (blue), CaM (red) and the visinin-like domain with autoinhibition/CaM complex (green). Labels show the elution volume for each peak and the corresponding species. Gel filtration was performed on an ÄKTA FPLC using a Superdex 10/300 GL S200 gel filtration column and data were processed using the Unicorn software package (GE Healthcare).

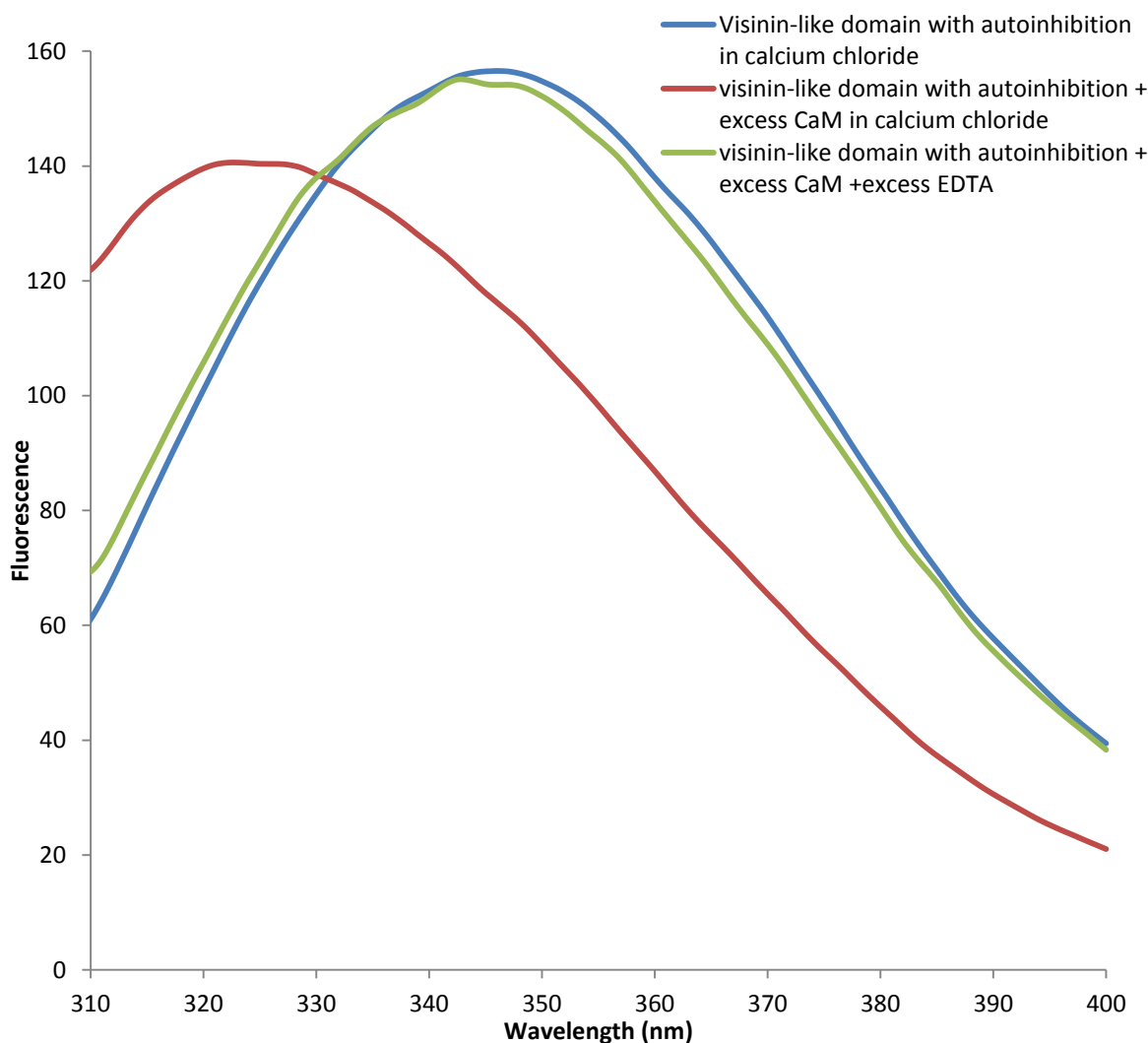


Figure. 5.2. Fluorescence spectra of CaM binding to the visinin-like domain with autoinhibition. Fluorescence spectra of the visinin-like domain with autoinhibition in 2 mM CaCl₂ (blue), visinin-like domain with autoinhibition with 2.5-fold excess CaM in 2 mM CaCl₂ (red) and the visinin-like domain in 2.5-fold excess CaM with all calcium ions stripped by the addition of 22.7 mM EDTA (green). The excitation wavelength was 290 nm slit widths were 10 nm and the scan speed was 500 nm min⁻¹. The spectra of visinin-like domain with autoinhibition with CaM in 2 mM CaCl₂ and in excess EDTA have been multiplied by 1.25 and 1.37, respectively, to correct for dilution.

Protein	Mw by AUC	Theoretical MW of monomer or 1:1 complex
	<i>kDa</i>	<i>kDa</i>
Visinin-like domain with autoinhibition	17.7 ± 0.2	23.5
CaM	14.4 ± 0.01	16.7
Visinin-like domain with autoinhibition + CaM (1:1 ratio)	34.9 ± 0.2	40.2
Visinin-like domain with autoinhibition + CaM (1:0.5 ratio)	35.0 ± 0.01	40.2

Table 5.1. Analytical ultracentrifugation of the CCaMK visinin-like domain with autoinhibition, CaM and the visinin-like domain with autoinhibitor/ CaM complex.

Data are shown for simultaneous fitting to 10 000, 20 000 and 30 000 RPM equilibrium data. Fitting was performed using the 1-component ideal model in the UltrascanII software package (126). Errors were estimated by Monte Carlo analysis.

As tryptophan residues can often report on protein-protein interactions, and a tryptophan residue is located at the end of the predicted CaM-binding site, fluorescence spectra were collected of the visinin-like domain with autoinhibition in isolation and with CaM in excess CaCl₂. This demonstrated that the tryptophan residue within the CaM binding site of the visinin-like domain with autoinhibition reported on CaM binding by shifting the emission wavelength from 240 nm to 320 nm. The addition of excess EDTA demonstrated that this shift is specific to calcium ion-bound CaM bound to the autoinhibitory domain as the maximum peak reverted to 340 nm, indistinguishable from the curve for the visinin-like domain with autoinhibition in excess CaCl₂ (Figure 5.2). CaM did not report in this assay as it does not contain any tryptophan residues and the excitation wavelength of 390 nm is too high for significant tyrosine fluorescence. When a titration of CaM was attempted, the binding curve was not ideal. The data suggested that there were more than two sites per protein, which does not agree with the AUC above (data not shown). The reason for this may be that some of the visinin-like domain with autoinhibition was not correctly folded and able to bind CaM. Additional problems with CaM were encountered by ITC where no binding was observed with CaM in excess (data not shown), in stopped flow where the association rate constant did not change as a function of CaM excess (data not shown), and by SPR (discussed below). Together these suggest that *M. truncatula* CaM does not behave ideally when used at high concentrations.

5.1.2 Determination of the CaM dissociation rate constant from the visinin-like domain with autoinhibition

As CaM binding is required for CCaMK activity, the rate at which calcium ions and CaM dissociate are important for relating CCaMK activity to calcium spiking. In addition dissociation rate constants from the ternary complex are often slower than from the corresponding binary complex.

Calcium ion-dissociation from the complex was monitored by Quin-2 absorbance at 15 °C as described for the visinin-like domain and visinin-like domain with autoinhibition in chapter four section 4.1.1 “Calcium ion-dissociation rate constants from the visinin-like domain and visinin-like domain with autoinhibition”. These data (shown in Figure 5.3 A and B) fitted best to the three exponent model as single exponent and two exponent models gave large residuals. Calibration of the signal revealed that 5.5 of the 7 expected sites were observed suggesting that there was a fourth fast-dissociation phase, which was complete within the 1 ms dead-time with a rate constant $>700 \text{ s}^{-1}$. The measured rates were 4.96 ± 0.06 , 0.536 ± 0.009 and 0.123 ± 0.002 with amplitudes of -0.0191 ± 0.0001 , -0.0196 ± 0.0002 and 0.0125 ± 0.0003 , respectively with an approximate ratio of 2:2:1.5, consistent with the 5.5 observed suggesting that the rates correspond to 2, 2 and 1.5 calcium ions, respectively. This means that the three rates observed are probably reporting on calcium ion-release from each lobe of CaM and from the visinin-like domain. Note that a significant portion at the beginning of the curve could not be fitted due to large residuals in this region. This may be because there were more than three rates being observed, which cannot be properly resolved from these data.

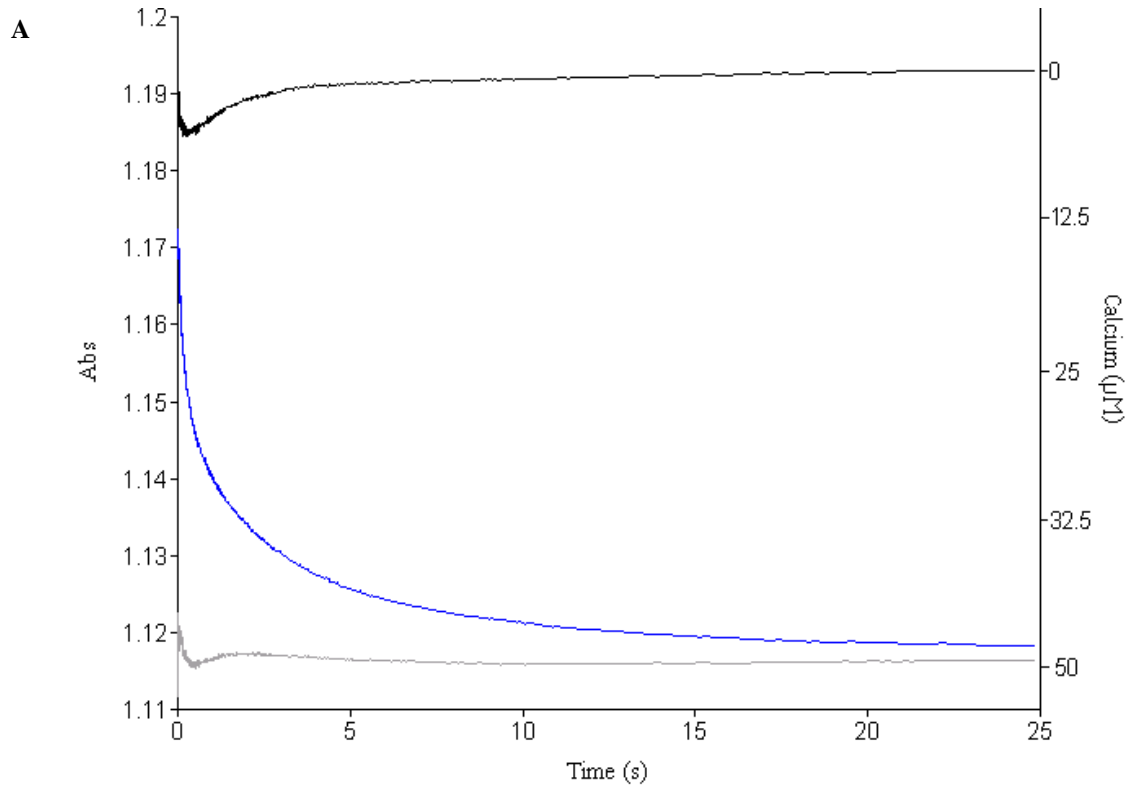
Dissociation kinetics of CaM was monitored using tryptophan fluorescence emission above 320 nm, which was expected to give an increase in signal as CaM dissociates based upon the spectra in Figure 5.2. This was achieved by mixing calcium ion-saturated visinin-like domain with autoinhibition/CaM complex with excess EDTA under stopped-flow conditions and monitoring on the millisecond timescale (shown in Figure 5.3 C and D). These data were best fit to a two exponential model suggesting that CaM dissociation is not a single process. These data also showed that CaM dissociation is similar to the observable rates of calcium ion dissociation with rate constants of 4.61 ± 0.06 and 0.529 ± 0.008 and amplitudes of 2.37 ± 0.02 and 2.28 ± 0.02 , respectively at 15 °C. The similar amplitudes demonstrate that both phases are significant in the CaM dissociation mechanism. As expected the rate constants increased with temperature. The rate constants were 6.4 ± 0.1 and 0.70 ± 0.01 at 20 °C, and 8.9 ± 0.1 and 0.83 ± 0.01 at 25 °C (data not shown). As a signal was seen for the visinin-like domain with autoinhibition vs EDTA control (shown in Figure 5.3 C and E), it cannot be determined whether both rates observed relate to CaM binding, or whether rates for a conformational change within the visinin-like domain with autoinhibition are also measured during complex dissociation. The visinin-like domain with

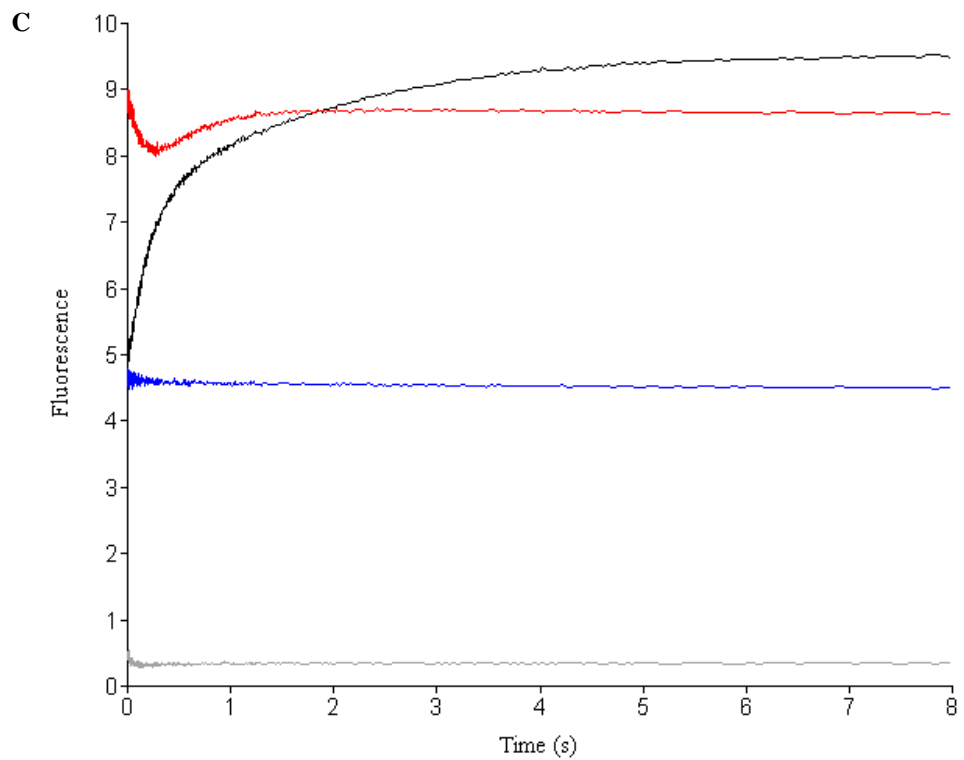
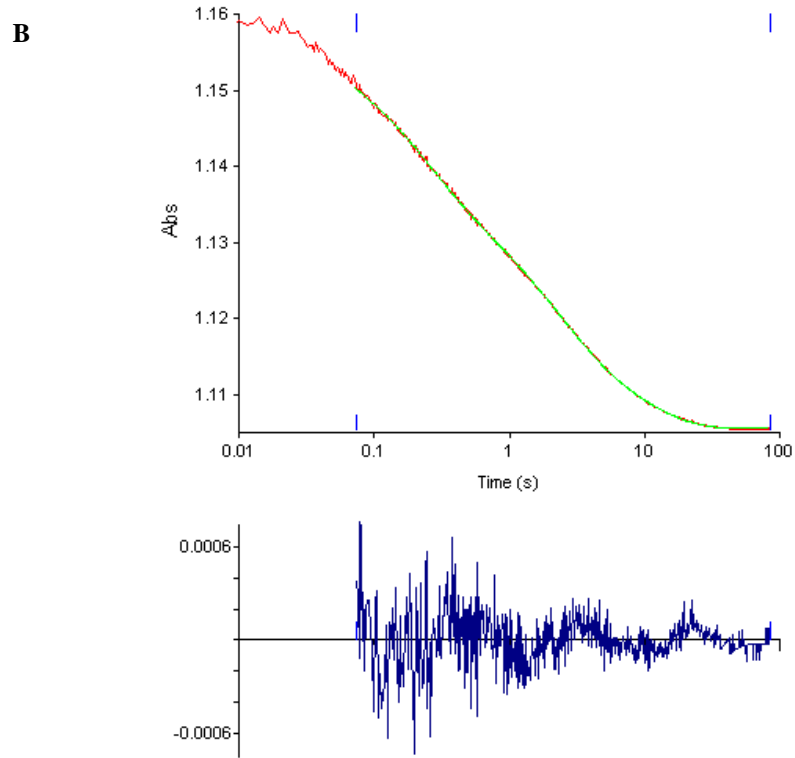
autoinhibition vs EDTA gave rate constants were 2.67 ± 0.05 and 5.46 ± 0.09 with amplitudes of 2.49 ± 0.09 and -2.65 ± 0.09 , respectively. However the overall signal is small compared to the CaM dissociation curve. The controls of complex vs buffer and visinin-like domain with autoinhibition in isolation vs EDTA demonstrate that the entire process of CaM dissociation is being observed. This is because the increase of fluorescence of the complex mixed with EDTA is of similar amplitude to the difference between these controls.

The rate constants of both calcium ion-dissociation and CaM-dissociation from the complex are similar to values published previously on bovine CaM dissociation from rat CaMKII by Meyer *et al.* (100) and from chicken CaM dissociation from CaMKII derived CaM binding peptides by Waxham *et al.* and dissociation of *xenopus* CaM by Jama *et al.* (101, 105). These values were 2.17, 0.26 and 0.3 s^{-1} . This demonstrates that CaM dissociation from the CCaMK visinin-like domain with autoinhibition occurs at a similar rate to that of non-autophosphorylated CaMKII. Jama *et al.* also determined that the observed slow rate constant was for calcium ion-dissociation from the C-terminal lobe of CaM as the N-terminal lobe dissociated rapidly with an estimated rate constant of 1000 s^{-1} (105). Research by Dodd *et al.* on human CaM binding to several Connexin 32 derived peptides showed that calcium ion-dissociation from CaM is also biphasic in this system. Calcium ion-dissociation rate constants of 10.8 and 1.7 s^{-1} were determined for human CaM bound to the peptide giving slower rate constants compared with ~ 1000 and 10.9 s^{-1} human CaM that was not in a protein complex (154). Taken together these reports suggest that biphasic calcium ion-dissociation from CaM in complex with its target is common. Furthermore, research on the *M. truncatula* CaM in our research group by L. Zhou *et al.* (unpublished) shows that calcium ion-dissociation from the apo protein is biphasic with rate constants of 19.6 ± 0.2 and $0.615 \pm 0.004 \text{ s}^{-1}$ with amplitudes of 0.0258 ± 0.0002 and 0.02519 ± 0.00006 , respectively, corresponding to three of the four sites.

Given the similarity in the fast and medium measured rate constants of calcium ion-dissociation and CaM dissociation, it is likely that these rate constants are related to the dissociation of the two lobes of CaM. By analogy to previous publications (100, 105) this is likely to mean that the N-terminal lobe of CaM dissociates with a half-time of approximately 0.15 s, followed by the C-lobe of CaM with a half-time of approximately 1.3 s. This is then likely to be followed by calcium-ion dissociation from the visinin-like domain with a half-time of 5.6 s to return the CaM binding site to its state at basal calcium-ion concentrations. The equal amplitudes of the calcium-ion dissociation rate constants would therefore suggest that each CaM lobe dissociates two calcium-ions per rate constant, and the visinin-like domain dissociates 1.5 ions to give a total of 5.5 observed. To confirm this interpretation experimentally, it may be necessary to analyse the dissociation kinetics of CaM from the isolated CCaMK visinin-like domain to remove the overlapping rate constants corresponding to calcium ion-dissociation from the visinin-like domain. This could be achieved by

using with synthetic peptides of the isolated autoinhibitory domain as the CaM binding protein and monitoring calcium ion and CaM dissociation by the same techniques as described above.





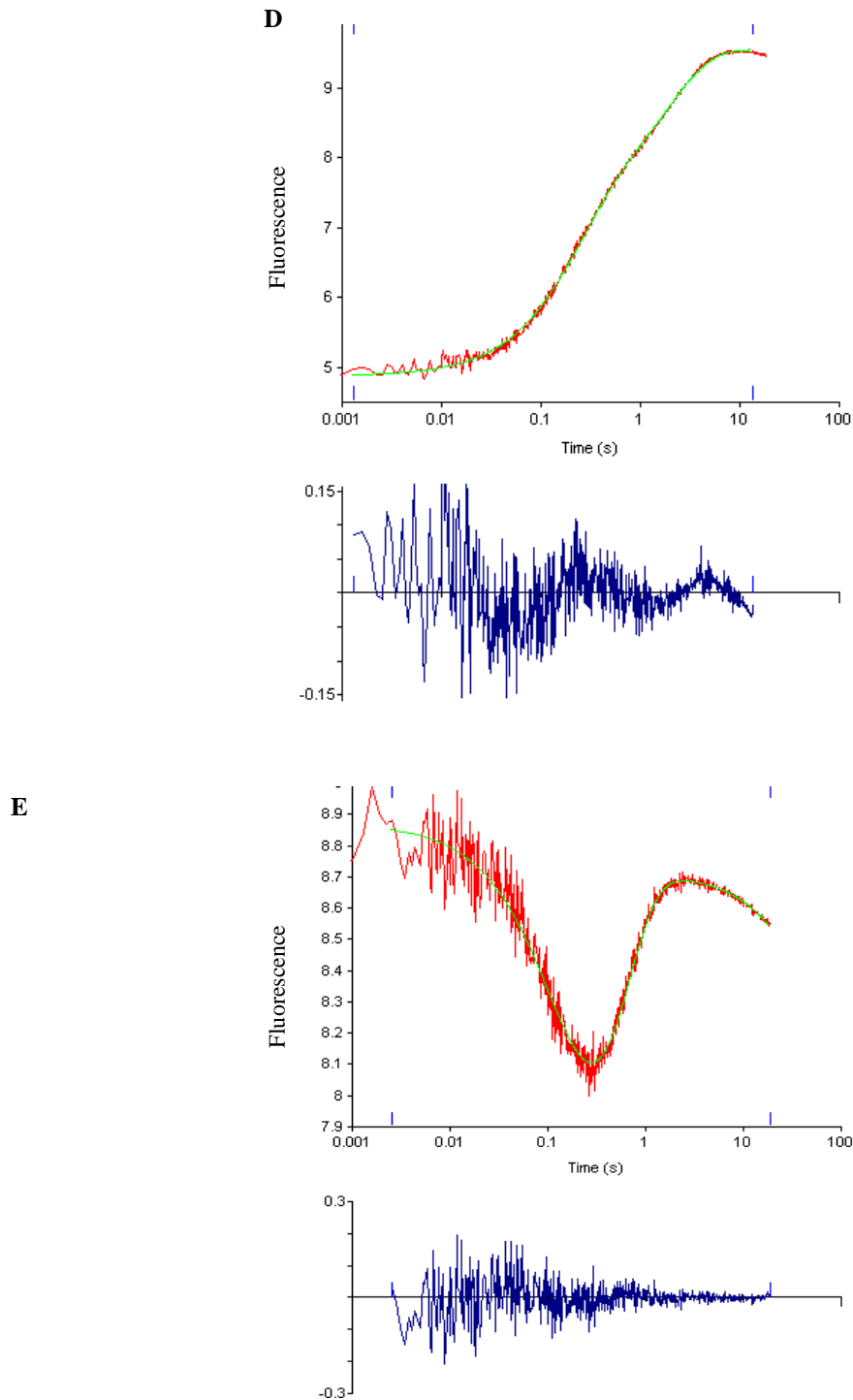


Figure. 5.3. Dissociation kinetics of the CCaMK visinin-like domain with autoinhibition/CaM/calcium ion complex. A, dissociation of calcium ions from the CCaMK visinin-like domain with autoinhibition/CaM complex monitored by Quin-2 absorbance (blue trace). The black and grey traces show buffer and 100 μM CaCl_2 controls, respectively, which were used to determine the expected range of calcium ion release from the proteins. Final concentrations were 7.2 μM complex (to provide a final binding site concentration of 50 μM) and 1 mM Quin-2 for calcium ion-dissociation experiments. Final concentrations were 0 or 50 μM CaCl_2 and 1 mM Quin-2 for the controls. B, fitting of the calcium ion-dissociation curve from the visinin-like

domain with autoinhibition/CaM complex with the three exponential model. The data are shown on a log timescale with the raw data in red and the fitted data in green. Residuals of the fit are shown in the lower panel. Rate constants were 4.96 ± 0.06 , 0.536 ± 0.009 and 0.123 ± 0.002 s⁻¹ with amplitudes of -0.0191 ± 0.0001 , -0.0196 ± 0.0002 and 0.0125 ± 0.0003 , respectively. C, stopped-flow fluorescence of Trp26 within the autoinhibitory domain of the visinin-like domain with autoinhibitor upon mixing the calcium ion-saturated CCaMK visinin-like domain with autoinhibition/CaM complex with excess EDTA (blue trace). The grey and blue traces show controls of CaM and complex mixed with buffer and the red trace shows the calcium ion-bound visinin-like domain with autoinhibition mixed with excess EDTA. Final concentrations were 2.5 μM visinin-like domain with autoinhibition and/or CaM and 1 mM EDTA. The buffer, in which all solutions were prepared, contained 0.1 mM CaCl₂. D, fitting of the CaM dissociation curve with the two exponential model. Rate constants were 0.529 ± 0.008 and 4.61 ± 0.06 s⁻¹ with amplitudes of 2.28 ± 0.02 and 2.37 ± 0.02 , respectively. E, fitting of the tyrosine fluorescence data for the calcium ion-saturated visinin-like domain mixed with excess EDTA to the two exponent model with sloping baseline. Rate constants were 2.67 ± 0.05 and 5.46 ± 0.09 s⁻¹ with amplitudes of 2.49 ± 0.09 and -2.65 ± 0.09 , respectively.

Species monitored	Reporter	Chelator	Sites	k_d slow	k_d med	k_d fast	$t^{1/2}$ slow	$t^{1/2}$ med	$t^{1/2}$ fast
				s ⁻¹	s ⁻¹	s ⁻¹	s	s	s
Ca ²⁺	Quin-2	Quin-2	5.5 of 7	0.123 ± 0.002	0.536 ± 0.009	4.96 ± 0.06	5.6	1.29	0.14
Complex	Tyr26	EDTA	n/a ^a	n/a ^a	0.529 ± 0.008	4.61 ± 0.06	n/a ^a	1.31	0.15

Table. 5.2. Measured rate constants for CaM and calcium ion-dissociation from the visinin-like domain with autoinhibition/CaM complex at 15 °C.

$t^{1/2}$ values were calculated from the rate data using the formula $t^{1/2} = \frac{1}{k} \times 0.693$.

^a not applicable

5.1.3 Binding and kinetics of CaM to the CCaMK visinin-like domain with autoinhibition

The K_D and k_d of CaM binding to CCaMK are known. However, the k_a remains undetermined and this is an important factor for the understanding of calcium spike decoding. In addition to the kinetics, the affinity of CaM for the CaM binding site has not been measured for the combination of *M. truncatula* CaM and CCaMK. The k_a and K_D were assessed using surface plasmon resonance (SPR). This technique involves the immobilisation of the protein, referred to as the ligand, on a

gold surface. Beneath the gold surface lays a prism, through which a laser is shone. The light from the laser will be reflected from the gold surface except at a specific angle, where the light is absorbed into the gold as plasmons. This angle is related to the refractive index of the solution within approximately 300 nm of the gold. When the aqueous target molecule is flowed over the surface, referred to as the analyte, it is bound to the ligand, which causes a change in the refractive index, which in turn alters the angle at which the light is absorbed. This angle is monitored and alterations are reported in response units on the second timescale.

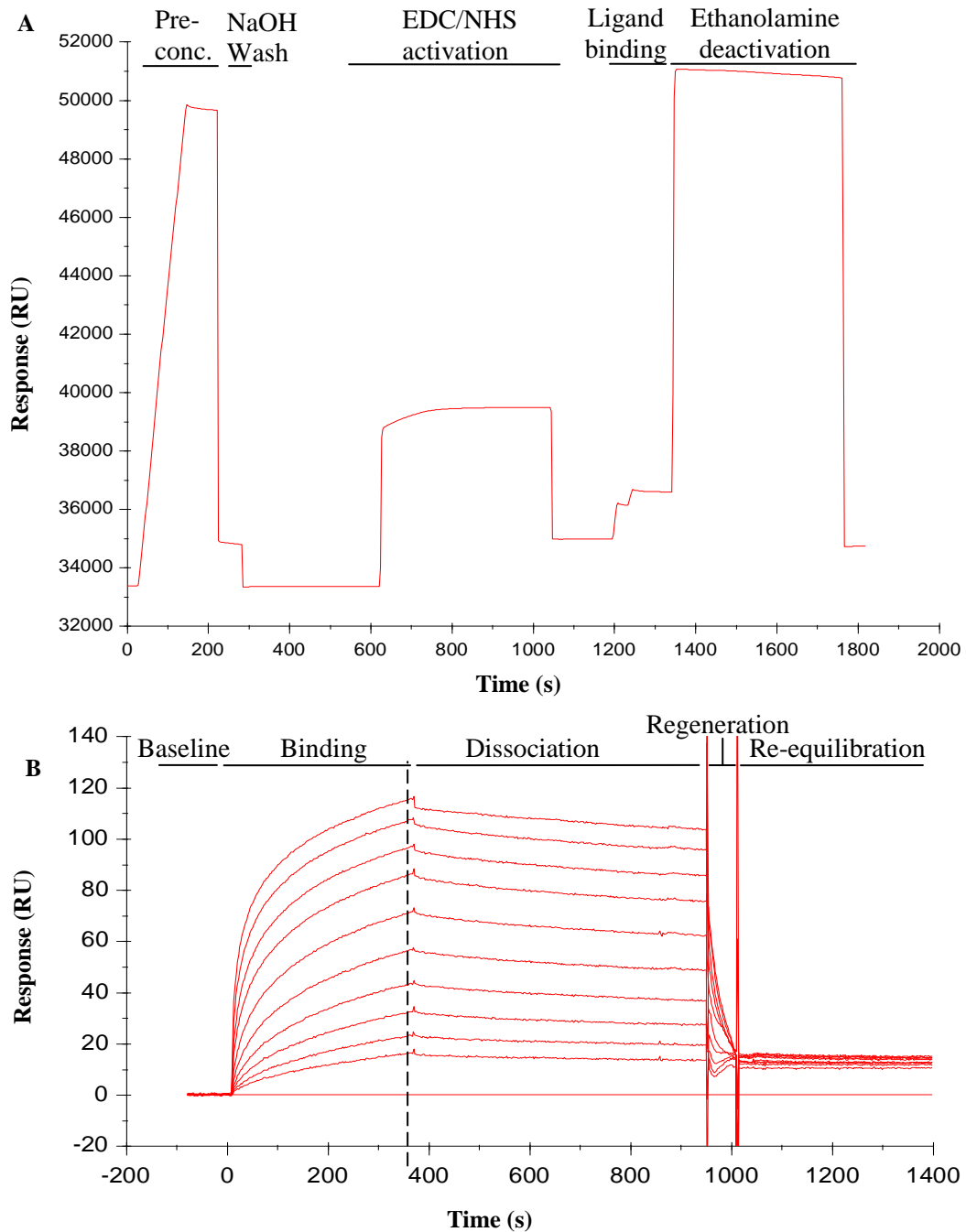
The chip used in these experiments was a CM5 (GE Healthcare). This chip is modified with a 100 nm thick layer of carboxymethyl dextran on the gold surface. This performs several functions. First it provides carboxymethyl groups onto which the ligand can be bound to ensure it is solvent accessible, and increases the amount that can be immobilised. This modification can be activated for immobilisation by many chemistries depending on the reactive groups on the ligand. Additionally the dextran protects the surface, reducing non-specific binding to the gold surface, which is hydrophobic and also interacts strongly with sulphur atoms contained within cysteine and methionine residues. Other chips are available with differing lengths of carboxymethyl dextran or reduced carboxymethylation; however, CM5 is the most effective for protein-protein interactions and thus was selected as the most appropriate.

The visinin-like domain with autoinhibition was selected as the ligand for these experiments and it was immobilised by amine coupling. This involved a pre-concentration step, which is used to assess the strength of interaction between the ligand and the surface to allow accurate immobilisation to a target level when the surface is activated. The surface is next washed with NaOH to remove all protein. To begin the immobilisation, the surface is treated with a mixture of 1-ethyl-3-(3-dimethylaminopropyl) carbodiimide and *N*-hydroxysuccinimide (EDC/NHS) to activate the carboxyl groups followed by the ligand. Amine groups, particularly those in lysine, react with the activated carboxyl groups to covalently link the ligand to the surface. Finally the surface is deactivated by blocking all remaining active carboxyl groups with ethanolamine. The immobilisation of the visinin-like domain with autoinhibition is shown in Figure 5.4 A. Preliminary experiments revealed that optimal immobilisation was achieved at pH 4 (data not shown). The low pH was required, it needs to be at least 1 pH units below the protein's pI to protonate its carboxyl groups and provide a net positive charge, which will be attracted to the negative charge of the chip surface. The theoretical pI was 5.12 for the visinin-like domain with autoinhibition. The minimum effective pH is approximately 3.5 as the pI of the surface is around pH 3. The maximum is set by the pI of the protein; the buffer should be at least one pH unit below this value for maximal efficiency. Immobilisation of CaM was attempted by this method. However, it was unsuccessful as CaM was unstable in the low pH buffer; possibly as pH 3.5-4 was too close to the theoretical pI of 4.12.

As the processes are monitored on the second timescale, it is possible to monitor the binding and dissociation of the analyte in real time. It is also possible to allow the binding to run to equilibrium and assess the affinity. A typical sensorgram consists of binding where the analyte is flowed over the surface and dissociation where it is washed off with buffer. These two phases are typically fitted when analysing kinetics by SPR. To prepare the surface for subsequent analyses, all remaining analyte must be removed in a regeneration step. In this experiment 2 mM EDTA was used to regenerate the surface (shown in Figure 5.4 B) as calcium-ion dissociation from CaM leads to dissociation as discussed in section 5.1.2 “Determination of the CaM dissociation rate constant from the visinin-like domain with autoinhibition”.

In these experiments CaM was flowed over the immobilised visinin-like domain with autoinhibition at concentrations between 1.95 and 1000 nM as shown in Figure 5.4 B. The end-points of the association phase were measured and fitted to the steady-state affinity model shown in Figure 5.4 C. This provided a K_D of 46 ± 8 nM, which is similar to a value of 55 nM published for potato CaM binding to lily CCaMK by Sathyanarayanan *et al.* (72). In this experiment the kinetic data were not ideal. Equilibrium was not reached even after long exposure to the analyte. This meant that the data could only be fit to the heterogeneous ligand model with R_{\max} allowed to float. This gave a poor fit with large residuals as shown in Figure 5.4 D and E. As it is usually not appropriate to float R_{\max} or to use the heterogeneous ligand model, the kinetic values obtained cannot be used. Association rate constants were $5.5 \times 10^5 \text{ M}^{-1} \text{ s}^{-1}$ and $2.2 \times 10^4 \text{ M}^{-1} \text{ s}^{-1}$ suggesting that CaM association to CCaMK lies in the $10^4 - 10^6 \text{ M}^{-1} \text{ s}^{-1}$ range but reliable data needs to be collected for this. Stopped flow absorbance under pseudo first order conditions is likely to be a suitable method. Qualitative assessment of the dissociation phase suggests that calcium-ion bound CaM is very slow to dissociate (rate constants of $1.26 \times 10^{-4} \text{ s}^{-1}$ and $2.01 \times 10^{-4} \text{ s}^{-1}$ were provided by the fit supporting this assessment). Dissociation with the addition of EDTA, shown in the regeneration step of Figure 5.4 B, suggest that removal of calcium is rapid and complete within several seconds, which is consistent with the stopped-flow data discussed in section 5.1.2 “Determination of CaM dissociation rate constants from the visinin-like domain with autoinhibitor”. The reason for the non-ideal binding curves is likely to be a non-specific interaction between the two proteins, or immobilisation leading to non-ideal kinetics whereby a secondary slow phase has a significant effect on the curve shape. This could be caused by heterogeneity caused by the immobilisation of the ligand in multiple orientations or a proportion of either protein not being correctly folded under the experimental conditions. A similar curve shape has previously been reported for CaM binding to vesicle associated membrane protein (VAMP2), a component of the soluble N-ethylmaleimide sensitive fusion protein attachment protein receptor (SNARE) complex involved in neurotransmitter release in synapses (155). This suggests that the non-ideal binding issue may not be isolated to the CCaMK/CaM system. Attempts to optimise the experiment

by immobilisation of biotinylated visinin-like domain with autoinhibition to a streptavidin-coated (SA) chip did not improve the data. Immobilisation of biotinylated CaM lead to an inability to regenerate the surface in the absence of reductant, which could not be used as DTT and TCEP gave large non-specific background signals (data not shown).



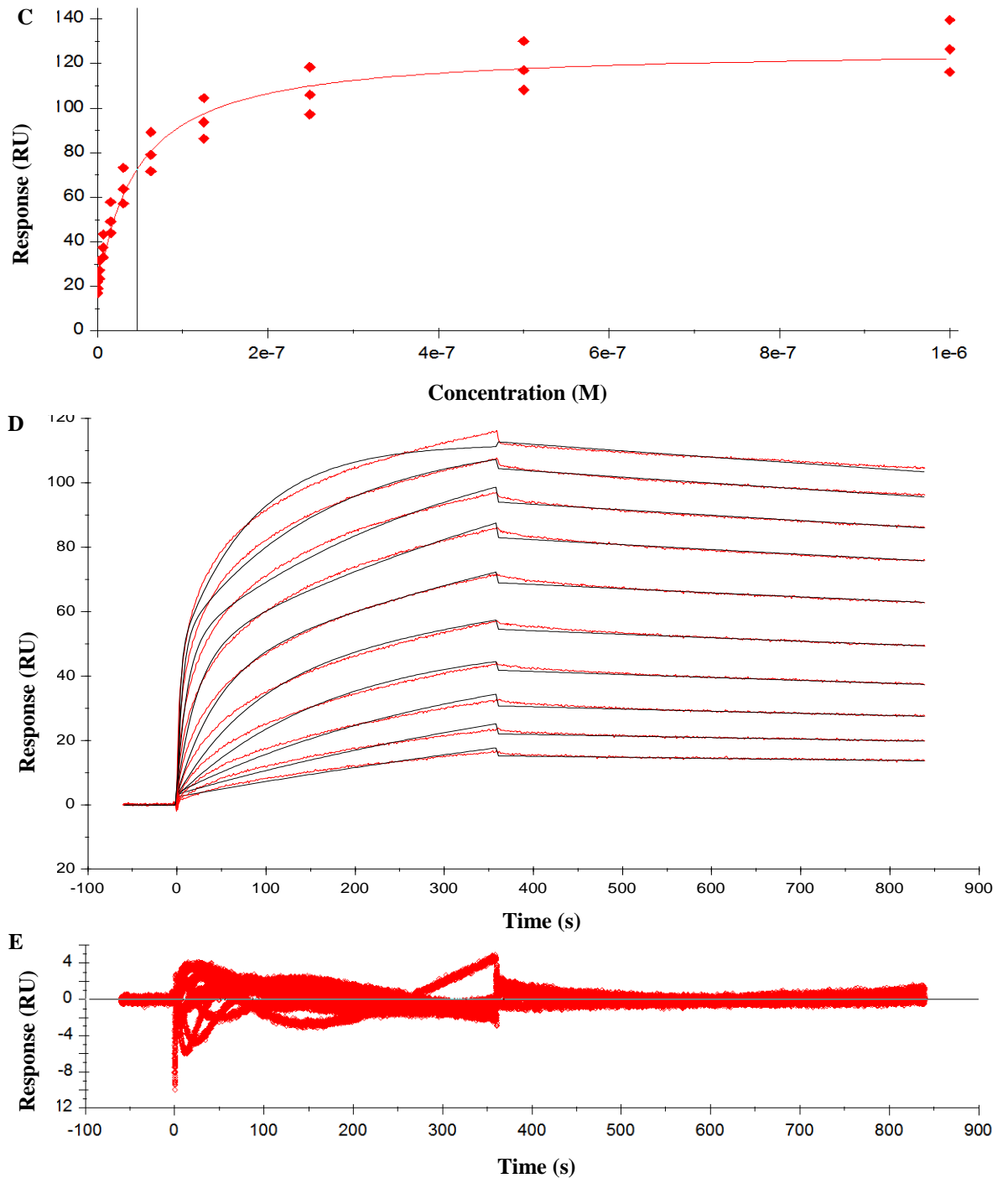


Figure. 5.4. CaM binding to the visinin-like domain with autoinhibition monitored by surface plasmon resonance. A, immobilisation of the CCaMK visinin-like domain construct on a CM5 carboxymethyl dextran chip (GE Healthcare) by amine coupling. Each phase in the sensorgram has been labelled. Binding was tested in a pre-concentration step, where protein was flowed over the surface to test the rate of binding followed by washing with 50 mM NaOH. The carboxyl groups within the carboxymethyl dextran were activated by flowing a mixture of EDS/NHS over the surface followed by protein, which bound covalently to the activated carboxyl

groups. Finally the remaining active groups were deactivated with ethanolamine. B, Sensorgrams of the binding of CaM over a range of 1.95 to 1000 nM. Sensorgrams have been corrected by baseline subtraction of a buffer control and subtraction of a sensorgram collected on a reference cell, which was prepared by EDC/NHS activation followed by immediate deactivation with ethanolamine. Sensorgrams have been aligned on the y axis by setting the value at the injection start to compensate for baseline drift over the course of the experiment. Each section of the sensorgram has been labelled and the injection end point, where values for affinity analysis were collected, is highlighted with a dashed line. For clarity only one of the three sets of data is shown. However this is typical as the data were reproducible. Experiments began by flowing buffer only for 100s followed by CaM solution for 360 s. Next, CaM was allowed to dissociate by flowing buffer-only for 600s. Finally the chip was regenerated by flowing 2 mM EDTA for 120 s, and the chip was reequilibrated by flowing buffer for 1000s. The running buffer was 50 mM Tris-HCl pH 7.5 containing 150 mM NaCl, 0.1 mM CaCl₂ and 0.005% P20. The flow rate was 30 $\mu\text{l min}^{-1}$. C, fitting of the end-point values to determine the CCaMK affinity for CaM. The K_D was calculated to be 46 ± 8 nM as highlighted by the vertical line. D, kinetic fitting to one set of sensorgrams with the heterogeneous ligand model with R_{max} allowed to float. The residuals of the fit are shown in E. As the residuals were poor and the model used was not appropriate, kinetic parameters were not collected from these data. All data were processed using the Biacore T100 evaluation software package (GE Healthcare).

5.2 DISCUSSION

As has been reported in other CaM-binding systems, CaM-dissociation occurs with multi-phase kinetics, which is likely to correspond to the separate dissociation rate constants for each lobe of calmodulin. This suggests that CaM binding to CCaMK may be similar to that with CaMKII in which the individual lobes of CaM appear to perform different roles in the enzyme. In this animal system it was determined that binding of the C-lobe of CaM, the slow dissociation lobe, increases the K_m of ATP whereas the N-terminal lobe raises the V_{max} of substrate phosphorylation. However full binding is required for full activity (105). Modelling of the differential dissociation kinetics of CaM, as well as the differing association rate constants and affinities by Pepke *et al.* suggests that the differing calcium ion-binding properties of the two lobes of CaM play important roles in the autophosphorylation of CaMKII. This is especially true when calcium ions are limiting, as is the case in animal systems (107). The data collected here suggest that similar considerations will be important in the future understanding of CaM binding to CCaMK. However, to allow similar modelling to take place, additional characterisation of CaM is required, such as the association kinetics (currently under investigation in our lab by stopped-flow tryptophan fluorescence under pseudo first order conditions) and influence of CaM mutants on the autophosphorylation rates. The medium and fast rate constants obtained for CaM dissociation from the CCaMK visinin-like

domain with autoinhibition (shown in Table 5.2) are similar to those for non-phosphorylated CaMKII (101, 105). However the N-terminal lobe dissociation appears to be approximately 200 fold slower. It should also be noted that the frequencies and maximal calcium ion-concentrations in the Pepke *et al.* animal model (107) differ significantly from those observed in calcium spiking in root hair cells (≤ 1 per 2 s vs 1 per 90 s, respectively) and therefore the behaviour of CaM binding to CCaMK *in vitro* will presumably differ from that of CaMKII. Combining the above data with the analysis of CaM binding by SPR shows that CaM dissociation is very slow in the presence of excess calcium ions. This suggests that calcium ion-dissociation is likely to drive CaM dissociation from CCaMK and therefore is likely to be the rate-limiting step with protein dissociation occurring immediately after.

Analysis of the equilibrium binding of *M. truncatula* CCaMK revealed that the affinity for *M. truncatula* CaM is high with a K_D of approximately 46 nM. This value is very similar to the value of 55 nM for the binding of potato CaM to lily CCaMK published by Sathyanarayanan *et al.* despite the non-ideal curves collected by SPR (72). This suggests that the CCaMK visinin-like domain with autoinhibition is a suitable model for the full length protein in biophysical studies. This value is also similar to the K_D of bovine CaM for unphosphorylated rat CaMKII reported by Meyer *et al.* of 14.5 nM (100).

Although the dissociation rate constants of calcium ions are slower for the complex than for the individual proteins, as was expected due to stabilisation upon complex formation, the slowest $t_{1/2}$ of 5.6 s is faster than the 90 s spike interval meaning that the populations of each species would be expected to oscillate with the calcium spiking as was the case for the CCaMK constructs as shown in the Chapter four discussion section. This means that CaM binding is unable to provide a mechanism for persistence of the active kinase, which is the key mechanism of decoding. In CaMKII, autophosphorylation leads to a slowing of the CaM dissociation rate constant by 100-1000 fold and an increase in affinity. This is termed CaM trapping and is one of the mechanisms by which CaMKII can persist between calcium spikes (100). The reduction in K_D by approximately 8-fold from 55 to 6.5 nM observed by Sathyanarayanan *et al.* suggests that CCaMK may have a CaM trapping mechanism, which is less potent than that of CaMKII (72). However, future experimental characterisation is required to assess the effect of this on the CaM dissociation rate constant and whether it is able to provide a mechanism for persistence.

When combined, these data allow a hypothesis for calcium ion and CaM dissociation from CCaMK to be proposed. It appears that initial dissociation from the visinin-like domain of one or two calcium ions is rapid. This is likely to be from EF-hand three, which was shown to be the fast dissociation site in chapter four section 4.1.2 “Dissection of the calcium ion-dissociation from the individual EF-Hands”. The next step is calcium ion-dissociation from the N-terminal EF-hands of CaM and dissociation of the CaM N-terminus from the autoinhibitory domain. Next, calcium ions

dissociate from the C-terminal EF-hands of CaM leading to complete CaM dissociation from the autoinhibitory domain. Finally one or two calcium ions dissociate from the visinin-like domain leading to a conformational change, which returns CCaMK to its apo state. This scheme is shown in Figure 5.5.

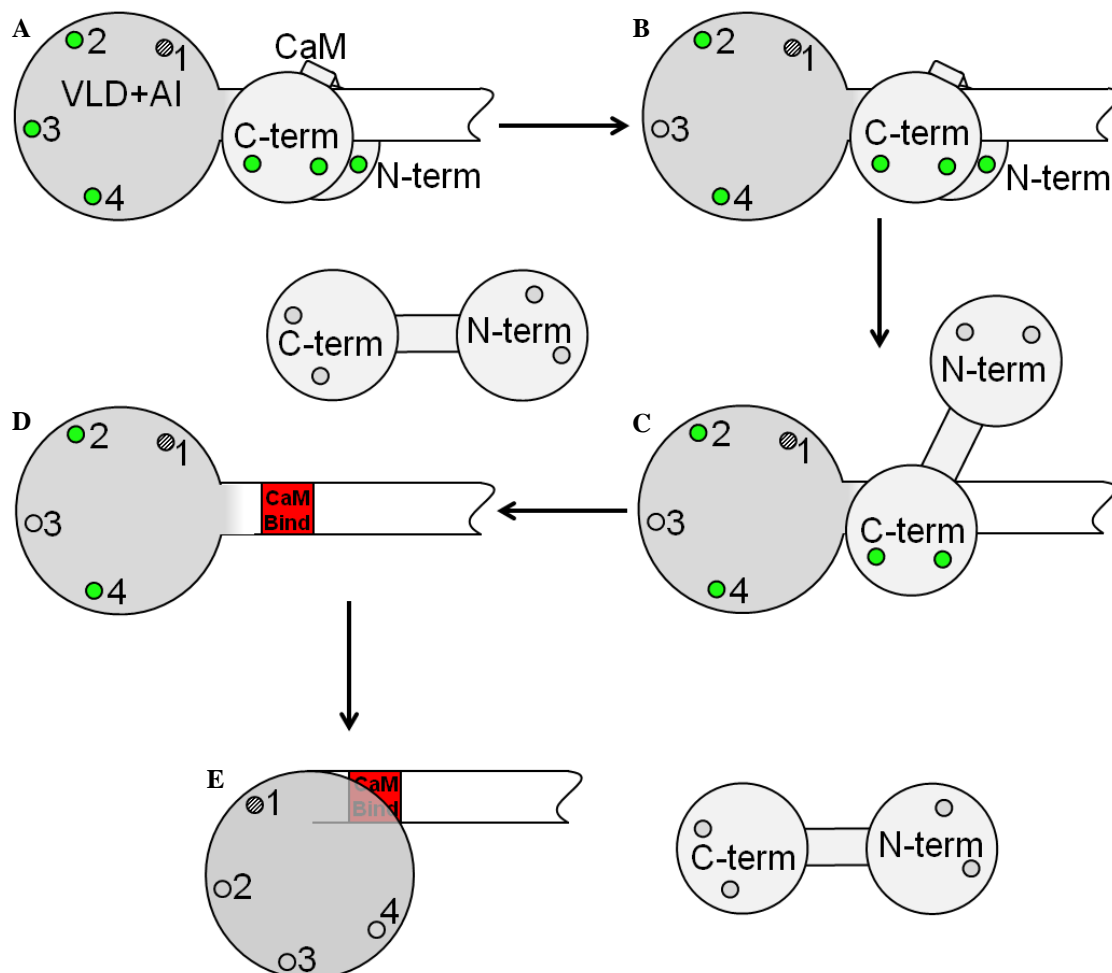


Figure 5.5. Proposed mechanism of CaM dissociation from the visinin-like domain with autoinhibition. The visinin-like domain with autoinhibition (VLD+AI) has the visinin-like domain shaded in grey, the autoinhibitory domain in white and the CaM binding site shaded in red. Each EF-hand labelled by number. The inactive EF-hand is shaded with diagonal lines, calcium ion-bound EF-hands are shaded green and apo EF-hands are shaded grey. CaM is shaded in light grey. The N and C terminal lobes of CaM are labelled N-term and C-term, respectively. A, calcium-ion saturated CCaMK visinin-like domain with autoinhibitor/CaM complex. B, complex after calcium ion-dissociation from EF-hand three of the visinin-like domain. C, calcium ion-dissociation from the CaM N-terminus and dissociation of the N-terminal lobe from the CaM binding site. D, calcium ion dissociation from the CaM C-terminus and complete dissociation of CaM. E, complete calcium ion-dissociation from the visinin-like domain and return to the apo conformation.

5.3 EXPERIMENTAL PROCEDURES

5.3.1 *Analytical gel filtration of the CCaMK visinin-like domain with autoinhibition, CaM and the visinin-like domain with autoinhibition/CaM complex.*

Solutions of 10 μM visinin-like domain with autoinhibition, CaM or of a mixture of the two proteins were passed through a Superdex 200 10/30 GL column (GE healthcare) pre-equilibrated with 50 mM Tris-HCl pH 7.5 containing 100 mM NaCl, 1 mM TCEP and 2 mM CaCl_2 . The column was calibrated as described in chapter two section 2.3.10 “Analytical gel filtration of visinin-like domain and visinin-like domain with autoinhibition”.

5.3.2 *Analytical ultracentrifugation of the CCaMK visinin-like domain with autoinhibition, CaM and the CCaMK visinin-like domain with autoinhibition/CaM complex*

CCaMK visinin-like domain with autoinhibition and CaM were dialysed into 10 mM HEPES pH 7.5 containing 50 mM NaCl, 1 mM TCEP and 2 mM CaCl_2 . Solutions of 50 μM visinin-like domain with autoinhibition, 50 μM CaM, 50 μM visinin-like domain with autoinhibition together with 50 μM CaM and 50 μM visinin-like domain with autoinhibition together with 25 μM CaM were analysed at spin speeds of 10 000, 20 000 and 30 000 RPM as described in chapter two section 1.3.12 “Analytical ultracentrifugation”.

5.3.3 *Tryptophan fluorescence spectroscopy of the visinin-like domain with autoinhibition to monitor CaM binding*

CCaMK visinin-like domain with autoinhibition and CaM were dialysed into 10 mM Tris-HCl pH 7.5 containing 50 mM NaCl, 1 mM TCEP and 2 mM CaCl_2 . A volume of 0.8 ml of 5 μM visinin-like domain with autoinhibition was placed into a reduced volume fluorescence cuvette, and a fluorescence spectrum was collected on a Perkin Elmer LS55 luminescence spectrometer between 310 and 400 nm with excitation at 290 nm, slit widths of 10 nm and a scan speed of 500 nm min^{-1} . A volume of 200 μl 50 μM CaM was added, then 100 μl of 0.25 M EDTA was added with additional spectra collected after each.

5.3.4 *Calcium ion-dissociation from the visinin-like domain with autoinhibition/CaM complex monitored by Quin-2 absorbance*

This experiment was performed as described in chapter four section 4.3.2 “Calcium ion-dissociation monitored by Quin-2 absorbance”. Samples of CaM and visinin-like domain with autoinhibition were dialysed separately and mixed in an equimolar ratio to produce a 14.4 μM stock of complex (100 μM binding site concentration).

5.3.5 *CaM dissociation from the CCaMK visinin-like domain with autoinhibition monitored by tryptophan fluorescence*

CaM and visinin-like domain with autoinhibition were dialysed into 10 mM Tris-HCl pH 7.5 containing 50 mM NaCl, 1 mM TCEP and 0.1 mM CaCl_2 . All solutions were prepared in this

buffer. Stock solutions of 5 μM visinin-like domain with autoinhibition, 5 μM CaM, 5 μM visinin-like domain with autoinhibition + 5 μM CaM, 2 mM EDTA and 20 mM EDTA were prepared. Each protein solution was mixed 1:1 with the 2 mM EDTA solution with a Hi-Tech scientific SF61 DX2 Double Mixing Stopped-Flow System equipped with a 100 W Hg arc-lamp in fluorescence mode. The excitation wavelength was 290 nm and emission was monitored above 320 nm, by installing a >320 nm filter, over a 20 s period. Data were collected with a logarithmic time base at 15, 20 and 25 $^{\circ}\text{C}$. Control experiments of complex or CaM vs buffer, and visinin-like domain with autoinhibition vs 2 mM EDTA were performed. An additional experiment was performed by mixing the complex with a 20 mM EDTA at 15 $^{\circ}\text{C}$. Final concentrations were 2.5 μM for the proteins and 1 or 10 mM EDTA.

5.3.6 *Surface Plasmon resonance*

CCaMK visinin-like domain with autoinhibition was exchanged into milliQ water by concentration and 10-fold dilution three times in a Sartorius Vivaspin 4, 10 000 MWCO filter. The protein was then exchanged into 10 mM pH 4 ammonium acetate by the same method. The protein was immobilised onto a CM5 chip in a Biacore T100 (GE Healthcare) by the EDC/NHS method as per the manufactures instructions to a target level of 1500 response units. A reference cell was prepared by EDC/NHS activation followed immediately by blocking with ethanolamine. Binding experiments were performed with CaM dialysed into 50 mM Tris-HCl pH 7.5 containing 150 mM NaCl, 0.1 mM CaCl_2 and 0.005% P20 surfactant. CaM solutions were prepared by serial dilution of a 1 μM stock down to 1.95 nM. Binding curves were produced by flowing CaM over the pre-equilibrated surface at 30 $\mu\text{l min}^{-1}$ for 360 s. The dialysis buffer without protein was flowed over the surface to allow CaM to dissociate for 600 s then the surface was regenerated with 2 mM EDTA for 120 s. Finally the surface was equilibrated by flowing buffer for 1000 s. The chip was preconditioned by performing ten binding experiments with 100 nM CaM before running the dilution series. All data were then processed in the Biacore T100 evaluation software package (GE Healthcare).

6. Chapter six - General discussion

The data presented in the above chapters begin to elucidate the mechanism by which the visinin-like domain of CCaMK operates in the decoding of calcium spiking in root hairs. The data show that each EF-hand contributes differently to the tertiary-level conformational changes and has different calcium ion-affinity and/or kinetics. These data allow for a hypothesis to be formed whereby the binding to each EF-hand initiates a specific conformational change and shifts the equilibrium between the inactive and active forms of CCaMK for autophosphorylation. This is supported by data presented in chapter two, which indicates that conformational changes are impaired when single EF-hands are inactivated and impaired further when two EF-hands are inactivated.

The affinities of EF-hands two and three are similar at 200 nM. This is ideal for decoding calcium spiking, which has a range of 5-800 nM (8). EF-hand four is a tight binding site with a significantly lower affinity as discussed in chapter three. This suggests that EF-hand four may be occupied at basal calcium ion concentrations meaning its occupancy remains unchanged during spiking. This would suggest that calcium ion-binding to EF-hands two and three is most important for the activation of CCaMK for autophosphorylation. This conclusion is supported by the fact that mutation of EF-hand four has little impact on the conformational changes observed in experiments described in chapter two. In addition to this, the binding of calcium ions to each EF-hand differ in their thermodynamic parameters. Calcium ion-binding to EF-hand two is exclusively driven by entropy and linked to conformational changes, which lead to the exposure of hydrophobic residues. As the exposure of hydrophobic residues is entropically unfavourable (156), other elements of calcium ion-binding and conformational changes within EF-hand two must be highly entropically favourable to yield an overall positive entropy change. To date, the function of this hydrophobic exposure remains unknown. It may be a driver of interactions with the kinase domain or CCaMK-interacting proteins. It is unlikely to be a method by which the visinin-like domain binds its own autoinhibitory domain as an increase in hydrophobic exposure was observed for both the visinin-like domain and visinin-like domain with autoinhibition constructs. EF-hand three binding is favourable in terms of entropy and enthalpy, and is linked to elongation of the visinin-like domain. The function of this also remains unknown in the context of the full-length protein. EF-hand four could not be characterised as contaminating calcium ions could not be removed from this site. Interestingly, EF-hand four is inactivated in many NCSs suggesting that it plays a mainly structural role (62). The suggestion that this site is occupied at basal concentrations may mean that the same is true for EF-hand four of CCaMK. From the conclusions described above, it was not possible to determine whether structural changes in CCaMKs visinin-like domain are similar to those of recoverin and the NCS family of proteins. The conformational changes are less

pronounced in the CCaMK visinin-like domain, but an elongation and alteration of interactions with the N-terminus do occur suggesting that a similar mechanism may exist. Future work to obtain crystal structures of CCaMK should be able to answer this question conclusively.

Although the affinities of EF-hands two and three are similar, their kinetics of calcium ion-binding and dissociation are not. As discussed in chapter four, EF-hand three releases calcium ions at a rate constant of greater than 700 s^{-1} suggesting that it returns to the apo state almost instantly after the end of a calcium spike. EF-hands two and four are much slower at releasing calcium ions at a rate constant of $2.11 \pm 0.01 \text{ s}^{-1}$. This suggests that EF-hands two will release calcium ions with only a slight delay at the end of a calcium spike. Presumably, conformational changes returning the EF-hands to the apo state occur at the same rate as calcium ion-dissociation, as has been determined to be the case in CaM in chapter five. However, this has not been determined experimentally for the visinin-like domain EF-hands. Although the slowest calcium-ion dissociation rate constants are measureable, they are too fast to allow persistence of calcium ion-bound CCaMK between spikes as the $t_{1/2}$ for calcium ion-dissociation was less than 1 s, much faster than the 90 s spike interval (36). This means that CaM binding and autophosphorylation are more likely to provide a mechanism for persistence between spikes. The effect of autophosphorylation on the kinetics and affinity of calcium ion-binding to the CCaMK EF-hands is currently not known.

As the dissociation kinetics of EF-hands two and three differ, the association kinetics must also differ as the affinities are indistinguishable. This suggests that EF-hand three binds calcium before EF-hand two. Assuming EF-hand four is occupied at basal calcium ion concentrations; this imposes an order of binding of EF-hand four, followed by EF-three followed by two. This scheme can be used to update the model of activation for the non-phosphorylated form of CCaMK as shown in Figure 6.1 A-C.

CaM affinity and dissociation kinetics from the CCaMK visinin-like domain with autoinhibition were discussed in chapter five. This revealed that CaM dissociation is too rapid to allow persistence of active CCaMK between spikes in the absence of autophosphorylation. These data also showed that the CaM binding properties of CCaMK are not dissimilar from CaMKII and other well characterised CaM binding proteins. Like with CaMKII, the C-terminal lobe of CaM may dissociate slower than the N-terminal lobe (Figure 6.1 G-I), although the dissociation of the N-terminal lobe is approximately 200-fold slower than in CaMKII (100, 105). The different binding properties of each lobe of CaM are thought to be important for the regulation of CaMKII (105, 107) and is possibly the case in CCaMK. This would suggest that *M. truncatula* CCaMK and CaM are not unique in terms of their CaM binding and kinetics. This is supported by data from L. Zhou *et al.* (unpublished) within our research group. It was shown that the affinity and kinetics of calcium ion-binding to *M. truncatula* CaM does not differ significantly to previously characterised animal CaMs. Where CCaMK does differ from CaMKII and all other known CaM kinases is in the presence of the visinin-like domain and its control of autophosphorylation. It is clear that CCaMK

must differ significantly from CaMKII as the spiking frequency is approximately ten-fold lower (0.5-4 Hz is relevant for CaMKII compared to 0.1 Hz in root hair nuclei). The concentration of calcium ions is also lower (low-mid μM in animal neurones, high nM in root hair nuclei) (8, 10, 36).

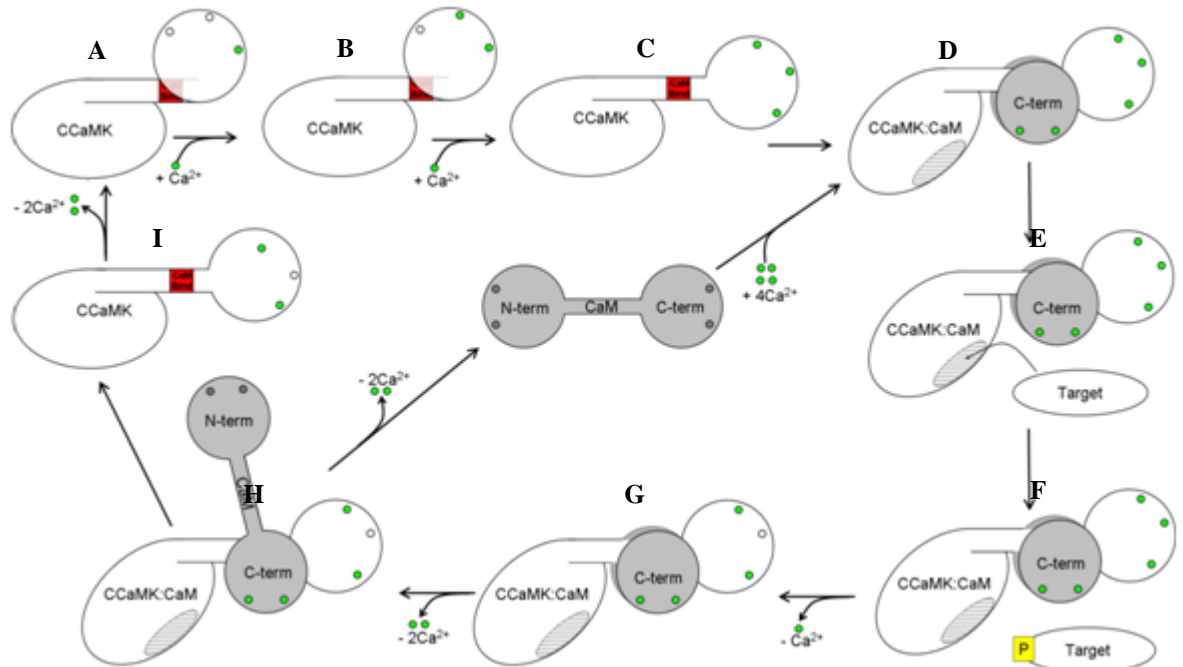


Figure. 6.1. Updated activation scheme for CCaMK with data from this thesis. Scheme based upon work by Sathyanarayanan *et al.* and Takezawa *et al.* (Chapter one, Figure 1.6) (61, 72) and updated with the biochemical data detailed in this thesis. This scheme includes the nonphosphorylated forms of CCaMK only. A-C, EF-hand four is likely to be occupied in the basal state. A calcium spike allows calcium ion-binding to EF-hand three, followed by EF-hand two, which initiates conformational changes. D, calcium ions bind to CaM and CaM binds to CCaMK. E-F, substrates bind and become phosphorylated. G-I, after a spike, calcium ions dissociate from EF-hand three, followed by the N-terminus of CaM leading to N-terminal CaM dissociation. Calcium ions then dissociate from the CaM C-terminus leading to full CaM dissociation. Finally calcium ions dissociate from CCaMK EF-hand two to return CCaMK to the apo state.

Although assessment of the data and basic models have allowed the function of CCaMK in response to calcium spiking to be predicted, comparison with *in vivo* data is required to truly understand the system in a biological context. In parallel with the work described in this thesis, B. Millar *et al.* in the Oldroyd group have produced multiple mutations of CCaMK in *M. truncatula* and assessed their effect on mycorrhization and nodulation. These include mutations of the EF-hands identical to those studied biochemically in the visinin-like domain construct. In the *in planta* experiments it was shown that single EF-hand mutants are reduced in their efficiency for both mycorrhization and nodulation by approximately 50-66%. Double mutants were completely

abolished for nodulation but mycorrhization was only reduced by approximately 66-90%. Finally the triple mutant was incapable of either symbiosis (Figure 6.2). This demonstrates that calcium ion-binding to CCaMK is essential for correct function. The finding that single mutants are only slightly impaired for symbiosis was instrumental to the hypothesis that two calcium ions binding can drive enough conformational change for activity, as discussed at the beginning of this section. These data suggest that part-loaded CCaMK is still functional, but to a lower level. This correlates well to the biochemical data, which suggest that the EF-hands each undergo different degrees of conformational change when calcium ions bind. Data showing that mutation of EF-hand four reduces the efficiency of nodulation shows that it is important for efficient activation of CCaMK, despite the fact that it is likely to be occupied at basal calcium ion-concentrations in the wild-type protein. Combined with the *in vivo* data, it is likely that calcium ion-binding to each EF-hand makes an individual contribution to the activation of CCaMK. This raises the possibility that different levels of saturation of the EF-hands could give different outputs. For instance, calcium ions bound to EF-hands two and four could be expected to yield a visinin-like domain with an exposed hydrophobic patch but no elongation, whereas calcium ions bound to three and four could yield an elongated visinin-like domain without an exposed hydrophobic patch. As EF-hand three fills before EF-hand two at the start of a calcium spike, around 80% of the low affinity sites will be filled at the top of the spike, and EF-hand two remains filled longer than EF-hand three at the end of a calcium spike, it is possible that the concentrations of part-loaded CCaMKs may be significant at certain time points. This hypothesis is supported by the fact that the double mutants can still undergo mycorrhization to a low level, but do not undergo nodulation. Furthermore, it was found that deletion of EF-hands four or four and three or leads to spontaneous nodule formation (Miller *et al.* unpublished). Complete deletion of the EF-hands does not lead to spontaneous nodulation. It should be noted that EF-hand deletion may affect the protein fold significantly. Nevertheless this demonstrates the importance of the EF-hands of CCaMK for its regulation, which these data suggest is negative. This is because the visinin-like domain appears to be a negative regulator when intact and able to bind calcium ions by preventing spontaneous nodulation. Its part-deletion appears to remove this function and suggests that CCaMK without a fully active visinin-like domain is deregulated. The *in vitro* and *in vivo* data suggest that consideration of part calcium ion-saturated forms of CCaMK are going to be important in complete computational models of how CCaMK decodes calcium spiking.

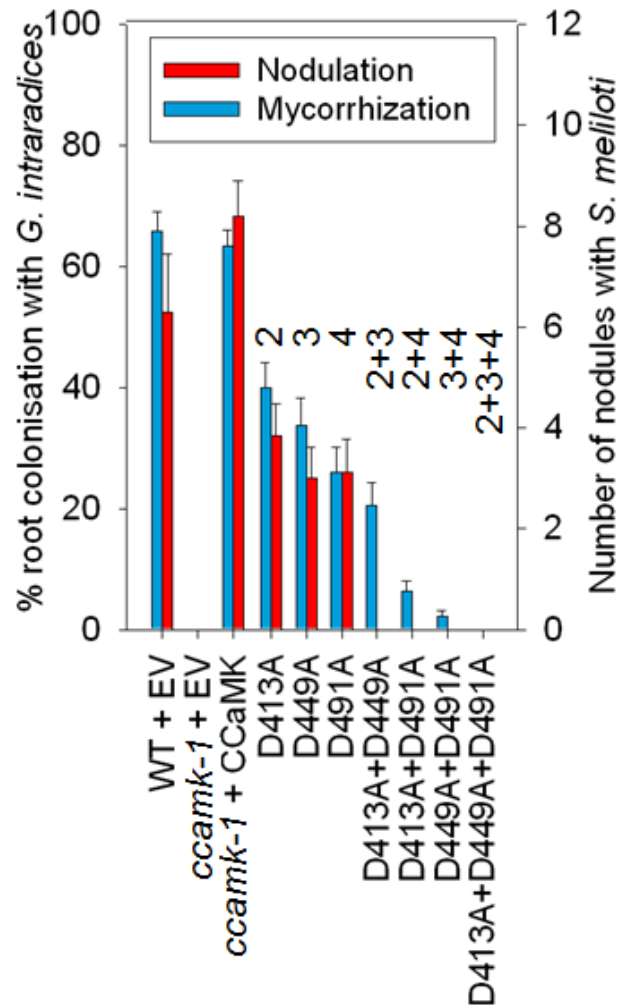


Figure. 6.2. Effects of CCaMK EF-hand mutation on the efficiency of symbiotic interactions in *M. truncatula*. Graph shows percent colonisation by *G. intraradices* (red bars) and mean nodule numbers per plant (blue bars). WT denotes wild-type plants, EV denotes empty vector transformation as a control, *ccamk-1* denotes a CCaMK mutant background, CCaMK denotes transformation with a vector containing the wild-type CCaMK, which restored wild-type activity. D#A denotes aspartic acids mutated to alanine in the CCaMK vector transformed into *ccamk-1* plants. Labels above indicate the EF-hands that have been inactivated. Figure kindly provided by B. Millar (unpublished data).

To date autophosphorylation has not been shown to lead to autonomous activity of CCaMK displaying another key difference to CaMKII. This means that autophosphorylation may be playing a very different role in CCaMK. Phosphorylation of Thr271 is known to enhance CaM affinity approximately eight-fold (72) which is much less than the 1000 fold seen in CaMKII (100).

Given that CaM dissociation is likely to occur between calcium spikes in root hair nuclei, any potential CaM/Ca²⁺ trapping in CCaMK may be important. However, this remains to be determined experimentally. Contradictory to the *in vitro* data, which shows that autophosphorylation enhances

CaM binding, which in turn enhances CCaMK activity, *in vivo* data suggest that a loss of autophosphorylation by mutation of Thr271 removes negative regulation of CCaMK and allows spontaneous nodulation. This means that autophosphorylation of Thr271 requires extensive additional characterisation. Additionally in biochemical assays CaM binding is known to inhibit autophosphorylation (61) which has been reproduced by A. Miyahara *et al.* in the Oldroyd group (unpublished), suggesting that CaM binding may also provide a mechanism for negative feedback on CCaMK activation. This has not been reported for CaMKII. Work by B. Millar, A. Miyahara *et al.* (unpublished) has also identified two additional potential autophosphorylation sites. These are Thr202 in the kinase domain, mutation of which to alanine almost abolishes mycorrhization whilst only slightly reducing nodulation efficiency. The second site is Ser343 located at the end of the CaM binding site. When Ser343 is mutated to alanine, nodulation is abolished but mycorrhization is only reduced by approximately 66% when compared to wild-type. This raises the possibility that differential autophosphorylation at these secondary sites may confer specificity of CCaMK in the output of the Sym pathway. From these conclusions it is clear that autophosphorylation of these additional sites also requires extensive characterisation to understand their exact function and mechanism. Additional CCaMK mutants of interest generated by Millar *et al.* were Glu319, Leu324 and Leu333, all within the CaM binding region of CCaMK. These mutants were all reduced for both symbioses. These data suggest that these residues may be important for CaM binding, and will make for interesting future characterisation of CaM binding and kinetics (Miller *et al.* unpublished).

The data presented in this thesis has characterised the calcium ion-binding and kinetics for the visinin-like domain, allowing an understanding of how it responds to the calcium spiking signal *in vivo*. Many of the parameters of CaM binding have also been characterised and combined with an understanding of the visinin-like domain to give an overall model of the binding and kinetics of calcium ions to CCaMK. It is known that these values will be critical for the complete computational modelling of CCaMK, and these values will, in future, be integrated with the understanding of other biophysical parameters of CCaMK activation to provide a complete picture of how calcium spiking is decoded by CCaMK.

7. Chapter seven – Outlook and future work

The data presented in this thesis have provided many parameters, which are required for the building of computational models. The aim of these models is to understand the function of CCaMK in the context of calcium spiking. Work by A. Pratap *et al.* within the Morris group is beginning to build models that include the values for affinity and kinetics determined in this thesis as well as the mechanisms of activation that have been elucidated.

It is clear that many characteristics have yet to be determined. For instance, it is not known whether calcium ion-binding to the visinin-like domain is required to allow CaM binding. This is under investigation in our research group by producing EF-hand mutants in the visinin-like domain with autoinhibition construct, which will be screened by equilibrium and possibly stopped-flow fluorescence as detailed in chapter five. It is conceivable that the visinin-like domain binds its own autoinhibitory domain to alleviate autoinhibition and allow autophosphorylation. This could be studied by mixing the isolated visinin-like domain with a synthetic peptide that mimics the autoinhibitory domain and monitoring mass change by DLS, analytical gel filtration or AUC.

Another key detail missing in chapter five is a reliable measure of the CaM association rate constant. A method for this was optimised as part of the stopped-flow studies by tryptophan fluorescence whereby CaM and CCaMK are mixed in the presence of excess calcium, and the signal above 320 nm is monitored with excitation at 290 nm. By measuring association rate constants at various visinin-like domain with autoinhibition concentrations, whilst keeping the CaM concentration constant, the association rate constant can be calculated under pseudo first-order conditions. Previous experiments determined that the data are not ideal when CaM is used in excess, as discussed in chapter five. In addition to the k_a , a reliable measure of K_D is also required. Although the SPR data agree closely with the data collected by Sathyanarayanan *et al.* (72) using fluorescence anisotropy of CaM labelled with dansyl chloride, the non-ideal behaviour of the SPR data means that they are not of publication quality. To this end, the fluorescence anisotropy method is currently being optimised for the study of *M. truncatula* CaM binding to the visinin-like domain with autoinhibition. Together these characterisations will allow a comprehensive understanding of CaM binding to CCaMK. Additionally, it may be possible to deconvolute the binding parameters of each lobe of CaM when these data are combined with data in chapter five, which will allow for more complex computational modelling. Along these lines, it may also be necessary to characterise mutants of the CaM EF-hands for all parameters of CCaMK binding in order to create complete models, such as the one published by Pepke *et al.* for CaMKII (107).

The suite of methods developed for the study of CaM binding will also be important for the study of interesting mutants in the CaM binding site of CCaMK that impact on the *in vivo* activity (identified by Millar *et al.* and discussed in the general discussion, chapter six). It is hoped that

biochemical characterisation of these mutants will allow for an understanding of the mechanisms behind these phenotypes.

Although the data thus far suggest that the visinin-like domain and visinin-like domain with autoinhibitor are good models for the behaviour of the full length protein, comparisons will need to be made to confirm this. To this end new constructs and/or conditions for the full length protein need to be identified. So far Miyahara and Zhou *et al.* (unpublished) have established that a maltose binding protein fusion of CCaMK is more suitable than the isolated protein for biochemical study. Additional early work on CCaMK constructs with short deletions of N-terminal residues suggests that stability may be enhanced without the addition of a tag. Unfortunately, these truncated constructs require further characterisation and optimisation before detailed study of CaM and calcium ion-binding can begin. These constructs of the full length CCaMK will be important in the future study of autophosphorylation on CaM and calcium ion-binding and kinetics. It is clear that autophosphorylation is critical in CCaMK regulation, and new sites Thr202 and Ser343, in addition to the known Thr271, require extensive characterisation. This means that many of the analyses carried out in this thesis require repeating with autophosphorylated CCaMK to define the influence of this modification on calcium spike decoding.

In parallel with the studies suggested above, detailed characterisation of substrate interaction and phosphorylation is required. Although Cyclops and Cip73 have been identified as substrates, with some sites of modification defined (refer to chapter one, section 1.3.3 “function of CCaMK” and references therein) the binding of these targets to CCaMK and the kinetics of phosphorylation have not been characterised. Understanding of these parameters will be critical in defining the output of CCaMK should the hypothesis that CCaMK decodes calcium spiking in terms of activity levels be upheld. Analysis of CCaMK mutants corresponding to those known to affect CaM and calcium ion-binding will also be critical in understanding the phenotypes observed by Millar *et al.* (unpublished) and discussed in the general discussion (chapter six).

An additional long term experiment relating to the work in this thesis will be obtaining a crystal structure of CCaMK, or of its individual domains. The structural analysis in chapter two gave many clues about the mechanism by which the visinin-like domain operates. However, an atomic resolution structure would give conclusive answers to the questions raised. It is clear that for the full length protein significant progress will need to be made. A crystallisation screen of the visinin-like domain construct after the N-terminal his-tag was cleaved with DAPase was set up in the closing stages of this study. Initial results suggested that stability was enhanced as almost all conditions gave clear drops at approximately 10 mg/ml protein concentration, whereas before cleavage this was closer to 50% clear drops. It remains to be seen whether this strategy can yield diffracting crystals with additional optimisation.

These proteins have proven challenging to work with meaning that future experiments will not be trivial. However, their continued study is worthwhile as an understanding of CCaMK will

contribute greatly to the long term goal of introducing nodulation into non-legume crops such as wheat. Achieving this goal would revolutionise agricultural methods and contribute to solving problems of food security and climate change. This outlook demonstrates that we are still in the early stages of characterisation of CCaMK. Today many of the tools exist, and the data thus far suggest that the future developments in this field will be both interesting and informative in bringing us closer to decoding calcium spiking through the calcium ion-binding properties of CCaMK.

References

1. Oldroyd, G. E. D., Harrison, M. J., and Udvardi, M. (2005) Peace talks and trade deals. Keys to long-term harmony in legume-microbe symbioses, *Plant Physiol.* *137*, 1205-1210.
2. Oldroyd, G. E. D. (2001) Dissecting symbiosis: developments in NOD factor signal transduction, *Ann. Bot.* *87*, 709-718.
3. Catoira, R., Galera, C., de Billy, F., Penmetsa, R. V., Journet, E.-P., Maillet, F., Rosenberg, C., Cook, D., Gough, C., and Dénarié, J. (2000) Four genes of *Medicago truncatula* controlling components of a Nod factor transduction pathway, *Plant Cell* *12*, 1647-1666.
4. Lévy, J., Bres, C., Geurts, R., Chalhoub, B., Kulikova, O., Duc, G., Journet, E.-P., Ane, J.-M., Lauber, E., Bisseling, T., Denarie, J., Rosenberg, C., and Debelle, F. (2004) A putative Ca²⁺ and calmodulin-dependent protein kinase required for bacterial and fungal symbioses, *Science* *303*, 1361-1364.
5. Oldroyd, G. E. D., and Geurts, R. (2001) *Medicago truncatula*, going where no plant has gone before, *Trends Plant Sci.* *6*, 552-554.
6. Berridge, M. J. (1997) The AM and FM of calcium signalling, *Nature* *386*, 759-760.
7. Sathyanarayanan, P., and Poovaiah, B. (2004) Decoding Ca²⁺ signals in plants, *Crit. Rev. Plant Sci.* *23*, 1-11.
8. Ehrhardt, D. W., Wais, R., and Long, S. R. (1996) Calcium spiking in plant root hairs responding to Rhizobium nodulation signals, *Cell* *85*, 673-681.
9. Berridge, M. J., Lipp, P., and Bootman, M. D. (2000) The versatility and universality of calcium signalling, *Nat Rev Mol Cell Biol* *1*, 11-21.
10. Meyer, T., and Stryer, L. (1991) Calcium spiking, *Annual. Rev. Biophys. Biophys. Chem.* *20*, 153-174.
11. Sanders, D., Pelloux, J., Brownlee, C., and Harper, J. F. (2002) Calcium at the crossroads of signaling, *Plant Cell* *14*, S401-417.
12. Michard, E., Lima, P. T., Borges, F., Silva, A. C., Portes, M. T., Carvalho, J. E., Gilliam, M., Liu, L.-H., Obermeyer, G., and Feijó, J. A. (2011) Glutamate receptor-like genes form Ca²⁺ channels in pollen tubes and are regulated by pistil d-Serine, *Science* *332*, 434-437.
13. Peiter, E., Maathuis, F. J. M., Mills, L. N., Knight, H., Pelloux, J., Hetherington, A. M., and Sanders, D. (2005) The vacuolar Ca²⁺-activated channel TPC1 regulates germination and stomatal movement, *Nature* *434*, 404-408.
14. Park, M. K., Ashby, M. C., Erdemli, G., Petersen, O. H., and Tepikin, A. V. (2001) Perinuclear, perigranular and sub-plasmalemmal mitochondria have distinct functions in the regulation of cellular calcium transport, *Embo J* *20*, 1863-1874.
15. Parekh, A. B. (2006) Cell biology: Cracking the calcium entry code, *Nature* *441*, 163-165.
16. Li, W.-h., Llopis, J., Whitney, M., Zlokarnik, G., and Tsien, R. Y. (1998) Cell-permeant caged InsP3 ester shows that Ca²⁺ spike frequency can optimize gene expression, *Nature* *392*, 936-941.
17. Friel, D. D., and Chiel, H. J. (2008) Calcium dynamics: analyzing the Ca²⁺ regulatory network in intact cells, *Trends Neurosci.* *31*, 8-19.
18. Chang, C. J. (2007) Chemical biology: ions illuminated, *Nature* *448*, 654-655.
19. Kits, K. S., and Mansvelder, H. D. (2000) Regulation of exocytosis in neuroendocrine cells: spatial organization of channels and vesicles, stimulus-secretion coupling, calcium buffers and modulation, *Brain Res. Rev.* *33*, 78-94.
20. Wagner, J., and Keizer, J. (1994) Effects of rapid buffers on Ca²⁺ diffusion and Ca²⁺ oscillations, *Biophys. J.* *67*, 447-456.
21. Hall, J. D., Betarbet, S., and Jaramillo, F. (1997) Endogenous buffers limit the spread of free calcium in hair cells, *Biophys. J.* *73*, 1243-1252.
22. Barrow, S. L., Sherwood, M. W., Dolman, N. J., Gerasimenko, O. V., Voronina, S. G., and Tepikin, A. V. (2006) Movement of calcium signals and calcium-binding proteins: firewalls, traps and tunnels, *Biochem. Soc. Trans.* *34*, 381-384.

23. Dolmetsch, R. E., Lewis, R. S., Goodnow, C. C., and Healy, J. I. (1997) Differential activation of transcription factors induced by Ca^{2+} response amplitude and duration, *Nature* 386, 855-858.
24. McCormack, E., Tsai, Y.-C., and Braam, J. (2005) Handling calcium signaling: Arabidopsis CaMs and CMLs, *Trends Plant Sci.* 10, 383-389.
25. Harmon, A. C., Gribskov, M., and Harper, J. F. (2000) CDPKs - a kinase for every Ca^{2+} signal?, *Trends Plant Sci.* 5, 154-159.
26. Gifford, J. L., Walsh, M. P., and Vogel, H. J. (2007) Structures and metal-ion-binding properties of the Ca^{2+} -binding helix-loop-helix EF-hand motifs, *Biochem. J.* 405, 199-221.
27. Yun, C.-H., Bai, J., Sun, D.-Y., Cui, D.-F., Chang, W.-R., and Liang, D.-C. (2004) Structure of potato calmodulin PCM6: the first report of the three-dimensional structure of a plant calmodulin, *Acta Crystallgr. D.* 60, 1214-1219.
28. Op den Camp, R., Streng, A., De Mita, S., Cao, Q., Polone, E., Liu, W., Ammiraju, J. S. S., Kudrna, D., Wing, R., Untergasser, A., Bisseling, T., and Geurts, R. (2011) LysM-Type mycorrhizal receptor recruited for rhizobium symbiosis in nonlegume parasponia, *Science* 331, 909-912.
29. Goormachtig, S., Capoen, W., James, E. K., and Holsters, M. (2004) Switch from intracellular to intercellular invasion during water stress-tolerant legume nodulation, *PNAS* 101, 6303-6308.
30. Capoen, W., Den Herder, J., Sun, J., Verplancke, C., De Keyser, A., De Rycke, R., Goormachtig, S., Oldroyd, G., and Holsters, M. (2009) Calcium spiking patterns and the role of the calcium/calmodulin-dependent kinase CCaMK in lateral root base nodulation of *Sesbania rostrata*, *Plant Cell*, tpc.109.066233.
31. Wang, W., and Poovaiah, B. W. (1999) Interaction of plant chimeric calcium/calmodulin-dependent protein kinase with a homolog of eukaryotic elongation factor-1 α , *J. Biol. Chem.* 274, 12001-12008.
32. Maillet, F., Poinot, V., Andre, O., Puech-Pages, V., Haouy, A., Gueunier, M., Cromer, L., Giraudet, D., Formey, D., Niebel, A., Martinez, E. A., Driguez, H., Becard, G., and Denarie, J. (2011) Fungal lipochitooligosaccharide symbiotic signals in arbuscular mycorrhiza, *Nature* 469, 58-63.
33. Parniske, M. (2008) Arbuscular mycorrhiza: the mother of plant root endosymbioses, *Nat Rev Micro* 6, 763-775.
34. Gutjahr, C., Banba, M., Croset, V., An, K., Miyao, A., An, G., Hirochika, H., Imaizumi-Anraku, H., and Paszkowski, U. (2008) Arbuscular mycorrhiza-specific signaling in rice transcends the common symbiosis signaling pathway, *Plant Cell*, tpc.108.062414.
35. Banba, M., Gutjahr, C., Miyao, A., Hirochika, H., Paszkowski, U., Kouchi, H., and Imaizumi-Anraku, H. (2008) Divergence of evolutionary ways among common sym genes: CASTOR and CCaMK show functional conservation between two symbiosis systems and constitute the root of a common signaling pathway, *Plant Cell Physiol.* 49, 1659-1671.
36. Kosuta, S., Hazledine, S., Sun, J., Miwa, H., Morris, R. J., Downie, J. A., and Oldroyd, G. E. D. (2008) Differential and chaotic calcium signatures in the symbiosis signaling pathway of legumes, *PNAS* 105, 9823-9828.
37. Sieberer, B. J., Chabaud, M., Timmers, A. C., Monin, A., Fournier, J., and Barker, D. G. (2009) A nuclear-targetedameleon demonstrates intranuclear Ca^{2+} spiking in medicago truncatula root hairs in response to rhizobial nodulation factors, *Plant Physiol.* 151, 1197-1206.
38. Radutoiu, S., Madsen, L. H., Madsen, E. B., Felle, H. H., Umehara, Y., Gronlund, M., Sato, S., Nakamura, Y., Tabata, S., Sandal, N., and Stougaard, J. (2003) Plant recognition of symbiotic bacteria requires two LysM receptor-like kinases, *Nature* 425, 585-592.
39. Oldroyd, G. E. D., Murray, J. D., Poole, P. S., and Downie, J. A. (2011) The rules of engagement in the legume-rhizobial symbiosis, *Annu. Rev. Genet.* 45, null.
40. Wais, R. J., Galera, C., Oldroyd, G., Catoira, R., Penmetsa, R. V., Cook, D., Gough, C., Denarie, J., and Long, S. R. (2000) Genetic analysis of calcium spiking responses in nodulation mutants of *Medicago truncatula*, *PNAS* 97, 13407-13412.

41. Chen, C., Ané, J.-M., and Zhu, H. (2008) OsIPD3, an ortholog of the *Medicago truncatula* DMI3 interacting protein IPD3, is required for mycorrhizal symbiosis in rice, *New Phytol.* 9999.
42. Chen, C., Gao, M., Liu, J., and Zhu, H. (2007) Fungal symbiosis in rice requires an ortholog of a legume common symbiosis gene encoding a Ca²⁺/calmodulin-dependent protein kinase, *Plant Physiol.* 145, 1619-1628.
43. Sinharoy, S., and DasGupta, M. (2009) RNA interference highlights the role of CCaMK in dissemination of endosymbionts in the aeschynomeneae legume arachis, *Mol. Plant-Microbe Interact.* 22, 1466-1475.
44. Oldroyd, G. E. D., Mitra, R. M., Wais, R. J., and Long, S. R. (2001) Evidence for structurally specific negative feedback in the Nod factor signal transduction pathway, *The Plant Journal* 28, 191-199.
45. Kalo, P., Gleason, C., Edwards, A., Marsh, J., Mitra, R. M., Hirsch, S., Jakab, J., Sims, S., Long, S. R., Rogers, J., Kiss, G. B., Downie, J. A., and Oldroyd, G. E. D. (2005) Nodulation signaling in legumes requires NSP2, a member of the GRAS family of transcriptional regulators, *Science* 308, 1786-1789.
46. Cook, D., Dreyer, D., Bonnet, D., Howell, M., Nony, E., and VandenBosch, K. (1995) Transient induction of a peroxidase gene in *Medicago truncatula* precedes infection by *Rhizobium meliloti*, *Plant Cell* 7, 43-55.
47. Oldroyd, G. E. D., and Long, S. R. (2003) Identification and characterization of nodulation-signaling pathway 2, a gene of *medicago truncatula* involved in NOD factor signaling, *Plant Physiol.* 131, 1027-1032.
48. Kanamori, N., Madsen, L. H., Radutoiu, S., Frantescu, M., Quistgaard, E. M. H., Miwa, H., Downie, J. A., James, E. K., Felle, H. H., Haaning, L. L., Jensen, T. H., Sato, S., Nakamura, Y., Tabata, S., Sandal, N., and Stougaard, J. (2006) A nucleoporin is required for induction of Ca²⁺ spiking in legume nodule development and essential for rhizobial and fungal symbiosis, *PNAS* 103, 359-364.
49. Groth, M., Takeda, N., Perry, J., Uchida, H., Draxl, S., Brachmann, A., Sato, S., Tabata, S., Kawaguchi, M., Wang, T. L., and Parniske, M. (2010) NENA, a *Lotus japonicus* homolog of Sec13, is required for rhizodermal infection by arbuscular mycorrhiza fungi and rhizobia but dispensable for cortical endosymbiotic development, *Plant Cell* 22, 2509-2526.
50. Murray, J. D., Muni, R. R. D., Torres-Jerez, I., Tang, Y., Allen, S., Andriankaja, M., Li, G., Laxmi, A., Cheng, X., Wen, J., Vaughan, D., Schultze, M., Sun, J., Charpentier, M., Oldroyd, G., Tadege, M., Ratet, P., Mysore, K. S., Chen, R., and Udvardi, M. K. (2011) Vapyrin, a gene essential for intracellular progression of arbuscular mycorrhizal symbiosis, is also essential for infection by rhizobia in the nodule symbiosis of *Medicago truncatula*, *The Plant Journal* 65, 244-252.
51. Kang, H., Zhu, H., Chu, X., Yang, Z., Yuan, S., Yu, D., Wang, C., Hong, Z., and Zhang, Z. (2011) A novel interaction between CCaMK and a protein containing the scythe_N ubiquitin-like domain in *Lotus japonicus*, *Plant Physiol.* 155, 1312-1324.
52. Oldroyd, G. E. D., Engstrom, E. M., and Long, S. R. (2001) Ethylene inhibits the NOD factor signal transduction pathway of *medicago truncatula*, *Plant Cell* 13, 1835-1849.
53. Marsh, J. F., Rakocevic, A., Mitra, R. M., Brocard, L., Sun, J., Eschstruth, A., Long, S. R., Schultze, M., Ratet, P., and Oldroyd, G. E. D. (2007) *Medicago truncatula* NIN Is essential for rhizobial-independent nodule organogenesis induced by autoactive calcium/calmodulin-dependent protein kinase, *Plant Physiol.* 144, 324-335.
54. Lohar, D. P., Sharopova, N., Endre, G., Penuela, S., Samac, D., Town, C., Silverstein, K. A. T., and VandenBosch, K. A. (2006) Transcript analysis of early nodulation events in *medicago truncatula*, *Plant Physiol.* 140, 221-234.
55. Fedorova, M., van de Mortel, J., Matsumoto, P. A., Cho, J., Town, C. D., VandenBosch, K. A., Gantt, J. S., and Vance, C. P. (2002) Genome-wide identification of nodule-specific transcripts in the model legume *medicago truncatula*, *Plant Physiol.* 130, 519-537.
56. Kiss, E., Olah, B., Kalo, P., Morales, M., Heckmann, A. B., Borbola, A., Lozsa, A., Kontar, K., Middleton, P., Downie, J. A., Oldroyd, G. E. D., and Endre, G. (2009) LIN, a

- novel type of U-Box/WD40 protein, controls early infection by rhizobia in legumes, *Plant Physiol.* *151*, 1239-1249.
57. Jones, K. M., Sharopova, N., Lohar, D. P., Zhang, J. Q., VandenBosch, K. A., and Walker, G. C. (2008) Differential response of the plant *Medicago truncatula* to its symbiont *Sinorhizobium meliloti* or an exopolysaccharide-deficient mutant, *PNAS* *105*, 704-709.
 58. Parádi, I., van Tuinen, D., Morandi, D., Ochatt, S., Robert, F., Jacas, L., and Dumas-Gaudot, E. (2010) Transcription of two blue copper-binding protein isogenes is highly correlated with arbuscular mycorrhizal development in *Medicago truncatula*, *Mol. Plant-Microbe Interact.* *23*, 1175-1183.
 59. Shaw, S. L., and Long, S. R. (2003) NOD factor elicits two separable calcium responses in *Medicago truncatula* root hair cells, *Plant Physiol.* *131*, 976-984.
 60. Patil, S., Takezawa, D., and Poovaiah, B. W. (1995) Chimeric plant calcium/calmodulin-dependent protein kinase gene with a neural visinin-like calcium-binding domain, *PNAS* *92*, 4897-4901.
 61. Takezawa, D., Ramachandiran, S., Paranjape, V., and Poovaiah, B. W. (1996) Dual regulation of a chimeric plant serine/threonine kinase by calcium and calcium/calmodulin, *J. Biol. Chem.* *271*, 8126-8132.
 62. Burgoyne, R. D., and Weiss, J. L. (2001) The neuronal calcium sensor family of Ca²⁺-binding proteins, *Biochem. J.* *353*, 1-12.
 63. Poovaiah, B. W., Xia, M., Liu, Z., Wang, W., Yang, T., Sathyanarayanan, P. V., and Franceschi, V. R. (1999) Developmental regulation of the gene for chimeric calcium/calmodulin-dependent protein kinase in anthers, *Planta* *209*, 161-171.
 64. Tirichine, L., Imaizumi-Anraku, H., Yoshida, S., Murakami, Y., Madsen, L. H., Miwa, H., Nakagawa, T., Sandal, N., Albrektsen, A. S., Kawaguchi, M., Downie, A., Sato, S., Tabata, S., Kouchi, H., Parniske, M., Kawasaki, S., and Stougaard, J. (2006) Deregulation of a Ca²⁺/calmodulin-dependent kinase leads to spontaneous nodule development, *Nature* *441*, 1153-1156.
 65. Pandey, S., and Sopory, S. K. (2001) *Zea mays* CCaMK: autophosphorylation-dependent substrate phosphorylation and down-regulation by red light, *J. Exp. Bot.* *52*, 691-700.
 66. Yano, K., Yoshida, S., Müller, J., Singh, S., Banba, M., Vickers, K., Markmann, K., White, C., Schuller, B., Sato, S., Asamizu, E., Tabata, S., Murooka, Y., Perry, J., Wang, T. L., Kawaguchi, M., Imaizumi-Anraku, H., Hayashi, M., and Parniske, M. (2008) CYCLOPS, a mediator of symbiotic intracellular accommodation, *PNAS* *105*, 20540-20545.
 67. Jeong, J. C., Shin, D., Lee, J., Kang, C. H., Baek, D., Cho, M. J., Kim, M. C., and Yun, D. J. (2007) Isolation and characterization of a novel calcium/calmodulin-dependent protein kinase, AtCK, from *Arabidopsis*, *Mol Cells* *24*, 276-282.
 68. Mitra, R. M., Gleason, C. A., Edwards, A., Hadfield, J., Downie, J. A., Oldroyd, G. E. D., and Long, S. R. (2004) From the cover: A Ca²⁺/calmodulin-dependent protein kinase required for symbiotic nodule development: Gene identification by transcript-based cloning, *PNAS* *101*, 4701-4705.
 69. Liu, Z., Xia, M., and Poovaiah, B. W. (1998) Chimeric calcium/calmodulin-dependent protein kinase in tobacco: differential regulation by calmodulin isoforms, *Plant Mol Biol* *38*, 889-897.
 70. Messinese, E., Mun, J.-H., Yeun, L. H., Jayaraman, D., Rouge, P., Barre, A., Lougnon, G., Schornack, S., Bono, J.-J., Cook, D. R., and Ane, J.-M. (2007) A novel nuclear protein interacts with the symbiotic DMI3 calcium- and calmodulin-dependent protein kinase of *medicago truncatula*, *Mol. Plant-Microbe Interact.* *20*, 912-921.
 71. Grimsrud, P. A., den Os, D., Wenger, C. D., Swaney, D. L., Schwartz, D., Sussman, M. R., Ane, J.-M., and Coon, J. J. (2010) Large-scale phosphoprotein analysis in *Medicago truncatula* roots provides insight into in vivo kinase activity in legumes, *Plant Physiol.* *152*, 19-28.
 72. Sathyanarayanan, P. V., Cremo, C. R., and Poovaiah, B. W. (2000) Plant chimeric Ca²⁺/calmodulin-dependent protein kinase. Role of the neural visinin-like domain in regulating autophosphorylation and calmodulin affinity, *J. Biol. Chem.* *275*, 30417-30422.

73. Sathyanarayanan, P. V., Siems, W. F., Jones, J. P., and Poovaiah, B. W. (2001) Calcium-stimulated autophosphorylation site of plant chimeric calcium/calmodulin-dependent protein kinase, *J. Biol. Chem.* 276, 32940-32947.
74. Gleason, C., Chaudhuri, S., Yang, T., Munoz, A., Poovaiah, B. W., and Oldroyd, G. E. D. (2006) Nodulation independent of rhizobia induced by a calcium-activated kinase lacking autoinhibition, *Nature* 441, 1149-1152.
75. Ramachandiran, S., Takezawa, D., Wang, W., and Poovaiah, B. W. (1997) Functional domains of plant chimeric calcium/calmodulin-dependent protein kinase: regulation by autoinhibitory and visinin-like domains, *J Biochem* 121, 984-990.
76. Peersen, O. B., Madsen, T. S., and Falke, J. J. (1997) Intermolecular tuning of calmodulin by target peptides and proteins: differential effects on Ca²⁺ binding and implications for kinase activation, *Protein Sci* 6, 794-807.
77. Sathyanarayanan, P. V., and Poovaiah, B. W. (2002) Autophosphorylation-dependent inactivation of plant chimeric calciumcalmodulin-dependent protein kinase, *Eur. J. Biochem.* 269, 2457-2463.
78. Kubota, Y., and Bower, J. M. (2001) Transient versus asymptotic dynamics of CaM kinase II: possible roles of phosphatase, *J. Comput. Neurosci.* 11, 263-279.
79. Du, L., and Poovaiah, B. W. (2005) Ca²⁺/calmodulin is critical for brassinosteroid biosynthesis and plant growth, *Nature* 437, 741-745.
80. Yang, T., and Poovaiah, B. W. (2003) Calcium/calmodulin-mediated signal network in plants, *Trends Plant Sci.* 8, 505-512.
81. Clapperton, J. A., Martin, S. R., Smerdon, S. J., Gamblin, S. J., and Bayley, P. M. (2002) Structure of the complex of calmodulin with the target sequence of calmodulin-dependent protein kinase I: Studies of the kinase activation mechanism, *Biochemistry* 41, 14669-14679.
82. Mann, D. M., and Vanaman, T. C. (1989) Topographical mapping of calmodulin-target enzyme interaction domains, *J. Biol. Chem.* 264, 2373-2378.
83. Martin, S. R., Andersson Teleman, A., Bayley, P. M., Drakenberg, T., and Forsen, S. (1985) Kinetics of calcium dissociation from calmodulin and its tryptic fragments, *Eur. J. Biochem.* 151, 543-550.
84. Porumb, T. (1994) Determination of calcium-binding constants by flow dialysis, *Anal. Biochem.* 220, 227-237.
85. Bayley, P., Ahlstrom, P., Martin, S. R., and Forsen, S. (1984) The kinetics of calcium binding to calmodulin: Quin 2 and ANS stopped-flow fluorescence studies, *Biochem. Biophys. Res. Commun.* 120, 185-191.
86. Gilli, R., Lafitte, D., Lopez, C., Kilhoffer, M. C., Makarov, A., Briand, C., and Haiech, J. (1998) Thermodynamic analysis of calcium and magnesium binding to calmodulin, *Biochemistry* 37, 5450-5456.
87. Luan, S., Kudla, J., Rodriguez-Concepcion, M., Yalovsky, S., and Gruissem, W. (2002) Calmodulins and calcineurin B-like proteins: calcium sensors for specific signal response coupling in plants, *Plant Cell* 14, S389-400.
88. Stefan, M. I., Edelstein, S. J., and Le NovÃˆre, N. (2008) An allosteric model of calmodulin explains differential activation of PP2B and CaMKII, *PNAS* 105, 10768-10773.
89. Hudmon, A., and Schulman, H. (2002) Neuronal Ca²⁺/calmodulin-dependent protein-kinase II: The role of structure and autoregulation in cellular function, *Annu. Rev. Biochem.* 71, 473-510.
90. Hudmon, A., and Schulman, H. (2002) Structure-function of the multifunctional Ca²⁺/calmodulin-dependent protein kinase II, *Biochem. J.* 364, 593-611.
91. Rosenberg, O. S., Deindl, S., Sung, R.-J., Nairn, A. C., and Kuriyan, J. (2005) Structure of the autoinhibited kinase domain of CaMKII and SAXS analysis of the holoenzyme, *Cell* 123, 849-860.
92. Liu, J., Miller, S. S., Graham, M., Bucciarelli, B., Catalano, C. M., Sherrier, D. J., Samac, D. A., Ivashuta, S., Fedorova, M., Matsumoto, P., Gantt, J. S., and Vance, C. P. (2006) Recruitment of novel calcium-binding proteins for root nodule symbiosis in *Medicago truncatula*, *Plant Physiol.* 141, 167-177.

93. Pellicena, P., and Kuriyan, J. (2006) Protein-protein interactions in the allosteric regulation of protein kinases, *Curr. Opin. Struct. Biol.* 16, 702-709.
94. Sjöström, P. J., and Nelson, S. B. (2002) Spike timing, calcium signals and synaptic plasticity, *Curr. Opin. Neurobiol.* 12, 305-314.
95. Gaertner, T. R., Kolodziej, S. J., Wang, D., Kobayashi, R., Koomen, J. M., Stoops, J. K., and Waxham, M. N. (2004) Comparative analyses of the three-dimensional structures and enzymatic properties of α , β , γ , and δ isoforms of Ca^{2+} -calmodulin-dependent protein kinase II, *J. Biol. Chem.* 279, 12484-12494.
96. Hoelz, A., Nairn, A. C., and Kuriyan, J. (2003) Crystal structure of a tetradecameric assembly of the association domain of Ca^{2+} /calmodulin-dependent kinase II, *Mol. Cell* 11, 1241-1251.
97. Kolodziej, S. J., Hudmon, A., Waxham, M. N., and Stoops, J. K. (2000) Three-dimensional reconstructions of calcium/calmodulin-dependent (CaM) kinase II alpha and truncated CaM kinase II alpha reveal a unique organization for its structural core and functional domains, *J. Biol. Chem.* 275, 14354-14359.
98. Hagiwara, T., Ohsako, S., and Yamauchi, T. (1991) Studies on the regulatory domain of Ca^{2+} /calmodulin-dependent protein kinase II by expression of mutated cDNAs in *Escherichia coli*, *J. Biol. Chem.* 266, 16401-16408.
99. Kanaseki, T., Ikeuchi, Y., Sugiura, H., and Yamauchi, T. (1991) Structural features of Ca^{2+} /calmodulin-dependent protein kinase II revealed by electron microscopy, *J. Cell Biol.* 115, 1049-1060.
100. Meyer, T., Hanson, P. I., Stryer, L., and Schulman, H. (1992) Calmodulin trapping by calcium-calmodulin-dependent protein kinase, *Science* 256, 1199-1202.
101. Waxham, M. N., Tsai, A.-I., and Putkey, J. A. (1998) A mechanism for calmodulin (CaM) trapping by caM-kinase II defined by a family of CaM-binding peptides, *J. Biol. Chem.* 273, 17579-17584.
102. De Koninck, P., and Schulman, H. (1998) Sensitivity of CaM kinase II to the frequency of Ca^{2+} oscillations, *Science* 279, 227-230.
103. Marhl, M., and Grubelnik, V. (2007) Role of cascades in converting oscillatory signals into stationary step-like responses, *BioSyst.* 87, 58-67.
104. Lantsman, K., and Tombes, R. M. (2005) CaMK-II oligomerization potential determined using CFP/YFP FRET, *Biochimica et Biophysica Acta: Molecular Cell Research* 1746, 45-54.
105. Jama, A. M., Gabriel, J., Al-Nagar, A. J., Martin, S., Baig, S. Z., Soleymani, H., Chowdhury, Z., Beesley, P., and Török, K. (2011) Lobe-specific functions of Ca^{2+} calmodulin in αCa^{2+} calmodulin-dependent protein kinase II activation, *J. Biol. Chem.* 286, 12308-12316.
106. Dupont, G., Houart, G., and De Koninck, P. (2003) Sensitivity of CaM kinase II to the frequency of Ca^{2+} oscillations: a simple model, *Cell Calcium* 34, 485-497.
107. Pepke, S., Kinzer-Ursem, T., Mihalas, S., and Kennedy, M. B. (2010) A dynamic model of interactions of Ca^{2+} , calmodulin, and catalytic subunits of Ca^{2+} /calmodulin-dependent protein kinase II, *PLoS Comput Biol* 6, e1000675.
108. Spilker, C., Richter, K., Smalla, K. H., Manahan-Vaughan, D., Gundelfinger, E. D., and Braunewell, K. H. (2000) The neuronal EF-hand calcium-binding protein visinin-like protein-3 is expressed in cerebellar Purkinje cells and shows a calcium-dependent membrane association, *Neuroscience* 96, 121-129.
109. Vijay-Kumar, S., and Kumar, V. D. (1999) Crystal structure of recombinant bovine neurocalcin, *Nat Struct Mol Biol* 6, 80-88.
110. Yamagata, K., Goto, K., Kuo, C.-H., Kondo, H., and Miki, N. (1990) Visinin: a novel calcium binding protein expressed in retinal cone cells, *Neuron* 4, 469-476.
111. Mathisen, P. M., Johnson, J. M., Kawczak, J. A., and Tuohy, V. K. (1999) Visinin-like protein (VILIP) is a neuron-specific calcium-dependent double-stranded RNA-binding Protein, *J. Biol. Chem.* 274, 31571-31576.
112. Lin, L., Jeanclos, E. M., Treuil, M., Braunewell, K.-H., Gundelfinger, E. D., and Anand, R. (2002) The calcium sensor protein visinin-like protein-1 modulates the surface expression

- and agonist sensitivity of the alpha 4beta 2 nicotinic acetylcholine receptor, *J. Biol. Chem.* 277, 41872-41878.
113. Feng, B., and Stemmer, P. M. (1999) Interactions of Calcineurin A, Calcineurin B, and Ca^{2+} , *Biochemistry* 38, 12481-12489.
114. Kolukisaoglu, Ü., Weigl, S., Blazevic, D., Batistic, O., and Kudla, J. (2004) Calcium sensors and their interacting protein kinases: Genomics of the arabidopsis and rice CBL-CIPK signaling networks, *Plant Physiol.* 134, 43-58.
115. Liu, J., and Zhu, J.-K. (1998) A calcium sensor homolog required for plant salt tolerance, *Science* 280, 1943-1945.
116. Kudla, J., Batistič, O., and Hashimoto, K. (2010) Calcium signals: the lead currency of plant information processing, *Plant Cell* 22, 541-563.
117. Ames, J. B., Ishima, R., Tanaka, T., Gordon, J. I., Stryer, L., and Ikura, M. (1997) Molecular mechanics of calcium-myristoyl switches, *Nature* 389, 198-202.
118. Naoe, Y., Arita, K., Hashimoto, H., Kanazawa, H., Sato, M., and Shimizu, T. (2005) Structural characterization of calcineurin B homologous protein 1, *J. Biol. Chem.* 280, 32372-32378.
119. Prilusky, J., Felder, C. E., Zeev-Ben-Mordehai, T., Rydberg, E. H., Man, O., Beckmann, J. S., Silman, I., and Sussman, J. L. (2005) FoldIndex(C): a simple tool to predict whether a given protein sequence is intrinsically unfolded, *Bioinformatics* 21, 3435-3438.
120. Lupas, A., Van Dyke, M., and Stock, J. (1991) Predicting coiled coils from protein sequences, *Science* 252, 1162-1164.
121. Yamagata, Y., Czernik, A. J., and Greengard, P. (1991) Active catalytic fragment of Ca^{2+} /calmodulin-dependent protein kinase II. Purification, characterization, and structural analysis, *J. Biol. Chem.* 266, 15391-15397.
122. Nettleship, J. E., Brown, J., Groves, M. R., and Geerloff, A. (2008) Methods for protein characterization by mass spectrometry, thermal shift (ThermoFluor) assay, and multiangle or static light scattering, In *Structural Proteomics*, pp 299-318.
123. Putkey, J. A., Sweeney, H. L., and Campbell, S. T. (1989) Site-directed mutation of the trigger calcium-binding sites in cardiac troponin C, *J. Biol. Chem.* 264, 12370-12378.
124. Peterson, B. Z., DeMaria, C. D., Adelman, J. P., and Yue, D. T. (1999) Calmodulin is the Ca^{2+} sensor for Ca^{2+} -dependent inactivation of L-type calcium channels, *Neuron* 22, 549-558.
125. Hu, P., Ye, Q.-Z., and Loo, J. A. (1994) Calcium stoichiometry determination for calcium binding proteins by electrospray ionization mass spectrometry, *Analytical Chemistry* 66, 4190-4194.
126. Scott, D. J., Harding, S. E., and Rowe, A. J. (2005) UltraScan - A comprehensive data analysis software package for analytical ultracentrifugation experiments, In *Analytical Ultracentrifugation* (Scott, D. J., Harding, S. E., and Rowe, A. J., Eds.), pp 210-230, The Royal Society of Chemistry.
127. Huang, H., Ishida, H., and Vogel, H. J. (2010) The solution structure of the Mg^{2+} form of soybean calmodulin isoform 4 reveals unique features of plant calmodulins in resting cells, *Protein Sci.* 19, 475-485.
128. Venyaminov, S. Y., Klimtchuk, E. S., Bajzer, Z., and Craig, T. A. (2004) Changes in structure and stability of calbindin-D_{28K} upon calcium binding, *Anal. Biochem.* 334, 97-105.
129. Marchand, S., and Roux, B. (1998) Molecular dynamics study of calbindin D_{9k} in the apo and singly and doubly calcium-loaded states, *Proteins: Struct. Funct. Bioinform.* 33, 265-284.
130. Whitmore, L., and Wallace, B. A. (2004) DICHROWEB, an online server for protein secondary structure analyses from circular dichroism spectroscopic data, *Nucleic Acids Res.* 32, W668-W673.
131. Sreerama, N., and Woody, R. W. (2000) Estimation of protein secondary structure from circular dichroism spectra: Comparison of CONTIN, SELCON, and CDSSTR Methods with an expanded reference set, *Anal. Biochem.* 287, 252-260.
132. Pain, R. (2001) *Determining the CD spectrum of a protein*, John Wiley & Sons, Inc.

133. Yamniuk, A. P., Nguyen, L. T., Hoang, T. T., and Vogel, H. J. (2004) Metal ion binding properties and conformational states of calcium- and integrin-binding protein, *Biochemistry* 43, 2558-2568.
134. Mertens, H. D. T., and Svergun, D. I. (2010) Structural characterization of proteins and complexes using small-angle X-ray solution scattering, *J. Struct. Biol.* 172, 128-141.
135. Petoukhov, M. V., Konarev, P. V., Kikhney, A. G., and Svergun, D. I. (2007) ATSAS 2.1 - towards automated and web-supported small-angle scattering data analysis, *J. Appl. Crystal.* 40, s223-s228.
136. Volkov, V. V., and Svergun, D. I. (2003) Uniqueness of *ab-initio* shape determination in small-angle scattering, *J. Appl. Crystal.* 36, 860-864.
137. Kozin, M. B., and Svergun, D. I. (2001) Automated matching of high- and low-resolution structural models, *J. Appl. Crystal.* 34, 33-41.
138. Rellos, P., Pike, A. C. W., Niesen, F. H., Salah, E., Lee, W. H., von Delft, F., and Knapp, S. (2010) Structure of the CaMKII δ /Calmodulin Complex Reveals the Molecular Mechanism of CaMKII Kinase Activation, *PLoS Biol* 8, e1000426.
139. Poirot, O., O'Toole, E., and Notredame, C. (2003) Tcoffee@igs: a web server for computing, evaluating and combining multiple sequence alignments, *Nucleic Acids Res.* 31, 3503-3506.
140. Belfield, E. J., Hughes, R. K., Tsesmetzis, N., Naldrett, M. J., and Casey, R. (2007) The gateway pDEST17 expression vector encodes a -1 ribosomal frameshifting sequence, *Nucleic Acids Res.* 35, 1322-1332.
141. Fromm, H., and Chua, N.-H. (1992) Cloning of plant cDNAs encoding calmodulin-binding proteins using 35 S-labeled recombinant calmodulin as a probe *Plant molecular biology reporter* 10, 7.
142. Studier, F. W. (2005) Protein production by auto-induction in high-density shaking cultures, *Protein Expression and Purification* 41, 207-234.
143. Gasteiger, E., Hoogland, C., Gattiker, A., Duvaud, S. e., Wilkins, M. R., Appel, R. D., and Bairoch, A. (2005) Protein identification and analysis tools on the ExPASy server, In *The Proteomics Protocols Handbook* (Walker, J. M., Ed.), pp 571-607, Humana Press.
144. Bondos, S. E., and Bicknell, A. (2003) Detection and prevention of protein aggregation before, during, and after purification, *Anal. Biochem.* 316, 223-231.
145. Shirran, S. L., and Barran, P. E. (2009) The use of ESI-MS to probe the binding of divalent cations to calmodulin, *J. Am. Soc. Mass Spectrom.* 20, 1159-1171.
146. Luedtke, N. W., Hwang, J. S., Glazer, E. C., Gut, D., Kol, M., and Tor, Y. (2002) Eilatin Ru(II) complexes display anti-HIV activity and enantiomeric diversity in the binding of RNA, *ChemBioChem* 3, 766-771.
147. Franke, D., and Svergun, D. I. (2009) DAMMIF, a program for rapid *ab-initio* shape determination in small-angle scattering, *J. Appl. Crystal.* 42, 342-346.
148. Svergun, D. I., Petoukhov, M. V., and Koch, M. H. J. (2001) Determination of domain structure of proteins from X-Ray solution scattering, *Biophys. J.* 80, 2946-2953.
149. Tanaka, T., Ames, J. B., Harvey, T. S., Stryer, L., and Ikura, M. (1995) Sequestration of the membrane-targeting myristoyl group of recoverin in the calcium-free state, *Nature* 376, 444-447.
150. Kuboniwa, H., Tjandra, N., Grzesiek, S., Ren, H., Klee, C. B., and Bax, A. (1995) Solution structure of calcium-free calmodulin, *Nat Struct Biol* 2, 768-776.
151. Karley, A. J., and White, P. J. (2009) Moving cationic minerals to edible tissues: potassium, magnesium, calcium, *Curr. Opin. Plant Biol.* 12, 291-298.
152. Chandler, D. (2005) Interfaces and the driving force of hydrophobic assembly, *Nature* 437, 640-647.
153. Hoops, S., Sahle, S., Gauges, R., Lee, C., Pahle, J., Simus, N., Singhal, M., Xu, L., Mendes, P., and Kummer, U. (2006) COPASI—a Complex Pathway Simulator, *Bioinformatics* 22, 3067-3074.
154. Dodd, R., Peracchia, C., Stolady, D., and Török, K. (2008) Calmodulin association with Connexin32-derived peptides suggests trans-domain interaction in chemical gating of gap junction channels, *J. Biol. Chem.* 283, 26911-26920.

-
155. Quetglas, S., Leveque, C., Miquelis, R., Sato, K., and Seagar, M. (2000) Ca^{2+} -dependent regulation of synaptic SNARE complex assembly via a calmodulin- and phospholipid-binding domain of synaptobrevin, *PNAS* 97, 9695-9700.
 156. Sturtevant, J. M. (1977) Heat capacity and entropy changes in processes involving proteins, *PNAS* 74, 2236-2240.